

Quantum phase transitions in transverse field spin models: From Statistical Physics to Quantum Information

Amit Dutta*

Department of Physics, Indian Institute of Technology, Kanpur 208 016, India

Uma Divakaran†

Theoretische Physik, Universität des Saarlandes, 66041 Saarbrücken, Germany

Diptiman Sen‡

Centre for High Energy Physics, Indian Institute of Science, Bangalore 560 012, India

Bikas K. Chakrabarti§

Theoretical Condensed Matter Physics Division and Centre for Applied Mathematics and Computational Science, Saha Institute of Nuclear Physics, 1/AF Bidhan Nagar, Kolkata 700 064, India

Thomas F. Rosenbaum¶

Department of Physics and the James Franck Institute, University of Chicago, Chicago, IL 60637

Gabriel Aeppli**

London Centre for Nanotechnology and Department of Physics and Astronomy, UCL, London, WC1E 6BT, United Kingdom

We review quantum phase transitions of spin systems in transverse magnetic fields taking the examples of some paradigmatic models, namely, the spin-1/2 Ising and XY models in a transverse field in one and higher spatial dimensions. Beginning with a brief overview of quantum phase transitions, we introduce the model Hamiltonians and discuss the equivalence between the quantum phase transition in such a model and the finite temperature phase transition in a higher dimensional classical model. We then provide exact solutions in one spatial dimension connecting them to conformal field theoretical studies when possible. We also discuss Kitaev models, and some other exactly solvable spin systems in this context. Studies of quantum phase transitions in the presence of quenched randomness and with frustrating interactions are presented in details. We discuss novel phenomena like Griffiths-McCoy singularities associated with quantum phase transitions of low-dimensional transverse Ising models with random interactions and transverse fields. We then turn to more recent topics like information theoretic measures of the quantum phase transitions in these models; we elaborate on the scaling behaviors of concurrence, entanglement entropy (for both pure and random models), quantum discord and quantum fidelity close to a quantum critical point. At the same time, we discuss the decoherence (or Loschmidt echo) of a qubit coupled to a quantum critical spin chain. We then focus on non-equilibrium dynamics of a variety of transverse field systems across quantum critical points and lines. After briefly mentioning rapid quenching studies, we dwell on slow dynamics and discuss the Kibble-Zurek scaling for the defect density following a quench across critical points and its modifications for quenching across critical lines, gapless regions and multicritical points. We present a brief discussion on adiabatic perturbation theory indicating the limits of slow and sudden quenching; we introduce the concept of a generalized fidelity susceptibility in this context. Topics like the role of different quenching schemes, local quenching, quenching of models with random interactions and quenching of a spin chain coupled to a heat bath are touched upon. The connection between non-equilibrium dynamics and quantum information theoretic measures (introduced in the previous section) is presented at some length. We indicate the connection between Kibble-Zurek scaling and adiabatic evolution of a state as well as the application of adiabatic dynamics as a tool of a quantum optimization technique known as quantum annealing (or adiabatic quantum computation). The final section is dedicated to a detailed discussion on recent experimental studies of transverse Ising-like systems.

*Electronic address: dutta@iitk.ac.in

†Electronic address: udiva@lusi.uni-sb.de

‡Electronic address: diptiman@cts.iisc.ernet.in

§Electronic address: bikask.chakrabarti@saha.ac.in

¶Electronic address: tfr@uchicago.edu

**Electronic address: gabriel.aeppli@ucl.ac.uk

Contents

I. Introduction and the aim of the review	3
(A). Quantum phase transitions	7
(B). Transverse Ising and XY models	10
(C). Some exactly solvable models related to transverse Ising and XY models	12
(D). Quantum-classical correspondence and scaling	14
(E). Quantum spin chains coupled to a bath	16
(F). Quantum rotor models	17
II. Exact solutions in one and two dimensions	18
(A). Jordan-Wigner transformation	18
(B). Connection to conformal field theory	20
(C). Exact solution of the Kitaev model	23
III. Role of quenched disorder	24
(A). Quantum Ising spin glass (QISG)	26
(B). Griffiths singularities and activated dynamics	27
(C). A generalized random transverse field Ising spin Chain	29
(D). Higher dimensional realization of IRFP	29
(E). Quantum Ising model in a random longitudinal field	31
IV. Related models with frustration	31
(A). Quantum ANNNI model	31
(B). Models with long-range antiferromagnetic interactions	35
V. Theoretical studies of quantum phase transition and information	36
(A). Entanglement	36
(a). Concurrence	37
(b). Entanglement entropy	39
(B). Quantum discord	41
(C). Quantum fidelity	41
(D). Quantum critical environment: decoherence and Loschmidt echo	47
VI. Non-equilibrium dynamics across quantum critical points	49
(A). Rapid quenching through a QCP	49
(B). Defect generation: Kibble-Zurek (KZ) scaling	51
(C). Adiabatic perturbation theory: Slow and Sudden Quenches	54
(D). Linear and non-linear slow evolution through critical points	56
(E). Quenching through multicritical points	59
(F). Generalized quenching schemes	61
(G). Quenching through gapless phases	62
(H). Quenching of a disordered chain	63
(I). Quenching with coupling to a bath	63
(J). Quenching and quantum information	64
(a). Slow quenches	64
(b). Sudden quenches	68
(K). Local quenching processes	69
(L). Thermalization	70
(M). KZ mechanism and adiabatic evolution	71
(N). A brief note on quantum annealing	71
VII. Experimental realizations of transverse field Ising systems	72
(A). Singlet ground state magnets	72
(B). Order/disorder transitions in hydrogen-bonded and other ferro/antiferroelectric systems	73
(C). Low-dimensional magnetic realizations of the transverse field Ising model	74
(D). Ising doublets in external magnetic fields in three-dimensions	76
(E). Disorder and the transverse field Ising model	76

VIII. Concluding remarks	81
Acknowledgments	81
A. Large spin limits: transverse XY spin chain	82
B. Derivation of a matrix product Hamiltonian	83
C. From Jordan-Wigner to bosonization	84
D. Scaling of the geometric phase close to a QCP	89
E. Landau-Zener tunneling	90
F. KZ mechanism in space	92
G. Effect of topology on quantum quenching	93
H. Studies of Tomonaga-Luttinger liquids	93
References	94

I. INTRODUCTION AND THE AIM OF THE REVIEW

A plethora of systems exhibit phase transitions as the temperature or some other parameter is changed. Examples range from the ice-water phase transition observed in our daily life to the loss of ferromagnetism in iron or to the more sophisticated Mott insulator-superfluid phase transition observed in optical lattices [1]. The last five decades have witnessed a tremendous upsurge in the studies of phase transitions at finite temperature [2–8]. The success of Landau-Ginzburg theories and the concepts of spontaneous symmetry breaking and the renormalization group [9–12] in explaining many of the finite temperature phase transitions occurring in nature has been spectacular.

In this review, we will consider only a subclass of phase transitions called quantum phase transitions (QPTs) [13–21]; these are zero temperature phase transitions which are driven by quantum fluctuations and are usually associated with a non-analyticity in the ground state energy density of a quantum many-body Hamiltonian. We will focus on continuous QPTs where the order parameter vanishes continuously at the quantum critical point (QCP) at some value of the parameters which characterize the Hamiltonian. We will not discuss first order quantum phase transitions associated with an abrupt change in the order parameter. Usually, a first order phase transition is characterized by a finite discontinuity in the first derivative of the ground state energy density. A continuous QPT is similarly characterized by a finite discontinuity, or divergence, in the second derivative of the ground state energy density, assuming that the first derivative is continuous. This is of course the classical definition; we will later mention some QPTs where the ground state energy density is not necessarily singular.

The central theme of the review is quantum phase transitions in transverse field models, (namely, Ising and XY models in a transverse magnetic field) which are paradigmatic models exhibiting zero temperature continuous QPTs, and the recent studies (both experimental and theoretical) involving these models. To the best of our knowledge, the one-dimensional version of the transverse Ising model (TIM) first appeared in the context of the exact solution of a two-dimensional nearest-neighbor ferromagnetic classical Ising model; the row-to-row transfer matrix of the two-dimensional model can be mapped to a transverse Ising chain in some limit [22] and the exact solution of this one-dimensional version of the model soon followed [23]. Shortly, the model was invoked to mimic the order-disorder transitions in KDP ferroelectrics [24]. Our review will attempt to highlight the aspects of the TIMs for which these models and their variants continue to be enormously useful, even more than fifty years after their first appearance, in understanding QPTs, non-equilibrium dynamics of quantum critical systems, and connections between QPTs, dynamics and quantum information, and in possible experimental and theoretical realizations of quantum annealing. Moreover, experimental realizations of these transverse Ising models have opened up new vistas of research.

Before presenting the section-wise plan of the review, let us first discuss in what sense the review will be useful to the community. Here, we place the most recent theoretical as well as experimental studies of QPTs in transverse field models under the same roof pointing to the open problems wherever possible. For example, a very recent experimental study of the exotic low lying spectrum of the transverse Ising systems in a longitudinal field [25] has been discussed here at some length mentioning the corresponding theoretical prediction of the same made decades ago (Sec. II (B)). Even when discussing conventional topics, also reviewed elsewhere, we emphasize recent developments and debates;

for example, we allude to recent studies of matrix product states and their connection to quantum information and dynamics. The correspondence between QPTs and classical finite-temperature phase transitions (in a model with one added dimension) is well studied for these models, but the possible breakdown of this established scenario in the context of the spin-boson model is relatively less familiar; we include this in the review. Although the novel features associated with random quantum Ising transitions have been reviewed previously, we mention the most generalized model introduced in connection to quantum information theory (more precisely, to the entanglement entropy, to be defined in Sec. V (A) (b)) and point to the recent debate on the possibility of a generalized c -theorem. Similarly, the long-standing debate concerning the width of the floating phase in the phase diagram of a one-dimensional transverse Ising model with regular frustrations is highlighted. At the same time, it needs to be emphasized that in Secs. 5 and 6, we have attempted to provide a general perspective of the related physical problems; the general theory is illustrated using the example of transverse field models. For example, we discuss the generic scaling of quantum fidelity in all limits (Sec. V (C)) and verify these scaling relations using one-dimensional transverse field models. It is to be noted that the section on regularly frustrated system (Sec. IV (A)) is model specific and in Sec. 3 we elaborate the features of quantum phase transitions in random systems which are the most prominent in TIMs.

In the first two sections we briefly present the phenomenology of the models and discuss at length their exact solution in one dimension. These discussions are intended to help a beginner to navigate through the more involved topics discussed in subsequent sections. Although the main emphasis is on the transverse Ising and XY models, we also briefly dwell on other one-dimensional exactly solvable models (closely related to the Ising and XY models) and the two-dimensional Kitaev model, and discuss their applications. In that sense, this review covers the entire gamut of Jordan-Wigner solvable models (to be explained below) especially from the viewpoint of quantum information and dynamics. Moreover, we use Appendix C to provide a discussion on the method of bosonization and QPTs in Tomonaga-Luttinger liquids which go beyond Jordan-Wigner solvable models.

With this preamble, let us elaborate on the section-wise plan of this review. In Sec. 1, we will briefly introduce QPTs and critical exponents. We then introduce the transverse Ising models in one and higher dimensions. This is followed by a discussion on a XY spin chain which is a generalized version of the Ising chain with XY -like interactions. The anisotropic version of the XY spin model has the same symmetry (Z_2) as the transverse Ising model and both the models are exactly solvable in one spatial dimension. However, the transverse XY chain exhibits a richer phase diagram with critical, multicritical points and gapless critical lines. Transverse Ising models have been extended to n -component quantum rotor models which are in fact quantum generalizations of classical n -vector models; we also briefly touch upon quantum rotor models. There are some variants of transverse Ising and XY spin chains (Sec. 1.3) which can be exactly solved and show rich phase diagrams (and are being studied extensively), e.g., the transverse XY spin chain with alternating interactions and fields, and a transverse Ising chain with three-spin interactions. The latter model is known to have a matrix product ground state and undergoes a quantum phase transition which has some unconventional properties as explained in Sec. 1.1.

Another useful aspect of the TIMs is their connection to classical Ising models in the sense of the universality class which we briefly mention in Sec. 1.4; we summarize the essential idea here. The zero-temperature transition of a d -dimensional TIM with nearest-neighbor ferromagnetic interactions belongs to the same universality class as the thermal phase transition of a classical Ising model with similar interactions in $(d + 1)$ -dimensions; this equivalence can be established using a Suzuki-Trotter formalism and through the imaginary time path-integral formalism of the quantum model where the additional dimension is the Trotter direction or imaginary time direction. Similarly, starting from the transfer matrix of the two-dimensional Ising model, one can arrive at the quantum Ising chain in a limit which is known as the τ -continuum limit. The underlying idea in both cases is that the extreme anisotropy in interactions along different spatial directions does not alter the universality class, i.e., the critical exponents. The quantum-classical correspondence holds even when the interactions in the quantum model are frustrated or random; in this case interactions along d spatial dimensions of the higher-dimensional classical models become frustrated or random as in the quantum model but the interactions in the Trotter (time) direction remain ferromagnetic and nearest-neighbor. Therefore, one ends up with a classical model with randomness or frustration correlated in the Trotter direction. The quantum-classical correspondence turns out to be useful for several reasons: (i) since classical models are well studied, one can infer some of the critical exponents of the equivalent quantum model beforehand. For example, one can immediately conclude that the upper critical dimension for a short-range interacting quantum Ising model would be three since this is equivalent to the thermal transition of a four-dimensional classical Ising model. (ii) Secondly, this mapping renders quantum Ising models ideal candidates for quantum Monte Carlo studies, and to understand the quantum transitions one has to study a classical Ising model with one additional dimension. Although an equivalent classical model exists for many quantum spin models (though not all), one usually ends up with a classical model with complicated interactions. Therefore, this equivalence is a unique property of TIMs which has been exploited intensively to gain a better understanding of QPTs in random models. In a similar spirit, one can show that the QPT in a quantum rotor model is equivalent to the thermal transition in a classical n -vector model with one additional dimension. However, this traditional notion has been challenged in the context of the spin-boson

model (Sec. 1.5).

The integrability of the transverse Ising and XY chains with nearest-neighbor interactions has possibly attracted the attention of the physicists the most¹. In Sec. 2, we will see how these spin models can be solved exactly using the Jordan-Wigner (JW) transformation. The reduced Hamiltonian in the Fourier space gets decoupled into 2×2 Hamiltonians; this two-level form eventually turns out to be extremely useful in calculating the defect density following a sweep of the spin chain across a QCP as we shall discuss in Sec. 5. Moreover, the ground state takes a direct product form of qubits; this simple form of the ground state wave function is extremely helpful in understanding the behavior and scaling of information theoretic measures close to a QCP which we shall discuss in Sec. 5. The Kitaev model on a honeycomb lattice is one of the very models which are exactly solvable in two dimensions; the solution employs a mapping of spin- $1/2$'s to Majorana fermions through a JW transformation. Hence the model has been widely used to understand non-equilibrium dynamics of quantum critical systems as well as in quantum information studies which we shall refer to in subsequent sections. We shall introduce the Kitaev model, the appropriate JW transformation and the phase diagram of the model in Sec. 2. Finally, we will briefly discuss the connection of various one-dimensional models to conformal field theory and show how the scaling dimensions of different operators can be extracted from the conformal properties of the equivalent action at the QCP. This information turns out to be useful, e.g., for the transverse Ising chain in the presence of a longitudinal field that destroys the integrability of the model. The recent study of the QPT of a model that challenges this quantum-classical equivalence will also be briefly mentioned.

It is well known that the presence of disorder or randomness in interactions or fields deeply influences the phase transition occurring in a classical system, often wiping it out completely. A modified Harris criterion points to a stronger dominance of randomness in the case of a zero-temperature quantum transition. Although the quantum versions of classical Ising and n -vector spin glasses have been studied in the last four decades and their quantum counterparts were introduced in the early eighties, the experimental results for LiHoF_4 and its disordered version $\text{LiHo}_x\text{Y}_{1-x}\text{F}_4$ which are ideal realizations of TIMs with long-range dipolar interactions led to a recent upsurge in exploring the QPT in quantum Ising spin-glasses which are briefly mentioned in Sec. 4. The most exciting feature associated with low-dimensional random quantum critical systems is the prominence of Griffiths-McCoy (GM) singular regions close to the QCP and the activated quantum dynamical scaling right at the QCP. We shall argue that these off-critical singularities are more prominent in transverse Ising models than in the rotor models due to the Ising symmetry in the former. These singular regions arise due to locally ordered large “rare” clusters, which can be viewed as a giant spin. If the spins are Ising-like, this giant spin can flip only through the barrier tunneling which is an activated process thereby leading to prominent GM regions. These issues and the contrast with the $O(n)$ symmetric quantum rotor models will be discussed in Sec. 3 where we allude to the effect of a random longitudinal field on the quantum Ising transitions. Experimental signatures of this GM phase are also discussed later. The role of these GM singularities in the quantum information theoretic measures and dynamics of disordered spin chains will be discussed in appropriate sections.

In Sec. 4, we shall introduce a version of the classical Ising model with competing interactions in which in addition to the nearest-neighbor ferromagnetic interactions along all the spatial directions, there is a next-nearest neighbor antiferromagnetic interactions along a particular direction, called the axial direction. This model is known as the axially anisotropic next-nearest-neighbor Ising (ANNNI) model which is the simplest model with non-trivial frustration and exhibits a rich phase diagram that has been studied for the last three decades. We focus on the bosonization study of the equivalent quantum model in one dimension. We show that different numerical studies and the bosonization studies contradict each other and whether a floating phase of finite width exists in the phase diagram of the one-dimensional transverse ANNNI is not clearly established till today. To make a connection with bosonization studies, we present the main ideas of bosonization and its applications to one-dimensional spin systems in Appendix C. In this context, we refer to the quantum rotor models with ANNNI-like frustrations and mention theoretical and experimental studies of the quantum Lifshitz point which appears in the phase diagram of these rotor models.

In Sec. 5, we will discuss some connections between quantum information theoretic measures and QPTs. It is interesting that these quantum information theoretic measures can capture the ground state singularities associated with a QPT. The quantum correlations of a state can be quantified in terms of bipartite entanglements. While the entanglement is a measure of the correlation based on the separability of two subsystems of the composite system, the quantum discord is based on the measurement on one of the subsystems. Both the concurrence (which is one of the measures of bipartite entanglement) and quantum discord show distinctive behaviors close to the QCP of a one-dimensional transverse XY spin model and interesting scaling relations which incorporate the information about the universality of the associated QPT. We also discuss the generic scaling for the entanglement entropy close to a

¹ We will discuss later what integrability means; here the expression implies that all the eigenfunctions and energies can be exactly obtained.

QCP and how these scaling relations are verified for transverse field spin models. Subsequently, we review the notion of quantum fidelity which is the modulus of the overlap of two ground state wave functions with different values of the parameters of the Hamiltonian. Although the fidelity vanishes in the thermodynamic limit, for a finite system it shows a dip at the QCP and hence is an ideal indicator of a QCP. We discuss the concept of fidelity susceptibility valid in the limit when two parameters under consideration are infinitesimally close to each other; this fidelity susceptibility shows a very interesting scaling behavior close to a QCP which can be verified analytically for transverse field spin chains. Moreover, one finds surprising results close to a multicritical point. In the process, we comment on the quantum geometric tensor defined on a multi-dimensional parameter space pointing to the close connection between the fidelity susceptibility and the geometric phase. Very recently, the fidelity has been studied for the case when the difference in the parameters characterizing two ground state wave functions is finite; this is referred to as the fidelity in the thermodynamic limit. A scaling of fidelity has been proposed in this limit also, which has again been verified for transverse field spin chains. Finally, we comment on the decoherence of a qubit (spin-1/2) or a central spin coupled to an environment which is conveniently chosen to be a transverse Ising/ XY spin chain. Due to the interaction between the qubit and the environment, the initial state (chosen to be the ground state) of the spin chain evolves with two different Hamiltonians and the corresponding Loschmidt echo is measured. The echo shows a sharp dip close to the QCP and shows a collapse and revival there which can be taken to be an indicator of quantum criticality. The sharp dip in the echo at the same time indicates a complete loss of coherence of the qubit which reduces from the initial pure state to a mixed state. The connection between the static fidelity and the dynamic Loschmidt echo is also mentioned.

In Sec. 6, we study in detail many aspects of the quenching dynamics of quantum systems across quantum critical points or lines; this is the longest section in this review. When a quantum system is driven across a quantum critical point by changing a parameter of the Hamiltonian following some protocol, defects are generated in the final state. This is due to the diverging relaxation time close to the QCP; no matter how slowly the system is quenched the dynamics is not adiabatic. The scaling of the density of defects in the final state is given by the rate of change of the parameter and some of the exponents of the QCP across which the system is driven. What is exciting about this problem is that the defects are generated through a non-equilibrium dynamics but the scaling of the defect density is dictated by the equilibrium quantum critical exponents. This scaling is known as the Kibble-Zurek scaling which can be readily verified using the integrability of the transverse field spin chains and the Landau-Zener transition formula for the non-adiabatic transition probability. We discuss in some detail adiabatic perturbation theory in order to arrive at the Kibble-Zurek scaling law; we also discuss the counterpart of this law in the limit when a parameter of the Hamiltonian is suddenly changed by a small amount starting from the QCP. We discuss how the scaling of the defect density following a sudden or adiabatic quench can be related to a generalized fidelity susceptibility. We indicate how to calculate the defect density following a quench across the critical points for the transverse XY spin chain. When the system is quenched across a multicritical point or a gapless critical line of the transverse XY spin chain or an extended gapless region of the Kitaev model, the traditional Kibble-Zurek scaling is non-trivially modified as we review at some length. Interesting results are obtained for non-monotonic variations of parameters and also when the spin chain is coupled to a bath. The effect of randomness in the interactions on the quenching is also discussed to indicate the role of GM singular regions (discussed in Sec. 3) in modifying the Kibble-Zurek scaling relations. It is natural to seek an optimized rate of quenching that minimizes defects in the final state within a fixed time interval ($-T$ to T). This knowledge would be extremely useful for the adiabatic evolution of a quantum state; we take up a discussion of related studies. One may wonder what happens when a parameter of the quantum Hamiltonian is changed locally; it so happens that in that case, one finds an interesting time evolution of the correlation function following the quench. Finally, we embark on establishing the connection between the non-equilibrium quantum dynamics and quantum information discussed in Sec. 5. As mentioned above, a sweep across a QCP generates defects in the final state which satisfy a scaling relation; interestingly the scalings of the concurrence, negativity, entanglement entropy and other measures of entanglement are also dictated by the scaling of the defect density although for the time evolution of the entanglement entropy one observes a clear signature of the Loschmidt echo for integrable models. In the last section, we comment on some recent studies of the possibilities of quantum annealing and adiabatic quantum computation. We reiterate that all the generic discussions presented in this section are illustrated using transverse field models and their variants.

A discussion of experimental realizations of Ising systems in transverse fields will be taken up in Sec. 7. As mentioned already, the model was introduced to study the order-disorder transition in KDP type ferroelectrics which we discuss at some length. We present a discussion of singlet ground state magnets where the ground state is well separated from higher lying spin multiplets, e.g., LiTbF_4 which was previously employed as an example of an ideal Ising dipolar coupled ferromagnet. The systems for which the most data are available is LiHoF_4 for which the ground state is a non-Kramers doublet with strong anisotropy effectively producing an Ising spin along the tetragonal c -axis. When a laboratory field is applied perpendicular to the c -axis, the ground state degeneracy is lifted and a transverse field is generated due to the mixing between the states which essentially leads, at the lowest order, to an Ising model representation of the system with an effective transverse field. The disordered version of the model (when the magnetic

Ho is substituted by non-magnetic Y), $\text{LiHo}_x\text{Y}_{1-x}\text{F}_4$, is an ideal realization of a quantum Ising spin glass. The phase diagram in the laboratory field and temperature plane shows a ferromagnetic phase for $x > x_c \simeq 0.2$ and a spin glass phase for $x < x_c$. This spin-glass transition and related experimental studies and observations which are not yet explained theoretically are discussed in detail in Secs. VII (D) and VII (E).

One of the most exciting experiments on the one-dimensional transverse field Ising model is discussed in Sec. VII (C), the material for the study being CoNb_2O_6 . The low-lying spectrum in the presence of a longitudinal field is described by the Lie algebra of the exceptional group E_8 which was theoretically predicted using a combination of CFT and an exact scattering matrix analysis for the low-energy particles that is discussed in Sec. II (B). The experimental study discussed in Sec. VII (C) in fact corroborates this finding. We shall make concluding remarks in Sec. 8.

Finally, we have strategically incorporated eight Appendices which are complementary to the material presented in the body of the review. In Appendix A, we discuss QPTs of a transverse XY spin chain in the limit when the spin magnitude S is large, known as the $S \rightarrow \infty$ limit; the results obtained here can be compared to the solution in the extreme quantum case (spin-1/2) discussed in Sec. II (A). At the same time, this section provides a thorough discussion of an interesting (mean field) method. In Appendix B, we have shown how a Hamiltonian (which is a variant of the transverse Ising spin chain Hamiltonian) with a given matrix product ground state can be constructed. We provide a brief overview of Tomonaga-Luttinger liquids in Appendix C while the corresponding studies of quantum dynamics and information are presented in Appendix H. The intention here is to enable the reader to get an idea of recent developments in these low-dimensional models. The discussion of Appendix C would also be useful in following the bosonization results used in Sec. IV (A). In Appendix D, we discuss the scaling of the geometric phase close to a QCP which is in fact closely related to the geometric tensor discussed in Sec. V (C). A derivation of the LZ transition formula that has been used extensively in estimating the defect density following a quantum quench across QCPs (discussed in Sec. 6) is given in Appendix E. Finally, in Appendices F and G, we briefly dwell on two exciting but involved topics, namely, the Kibble-Zurek mechanism in space and the effect of topology on quantum quenching; these studies in fact complement those presented in Sec. 6.

(A). Quantum phase transitions

Let us first recall some features of classical phase transitions driven by thermal fluctuations before considering QPTs in detail. Suppose that a translation invariant classical system in d spatial dimensions has a critical point at some finite temperature $T = T_c$. Such a critical point is associated with a number of critical exponents which are defined as follows [5, 9]. Let $\mathcal{O}(\vec{x})$ denote an order parameter so that the thermal expectation value $\langle \mathcal{O}(\vec{x}) \rangle = 0$ for $T \geq T_c$ and $\neq 0$ for $T < T_c$. If $T > T_c$, the two-point correlation function $\langle \mathcal{O}(\vec{x}_1)\mathcal{O}(\vec{x}_2) \rangle$ falls off at large distances as $\exp(-|\vec{x}_1 - \vec{x}_2|/\xi)$. This defines a correlation length ξ which is a function of T . Then ξ diverges when $T \rightarrow T_c^+$ as $\xi \sim (T - T_c)^{-\nu}$, where ν is called the correlation length exponent. Another exponent is β which is defined by the way the order parameter approaches zero as $T \rightarrow T_c^-$, namely, $\langle \mathcal{O}(\vec{x}) \rangle \sim (T_c - T)^\beta$. The specific heat diverges as $T \rightarrow T_c^+$ as $C \sim (T - T_c)^{-\alpha}$. Next, if h denotes the field which couples to the order parameter in the Hamiltonian of the system, then the zero-field susceptibility $\chi \equiv (d\langle \mathcal{O}(\vec{x}) \rangle / dh)_{h=0}$ diverges as $T \rightarrow T_c^+$ as $\chi \sim (T - T_c)^{-\gamma}$. Exactly at $T = T_c$, the order parameter scales with h as $\langle \mathcal{O}(\vec{x}) \rangle \sim |h|^{1/\delta}$ as $h \rightarrow 0$, while the two-point correlation function falls off at large distances as $|\vec{x}_1 - \vec{x}_2|^{-(d-2+\eta)}$. Finally, there is a dynamical critical exponent, z , which determines the response of the system to time-dependent fields; there is a response time τ which diverges as $\tau \sim \xi^z$ as $T \rightarrow T_c^+$. The connection between a finite temperature classical phase transition (CPT) and the corresponding QPT in transverse field models will be discussed below.

The critical exponents defined above are not independent of each other; they are connected through scaling relations like $\alpha + 2\beta + \gamma = 2$, $\gamma = (2 - \eta)\nu$, $2\beta + \gamma = \beta(\delta + 1)$, etc., so that only two of the six exponents are independent [2, 3]. These scaling relations stem from the fact that close to a critical point, quantities like the free energy density, correlation functions, etc., can be expressed as homogeneous functions of dimensionless variables scaled with the diverging correlation length ξ . Let us consider a correlation volume in a d -dimensional hyper-space of size ξ^d so that the free energy density (f) scales as $f \sim \xi^{-d}$. Noting that $f \sim |T - T_c|^{2-\alpha}$ (as $C \sim |T - T_c|^{-\alpha}$) and $\xi \sim |T - T_c|^{-\nu}$, one readily arrives at one of the scaling relations $2 - \alpha = \nu d$; this is known as the hyperscaling relation. This hyperscaling relation is valid at or below the upper-critical dimension d_u^c of the model considered. For $d > d_u^c$, the critical exponents are determined by the mean field theory. For classical Ising and n -vector models $d_u^c = 4$.

The striking feature of any continuous phase transitions is the concept of “*universality*”, which means that the critical exponents depend only upon the dimensionality of the system, the symmetry of the order parameter, and the nature of the fixed point, irrespective of the microscopic details of the Hamiltonian. Thus, the critical exponents of the phase transitions occurring in nature can in principle be studied by exploring a simpler model Hamiltonian belonging to the same universality class.

We now present a brief overview of quantum phase transitions [14–16]. QPTs are phase transitions which occur at

zero temperature by driving a non-thermal parameter of a quantum system. At zero temperature, the system will be in the ground state dictated by the values of the parameters of its Hamiltonian. Each term of the Hamiltonian, when dominant, corresponds to a specific ground state and determines a phase in the phase diagram. The presence of non-commuting terms in the Hamiltonian produces a superposition between various states. By varying different terms of the Hamiltonian, one can access the entire phase diagram, crossing different phase boundaries involving second order QPTs. In QPTs, it is the quantum fluctuations (due to non-commuting terms in the Hamiltonian) which are responsible for taking the system from one phase to another, in contrast to the thermal fluctuations in finite temperature phase transitions. One might think that such phase transitions are not relevant to the real world due to the unattainability of zero temperature. However, it has been found that many finite temperature properties of a system can be explained by understanding its quantum critical point (QCP).

We now discuss various critical exponents which characterize a QCP [14, 16]. A QCP is a point at which the ground state energy of the system is a non-analytic function of some parameter which is different from temperature, such as the pressure, magnetic field or interaction strength. At this point, the energy difference Δ between the ground state and the first excited state vanishes. As a parameter g in the Hamiltonian is increased from zero, Δ decreases till it vanishes at the quantum critical point as

$$\Delta \propto |g - g_c|^{\nu z}, \quad (1)$$

where ν and z are the critical exponents associated with the critical point g_c and are defined as follows. In a continuous phase transition, one can associate a length scale ξ which determines the exponential decay of the equal-time two-point correlation in the ground state. For example, the equal-time connected correlation function $G(r)$ of the order parameter between two points separated by a distance r is given by

$$G(r) = \langle O(0, t)O(r, t) \rangle - \langle O(0, t) \rangle \langle O(r, t) \rangle \propto \frac{e^{-r/\xi}}{r^{d-2+\eta}}, \quad (2)$$

where d is the dimensionality of the system and η is called the Fisher exponent associated with the critical point. As the critical point is approached, the length scale ξ diverges with a critical exponent ν as

$$\xi \propto |g - g_c|^{-\nu}. \quad (3)$$

At the critical point, $\xi \rightarrow \infty$ and the correlation function $G(r)$ decays as a power law. Similarly, one can define a time scale ξ_τ for the decay of equal-space correlations analogous to (2), which diverges as

$$\xi_\tau \sim \Delta^{-1} \propto \xi^z \propto |g - g_c|^{-\nu z}. \quad (4)$$

The above equation shows that, unlike CPTs, space and time are connected with each other in QPTs. This complex interplay between space and time in QPTs makes it a challenging area of research.

At the critical point, the correlation length and time are both infinite; fluctuations occur on all length and time scales, and the system is said to be scale invariant. As a result, all observables show power-law behaviors near the critical point. For example, the order parameter \mathcal{O} , characterizing order in the system, is given by

$$\begin{aligned} \mathcal{O} &\propto (g_c - g)^\beta \quad \text{for } g < g_c, \\ &= 0 \quad \text{for } g \geq g_c. \end{aligned} \quad (5)$$

The specific heat C in QPTs is defined as the change in the ground state energy due to a small change in the varying parameter. Although there are seven critical exponents (as shown in Table I for transverse Ising models), not all are independent. As in the classical continuous phase transitions, one can obtain four scaling relations connecting these exponents and hence only three of the exponents are independent [3, 4].

Till now, we have discussed everything at zero temperature where there are no thermal fluctuations. For the sake of completeness, we briefly describe the effect of finite temperature on the QPTs. Let us introduce the frequency associated with the diverging relaxation time by ω_c . As discussed before, the energy associated with this frequency vanishes as

$$\hbar\omega_c \propto |g - g_c|^{\nu z}$$

when the critical point is approached. Quantum mechanics is important as long as this typical energy scale is larger than the thermal energy $k_B T$. In the regions of the phase diagram where $k_B T$ is larger than $\hbar\omega_c$, the classical description of the phase transition can be applied. Namely, quantum mechanics can still be important on microscopic scales but it is the thermal fluctuations which dominate the macroscopic scales and is more relevant in determining the critical behavior.

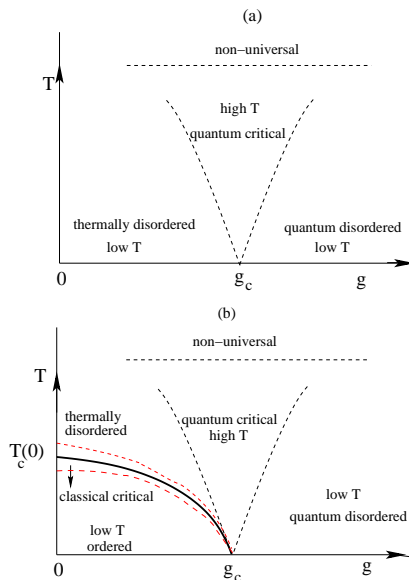


FIG. 1: (Color online) Schematic phase diagram in the vicinity of a quantum critical point. Fig. (a) corresponds to the case where order exists only at $T = 0$, for example, the one-dimensional transverse Ising model (TIM) with g denoting the transverse field. Fig. (b) refers to the case where order can exist even at finite temperatures, for example, the two-dimensional TIM. We discuss Fig. (b) with respect to the two-dimensional TIM. The phase transition at $T = 0$ and $g = g_c$ has the critical exponents of a two-dimensional TIM or the thermal phase transitions of the three-dimensional classical Ising model as obtained by the Suzuki-Trotter formalism (to be discussed in Sec. I (D)). The classical critical point at $g = 0$ and $T = T_c(0)$ denotes the thermal phase transition of a two-dimensional classical Ising model. The solid line marks the phase boundary between ordered and disordered phases. Phase transitions at any finite temperature belong to the universality class of the two-dimensional classical Ising transition governed by $T_c(0)$. The region between the two dashed red lines is dominated by classical fluctuations. The crossover from a low T quantum disordered region to a high T quantum critical region occurs when $\hbar\omega \simeq k_B T$, where ω is the characteristic frequency scale (see Sec. I (D)). (After Sachdev, 1999).

The phase diagram of a quantum system can be of two types depending on whether a finite temperature phase transition exists or not in the system. Figure 1 (a) describes the situation where the order exists only at $T = 0$, for example, the one-dimensional transverse Ising model (discussed later) with the critical temperature $T_c = 0$ at $g = g_c$. In this case, there will be no true phase transition in any real experiment carried out at finite temperatures. However, the finite temperature region in the same figure is characterized by three different regions, separated by crossovers, depending on whether the behavior is dominated by thermal or quantum fluctuations. In the thermally disordered region, the long-range order is destroyed by thermal fluctuations whereas in the quantum disordered state, the physics is dominated by quantum fluctuations. In the quantum critical region, both types of fluctuations are important. In the other type of systems undergoing phase transitions at finite temperatures, for example, the two-dimensional transverse Ising model, the phase diagram is richer as shown in Fig. 1 (b). There is an additional line of finite temperature transitions, the regions surrounding which are referred to as “classical critical” where classical fluctuations dominate. Each of these regions has some special properties [14] which will be discussed later.

There have been many experimental demonstrations of QPTs. The cuprate superconductors which can be tuned from a Mott insulating phase to a d -wave superconducting phase by carrier doping are a paradigmatic example of QPTs. LiHoF_4 , La_2CuO_4 and the heavy fermion $\text{CeCu}_{6-x}\text{Au}_x$ are some other examples of materials which show phase transitions at zero temperature when a particular parameter, say, the transverse field or the concentration x of a component is varied. The systems LiHoF_4 and its disordered version $\text{LiHo}_x\text{Y}_{1-x}\text{F}_4$ are ideal realizations of the transverse Ising model (TIM) with long-range dipolar interactions (to be discussed in Secs. VII (D) and VII (E)) which exhibit QPTs.

So far we have discussed QPTs which are associated with a singularity in the ground state of the quantum Hamiltonian. Before ending this section, let us mention a different class of QPTs in which the ground state has a matrix product form [26]. In these QPTs, the ground state may be completely analytic near $g = g_c$, there may not be any spontaneous symmetry breaking on either side of $g = g_c$, and the two-point correlation function may not approach zero as a power of the separation between the two points at $g = g_c$; in these respects, these QPTs are quite different from those discussed above. However, as $g \rightarrow g_c$, the correlation length diverges and the energy gap approaches zero

as powers of $|g - g_c|$ as in conventional QPTs. In this review, we will mainly discuss conventional QPTs. However, the concept of a matrix product wave function is useful in many problems, including the exact ground state of the Affleck-Kennedy-Lieb-Tasaki model which describes a spin-1 chain with isotropic nearest-neighbor interactions [27]. A matrix product wave function has the form [26, 28]

$$|\psi\rangle = \sum_{i_1, \dots, i_N=1}^d \text{tr}(A_{i_1} \cdots A_{i_N}) |i_1, \dots, i_N\rangle, \quad (6)$$

where N denotes the number of sites, d is the Hilbert space dimension at each site of the system, and $\{A_i\}$ is a set of d D -dimensional matrices where D is an appropriately chosen integer known as the bond dimension². For such a wave function, correlation functions can be calculated by transfer matrix methods; they typically decay exponentially at large distances, where the correlation length is related to the ratio of the second largest eigenvalue to the largest eigenvalue of the transfer matrix. Further, given a matrix product wave function, one can usually construct a Hamiltonian for which it is the ground state [26] (see Sec. I (C) and Appendix B).

Finally, we note that there have been many studies of QPTs which occur between a topological phase and a conventional phase. It is to be noted that a phase with topological order cannot be characterized by any local order parameter; rather it is characterized in other ways such as the ground state degeneracy and the nature of the low-lying excitations. The toric code model is a microscopic lattice model that has been used in this context of topological order and quantum criticality [29]. We shall not discuss this issue here and refer interested readers to a recent review article [30].

(B). Transverse Ising and XY models

One of the prototypical examples capturing the essence of QPTs is the transverse Ising model (TIM) [23, 31]. On a d -dimensional hypercubic lattice, the model consisting of N spins is described by the Hamiltonian

$$H = - \sum_{\langle \mathbf{ij} \rangle} J_{\mathbf{ij}} \sigma_{\mathbf{i}}^x \sigma_{\mathbf{j}}^x - h \sum_{\mathbf{i}} \sigma_{\mathbf{i}}^z, \quad (7)$$

where $\sigma_{\mathbf{i}}^a$, $a = x, y, z$, denote the Pauli spin matrices which satisfy the commutation relations $[\sigma_{\mathbf{i}}^a, \sigma_{\mathbf{i}}^b] = 2i\epsilon_{abc}\sigma_{\mathbf{i}}^c$ at the same site and commute at two different sites (we will generally set $\hbar = 1$). The number of spins $N = (L/a)^d$, where L is the linear dimension of the system, and a is the lattice spacing; we will usually set $a = 1$ in subsequent sections if it is not explicitly mentioned. Here, $\langle \mathbf{ij} \rangle$ denotes nearest-neighbor interactions. This Hamiltonian is invariant under the Z_2 symmetry $\sigma_{\mathbf{i}}^x \rightarrow -\sigma_{\mathbf{i}}^x$, $\sigma_{\mathbf{i}}^y \rightarrow -\sigma_{\mathbf{i}}^y$, and $\sigma_{\mathbf{i}}^z \rightarrow \sigma_{\mathbf{i}}^z$. In this section, we assume that $J_{\mathbf{ij}} = J_x \geq 0$, i.e., a ferromagnetic (FM) interaction between the nearest-neighbor spins. We take $h \geq 0$ without loss of generality. The non-commuting transverse field term introduces quantum fluctuations in the model causing a QPT from an ordered phase ($m_x = \langle \sigma^x \rangle \neq 0$, where $\langle \cdots \rangle$ represents the ground state average of an operator) to a disordered paramagnetic (PM) phase ($m_x = 0$) at a critical value of $h = h_c$. For $h < h_c$, there are two degenerate ground states with FM ordering in which the Z_2 symmetry is broken. For a finite chain, there is a finite rate of tunneling between the two states which is exponentially small in the system size (due to a large barrier); the tunneling leads to a breaking of the exact degeneracy which exists for an infinite system and produces an exponentially small energy gap ($\sim \exp(-cL^d)$) between the two lowest energy states. The long-range order persists up to h_c . For $h > h_c$, the field term h wins over the cooperative interaction J_x , leading to the vanishing of the order parameter, and the system is in a PM phase. The TIM Hamiltonian can be further generalized incorporating a longitudinal magnetic field h_L such that

$$H = - \sum_{\langle \mathbf{ij} \rangle} J_{\mathbf{ij}} \sigma_{\mathbf{i}}^x \sigma_{\mathbf{j}}^x - h \sum_{\mathbf{i}} \sigma_{\mathbf{i}}^z - h_L \sum_{\mathbf{i}} \sigma_{\mathbf{i}}^x. \quad (8)$$

In Table I, we present definitions of all the major critical exponents taking the example of TIM with magnetization m_x as the order parameter \mathcal{O} , h_L as the conjugate field or the longitudinal field, and h (analogous to g in (1)) as the non-commuting transverse field which leads to quantum fluctuations resulting in a QPT.

We mention here some of the very early studies of the phase transitions in TIMs. This system was studied by de Gennes [24], to theoretically model the order-disorder transition in some double well ferroelectric systems such

² Typically, variational states of the matrix product form become more accurate as D is increased.

TABLE I: Definition of critical exponents associated with a quantum critical point occurring in magnetic system (see text) [16].

Quantity	Exponent	Definition	Conditions
Correlation length ξ	ν	$\xi \propto h - h_c ^{-\nu}$	$h \rightarrow h_c$ and $h_L = 0$
Order parameter m_x	β	$m_x \propto (h_c - h)^\beta$	$h \rightarrow h_c$ from below and $h_L = 0$
Specific heat C	α	$C \propto h - h_c ^{-\alpha}$	$h \rightarrow h_c$ and $h_L = 0$
Susceptibility χ	γ	$\chi \propto h - h_c ^{-\gamma}$	$h \rightarrow h_c$ and $h_L = 0$
Critical isotherm	δ	$h_L \propto m_x ^\delta \text{sign } m_x$	$h_L \rightarrow 0$ and $h = h_c$
Correlation function G	η	$G(r) \propto r ^{-d+2-\eta}$	$h = h_c$ and $h_L = 0$
Correlation time ξ_τ	z	$\xi_\tau \propto \xi^z$	$h \rightarrow h_c$ and $h_L = 0$

Category	Some specific examples	References
Order disorder ferroelectrics	KH ₂ PO ₄ KD ₂ PO ₄	[46] [47–49]
Jahn-Teller systems	DyVO ₄ TbVO ₄	[50] [51]
Mixed hydrogen bonded ferroelectrics (proton glasses)	Rd _{1-x} (NH ₄) _x H ₂ PO ₄	[52]
Dipolar magnets (quantum spin-glass)	LiHo _x Y _{1-x} F ₄	[53, 54]
Quasi-one-dimensional Ising systems	CoNb ₂ O ₆	[25]

TABLE II: Systems described by to Ising model in a transverse field; for a more exhaustive list we refer to [34]

as potassium dihydrogen phosphate (KDP or KH₂PO₄) crystals [32]; we shall provide a detailed discussion on this in Sec. VII (B). The connection to KDP ferroelectrics led to studies of the mean field phase diagram [33, 34], series studies [35] of the model, and the exact solution in one dimension [23, 31]; perturbative calculations of transverse susceptibilities in one dimension and on the Bethe lattice were also carried out [36]. The major experimental systems which are modeled in terms of TIMs are summarized in Table II. In addition, an experimental study of quantum simulations of a transverse Ising Hamiltonian of three spins with frustrating interactions between them has been reported recently; this is realized in a system of three trapped atomic ions whose interactions can be precisely controlled using optical forces [37].

For the sake of completeness, we mention here some mean field studies of the model in higher dimensions (or for higher spin values). The TIM in a general dimension was studied by Brout *et al.* [33], within mean field theory by reducing it to an effective single-site problem; this method has been generalized to study the elementary (spin-wave) excitations around the mean field state for pure [33] as well as a dilute TIM [38] (for details see [13, 39]). Quantum spin models can also be solved in the large spin ($S \rightarrow \infty$) limit when one incorporates quantum fluctuations over the classical ground state to first order in $1/S$ by applying the Holstein-Primakoff transformation [40–42] (see Appendix A).

The one-dimensional version of the model (7) with nearest-neighbor FM interactions can be written as

$$H = -J_x \sum_{i=1}^{N-1} \sigma_i^x \sigma_{i+1}^x - h \sum_{i=1}^N \sigma_i^z. \quad (9)$$

A duality transformation between low field and high field, which is a quantum generalization of the duality relation between the low and high temperature phases of the two-dimensional classical Ising model [43], enables one to locate the QCP exactly [44, 45]. Defining Pauli spin operators on a dual lattice (using for example, $\mu_i^x = \sigma_{i+1}^z \sigma_i^z$ and $\mu_i^z = \prod_{j < i} \sigma_j^x$) and exploiting the self-duality of the QCP, one finds $h_c = J_x$ (see Kogut, 1979, for a review) which turns to be the exact value (see Sec. II (A)). In subsequent sections, we will often set $J_x = 1$ so that $h_c = 1$. In Sec. II (A), we shall present the exact diagonalization of (9) using the Jordan-Wigner transformation.

The TIM can be generalized to the XY Hamiltonian in a transverse field incorporating additional interactions

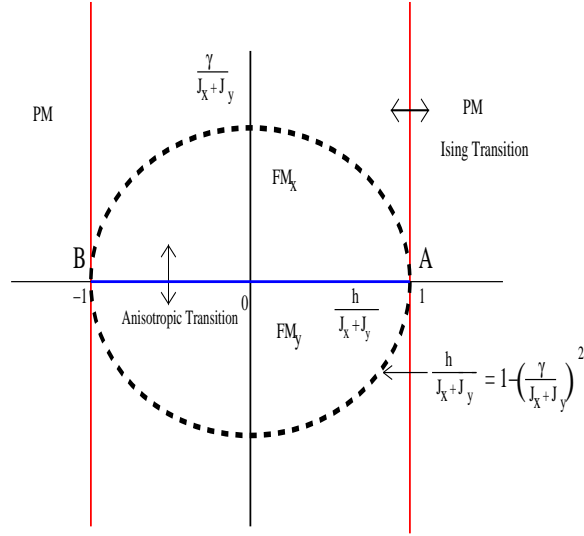


FIG. 2: (Color online) The phase diagram of a spin-1/2 transverse XY chain. The vertical red lines denote the Ising transitions between the FM phase and the PM phase. The horizontal bold line ($\gamma = J_x - J_y = 0, -(J_x + J_y) < h < J_x + J_y$) stands for the anisotropic phase transition between the ferromagnetic phases FM_x and FM_y with magnetic ordering along \hat{x} and \hat{y} directions, respectively. The multicritical points where the Ising and anisotropic transitions line meet ($\gamma = 0, h = \pm(J_x + J_y)$) are denoted by A and B in the figure. The dotted line given by the equation $h/(J_x + J_y) = 1 - \gamma^2/(J_x + J_y)^2$, denotes the boundary between the commensurate and incommensurate ferromagnetic phases. For the Ising and the anisotropic transitions critical exponents are $\nu = z = 1$ while for the transition at the MCPs, $\nu_{mc} = 1/2$ and $z_{mc} = 2$. (After Bunder and McKenzie, 1999).

defined by the following Hamiltonian in one dimension [23, 55–58],

$$H = - \sum_i [J_x \sigma_i^x \sigma_{i+1}^x + J_y \sigma_i^y \sigma_{i+1}^y + h \sigma_i^z]. \quad (10)$$

Without loss of generality, we can assume that $J_x \geq |J_y| \geq 0$ and therefore that $J_x + J_y > 0$. The higher dimensional version of the model appears in the pseudo-spin representation of the BCS Hamiltonian, and its mean field treatment yields exactly the BCS gap equation [59]. The spin chain defined in (10) is exactly solvable as will be shown in Sec. II. The phase diagram of the one-dimensional model is shown in Fig. 2 with the anisotropy parameter $\gamma = J_x - J_y$. The system undergoes transitions from PM to FM phase at $h = \pm(J_x + J_y)$; these transitions belong to the universality class of the transverse Ising chain and are hence called Ising transitions. The ferromagnetic order in the XY plane is in the \hat{x} direction (\hat{y} direction) if $J_x > J_y$ ($J_x < J_y$) and $|h| < J_x + J_y$; there is a QPT between these two phases at $J_x = J_y$ referred to as anisotropic transition. On this anisotropic transition line ($J_x = J_y$) between two FM phases (referred to as FM_x and FM_y phases) the energy gap vanishes for a non-commensurate wave vector k_0 ; $k_0 = 0$ or π when $h \rightarrow -(J_x + J_y)$ or $h \rightarrow J_x + J_y$. There are two multicritical points (MCP) (at $h = \pm(J_x + J_y)$ and $\gamma = 0$) denoted by A and B in the phase diagram (2) where the Ising and anisotropic transition lines meet [60]. In subsequent sections, we will often set $J_x + J_y = J = 1$. Due to its exact solvability and rich phase diagram with critical and multicritical points as well as gapless critical lines, the model in (10) has been used throughout Secs. 5 and 6.

(C). Some exactly solvable models related to transverse Ising and XY models

In this section, we shall briefly introduce a few spin models which are closely related to the transverse Ising and XY spin chains. These models are exactly solvable and hence have turned out to be extremely useful in recent studies of quantum information and dynamics as discussed later.

Let us first introduce an extended transverse Ising spin chain whose ground state is given exactly by a finite rank matrix product state (see the discussion at the end of Sec. I(A)). Referring to Eq. (6), with $D = d = 2$, and defining $A_1 = (I - \sigma^z)/2 + \sigma^-$ and $A_2 = (I + \sigma^z)/2 + g\sigma^+$, where I is 2×2 identity matrix and $\sigma^\pm = \sigma^x \pm i\sigma^y$, we obtain a

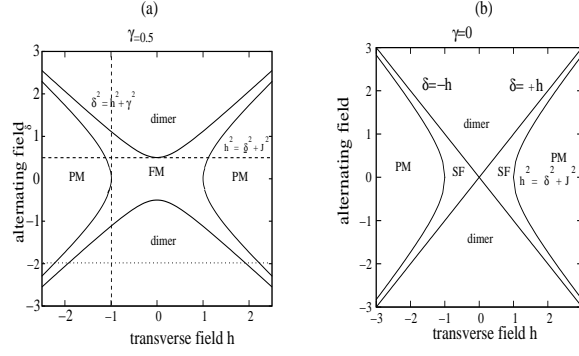


FIG. 3: Phase diagram of the XY chain in an alternating transverse field for $\gamma = 0.5$ (Fig. (a)) and $\gamma = 0$ (Fig. (b)). In (a), the PM \leftrightarrow FM and FM \leftrightarrow dimer phase transitions with critical exponents $\nu = z = 1$ are shown by the phase boundaries $h^2 = \delta^2 + J^2$ and $\delta^2 = h^2 + \gamma^2$, respectively. There is also a QPT with $\nu = 2$ and $z = 1$ when two special points ($h = \pm 1, \delta = 0$) and ($h = 0, \delta = \pm\gamma$) points are approached along the dashed line. In (b), the gapless $U(1)$ -symmetric superfluid (SF) \leftrightarrow PM phase boundary is given by $h^2 = \delta^2 + J^2$ with ordering wave vector $\cos k_0 = \sqrt{h^2 - \delta^2}/J$ for $\delta^2 < h^2 < \delta^2 + J^2$; this transition belongs to the Lifshitz universality class with critical exponents $\nu = 1/2, z = 2$. A different critical behavior occurs at $h = \pm 1, \delta \rightarrow 0$ where $\nu = 1, z = 2$. Ising exponents are recovered while approaching the point $h = 0, \delta = 0$ along every path other than $\delta = 0, h \rightarrow 0$ when the spin chain is on the anisotropic critical line of Fig. 2. (After Deng *et al.*, 2008).

Z_2 symmetric Hamiltonian [26]

$$H = \sum_i [2(g^2 - 1)\sigma_i^z \sigma_{i+1}^z - (1 + g)^2 \sigma_i^x + (g - 1)^2 \sigma_i^z \sigma_{i+1}^x \sigma_{i+2}^z] \quad (11)$$

with periodic boundary conditions; see Appendix B for the derivation. This Hamiltonian undergoes a QPT at $g_c = 0$ with a diverging correlation length with critical exponents $\nu = 1$ and $z = 2$; the state at the QCP is a Greenberger-Horner-Zeillinger state [61]. The QCP at $g_c = 0$ is unconventional in the sense that the ground state energy is analytic at this point.

We can define a duality transformation to a spin-1/2 chain whose site labels run over $i + 1/2$, with the mappings

$$\tau_{i+1/2}^z = \sigma_i^z \sigma_{i+1}^z, \quad \tau_{i-1/2}^x \tau_{i+1/2}^x = \sigma_i^x, \quad \tau_{i-1/2}^y \tau_{i+1/2}^y = -\sigma_{i-1}^z \sigma_i^x \sigma_{i+1}^z, \quad (12)$$

where $\tau_{i+1/2}^a$ denote Pauli matrices for the dual spin-1/2 chain. Under this transformation, Hamiltonian in Eq. (11) gets mapped to the transverse XY model in Eq. (10), with $h/(J_x + J_y) = (1 - g^2)/(1 + g^2)$ and $\gamma/(J_x + J_y) = 2g/(1 + g^2)$. We then see that the QPT at $g = 0$ corresponds to the multicritical point lying at $h/(J_x + J_y) = 1$ and $\gamma/(J_x + J_y) = 0$ in Fig. 2 and g parametrizes a path along the dotted line. The notion of a matrix product state and the Hamiltonian in (11) have been useful in recent quantum information theoretic studies [28, 62–64] (see Secs. V (A) (b) and V (C)).

We note that a transverse Ising spin chain incorporating three-spin interactions, given by the Hamiltonian

$$H = - \sum_i \sigma_i^z [h + J_3 \sigma_{i-1}^x \sigma_{i+1}^x] + J_x \sum_i \sigma_i^x \sigma_{i+1}^x \quad (13)$$

which is dual to the transverse XY spin chain in Eq. (10), has already been studied [65].³ The model is exactly solvable and hence has been useful in studying quantum dynamics across its QCPs [67].

Let us also introduce an anisotropic spin-1/2 XY spin chain Hamiltonian in which the strength of the transverse field alternates between $h + \delta$ and $h - \delta$ at odd and even sites, respectively, [68–70] given by

$$H = - \sum_j \left[\frac{(J_x + J_y)}{4} (\sigma_j^x \sigma_{j+1}^x + \sigma_j^y \sigma_{j+1}^y) + \frac{(J_x - J_y)}{4} (\sigma_j^x \sigma_{j+1}^x - \sigma_j^y \sigma_{j+1}^y) + \frac{(h - (-1)^j \delta)}{2} \sigma_j^z \right]. \quad (14)$$

³ The interaction J_3 which is generated in the first step of a real space renormalization group (RSRG) study of transverse Ising models [66] has been found to be irrelevant in determining the critical behavior of the system.

The rich phase diagram of the model in (14), obtained by exact solution using the Jordan-Wigner transformation, is shown in Fig. 3 (with $\gamma = J_x - J_y$ and $J_x + J_y = J$) for $\gamma = 0$ and $\gamma = 0.5$. We list below the associated QCPs and corresponding critical exponents.

For $\gamma > 0$: The PM \leftrightarrow FM and FM \leftrightarrow dimer phase transitions are given by the phase boundaries $h^2 = \delta^2 + J^2$ and $\delta^2 = h^2 + \gamma^2$, respectively. (The dimer phase is one in which $\langle \sigma_j^z \rangle$ has a staggered order).

(i) In general, for $\gamma > 0$, the QCPs belong to the $d = 2$ Ising universality class with critical exponents $\nu = z = 1$.

(ii) A different critical behavior is observed for $h \rightarrow 0, \delta = \pm\gamma$ and $h = \pm 1, \delta \rightarrow 0$ with $\nu = 2, z = 1$.

For $\gamma = 0$:

(i) Superfluid (SF) \leftrightarrow dimer and SF \leftrightarrow PM phase transitions. The ordering wave vector in the gapless SF phase is k_0 given by $\cos k_0 = \sqrt{h^2 - \delta^2}/J$ for $\delta^2 < h^2 < \delta^2 + J^2$.

(ii) In general, the QCPs on the boundary line belongs to the Lifshitz universality class with critical exponents $\nu = 1/2, z = 2$.

(iii) Once again, a different critical behavior occurs at $h = \pm 1, \delta \rightarrow 0$ where $\nu = 1, z = 2$.

(iv) The Ising exponents are recovered while approaching the point $h = 0, \delta = 0$ along every path other than $\delta = 0, h \rightarrow 0$ where there is no critical behavior.

Because of the exact solvability and the possibility of exploring different QCPs, this model has turned out to be extremely useful [70, 71] (see Sec. VI(G)).

Finally, let us briefly mention an infinite range interacting XY Hamiltonian known as the Lipkin-Meshkov-Glick (LMG) model [72]; this is an exactly solvable model with infinite coordination number [73, 74]. Although this model is not discussed in detail in this review, it has been studied extensively in recent years, particularly from the point of view of quantum information [75–81] and dynamics [82]. The model consists of N spin-1/2 objects and given by

$$H = -\frac{J}{N} \sum_{i < j} (\sigma_i^x \sigma_j^x + \gamma \sigma_i^y \sigma_{i+1}^y) - h \sum_i \sigma_i^z, \quad (15)$$

where N is the number of spins and $\gamma \leq 1$ is the anisotropy parameter. Introducing $\vec{S}_a = \sum_i \vec{\sigma}_i^a, a = x, y, z$, the Hamiltonian in (15) can be written up to a constant as $-(1/2N)(S_x^2 + \gamma S_y^2) - h S_z$. The Hamiltonian satisfies the commutation relations $[H, \vec{S}^2] = 0$ and also $[H, \prod_i \sigma_i^z] = 0$ which implies that the parity of the number of spins pointing in the direction of the field is conserved. Moreover, $[H, S_z] = 0$ for $\gamma = 1$.

In the $N \rightarrow \infty$ limit, the LMG model shows a QPT as $2h/J \rightarrow 1^-$ characterized by mean field exponents for all values of γ [83]; the magnetization in the \hat{x} direction (or in the xy -plane for the isotropic case $\gamma = 0$) is given by $m = \sqrt{1 - 4h^2/J^2}$ for $h \leq J/2$ and vanishes for $h > J/2$. For $h > J/2$, the ground state is non-degenerate for any γ ; for $h < J/2$, it is doubly degenerate for any $\gamma \neq 0$, indicating the breakdown of Ising symmetry. The energy gap vanishes at the QCP as $\sqrt{(h - J/2)(h - \gamma)}$ for $h \geq J/2$. For finite N (which also means finite S for this model), the model can be diagonalized using Holstein-Primakoff transformation [40–42] both for $\gamma = 0$ [84] and $\gamma \neq 0$ [76]. The finite temperature phase diagram in the $N \rightarrow \infty$ limit can be found by using the self-consistent method for the equivalent single particle Hamiltonian [84]; see Sec. 6.1.

(D). Quantum-classical correspondence and scaling

The mapping from temperature to imaginary time ($\bar{\tau}$), given by $\bar{\tau} = \beta$ where $\beta = 1/(k_B T)$, enables us to make use of an imaginary time path integral formalism of a quantum Hamiltonian [85] which states that the transition amplitude between two states can be calculated by summing over the amplitudes of all possible paths going between them. To formulate the corresponding path integral, one divides the temperature interval $L_\tau = 1/(k_B T)$, where k_B is the Boltzmann constant, into M small intervals $\delta\bar{\tau}$ such that $M\delta\bar{\tau} = \beta$ in the limit of $\delta\bar{\tau} \rightarrow 0$ and $M \rightarrow \infty$ with β remaining finite. The path integral formalism of the partition function of a d -dimensional quantum system effectively gives us an equivalent action of a $(d + 1)$ -dimensional classical system, with the additional time dimension being of finite size ($= 1/(k_B T)$). In the limit $T \rightarrow 0$, the size of the temporal direction diverges and one gets a truly $(d + 1)$ -dimensional classical action. For $T \neq 0$, the time direction L_τ is finite and does not contribute close to the critical point when $\xi \rightarrow \infty$ and one arrives at a d -dimensional classical action [15]. A QPT at $T = 0$ is therefore associated with a diverging correlation length in the temporal direction (or the relaxation time) which scales as $\xi_\tau \sim 1/\Delta$, where Δ is the energy gap between the ground and the first excited state [45]. Although as mentioned above, such a correspondence exists for all models discussed before, we shall illustrate this classical quantum correspondence using the example of the transverse Ising models.

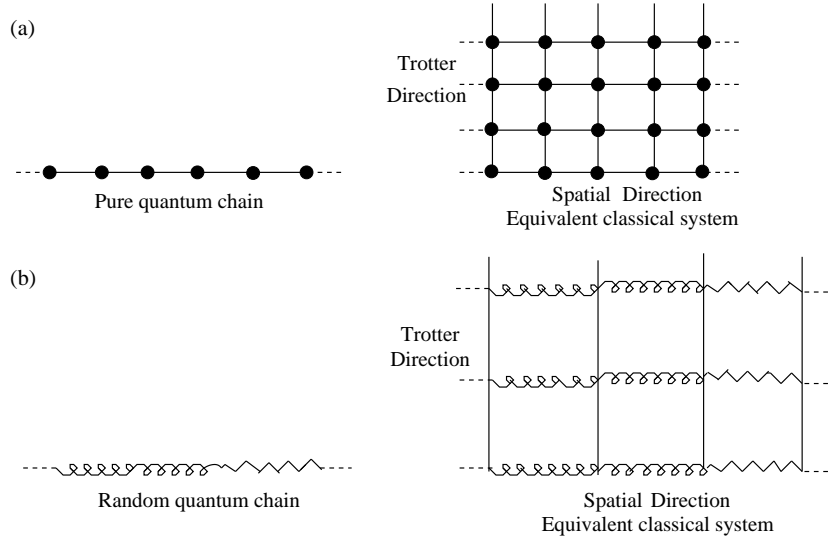


FIG. 4: The equivalent classical model: (a) for a pure transverse Ising chain, and (b) for a chain with random interactions but uniform transverse field. Here continuous lines indicate ferromagnetic interactions and zig-zag lines denote random interactions. Figure (b) shows that the randomness is infinitely correlated along the Trotter direction (i.e., the same pattern is replicated) of the equivalent classical random model. This represents a version of the McCoy-Wu model [94].

For a TIM in d dimensions, the classical-quantum correspondence was established [86, 87] using the imaginary time path integral in the Matsubara representation with Matsubara frequencies (MFs) $\omega_m = 2\pi m k_B T$, $m = 0, 1, 2, \dots$ [88]. At $T = 0$, these MFs become continuous and one arrives at the Landau-Ginzburg-Wilson (LGW) action of a classical model with an additional temporal direction. This correspondence establishes that the upper critical dimension (d_u^c) for the QPT of TIM is $(3 + 1)$; one can calculate the associated critical exponents using the ϵ -expansion technique [9] around the upper critical dimension [14]. For $T \neq 0$, the MFs become discrete and only the mass term corresponding to $m = 0$ vanishes at the critical point, whereas the mass terms for $m \neq 0$ become irrelevant under renormalization. This effectively results in a LGW action of a classical Ising model in d dimensions.

We can use the Suzuki-Trotter (ST) [89, 90] formalism to show that the QPT of a d -dimensional TIM is equivalent to a $(d + 1)$ -dimensional classical Ising model [91]. The ST formalism relies on the Trotter formula $\exp(\hat{A}_1 + \hat{A}_2) = \lim_{M \rightarrow \infty} [\exp(\hat{A}_1/M) \exp(\hat{A}_2/M)]^M$, where \hat{A}_1 and \hat{A}_2 are quantum mechanical bounded operators which may not commute with each other. Starting from a transverse Ising chain (9) of length L with interaction term $K = \beta J_x$, we use the Trotter formula; inserting M complete set of eigenstates of the operator σ_x , we arrive at the partition function of a classical Ising model on a $L \times M$ square lattice, where M denotes the size of the Trotter direction, with anisotropic interactions K/M and $K_M = (1/2) \ln \coth(\beta h/M)$ in the spatial and Trotter directions, respectively (for details, see Ref. [92]). We note that in the limit $M \rightarrow \infty$, K/M vanishes while K_M diverges logarithmically unless $T = 0$. We take $M \rightarrow \infty$ and $\beta \rightarrow \infty$ simultaneously so that β/M is finite; then the model becomes equivalent to a two-dimensional classical Ising model. The above calculation can be generalized to higher dimensions. If the interactions of the spins are random, the ST mapping leads to a higher dimensional classical Ising Hamiltonian with randomness being striped or infinitely correlated along the Trotter direction (see Fig. 4). The ST formalism and imaginary time path integral formalism are at the root of quantum Monte Carlo methods; for example, Rieger and Kawashima used continuous imaginary time cluster Monte Carlo algorithms for a transverse Ising model in $d = 2$ [93].

In a similar spirit, one can derive an equivalent quantum Hamiltonian starting from the partition function of a classical Hamiltonian in an extreme anisotropic limit; this is known as the τ -continuum formulation [44, 45]. Let \hat{T} denote the transfer matrix of a d -dimensional classical Hamiltonian H_{cl} . The equivalent quantum Hamiltonian \hat{H} is defined through the relation $\hat{T} = 1 - \delta\tau \hat{H} + O(\delta\tau^2)$ where $\delta\tau$ ($\rightarrow 0$) is the infinitesimal lattice spacing along one of the spatial directions. For example, one considers the row-to-row transfer matrix of the two-dimensional anisotropic classical Ising model at temperature T [95]. In the extreme anisotropic limit, in which the interaction between spins of neighboring rows vanishes as $\delta\tau$ and between spins of the same row as $g\delta\tau$ so that the ratio of these two interactions ($= g$) remains finite, one gets the equivalent one-dimensional quantum Hamiltonian (defined along the row) given in (9). The temperature T in the classical model maps to the transverse field h in the quantum Hamiltonian.

The scaling relations associated with QCP are discussed in detail in Ref. [14], and in Ref. [15]; we present here a brief recapitulation. The inherent quantum dynamics and the diverging correlation length as well as diverging relaxation

time $\xi_\tau \sim \xi^z$ modify the scaling relation when compared to a classical phase transition. For example, close to the QCP, the energy gap between the ground state and the first excited state scales as $\lambda^{z\nu}$, where $\lambda = g - g_c$ is the measure of the deviation from the critical point. Exactly at $\lambda = 0$, the energy gap vanishes at some momentum \vec{k}_c as $|\vec{k} - \vec{k}_c|^z$; if $z = 1$, the QCP is Lorentz invariant. The ground state energy density therefore scales as $E_g \sim \xi^{-(d+z)} f(k\xi, \omega\xi^z, \lambda\xi^{1/\nu})$, where we have used the fact that the correlation volume is ξ^{d+z} . Using the scaling relation $\xi \sim \lambda^{-\nu}$ and the definition of the exponent α (see Sec. I(A)) which yields $E_g \sim \lambda^{2-\alpha}$, we get the modified hyperscaling relation for a QPT given by

$$2 - \alpha = \nu(d + z), \quad (16)$$

which is valid below the upper critical dimension. When compared with the hyperscaling relation $2 - \alpha_{cl} = \nu_{cl}d$ of a classical system [2] where α_{cl} and ν_{cl} are critical exponents of the equivalent CPT, the modified hyperscaling relation once again implies the following: the QPT is equivalent to the finite temperature transition of an equivalent classical model with one additional dimension, i.e., the Trotter dimension, along which the correlation length $\xi_\tau \sim \xi^z$, and the exponent z manifests in (16); if $z = 1$, one gets a $d_{quantum} \rightarrow (d + 1)_{classical}$ correspondence. Therefore the upper critical dimension of the QPT of the TIM ($\nu = z = 1$) is $d_u^c = 3$ in comparison to $d_u^c = 4$ for the thermal transition of the classical Ising model [3].

At a finite temperature, the size of the temporal direction is finite and given by $L_\tau = \beta$. Using the finite size scaling [96], one gets the relation

$$g_c(T) = g_c(T = 0) + BL_\tau^{-1/\nu z} = g_c(T = 0) + BT^{1/\nu z}, \quad (17)$$

where B is a constant, implying that the quantum critical exponents determine the phase boundary at a finite temperature close to the QCP (see Fig. 1). Referring to Fig. 1 (a), the crossover from the quantum paramagnetic region to the quantum critical region occurs when $\hbar\omega \sim k_B T$, where ω is the characteristic frequency scale. In the vicinity of the phase boundary, the phase transition is classical in nature due to the critical slowing down as mentioned already. Now consider a TIM in $d = 1$ which exhibits long-range order only at $T = 0$. In this case, the ordered region is replaced by a “renormalized” classical state (see Fig. 1 (a)) [14]. In this region, the fluctuations are classical because ξ diverges as $T \rightarrow 0$ for $g < g_c$. For the one-dimensional classical Ising model, $\xi \sim \exp(\beta)$ [3] grows much faster than the de Broglie wavelength and hence the fluctuations are classical.

(E). Quantum spin chains coupled to a bath

The quantum-classical correspondence discussed in the previous section has been critically looked at and also challenged in recent years in the context of the quantum phase transition in a two-level system (or a single spin-1/2) coupled to an infinite number of bosonic degrees of freedom which are characterized by a spectral function $J(\omega)$; this is known as the spin-boson model [97–99]. The Hamiltonian is

$$H = \Delta \frac{\sigma^x}{2} + \frac{\sigma^z}{2} \sum_i \lambda_i (a_i + a_i^\dagger) + \sum_i \omega_i a_i^\dagger a_i, \quad (18)$$

where σ^a , $a = x, z$, are Pauli matrices, a_i , a_i^\dagger are bosonic annihilation and creation operators, Δ represents the tunneling matrix element, and ω_i denote the oscillator frequencies of the bosonic degrees of freedom. The coupling between the spin and the oscillator bath via λ_i is determined by the spectral function of the bath,

$$J(\omega) = \pi \sum_i \lambda_i^2 \delta(\omega - \omega_i). \quad (19)$$

This is parametrized as $2\pi\alpha\omega_c^{1-s}\omega^s$ for $0 < \omega < \omega_c$, where ω_c is the cut-off frequency and α represents the coupling strength; we take $s > -1$. When the exponent s lies in the range $0 < s < 1$, the model is said to be in the sub-ohmic range. The case $s = 1$ refers to the ohmic situation; then $J(\omega) \sim \omega$ and is independent of ω_c . The case $s > 1$ is called super-ohmic.

The quantum critical behavior of the model in (18) depends crucially on the value of the exponent s . For $s < 1$, the spin-boson model shows a QPT from a delocalized phase (when tunneling dominates) to a localized phase at a critical value of $\alpha = \alpha_c(s, \Delta, \omega_c)$. In view of the quantum-classical mapping discussed earlier, this QPT is expected to be in the same universality class as that of the finite-temperature transition of a classical Ising chain with long-range interactions [100, 101]. The case $s = 1$ corresponds to a classical Ising chain with inverse-square interactions [102, 103]

which exhibits a Berezinskii-Kosterlitz-Thouless (BKT) transition [104] from a power-law correlated phase below T_c to a disordered phase with exponentially decaying correlations above T_c .

Studies using numerical RG techniques [105] have established the existence of the aforementioned QPT for both the ohmic ($s = 1$) and sub-ohmic ($s < 1$) situations [105]. Moreover, the possibility of a breakdown of the quantum-classical mapping for $0 < s < 1/2$ has been pointed out in [106]. In this range of s , the equivalent classical Ising chain shows a mean field behavior [100], whereas ϵ -expansion studies indicate that the QPT is governed by the interacting fixed point which implies a non-mean field critical behavior [106]. However, the critical exponents obtained by an accurate quantum Monte Carlo method with a continuous imaginary time cluster algorithm including finite temperature corrections indicated the correctness of the quantum-classical mapping for all values of s [107] and predicted mean field behavior for the QPT for this range of s (see also [108])⁴. A very recent study [109], on the other hand, again points to the breakdown of the quantum-classical correspondence⁵ for the QPT with $s < 1/2$ implying that the debate on this issue is far from being settled. It should be mentioned here that dissipative spin dynamics in this model has also been studied using the Majorana representation and numerical RG techniques [110, 111].

Let us note that the quantum Ising spin chain coupled to a heat bath has been studied in recent years. The Hamiltonian is given by [112]

$$H = -J \sum_i \sigma_i^x \sigma_{i+1}^x - h \sum_i \sigma_i^z + \sum_{i,k} \lambda_k (a_{ik} + a_{ik}^\dagger) \sigma_i^x + \sum_{ik} \omega_{ik} a_{ik}^\dagger a_{ik}, \quad (20)$$

where the spin at each site i is linearly coupled via λ_k to an independent set of bosons denoted by the operators a_{ik} and a_{ik}^\dagger with frequencies ω_{ik} . Using the Suzuki-Trotter formalism, the above chain can be mapped to the two-dimensional classical Ising Hamiltonian with a long-range interaction in the temporal direction. The phase boundary between the FM and PM phases in the presence of dissipation (denoted by α as above) has been obtained using extensive Monte Carlo studies for the ohmic case $s = 1$ [112]. These studies also established a new quantum critical behavior in the presence of dissipation with critical exponents independent of the value of α .

The QCP mentioned above has been experimentally studied in [113] for the system LiHoF₄ where the electron spins are effectively coupled to a spin bath consisting of the nuclear spins (see also Sec. VII (D)). This coupling modifies the QCP of the transverse Ising model describing the electron spins, so that the energy gap, defined by following the most prominent feature of the magnetic exciton dispersion, does not go to zero but reaches a minimum (and the corresponding coherence length reaches a maximum) at some value of the transverse field. This work demonstrates an intrinsic limitation to the observation of a QCP for an electronic system which is coupled to a nuclear spin bath even at very low temperatures where the coupling to a phonon bath becomes unimportant.

(F). Quantum rotor models

Finally, we provide a brief note on the quantum lattice rotor models because of their close connection to the TIMs. These models were introduced [114] as a version of the non-linear σ -models to study the low-temperature properties of two-dimensional quantum Heisenberg antiferromagnetic systems. The Hamiltonian of a quantum rotor (QR) model on a d -dimensional regular lattice is given by

$$H_R = \frac{g}{2} \sum_{\mathbf{i}} \hat{L}_{\mathbf{i}}^2 - J \sum_{\langle \mathbf{i}\mathbf{j} \rangle} \hat{x}_{\mathbf{i}} \cdot \hat{x}_{\mathbf{j}}. \quad (21)$$

The n -component unit-length vectors $\hat{x}_{\mathbf{i}}$'s denote the orientation of the rotors on the surface of a sphere in the n -dimensional rotor space, where $n \geq 2$. For simplicity, we have assumed only nearest-neighbor ferromagnetic interactions between the rotors. The operators $\hat{L}_{\mathbf{i}\alpha\beta}$ ($\alpha, \beta = 1, 2, \dots, n$) are the $n(n-1)/2$ components of the angular momentum generator operator in the rotor space which can be put in the differential form as

$$L_{\mathbf{i}\alpha\beta} = -i\hbar \left(x_{\mathbf{i}\alpha} \frac{\partial}{\partial x_{\mathbf{i}\beta}} - x_{\mathbf{i}\beta} \frac{\partial}{\partial x_{\mathbf{i}\alpha}} \right).$$

The non-commutativity between the operators $\hat{x}_{\mathbf{i}}$ and $\hat{L}_{\mathbf{i}}$ introduces quantum fluctuations in the model which can be tuned by changing the kinetic term g . In the limit $g = 0$, the rotors at different sites choose a particular orientation

⁴ The failure of the numerical RG technique in the localized phase for $s < 1/2$ is argued to be due to the presence of a dangerously irrelevant operator [107] so that the exponents are determined by the Gaussian fixed point, as happens in Landau theory for $d > d_u^c$ [3].

⁵ This breakdown is attributed to the presence of a Berry-phase term in a continuum path-integral representation of the model.

(ferromagnetic phase) thereby breaking the underlying $O(n)$ symmetry, while for $g \gg J$ the symmetry is restored. We therefore expect a QPT from a symmetric PM phase to a symmetry-broken FM phase at a critical value $g = g_c$ at $T = 0$.

For example, consider the case for $n = 2$ and $d = 2$, when the Hamiltonian in (21) describes an array of Josephson junctions on a d -dimensional lattice which is in fact the quantum counterpart of the d -dimensional classical XY model [15, 115]. The Hamiltonian in Eq. (21) can be written in the form

$$H = \frac{2e^2}{C} \sum_i \frac{\partial^2}{\partial \theta_i^2} - E_J \sum_{\langle ij \rangle} \cos(\hat{\theta}_i - \hat{\theta}_j), \quad (22)$$

where we have set $\hat{x}_i = \cos \hat{\theta}_i$, $g/2 = 2e^2/C$, $J_{ij} = J = E_J$, and $\hat{L}_i^z = -(i\hbar)\partial/\partial\theta_i$. Here, the operator $\hat{\theta}_j$ represents the phase of the superconducting order parameter on the j -th grain, while the term $-i\hbar(2e/C)\partial/\partial\theta_i$ is canonically conjugate to the phase and denotes the voltage on the j -th junction. The Cooper pair charge is $2e$ and C is the capacitance of each grain. The interaction term E_J represents the Josephson coupling energy between the superconducting grains. In the Hamiltonian in (22), the kinetic term tends to destroy any long-range order in the phases θ_i ; hence the model exhibits a QPT from a superconducting to an insulating phase when the ratio E_C/E_J exceeds a critical value, where $E_C (= 2e^2/C)$ is called the charging energy. One can construct an imaginary time path integral [116] which is in fact identical to that of the TIM with the order parameter field being two-component. As argued in Sec. I (D), the finite temperature transition (when the non-commuting kinetic term is irrelevant) belongs to the universality class of the d -dimensional classical XY model given by the XY term $E_J \sum_{\langle ij \rangle} \cos(\hat{\theta}_i - \hat{\theta}_j)$ in (22). On the other hand, the QPT corresponds to a XY model with one added dimension coming from the kinetic term. The finite temperature transition of a two-dimensional array (or the equivalent zero-temperature transition of a one-dimensional array) is therefore a BKT transition [104].⁶

The discussion above shows that the QR Hamiltonian is in fact a n -component generalization of the transverse Ising Hamiltonian from the viewpoint of universality of QPTs. Noting that the components of the operators \hat{x}_i commute with each other (unlike the Pauli spin operators), one can show that the zero temperature phase transition of a d -dimensional QR model belongs to the universality class of the finite temperature transition of a $(d+1)$ -dimensional classical n -vector model as shown above for $n = 2$. On the other hand, the finite temperature transition for the QR corresponds to the finite temperature transition of a d -dimensional classical n -vector model. In the limit $n \rightarrow \infty$, the Hamiltonian reduces to a quantum version of a spherical model [117] with the quantum critical behavior belonging to the universality class of the finite temperature transition of a classical spherical model [118] with one dimension added. The QR model has been extensively studied in the presence of random interactions [119–121] and random longitudinal fields [122, 123] in order to investigate the zero temperature and finite temperature properties of quantum spin glass models of rotors. We refer to Ref. [14], for exhaustive discussions on quantum rotor models; however, we shall briefly refer to these models in the context of GM singularities (Sec. III (B)) and the quantum Lifshitz point (Sec. IV (A)).

II. EXACT SOLUTIONS IN ONE AND TWO DIMENSIONS

(A). Jordan-Wigner transformation

Let us consider the spin-1/2 XY model placed in a magnetic field pointing in the \hat{z} direction. The Hamiltonian is given by

$$H = - \sum_{n=1}^{N-1} [J_x \sigma_n^x \sigma_{n+1}^x + J_y \sigma_n^y \sigma_{n+1}^y] - \sum_{n=1}^N h \sigma_n^z, \quad (23)$$

with $J_x + J_y > 0$, where σ_n^a denote the Pauli matrices at site n , and we will assume periodic boundary conditions so that $\vec{\sigma}_{N+1} \equiv \vec{\sigma}_1$. Clearly, for $J_y = 0$, the Hamiltonian in (23) reduces to that of the transverse Ising chain. A discussion of QPTs in this model in the $S \rightarrow \infty$ limit is presented in Appendix A.

The above system can be mapped to a model of spinless fermions using the Jordan-Wigner (JW) transformation [22]. We map an \uparrow spin or a \downarrow spin at any site to the presence or absence of a spinless fermion at that site. This can

⁶ A similar scenario is shown in a 1d TIM with FM interactions falling as the inverse square of the distance between the spins [101].

be done by introducing a fermion annihilation operator c_n at each site, and writing the spin at that site as

$$\begin{aligned}\sigma_n^z &= 2c_n^\dagger c_n - 1 = 2\rho_n - 1, \\ \sigma_n^- &= \frac{1}{2}(\sigma_n^x - i\sigma_n^y) = c_n e^{i\pi \sum_{j=1}^{n-1} \rho_j},\end{aligned}\tag{24}$$

where $\rho_n = c_n^\dagger c_n = 0$ or 1 is the fermion occupation number at site n . The expression for σ_n^+ can be obtained by taking the Hermitian conjugate of σ_n^- . The string factor in the definition of σ_n^- is necessary to ensure the correct anticommutation relations between the fermionic operators, namely, $\{c_m, c_n^\dagger\} = \delta_{mn}$ and $\{c_m, c_n\} = 0$.

Following the JW transformation, (23) takes the form

$$\begin{aligned}H &= \sum_{n=1}^{N-1} \left[-(J_x + J_y) (c_n^\dagger c_{n+1} + c_{n+1}^\dagger c_n) + (J_x - J_y) (c_{n+1}^\dagger c_n^\dagger + c_n c_{n+1}) \right] \\ &\quad - (-1)^{N_f} [-(J_x + J_y) (c_N^\dagger c_1 + c_1^\dagger c_N) + (J_x - J_y) (c_1^\dagger c_N^\dagger + c_N c_1)] \\ &\quad - \sum_{n=1}^N h (2c_n^\dagger c_n - 1),\end{aligned}\tag{25}$$

where N_f denotes the total number of fermions: $N_f = \sum_{n=1}^N c_n^\dagger c_n$. (Note that N_f commutes with H , hence it is a good quantum number). We now Fourier transform to the operators $c_k = \sum_{n=1}^N c_n e^{-ikna}/\sqrt{N}$, where a is the lattice spacing and the momentum k lies in the range $[-\pi/a, \pi/a]$ and is quantized in units of $2\pi/(Na)$. [The factor of $-(-1)^{N_f}$ in Eq. (25) implies that $k = 2j\pi/(Na)$ if N_f is odd, while $k = (2j+1)\pi/(Na)$ if N_f is even; here j runs over a total of N integer values. The chain length $L = Na$; in subsequent sections we will usually set $a = 1$]. We then obtain

$$\begin{aligned}H &= \sum_{k>0} \begin{pmatrix} c_k^\dagger & c_{-k} \end{pmatrix} H_k \begin{pmatrix} c_k \\ c_{-k}^\dagger \end{pmatrix}, \\ H_k &= 2 \begin{pmatrix} -(J_x + J_y) \cos(ka) - h & i(J_x - J_y) \sin(ka) \\ -i(J_x - J_y) \sin(ka) & (J_x + J_y) \cos(ka) + h \end{pmatrix},\end{aligned}\tag{26}$$

where k now lies in the range $[0, \pi/a]$. Since this Hamiltonian is quadratic in the fermion operators, it can be diagonalized using a fermionic Bogoliubov transformation,

$$\begin{aligned}d_k^\dagger &= \sin \theta_k c_k + i \cos \theta_k c_{-k}^\dagger, \\ d_{-k}^\dagger &= \sin \theta_k c_{-k} - i \cos \theta_k c_k^\dagger,\end{aligned}\tag{27}$$

where θ_k is fixed by the condition

$$\tan(2\theta_k) = - \frac{(J_x - J_y) \sin(ka)}{(J_x + J_y) \cos(ka) + h}.\tag{28}$$

We then arrive at a Hamiltonian given by [22, 124]

$$H = \sum_{k>0} \omega_k (d_k^\dagger d_k + d_{-k}^\dagger d_{-k} - 1),\tag{29}$$

where $\omega_k = 2 [h^2 + J_x^2 + J_y^2 + 2h(J_x + J_y) \cos(ka) + 2J_x J_y \cos(2ka)]^{1/2}$. The ground state $|GS\rangle$ of the Hamiltonian in (29) satisfies $d_k |GS\rangle = d_{-k} |GS\rangle = 0$ for all $k > 0$. If we define the vacuum state $|\phi\rangle$ to be the state satisfying $c_k |\phi\rangle = c_{-k} |\phi\rangle$ for all $k > 0$, the ground state of (29) can be written as

$$\begin{aligned}|GS\rangle &= \bigotimes_{k>0} (\cos \theta_k + i \sin \theta_k c_k^\dagger c_{-k}^\dagger) |\phi\rangle \\ &\equiv \bigotimes_{k>0} (\cos \theta_k |0\rangle + i \sin \theta_k |k, -k\rangle).\end{aligned}\tag{30}$$

In the thermodynamic limit $N \rightarrow \infty$, the ground state energy is given by $E_0 = -N \int_0^{\pi/a} dk / (2\pi) \omega_k$.

As a function of k , ω_k has extrema at the points 0 , π/a and k_0 which is given by

$$\cos(k_0 a) = - \frac{h(J_x + J_y)}{4J_x J_y}, \quad (31)$$

provided that $h(J_x + J_y)/(4J_x J_y)$ lies in the range $[-1, 1]$. The values of ω_k at these three points are given by $2|J_x + J_y + h|$, $2|J_x + J_y - h|$ and $2|J_x - J_y|\sqrt{1 - h^2/(4J_x J_y)}$ respectively. The system is therefore gapless for the following three cases: (i) $J_x + J_y = -h$, (ii) $J_x + J_y = h$, and (iii) $J_x = J_y$ and $|h/J_x| \leq 2$. In all three cases, ω_k vanishes linearly as $k \rightarrow 0$, π/a or k_0 ; hence the dynamical critical exponent is given by $z = 1$. Further $\nu z = 1$, hence $\nu = 1$. Similarly, one can show that for a transition across the MCP in Fig. 2, $\nu_{mc} = 1/2$ and $z_{mc} = 2$. At the MCP, $\omega_k \sim k^2$ yielding $z_{mc} = 2$, and $\omega_k \sim (h + 2J_x)$ for $k = 0$, as the MCP B is approached along the anisotropic transition line, i.e., $h \rightarrow -(J_x + J_y) = -2J_x$, so that $\nu_{mc} z_{mc} = 1$.

The QPTs in cases (i) and (ii) belong to the universality class of the critical transverse Ising model in one dimension [31, 124] which is also related to the classical Ising model in two dimensions at the critical temperature. We will therefore refer to these cases as the “Ising transition”. The quantum phase transition in case (iii) will be referred to as the “anisotropic transition” since this line is crossed when the XY couplings J_x and J_y are made unequal giving rise to an anisotropic XY model.

The generally incommensurate value of k_0 given by (31) becomes equal to the commensurate value of π/a if $h/(J_x + J_y) = 1 - \gamma^2/(J_x + J_y)^2$, where $\gamma = (J_x - J_y)$. This corresponds to the dotted line shown in Fig. 2 where there is a transition from an incommensurate to a commensurate phase. On that line, the model can be mapped by a duality transformation (12) to the model given in (11).

The gaplessness of the three cases discussed above suggests that it may be possible to describe them in terms of quantum field theories (at length scales which are much larger than a) which are conformally invariant. We will now identify the appropriate conformal field theories.

Cases (i) and (ii) with $J_x + J_y = \pm h$ are similar, so we will consider only one of them, say, $J_x + J_y = -h$. Eq. (29) shows that there are two modes, d_k and d_{-k} , whose energies vanish linearly as $\omega_k = 2a|J_x - J_y|k$ as $k \rightarrow 0^+$. The velocity of these modes is given by $v = (d\omega_k/dk)_{k=0} = 2a|J_x - J_y|$. Further, the operators d_k and d_{-k} describe right- and left-moving modes whose wave functions are given by $e^{ik(x-vt)}$ and $e^{-ik(x+vt)}$ respectively, where $k > 0$. These are precisely the modes of a massless Majorana fermion described in Sec. II (B).

Case (iii) with $J_x = J_y$ and $|h/J_x| \leq 2$ has ω_k vanishing linearly as $k \rightarrow k_0$ from both above and below. The velocity is given by $v = (d\omega_k/dk)_{k=k_0} = 2a\sqrt{4J_x^2 - h^2}$. Let us redefine the operators $d_k \rightarrow d_k^\dagger$ and $d_{-k} \rightarrow d_{-k}^\dagger$ for $k < k_0$. Since this transforms $d_k^\dagger d_k \rightarrow d_k d_k^\dagger = -d_k^\dagger d_k$ plus 1 (and similarly for d_{-k}), we see that the energy ω_k becomes negative for $k < k_0$. Further, the wave functions for d_k are given by $e^{i[kx - (k-k_0)vt]}$ and $e^{-i[kx - (k-k_0)vt]}$ for $k > k_0$ and $k < k_0$ respectively, while the wave functions for d_{-k} are given by $e^{-i[kx + (k-k_0)vt]}$ and $e^{i[kx + (k-k_0)vt]}$ for $k > k_0$ and $k < k_0$ respectively. Upon noting that $k - k_0$ can take both positive and negative values, and redefining the momentum from $k - k_0$ to k , we see that these are the modes of a massless Dirac fermion, with d_k and d_{-k} describing right- and left-moving modes respectively.

We see that the velocities v of the above field theories vanish at the two points given by $J_x = J_y$ and $h = \pm 2J_x$. These correspond to multicritical points. At these points, ω_k vanishes quadratically, rather than linearly, as $k \rightarrow 0$ or π ; this implies that $z = 2$. Hence, the corresponding field theories are not Lorentz invariant and therefore not conformally invariant.

We can consider small perturbations from the gapless theories discussed above, namely, making $J_x + J_y$ slightly different from $|h|$ in cases (i) and (ii), and making J_x slightly different from J_y in case (iii). In the quantum field theoretic language, such a perturbation gives rise to a Majorana mass term for cases (i) and (ii), and to a Dirac mass term for case (iii). The forms of these mass terms are given in Sec. II (B).

Finally, we consider a transverse Ising chain in a longitudinal field given by the Hamiltonian

$$H = -J_x \sum_{\langle ij \rangle} \sigma_i^x \sigma_j^x - h \sum_i \sigma_i^z - h_L \sum_i \sigma_i^x. \quad (32)$$

Due to the presence of a longitudinal field, the model is no longer exactly solvable; we will discuss the effect of this field in a particular limit below.

(B). Connection to conformal field theory

Near a QCP, we can generally use a continuum field theory to describe the system since the correlation length ξ is much larger than microscopic length scales such as the lattice spacing (if the quantum model is defined on a lattice)

or the distance between nearest-neighbor particles. Exactly at $g = g_c$, the field theory will be scale invariant since $\xi = \infty$. Further, if the dynamical critical exponent $z = 1$, time and space will be on the same footing (apart from a factor given by the velocity v of the low-energy excitations), and the field theory would be expected to have a Lorentz invariant form. A combination of Lorentz invariance and scale invariance turns out to put rather powerful constraints on the correlation functions of the quantum theory, particularly in two space-time dimensions, i.e., if the original classical system is in two spatial dimensions. We will now discuss this case a little more [125].

Consider a quantum field theory in two-dimensional Minkowski space-time with coordinates (x, t) . It is convenient to transform to two-dimensional Euclidean space-time with coordinates (x, \bar{t}) , by making the substitution $t = -i\bar{t}$; when we analytically continue from real t to imaginary t , \bar{t} becomes real. Let us introduce the complex coordinates $z = \bar{t} - ix/v$ and $z^* = \bar{t} + ix/v$, where v denotes the velocity. It turns out that a theory in two Euclidean dimensions which is invariant under translations, rotations and scaling is also invariant under the full conformal group corresponding to transformations given by all possible analytical functions, $z \rightarrow z' = f(z)$; such a theory is called a conformal field theory (CFT). The Lie algebra for the conformal group in two dimensions is infinite-dimensional since a transformation close to the identity can be written as a Laurent series

$$z' = z - \sum_{m=-\infty}^{\infty} \epsilon_m z^{m+1}, \quad (33)$$

where the ϵ_m 's are infinitesimal quantities. The generators of the transformations are given by $l_m = -z^{m+1} \partial_z$ which satisfy the Lie algebra $[l_m, l_n] = (m - n) L_{m+n}$. It turns out that in the quantum theory, the Lie algebra of the generators, now denoted by L_m , contains an extra term if $m = -n$; namely, we find that

$$[L_m, L_n] = (m - n) L_{m+n} + \frac{c}{12} (m^3 - m) \delta_{m+n,0}. \quad (34)$$

This is called the Virasoro algebra and c is called the central charge of the theory. The number c plays an important role in several properties of the theory, such as finite size corrections to the free energy of the theory at finite temperature [126, 127], the entropy of a finite region of the system [128], and the entropy of entanglement between two parts of the system [129] (see Sec. V (A) (b)).

In a CFT, the correlation functions of various field operators fall off as powers of their space-time separations. Consider an operator $\mathcal{O}(z, z^*)$ whose two-point correlation function takes the form

$$\langle \mathcal{O}(z_1, z_1^*) \mathcal{O}(z_2, z_2^*) \rangle = \frac{C}{(z_1 - z_2)^{2x_{\mathcal{O}}} (z_1^* - z_2^*)^{2\bar{x}_{\mathcal{O}}}}, \quad (35)$$

where C is a constant which depends on \mathcal{O} . Then $d_{\mathcal{O}} = x_{\mathcal{O}} + \bar{x}_{\mathcal{O}}$ is called the scaling dimension and $x_{\mathcal{O}} - \bar{x}_{\mathcal{O}}$ is called the spin of the operator \mathcal{O} .

We now present three simple examples of CFTs. The first example is a massless Dirac fermion. In Minkowski space-time, the action for this is given by

$$S = i \int dt dx [\psi_R^\dagger (\partial_t + v \partial_x) \psi_R + \psi_L^\dagger (\partial_t - v \partial_x) \psi_L]. \quad (36)$$

The Euler-Lagrange equations of motion imply that ψ_R and ψ_L are functions of $x - vt$ and $x + vt$ respectively. We find that the central charge of this theory is $c = 1$. The scaling dimension and spin of the fields ψ_R and ψ_L are given by $(1/2, 1/2)$ and $(1/2, -1/2)$ respectively. The second example is a massless Majorana fermion; such a fermion is described by a field operator which is equal to its own Hermitian conjugate. Given a Dirac field ψ_R , we can form two Majorana fields from it, namely, $\chi_R = \psi_R + \psi_R^\dagger$ and $\xi = i(\psi_R - \psi_R^\dagger)$. Using only one of these fields, say, χ_R and a similar field χ_L formed from ψ_L , we can write down the action

$$S = i \int dt dx [\chi_R (\partial_t + v \partial_x) \chi_R + \chi_L (\partial_t - v \partial_x) \chi_L]. \quad (37)$$

As before, the equations of motion show that χ_R and χ_L are functions of $x - vt$ and $x + vt$ respectively. The central charge of this theory is given by $c = 1/2$. The third example of a CFT is a massless boson whose action is given by

$$S = \int dt dx \left[\frac{1}{2v} (\partial_t \phi)^2 - \frac{v}{2} (\partial_x \phi)^2 \right]. \quad (38)$$

The equations of motion show that ϕ can be written as $\phi = \phi_R + \phi_L$, where ϕ_R and ϕ_L are functions of $x - vt$ and $x + vt$ respectively. The central charge of this theory is also given by $c = 1$. The fields $\partial_z \phi_R$, $e^{i2\sqrt{\pi}\phi_R}$ and $e^{-i2\sqrt{\pi}\phi_R}$

have scaling dimension and spin equal to $(1, 1)$, $(1/2, 1/2)$ and $(1/2, 1/2)$ respectively. Similarly, we can use ϕ_L to construct three fields with scaling dimension and spin equal to $(1, -1)$, $(1/2, -1/2)$ and $(1/2, -1/2)$. We will discuss later how these fermionic and bosonic theories can be related to each other by bosonization.

The three CFTs mentioned above are massless; indeed, masslessness is a necessary condition for a theory to be scale invariant. However, one can perturb a CFT to give the particles a small mass. The corresponding mass terms in the action are given by $\int dtdx \mu(\psi_R^\dagger \psi_L + \psi_L^\dagger \psi_R)$ for the Dirac fermion, $\int dtdx i\mu\chi_R\chi_L$ for the Majorana fermion, and $\int dtdx \mu^2 \cos(2\sqrt{\pi}\phi)$ for the boson respectively. The last term assumes that the bosonic theory is invariant under $\phi \rightarrow \phi + \sqrt{\pi}$.

The effect of a perturbation of a CFT is governed by the scaling dimension of the corresponding operator \mathcal{O} as follows. Under a perturbation of the action of the CFT by an amount $\delta S = \lambda \int dtdx \mathcal{O}$, it turns out that the parameter λ effectively becomes a function of the length scale L , and it satisfies the renormalization group (RG) equation

$$\frac{d\lambda}{d\ln L} = (2 - d_{\mathcal{O}}) \lambda \quad (39)$$

to first order in λ . The perturbation given by \mathcal{O} is relevant, irrelevant and marginal for $d_{\mathcal{O}} < 2$, > 2 and $= 2$ respectively. If $d_{\mathcal{O}} < 2$, a small value of λ at the microscopic length scale (say, the lattice spacing a if the underlying model is defined on a lattice) will grow to be of order 1 at a length scale L_0 given by $L_0/a \sim 1/(\lambda(a))^{1/(2-d_{\mathcal{O}})}$. This implies that the perturbation gives rise to a finite correlation length ξ of the order of L_0 , or, equivalently, produces an energy gap (sometimes also called a mass) which scales with $\lambda(a)$ as

$$\Delta E \sim v (\lambda(a))^{1/(2-d_{\mathcal{O}})}, \quad (40)$$

since energy scales as v/length . If the correlation or energy gap can be experimentally measured as a function of $\lambda(a)$, one can deduce the value of $d_{\mathcal{O}}$. Conversely, if the value of $d_{\mathcal{O}}$ can be found using analytical or numerical methods, one can predict the power-law for ξ or ΔE . If $d_{\mathcal{O}} > 2$, the perturbation is irrelevant and the correlation length (energy gap) will remain infinite (zero) respectively.

We now apply these ideas about scaling dimensions and the effects of perturbations to the Ising transition mentioned in Sec. II (A). To be specific, let us consider the Hamiltonian given in (9). Close to the critical point $h = J_x$, the system is described by a CFT which is the theory of a massive Majorana fermion; from (29), we see that the energy-momentum dispersion near $k = \pi/a$ is given by $\omega_k = \sqrt{v^2 \delta k^2 + m^2}$, where $\delta k = k - \pi/a$, the velocity is $v = 2ha$ and the mass is $m = 2|h - J_x|$. The exact values of the various critical exponents in this theory are known and are given by $z = 1$ (since the energy gap scales as $|\delta k|$ for $h = J_x$), $\nu = 1$ (since $z = 1$ and the energy gap scales as $|h - J_x|$ for $\delta k = 0$), $\beta = 1/8$, $\alpha = 0$, $\gamma = 7/4$, $\delta = 15$, and $\eta = 1/4$. The value $\nu = 1$ and the equivalence of the temperature in the two-dimensional classical Ising model and the transverse field h in (9) implies that near the critical point, the correlation length scales as $(T - T_c)^{-1}$ or $|h - J_x|^{-1}$. Next, the combination $\nu = 1$ and $\beta = 1/8$ implies that the scaling dimension of the longitudinal magnetization ($\langle \sigma_n^x \rangle$) is given by $1/8$. (This implies that at criticality, the two-point correlation function $\langle \sigma_n^x \sigma_0^x \rangle \sim 1/n^{1/4}$, and hence that $\eta = 1/4$ as noted above). At the critical point, the addition of a small longitudinal magnetic field h_L (pointing in the \hat{x} direction as in (32)) will produce an energy gap scaling as $h_L^{1/(2-1/8)} = h_L^{8/15}$, and a longitudinal magnetization scaling as $(\text{gap})^{1/8} \sim h_L^{1/15}$; the latter implies that $\delta = 15$. We note that the value of critical exponent ν depends upon the scaling dimension of the perturbing operator that takes the system away from the gapless QCP and thereby generates a gap. As shown above, if the perturbation is due to the transverse field h , $\nu = 1$. In contrast, if the gap is generated by applying a longitudinal field in the \hat{x} direction, the resultant ν would be different (see (131) and discussions preceding that).

It turns out that the addition of a small longitudinal magnetic field at criticality produces a rather intricate pattern of energy gaps for the low-lying excitation spectrum. This was shown using a combination of CFT and an exact scattering matrix analysis for the low-energy particles in Ref. [130–133]. This was confirmed experimentally by Coldea *et al.* [25] (see also Ref. [134], and Sec. VII (C)); for a recent theoretical analysis, see Ref. [135]. The low-lying spectrum is described by the Lie algebra of the exceptional group E_8 , and the scattering matrix approach gives the exact ratios of the energy gaps of the 8 states; in particular, the ratio of the energies of the second and first excited states is predicted to be the golden ratio $(1 + \sqrt{5})/2 \simeq 1.618$. This was found to be the case in the quasi-one-dimensional Ising ferromagnet CoNb_2O_6 ; the Co^{2+} ions form spin-1/2 chains which are coupled very weakly to each other. A small longitudinal field h_L is believed to be present intrinsically in this system due to the interchain couplings. The ratio of the energies of the two lowest-lying states was found to approach the golden ratio when the transverse field was tuned to be close to the critical value of about 5.5 T [25] (see Fig. 32).

Before ending this section, we note that a huge literature exists on the dynamic correlation function of a transverse Ising chain [55–57, 136–138]. We will not discuss this in this review and refer to Ref. [14] (see also [139], and references therein).

(C). Exact solution of the Kitaev model

The two-dimensional Kitaev model defined on a honeycomb lattice is described by the Hamiltonian [140]

$$H_{2d} = \sum_{j+l=\text{even}} (J_1 \sigma_{j,l}^x \sigma_{j+1,l}^x + J_2 \sigma_{j-1,l}^y \sigma_{j,l}^y + J_3 \sigma_{j,l}^z \sigma_{j,l+1}^z), \quad (41)$$

where j and l defines the column and row indices of the lattice shown in Fig. 5. One of the main properties of the Kitaev model which makes it theoretically attractive is that, even in two dimensions, it can be mapped onto a non-interacting fermionic model by a JW transformation [140–144].

The one-dimensional Kitaev model, namely, just one row of interacting spins in Fig. 5, is described by the Hamiltonian

$$H_{1d} = \sum_{n=1}^{N/2} (J_1 \sigma_{2n}^x \sigma_{2n+1}^x + J_2 \sigma_{2n-1}^y \sigma_{2n}^y), \quad (42)$$

The summation label n takes $N/2$ values where N is the total number of sites and the number of unit cells is $N/2$.

As before, the Hamiltonian in (42) can be diagonalized using the JW transformation [22] (for details, see [145, 146]), defined as

$$a_n = \left(\prod_{j=-\infty}^{2n-1} \sigma_j^z \right) \sigma_{2n}^y \quad \text{and} \quad b_n = \left(\prod_{j=-\infty}^{2n} \sigma_j^z \right) \sigma_{2n+1}^x, \quad (43)$$

where a_n and b_n are independent Majorana fermions at site n , satisfying the relations $a_n^\dagger = a_n$, $b_n^\dagger = b_n$, $\{a_m, a_n\} = 2\delta_{m,n}$, $\{b_m, b_n\} = 2\delta_{m,n}$, $\{a_m, b_n\} = 0$. [Eq. (43) has the same content as Eq. (24) but is more useful here because we want to work with Majorana fermions a_n and b_n rather than Dirac fermions c_n]. We perform a Fourier transformation of a_n and b_n , to a_k and b_k , and note that the sum over k goes only over half the Brillouin zone as the a_n 's are Majorana fermions. One can check that the number of modes lying in the range $0 \leq k \leq \pi$ is $N/4$ so that k ranges from 0 to π . By defining $\psi_k = (a_k, b_k)$, the Hamiltonian in (42) can be rewritten as $H_{1d} = \sum_{k=0}^{\pi} \psi_k^\dagger H_k \psi_k$ where

$$H_k = 2i \begin{bmatrix} 0 & -J_1 - J_2 e^{-ik} \\ J_1 + J_2 e^{ik} & 0 \end{bmatrix}. \quad (44)$$

The above Hamiltonian can be diagonalized by a Bogoliubov transformation, and the eigenvalues are given by $E_k^\pm = \pm 2\sqrt{J_1^2 + J_2^2 + 2J_1 J_2 \cos k}$. In the ground state, one of the bands is fully occupied while the other is empty. The gap in the spectrum $\Delta_k = E_k^+ - E_k^-$ vanishes at $J_1 = \pm J_2$ for $k = \pi$ and 0 respectively. The critical exponents ν and z can be calculated using the definition $\Delta_{k=k_c} = (J_1 - J_c)^{\nu z}$ and $\Delta_{J_1=J_c} \sim k^z$, where J_c is the value of the coupling J_1 at which the gap closes at the critical mode k_c . In this case, we have $J_c = \pm J_2$ for $k_c = \pi$ and 0, respectively, and $\nu = z = 1$. It can be shown by introducing a duality transformation that the transition between the two gapped phases at $J_1/J_2 = 1$ does not involve any change of symmetry but there is a change of topological order [141, 143, 148, 149]⁷.

For $J_3 \neq 0$, we define the JW transformation as

$$\begin{aligned} a_{j,l} &= \left(\prod_{i=-\infty}^{j-1} \sigma_{i,l}^z \right) \sigma_{j,l}^y \quad \text{for even } j+l, \\ a'_{j,l} &= \left(\prod_{i=-\infty}^{j-1} \sigma_{i,l}^z \right) \sigma_{j,l}^x \quad \text{for even } j+l, \\ b_{j,l} &= \left(\prod_{i=-\infty}^{j-1} \sigma_{i,l}^z \right) \sigma_{j,l}^x \quad \text{for odd } j+l, \\ b'_{j,l} &= \left(\prod_{i=-\infty}^{j-1} \sigma_{i,l}^z \right) \sigma_{j,l}^y \quad \text{for odd } j+l, \end{aligned} \quad (45)$$

⁷ We reiterate that states with different topological order cannot be distinguished from each other by any local order parameter, but they differ in other ways such as the ground state degeneracy and the nature of the low-lying excitations.

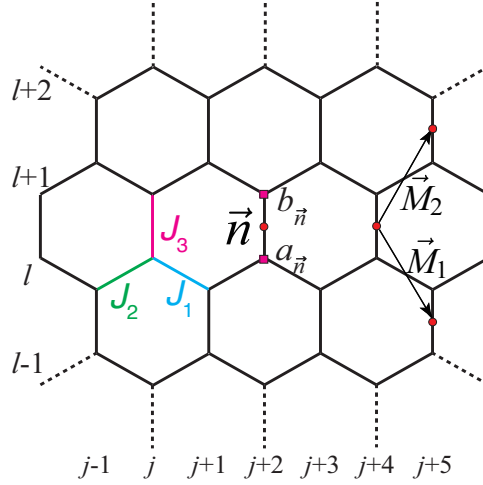


FIG. 5: (Color online) Schematic representation of a Kitaev model on a honeycomb lattice showing the interactions J_1 , J_2 and J_3 between x , y and z components of the spins respectively. \vec{n} represents the position vector of each vertical bond (unit cell). The vectors \vec{M}_1 and \vec{M}_2 are spanning vectors of the lattice. In the fermionic representation of the model, the Majorana fermions $a_{\vec{n}}$ and $b_{\vec{n}}$ sit at the bottom and top sites of the vertical bond with center coordinate \vec{n} as shown. (After [147].)

where $a_{j,l}$, $a'_{j,l}$, $b_{j,l}$ and $b'_{j,l}$ are all Majorana fermions. The spin Hamiltonian in (41) gets mapped to a fermionic Hamiltonian given by

$$H_{2d} = i \sum_{\vec{n}} [J_1 b_{\vec{n}} a_{\vec{n}-\vec{M}_1} + J_2 b_{\vec{n}} a_{\vec{n}+\vec{M}_2} + J_3 D_{\vec{n}} b_{\vec{n}} a_{\vec{n}}], \quad (46)$$

where $D_{\vec{n}} = i b'_{\vec{n}} a'_{\vec{n}}$ and $\vec{n} = \sqrt{3}\hat{i} n_1 + (\frac{\sqrt{3}}{2}\hat{i} + \frac{3}{2}\hat{j}) n_2$ denote the midpoints of the vertical bonds. Here n_1, n_2 run over all integers so that the vectors \vec{n} form a triangular lattice whose vertices lie at the centers of the vertical bonds of the underlying honeycomb lattice; the Majorana fermions $a_{\vec{n}}$ and $b_{\vec{n}}$ sit at the bottom and top sites respectively of the bond labeled \vec{n} . The vectors $\vec{M}_1 = \frac{\sqrt{3}}{2}\hat{i} - \frac{3}{2}\hat{j}$ and $\vec{M}_2 = \frac{\sqrt{3}}{2}\hat{i} + \frac{3}{2}\hat{j}$ are spanning vectors for the reciprocal lattice. We note that the operators $D_{\vec{n}}$ have eigenvalues ± 1 , and commute with each other and with H_{2d} ; hence all the eigenstates of H_{2d} can be labeled by specific values of $D_{\vec{n}}$. The ground state can be shown to correspond to $D_{\vec{n}} = 1$ for all \vec{n} for any value of the interaction parameter [140]. For $D_{\vec{n}} = 1$, it is straightforward to diagonalize H_{2d} in momentum space (for details, see [150]). We then obtain $H_{2d} = \sum_{\vec{k}} \psi_{\vec{k}}^\dagger H_{\vec{k}} \psi_{\vec{k}}$, where $\psi_{\vec{k}}^\dagger = (a_{\vec{k}}^\dagger, b_{\vec{k}}^\dagger)$, and $H_{\vec{k}}$ can be expressed in terms of Pauli matrices

$$H_{\vec{k}} = 2 [J_1 \sin(\vec{k} \cdot \vec{M}_1) - J_2 \sin(\vec{k} \cdot \vec{M}_2)] \sigma^x + 2 [J_3 + J_1 \cos(\vec{k} \cdot \vec{M}_1) + J_2 \cos(\vec{k} \cdot \vec{M}_2)] \sigma^y. \quad (47)$$

The energy spectrum of H_{2d} therefore consists of two bands with energies

$$E_{\vec{k}}^\pm = \pm 2 [(J_1 \sin(\vec{k} \cdot \vec{M}_1) - J_2 \sin(\vec{k} \cdot \vec{M}_2))^2 + (J_3 + J_1 \cos(\vec{k} \cdot \vec{M}_1) + J_2 \cos(\vec{k} \cdot \vec{M}_2))^2]^{1/2}. \quad (48)$$

We note for $|J_1 - J_2| \leq J_3 \leq J_1 + J_2$, these bands touch each other so that the energy gap $\Delta_{\vec{k}} = E_{\vec{k}}^+ - E_{\vec{k}}^-$ vanishes for special values of \vec{k} for which $J_1 \sin(\vec{k} \cdot \vec{M}_1) - J_2 \sin(\vec{k} \cdot \vec{M}_2) = 0$ and $J_3 + J_1 \cos(\vec{k} \cdot \vec{M}_1) + J_2 \cos(\vec{k} \cdot \vec{M}_2) = 0$. The gapless phase in the region $|J_1 - J_2| \leq J_3 \leq J_1 + J_2$ is shown in Fig. 6 [140–144]. It is straightforward to show that the transition on the critical line $J_3 = J_1 + J_2$ that separates one of the gapped phase from the gapless phase in Fig. (6) belongs to the universality class of an anisotropic quantum critical point with exponents $\nu_1 = 1/2, z_1 = 2$ and $\nu_2 = 1, z_2 = 2$, respectively [147, 150]. Both the one-dimensional and two-dimensional versions of the Kitaev model have been used extensively in studies of quantum information and non-equilibrium dynamics (see e.g., Secs. V (C), VI (G), Appendix G, etc.).

III. ROLE OF QUENCHED DISORDER

In this section, we will discuss quantum phase transitions in TIMs in the presence of random interactions or fields. We will provide a brief overview and refer to some review articles [151–155] for extensive discussions. Randomness has

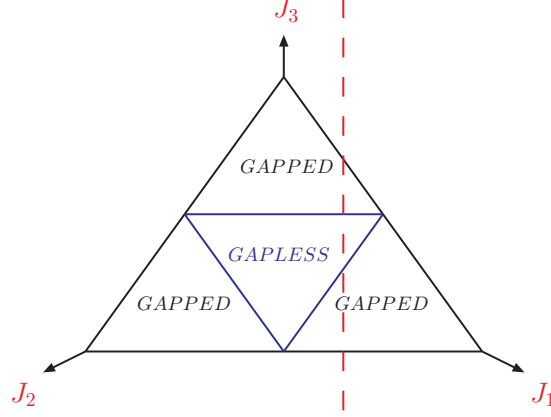


FIG. 6: (Color online) Phase diagram of the Kitaev model showing one gapless and three gapped phases inside the equilateral triangle in which $J_1 + J_2 + J_3$ is a constant. (The symbols J_i denote that the values of J_i are measured from the opposite side of the triangle). The red dashed line indicates the quenching of J_3 from $-\infty$ to ∞ to be discussed in Sec. VI(G). (After Sengupta *et al.*, 2008).

a drastic effect on QPTs, especially in low dimensions which has been a subject of extensive research both theoretically and experimentally.

In a seminal paper [156] Harris addressed the question of the relevance of disorder close to a finite temperature classical transition using the following argument. For a model with a random local critical temperature [157], one can use the central limit theorem to argue that the fluctuation in T_c for a domain of size ξ is of the order of $\Delta T_c \sim \xi^{-d/2} \sim (T - T_c)^{\nu_{\text{pure}} d/2}$, where ν_{pure} is the correlation length exponent corresponding to the critical point of the non-random version of the model. This shows that $\Delta T_c / |T - T_c|$ grows as $T \rightarrow T_c$, if $\nu_{\text{pure}} < 2/d$ (or $\alpha_{\text{pure}} > 0$ because of the hyperscaling relation $2 - \alpha_{\text{pure}} = \nu_{\text{pure}} d$ valid for $d < d_u^c$), and hence randomness is a relevant perturbation. If $\nu_{\text{pure}} > 2/d$, randomness is irrelevant in determining the critical behavior which remains that of the pure system. When disorder is relevant, it has been shown that the correlation length critical exponent ν_{random} associated with the random critical fixed point satisfies $\nu_{\text{random}} \geq d/2$; this is known as the Chayes criterion [158]. However, this criterion is not universally valid; there exist a number of systems, including the metal-insulator transition in uncompensated, doped semiconductors and helium in aerogel, that have experimental results in conflict with this (see Ref. [159] and references therein)⁸.

Let us consider a TIM in d -dimensions with randomness only in the interactions (assumed to be nearest neighbor for the time being) given by the Hamiltonian

$$H = - \sum_{\langle ij \rangle} J_{ij} \sigma_i^x \sigma_j^x - h \sum_i \sigma_i^z, \quad (49)$$

where the J_{ij} 's are chosen from a random distribution. Similarly one can define QR models (21) with random interactions [119]. As discussed already, the QPT of the Hamiltonian in (49) is equivalent to the finite temperature CPT in a $(d+1)$ -dimensional classical Ising model with randomness infinitely correlated in the Trotter direction (see Fig. 7). Due to this correlated nature of randomness, this additional dimension does not influence the fluctuation ΔT_c of the $(d+1)$ -dimensional model which is still given by $\Delta T_c \sim (T - T_c)^{\nu_{\text{pure}}^q d/2}$, where ν_{pure}^q is the correlation length exponent for the QPT in the corresponding pure system. Therefore, following similar arguments as given above, we find that disorder is relevant when $\nu_{\text{pure}}^q < 2/d$ or $\alpha_{\text{pure}}^q + \nu_{\text{pure}}^q > 0$ [160, 161] where we have used the hyperscaling relation in (16) with $z = 1$. Since $\nu_{\text{pure}}^q > 0$, randomness is usually relevant for a QPT.

⁸ The Chayes criterion is obtained using finite size scaling and disorder averaging of a particular type. This leads to an additional length scale in the problem, as well as noise. It has been posited that self-averaging is not the appropriate treatment of the disorder in all cases, circumventing the strict bound on the critical exponent at $2/d$ in such instances [159].

(A). Quantum Ising spin glass (QISG)

The free energy \mathcal{F} of a random system is a self-averaging quantity which means that in the $N \rightarrow \infty$ limit, $\mathcal{F} = -1/(\beta N) \overline{\ln \mathcal{Z}(J)} = \mathcal{F}_\infty(\beta)$ where \mathcal{Z} is the partition function for a given configuration of disorder. The overline bar denotes the average over disorder such that $\overline{A} = \int dJ P(J) A(J)$ where $P(J)$ is distribution of disorder. For a self-averaging quantity, the fluctuation falls off as $1/N$. To calculate $\overline{\ln \mathcal{Z}(J)}$, the method of replicas [162] turns out to be extremely useful. This involves using the mathematical formula $\ln \mathcal{Z} = \lim_{n \rightarrow 0} (\mathcal{Z}^n - 1)/n$, which means that we are in fact considering n identical copies of the system for a given disorder configuration. As a result of disorder averaging, i.e., in evaluating the disorder-averaged $\overline{\ln \mathcal{Z}(J)} = \int dJ P(J) \ln \mathcal{Z}$ (using its replicated form), the different replicas get coupled; eventually one takes the limit $n \rightarrow 0$.

This method has been used to study classical Ising spin glasses (for reviews see [163–167]) given by the Hamiltonian

$$H = - \sum_{ij} J_{ij} S_i S_j, \quad (50)$$

where the S_i 's are classical binary variables ($S_i = \pm 1$). In the Edwards-Anderson (EA) version of Hamiltonian (50) [162], the interactions are Gaussian distributed but are restricted to nearest neighbors only. In the mean field Sherrington-Kirkpatrick (SK) version [168], all the spins in (49), interact with each other, and the interactions J_{ij} 's are chosen from a Gaussian distribution,

$$P(J_{ij}) = \left(\frac{N}{2\pi\tilde{J}^2} \right) \exp \left(-\frac{N J_{ij}^2}{2\tilde{J}^2} \right), \quad (51)$$

where we have set $\overline{J_{ij}} = 0$ and \tilde{J}/\sqrt{N} is the variance of the distribution. The presence of $1/N$ in the expression of the variance is essential for the extensivity of the model, i.e., to obtain finite thermodynamic quantities in the thermodynamic limit ($N \rightarrow \infty$).

The natural choice for the spin-glass order parameter is the EA parameter defined as $q = 1/N \sum_{i=1}^N \overline{\langle S_i \rangle^2}$, which is the configuration averaged mean-squared local magnetization. Note that one applies a conjugate longitudinal field \tilde{H} (that breaks the spin-reversal symmetry of (51)), which is set equal to zero after the thermodynamic limit is taken; the precise definition of q is therefore given by $q = \lim_{\tilde{H} \rightarrow 0} \lim_{N \rightarrow \infty} (1/N) \sum_{i=1}^N \overline{\langle S_i \rangle^2}$. Otherwise, $\langle S_i \rangle = 0$ due to the symmetry. On the other hand, the overlap between different replicas defined by $q_{\alpha\beta} = 1/N \sum_{i=1}^N \langle S_i^\alpha \rangle \langle S_i^\beta \rangle$, is also a measure of spin glass order. In the saddle point solution (obtained in the $N \rightarrow \infty$ limit) [168]⁹ of the classical SK model, one assumes a replica symmetric (RS) ansatz $q_{\alpha\beta} = q_0$ for $\alpha \neq \beta$ and $q_{\alpha\alpha} = 0$. However, the stability analysis of the RS saddle point solution shows that the spin glass phase with $q \neq 0$ is unstable at low temperature because of the emergence of a negative entropy. In a magnetic field (\tilde{H}), the RS solution is unstable below a line in the $T - \tilde{H}$ plane, this is known as the Almeida-Thouless (AT) line [169].

To cure this problem, the concept of replica symmetry breaking (RSB) was introduced [170–173] (see also [163]). In this ansatz, the $n \times n$ order-parameter matrix $q_{\alpha\beta}$ is divided into $n/m_1 \times n/m_1$ blocks of size $m_1 \times m_1$. In the off-diagonal blocks, nothing is changed while in the diagonal blocks q_0 is replaced by q_1 . The method is repeated for each of the blocks along the diagonal which are split into $m_1/m_2 \times m_1/m_2$ subblocks each of size $m_2 \times m_2$ and along the diagonal of the sub-block q_1 is replaced by q_2 ; the procedure is repeated k times such that $n \geq m_1 \geq m_2 \dots > m_k \geq 1$. While the procedure is meaningful for positive integer n and finite k , one assumes that an analytical continuation to the limit $n \rightarrow 0$ and $k \rightarrow \infty$ is possible such that $0 \leq m_i \leq 1$ as $k \rightarrow \infty$. In this limit m_i becomes continuous, $m_i \rightarrow x$, $0 < x < 1$ and $q_i \rightarrow q(x)$; the EA order parameter is given by $q = q(x=1)$. The RSB is related to the rugged free energy landscape of the spin glass phase when the system may get trapped in a local minima leading to the breaking of ergodicity. The ground state of SK model is expected to be infinitely replica symmetry broken and there are thermodynamically large number of local minima. Later works showed the RSB solution is stable [174] and exact for SK spin glass [175]. We note that an alternative picture known as the “droplet picture” [176, 177] in fact rules out the possibility of an AT line and RSB for any finite dimensional spin-glass. Whether the AT line exists for a real short-range interacting spin glass is still not clear [178]; a recent study [179] shows that it occurs only for $d > d_u^c (= 6$ for short-range spin glass [163]), i.e., in the mean field region. However, we shall comment below that in a quantum spin glasses there is a possibility of restoration of replica symmetry due to quantum tunneling at zero-temperature.

⁹ One in fact interchanges the limits $n \rightarrow 0$ and $N \rightarrow \infty$ to arrive at the saddle point solution; first the $N \rightarrow \infty$ limit is taken keeping n finite, and then the limit $n \rightarrow 0$ is applied.

The quantum counterpart of classical Ising spin glasses given by Hamiltonian (49) was introduced in the early 1980's [180]. The SK version (with P_{ij} 's given by (51)) has been studied extensively [181–185]; in particular, the possibility of the restoration of replica symmetry of the replica symmetric broken classical ground state was addressed [182]. There is a possibility that quantum fluctuations due to the transverse field may help tunneling across macroscopically large but narrow barriers which is not possible through thermal activated dynamics.

In the $N \rightarrow \infty$ limit, the classical SK model can be reduced to a single spin problem in a Gaussian distributed random field h_{eff}^r , with zero mean and variance $J^2 q$, where q is the replica symmetric version of the spin-glass order parameter $q_{\alpha\beta}$. For the quantum case, one can intuitively write an effective single spin Hamiltonian (H_{SP}) [186, 187] given by $H_{\text{SP}} = -h_{\text{eff}}^r \sigma^x - h \sigma^z$. The Hamiltonian H_{SP} can then be solved using a self-consistent method which necessitates random averaging in addition to the thermal averaging. The phase boundary between the spin-glass phase ($q = 1/N \sum_{i=1}^N \overline{\sigma_{i\alpha}^x \sigma_{i\beta}^x} \neq 0$) and the PM phase ($q = 0$) is given by the condition $h_c(T)/J = \tanh(h_c(T)/(k_B T))$.

The random averaged quantum SK model can be mapped to a single spin problem due to the infinite range of interactions. However, a non-local interaction in imaginary time $\mathcal{R}(\bar{\tau} - \bar{\tau}')$ is generated due to the infinite correlation of disorder in the temporal direction as happens also for a vector quantum spin glass [188]; here the replica symmetric case is assumed. Within the static approximation which ignores the time dependence of \mathcal{R} , the phase diagram of the model has been studied [184, 189]. Miller and Huse [190] used a non-perturbative argument that goes beyond the static approximation to estimate the critical value of the transverse field h_c at $T = 0$, starting from the replica symmetric PM phase.

Following the experimental realization of a QISG with long-range dipolar interaction in the material $\text{LiHo}_x\text{Y}_{1-x}\text{F}_4$ [53, 54, 191] (see Sec. 9 for details), a number of studies have been directed towards understanding the QPT in the EA QISG. The equivalent classical spin-glass model with correlated randomness (Fig. 4) has been studied using quantum Monte Carlo methods for spatial dimension $d = 2$ [192] and $d = 3$ [193]. The critical temperature and the exponents are obtained by a finite-size scaling analysis of the Binder cumulant \tilde{g} [163], given by

$$\tilde{g} = \frac{1}{2} \left(3 - \frac{\langle q^4 \rangle}{\langle q^2 \rangle^2} \right) = \bar{g}_0 \left(L^{1/\nu} (T - T_c), \frac{M}{L^z} \right), \quad (52)$$

where \bar{g}_0 is the scaling function and L (M) is the size of the spatial (Trotter) direction. It is found that the Binder cumulant shows a maximum as a function of M , and the value of this maximum becomes independent of the spatial size L at $T = T_c$; knowing T_c , one can find the dynamical exponent z using the scaling relation in (52). Similarly, by studying the variation of \tilde{g} as a function of temperature for fixed M/L^z , one can estimate T_c (at which \tilde{g} becomes independent of L) and also the critical exponent ν . These studies show that $\nu \approx 1.0$ and $z \approx 1.7$ for $d = 2$ [192], and $\nu \approx 0.8$ and $z \approx 1.3$ for $d = 3$ [193]. Both the linear and non-linear susceptibilities were found to diverge for $d = 3$, while for $d = 2$ only the non-linear susceptibility was shown to diverge.

The LGW actions in terms of the spin glass order parameter $q_{\alpha\beta}$ for an EA QISG and also a QR were proposed in [120] where it was shown that the quantum fluctuations are dangerously irrelevant (see [3], for a discussion of dangerously irrelevant variables) close to the QCP. Below the upper critical dimension $d_u^c (= 8$ for this model, consistent with the hyperscaling relation in (16) since the mean field $z = 2$, $\nu = 1/4$ for QISG and $d_u^c = 6$ for classical spin glass), the renormalization group calculations fail to locate any stable weak coupling fixed point, and a run-away to strong coupling was observed. This was attributed to the existence of an infinite randomness fixed point (see below) for $d < d_u^c$. A similar result was obtained [194] for the quantum version of the classical spin-glass where the random interaction decays algebraically with the distance between the spins [179, 195, 196]. A quantum version of the droplet model has also been proposed [197].

(B). Griffiths singularities and activated dynamics

The free energy of a dilute Ising ferromagnet is a non-analytic function of the external field below the critical temperature of the corresponding pure model; this is known as a Griffiths-McCoy (GM) singularity [198]. More generally speaking, a random magnetic system is in its GM phase if it is above its ordering temperature but below the highest ordering temperature allowed by the distribution [199]. The GM singular regions occur due to locally ordered “rare regions” [198, 200, 201] as seen for example in two-dimensional Ising models with frustration as well as randomness [202, 203], and it strongly influences the dynamical response of the system [204–206].

In a QPT, statistics and dynamics are mingled and hence these “rare regions” have a more prominent effect on the QPT of a low-dimensional system as we shall indicate below using the example of a dilute transverse Ising chain in the ferromagnetic phase; the existence of these regions results in fascinating features associated with random QPTs in low-dimensional systems. These features are the activated quantum dynamical scaling ($z \rightarrow \infty$) at the QCP and the existence of GM singular regions where the susceptibility diverges even away from the critical point [207–209]. The

role of these GM singular regions in quantum information and dynamics will be discussed in Secs. V (A) (b), VI (H), etc. For a discussion on experimental signature of such singularities see the discussion around Eq. (162).

Let us consider a random one-dimensional transverse Ising chain given by the Hamiltonian

$$H = - \sum_{i=1}^{N-1} J_{i,i+1} \sigma_i^x \sigma_{i+1}^x - \sum_{i=1}^N h_i \sigma_i^z, \quad (53)$$

which includes randomness in the transverse field also. For $d = 1$, one can perform a gauge transformation to make all the $J_{i,i+1}$ and h_i positive. Moreover, using the duality transformation [45] (see also Sec. I (B)), one can argue that the critical point is expected when the distribution of bonds and fields are identical. Hence, defining variables $\Delta_h = \overline{\ln h}$ and $\Delta_J = \overline{\ln J}$, the QCP occurs when $\Delta_h = \Delta_J$. The deviation from the QCP is measured as $\lambda = (\Delta_h - \Delta_J)/(\text{var}[h] + \text{var}[J])$; here var stands for the variance of the distribution.

The model in (53) has been studied by Fisher [207, 209–211] using a strong disorder renormalization group (SDRG) technique introduced in [212]. In this approach, we choose the strongest bond or the strongest field and minimize the corresponding term in the Hamiltonian; therefore the degrees of freedom associated with the maximum energy scale (Ω_0) are frozen at the lowest energy scale. If the strongest coupling is a field h_i at the site i , then the spin variable at this site is fixed in the direction of the field (i.e., decimated) and an effective interaction generated due to quantum fluctuations between neighboring spins $\tilde{J}_{i-1,i+1}$ (much smaller than Ω) is calculated using second-order perturbation theory. In contrast, if the interaction between two sites $J_{i,i+1}$ are the strongest, we set the spins at those two sites i and $i+1$ to point in the same direction, i.e., they form a ferromagnetic cluster which can be viewed as a single spin with higher magnetic moment in an effective transverse field again calculated by second-order perturbation. In the process, the maximum energy scale decreases to $\Omega < \Omega_0$. The process is iterated and the renormalization group flow equations for the distributions of h_i and $J_{i,i+1}$ as a function of $\Lambda = \ln(\Omega_0/\Omega)$ have a fixed point solution which is an attractor for all initial distribution of randomness. This is the infinite randomness fixed point (IRFP) distribution, so called because disorder grows beyond limit under renormalization as $\Omega \rightarrow 0$; in this sense, SDRG is asymptotically exact in describing the low-energy properties near a random QCP ($\lambda = 0$). We see that the clusters grow in the ordered phases while bonds become disconnected in the disordered phase. Qualitatively one can argue that at the QCP the annihilation and aggregation of clusters compete with each other at each energy scale.

An IRFP is characterized by three critical exponents ψ , ϕ and ν . For a rare large cluster at energy scale Ω , the linear dimension L of the cluster is related to Ω through the exponent ψ as $\ln(\Omega/\Omega_0) \sim L^\psi$. This logarithmic dependence is the signature of the activated quantum dynamics. Similarly, the magnetization of the cluster scales as $L^{\phi\psi}$ and the correlation length exponent ν determines the decay of the average correlation function [207]. Fisher showed that [207, 209] for the one-dimensional chain (53), $\psi = 1/2$, $\phi = (\sqrt{5} + 1)/2$ and $\nu = 2$. Close to the QCP (λ non-zero but small), the spin chain is in the GM phase, where the low-energy behavior is dominated by gapless but well-localized excitations which lead to off-critical singularities; at early stages the chain obeys the critical scaling. However, when the typical sizes and bond length is of the order of the correlation length $\xi \sim \lambda^{-2}$ and $\Lambda = \ln(\Omega_0/\Omega) \sim \lambda^{-1}$, a crossover to ordered ($\lambda < 0$) or disordered ($\lambda > 0$) phase takes places. For small λ , in both phases $\Omega \sim L^{-z(\lambda)}$ with the effective dynamical exponent $z(\lambda) \sim |\lambda|^{-1}$ diverging at the QCP where dynamics is activated. We mention that the SDRG method has been extended to $d = 2$ [213, 214].

Numerical diagonalization of a one-dimensional random Ising chain using a JW mapping to fermions [215] confirmed the SDRG predictions; the dynamical properties of a random chain has also been studied [216, 217]. Long-range spatial correlations of disorder [218] were found to enhance the GM singularities [219]. Similar results have been obtained for a random transverse XY chain by mapping to a Dirac equation with random mass [124] and also exploiting the analogy between a one-dimensional random TIM and a random walk [220, 221].

Quantum Monte Carlo studies of EA QISG [222, 223] as well as of two-dimensional random bond Ising models [224] show that critical points in all these cases happen to be an IRFP and hence one can conclude that at an IRFP frustration is irrelevant. However, the situation of QISG needs more attention at this point. For QISG in spatial dimension two [222], signatures of strong GM singularities are observed in the disordered phase near the quantum transition where one finds power-law distributions of the local susceptibility and local non-linear susceptibility characterized by a smoothly varying dynamical exponent. The local non-linear susceptibility diverges in the GM phase though the local susceptibility does not; it diverges only at the QCP. Approaching from the disordered phase, the limiting value of the dynamical exponent apparently tends to its value ($z \simeq 1.7$) at the QCP quoted in the previous section. This is in contrast to the one-dimensional situation where $z \rightarrow \infty$ at the QCP and if one assumes that z is finite, the dynamical scaling should be conventional. However, one can not rule out the possibility of increasing z for larger system size and hence an activated quantum critical dynamics.

The SDRG studies of the random spin-1/2 Heisenberg chain [208] has revealed that the ground state is a random singlet phase which is another example of IRFP. This is true also for higher spin values [225]. We note that the

existence of GM phases and an infinite randomness fixed point has been reported for the finite temperature transition of a layered Heisenberg ferromagnet [226].

The effect of GM singularities are less prominent for QR models. This can be argued [120] taking the example of a random Ising (rotor) model with a uniform transverse field (kinetic term). A locally ordered region of size L^d can be viewed as a single spin with a large magnetic moment L^d coupled ferromagnetically with similar blocks along the Trotter direction, so that we have an equivalent one-dimensional chain of these giant moments. If the moments are Ising-like, then the correlation time goes as $\xi_\tau \sim \exp(L^d)$ which is an activated behavior, while for the n -vector case $\xi_\tau \sim L^d$ [3]. The latter suggests a power-law quantum critical dynamics and hence less prominence of GM singularities for $n > 1$. Therefore, it is the Ising nature of interactions that lead to activated quantum dynamical scaling which in turn results in exotic GM singular phases associated with low-dimensional random quantum Ising transitions.

(C). A generalized random transverse field Ising spin Chain

We now briefly mention a generalized random transverse field Ising chain with spins having q states (labeled by $|s_i\rangle = |0_i\rangle, |1_i\rangle, \dots, |(q-1)_i\rangle$). The spin chain described by the Hamiltonian [227]

$$H_q = - \sum_i J_i \sum_{n=1}^{q-1} \alpha_n (S_i^{z\dagger} S_i^z)^n - \sum_i h_i \sum_{n=1}^{q-1} \alpha_n \Gamma_i^n. \quad (54)$$

is useful in studying the entanglement entropy of a random system to be discussed in Sec. V (A) (b). Here, S^z is a $q \times q$ matrix with $(S^z)_{lm} = \exp[(2i\pi l)/q] \delta_{lm}$ (with $l, m = 0, \dots, q-1$), $\Gamma = |s\rangle\langle s+1|$ is the spin-raising operator, i.e., $\Gamma|s\rangle = |s+1\rangle$; the variables α_n are disorder-free and satisfy $\alpha_n = \alpha_{q-n}$ for Hermiticity. For each set of α_n , there exist a duality transformation $S_i^{z\dagger} S_i^z = \Gamma_i^*$ and $\prod_{j<i} \Gamma_j = S_i^{z*}$ which interchanges h and J . For $\alpha_n = 1$ for all n , the Hamiltonian describes a q -state random quantum Potts chain. The disorder free ferromagnetic quantum Potts chain has a first order quantum transition for $q > 4$ and a continuous transition for $q \leq 4$ [228]. For $\alpha_n = \delta_{1,n}$, model (54) represents a random Z_q clock model. We note that the ferromagnetic clock chains have, for $q > 4$, a quasi-long-range ordered phase sandwiched between a FM phase and a PM phase with the corresponding transitions being of BKT type; for $q \leq 4$, the model has a second order phase transition [229]. SDRG studies of random q -state Potts model and Z_q clock model show that the critical fixed point is in fact the IRFP of the model (53) [230]. In particular, for the Z_q clock model with $q > 4$, the existence of an unstable intermediate-disorder fixed point separating a low disorder fixed point and the IRFP has been found both analytically and using density matrix renormalization group [230, 231].

An important realization of (54) is obtained by choosing $\alpha_n = \sin(\pi/q)/\sin(\pi n/q)$. The pure version of the model is critical along the self-dual line $J = h$, (unlike Potts and clock models) for each q [232] and its fluctuations are governed by the Z_q parafermionic field theories with central charge $c_q^{\text{pure}} = 2(q-1)/(q+2)$ [233]; $q = 2$ for Ising model and $q = 3$ for 3-state Potts model. Reference [227] suggests that even for infinitesimal disorder the Hamiltonian flows to an IRFP for all values of q . However, under SDRG, the set α_n renormalizes to $\alpha_n = \delta_{1,n}$ which coincides with the random clock model discussed in the previous paragraph for which there is an intermediate fixed point. Therefore, whether the Hamiltonian (54) with $q > 4$ flows to the IRFP upon introduction of a weak disorder (as indicated in [227]) is still an open question although it happens for $q < 4$.

(D). Higher dimensional realization of IRFP

The ideal higher-dimensional realization of an IRFP is provided by a random TIM on a d -dimensional dilute lattice which is again given by (49) where the bonds J_{ij} are present with a probability p , i.e.,

$$P(J_{ij}) = p\delta(J_{ij} - J) + (1-p)\delta(J_{ij}). \quad (55)$$

This model connects the QPT of the TIM (from a FM to a PM phase) to a geometrical phase transition, namely, the percolation transition [234, 235]. For $h = 0$ (see Fig. 7), if $p > p_c$ (the percolation threshold), at least one system spanning cluster exists, while for $p < p_c$, only finite clusters appear. The geometrical transition at $p = p_c$ belongs to the universality class of the thermal transition of a q -state Potts model in the limit $q \rightarrow 1$ [236]. The critical line at p_c in Fig. 7 is vertical due to the fact that even at the percolation threshold there exists an infinitely connected cluster with a fractal dimension $d_f (< d)$, and hence a finite amount of h is necessary to destroy the long-range order [160]. This prediction was verified [237] by extending the real space renormalization group applicable to classical dilute magnets [238, 239].

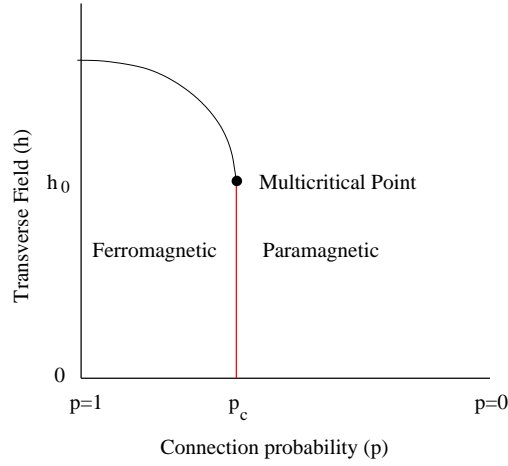


FIG. 7: The phase diagram of a dilute TIM for $d \geq 2$. The quantum phase transition across the vertical line at the percolation threshold p_c is governed by the percolation fixed point. Here, h_0 denotes the value of h corresponding to the multicritical point (After Harris, 1974b).

The exponents associated with quantum transitions across this vertical line below the multicritical point ($h < h_0$) (see Fig. 7) are the exponents of the percolation transition [234]; in this case the fixed point at $p = p_c, h = 0$, plays the role of an IRFP [240]. This has been verified numerically [241]. These exponents can be found in the following way: the energy of a cluster of diameter L scales as L^{d_f} showing that the exponent $\psi = d_f$, while the exponent $\nu = \nu_p$ and $\phi = (d - \beta_p/\nu_p)/d_f = 1$. Here the subscript p denotes the corresponding percolation exponents which are well known from numerical studies, e.g., for $d = 2$, $\nu_p = 4/3$, $d_f = 91/48$ and $\beta_p = 5/36$. [234]. Senthil and Sachdev [240], also showed that either side of the percolation threshold p_c is flanked with off-critical GM singular phases. For example, in the disordered phase ($p < p_c$), the disorder averaged imaginary time part of the local dynamical susceptibility satisfies a power-law scaling $\chi_L''(\omega) \sim \omega^{d/z-1}$. This power-law behavior shows that the PM phase is gapless, and the average local susceptibility diverges as $T^{d/z-1}$ as $T \rightarrow 0$. The dynamical exponent is related to the percolation correlation length ξ_p as $z \sim \xi_p^{d_f} \sim (p_c - p)^{-\nu d_f}$ and diverges as $p \rightarrow p_c$.

Similar results are obtained in [67, 242] for a TIM on dilute lattices with long-range connection probabilities [243, 244], and for contact processes [245] on dilute lattices [246]. For quantum rotors on dilute lattices, the quantum dynamics at the percolation threshold is of the conventional power-law type with $z = d_f$ which is consistent with the argument given above [247]. Let us also mention some interesting studies that connect geometrical and quantum phase transitions of magnetic models [248–252].

Finally, let us comment on the reason behind the greater prominence of GM regions in a QPT compared to a CPT using the example of a dilute Ising model in the FM phase [154]. The probability of a rare cluster of size L^d is exponentially small and goes as $p^{L^d} \sim \exp(-cL^d)$, where c is a constant. However, for the classical system, the spins within this cluster have a relaxation time that is exponentially large (because of the activation energy that is needed to pull a domain wall through the cluster to turn it over), where the relaxation time $\sim \exp(\sigma L^{d-1})$, and σ is the surface tension. These two together render the final decay of the autocorrelation function faster than algebraic. Let us now consider the dynamics of a similar rare cluster of size L in the case of the dilute quantum Ising system in (55) which again occurs with a probability $\sim \exp(-cL^d)$. The quantum dynamics in this model is essentially due to barrier tunneling between two nearly degenerate minima of the cluster; for a small transverse field h , the energy gap between these two minima scales as $\exp(-\sigma' L^d)$. Consequently, the inverse of the tunneling rate (or the relaxation time) of the cluster scales as $\exp(\sigma' L^d)$; this (together with the probability $\sim \exp(-cL^d)$) in turn leads to an algebraic decay of the autocorrelation function. This algebraic decay is in fact a signature of gaplessness which signals the existence of GM singularities. We emphasize that it is the difference in the nature of dynamics (activated for a random CPT and barrier tunneling for a random QPT in transverse Ising models) which is at the root of the stronger GM singularities in a QPT.

(E). Quantum Ising model in a random longitudinal field

The classical Ising model in a site-dependent random longitudinal field with zero mean and non-zero variance is given by the Hamiltonian [253–256]

$$H = -J \sum_{\langle ij \rangle} S_i S_j - \sum_i h_i S_i. \quad (56)$$

This model shows an order-disorder transition from a FM phase ($m = \overline{S_i} \neq 0$) to PM phase ($m = 0$) at a critical temperature in dimensions greater than the lower critical dimension (d_l^c); the domain wall argument by Imry and MA [257] and also calculations on hierarchical lattices [258] showed that $d_l^c = 2$. Moreover, from LGW calculations it has been shown that $d_u^c = 6$ and thermal fluctuations are dangerously irrelevant for $d < d_u^c$ [259, 260]. The phase transition of a random field Ising model (RFIM) has been shown to be of the same universality class as that of a site-dilute Ising antiferromagnet in a longitudinal field [261, 262].

The quantum version of the model (56) is given as

$$H = -J_x \sum_{\langle ij \rangle} \sigma_i^x \sigma_j^x - h \sum_i \sigma_i^z - \sum_i h_L^i \sigma_i^x, \quad (57)$$

where $\overline{h_L^i} = 0$ and $\overline{h_L^i h_L^j} = \Delta \delta_{ij}$. The order-disorder transition in model (57) has been studied [92, 123, 161, 263–265] within mean field theory and ϵ -expansion calculations around the upper critical dimension. It has been shown that a TIM model in a random longitudinal field (57) is equivalent to a site-dilute Ising antiferromagnet in a transverse field [92].

The model in (57) has been studied using the imaginary time path integral formalism [123, 161, 264]; it can be shown that the random field couples only to the static ($\omega = 0$) part of the order parameter, and hence the lower and upper critical dimensions of the quantum models remain the same as those of the classical counterpart (see also [266]). It has also been shown that the quantum fluctuations are dangerously irrelevant. The critical exponents for the QPT are therefore identical to the classical model. In short, the random field fluctuations mask the quantum fluctuations and random field fixed point at ($T = h = 0$) is the critical fixed point. This has been established using a phenomenological scaling for quantum systems [265] which is an extension of the real space renormalization group (RSRG) studies of the classical model in (56) [267, 268]. The classical RFIM shows an activated dynamical behavior [269] due to the presence of free energy barriers which scale with the cluster size close to the critical point; it has been argued that in a quantum RFIM this effect is expected to be stronger as the domains are correlated in the Trotter direction [265].

Finally, let us point out some recent theoretical studies of the system LiHoF_4 . The magnetic phase diagram has been obtained by quantum Monte Carlo studies which go beyond the mean field theory and include the on-site hyperfine interaction through a renormalization of the transverse magnetic field [270], and also by employing a perturbative quantum Monte Carlo technique [271]. Although domain wall formation in these systems is favored due to the combination of strong Ising anisotropy and long-range forces, the long-range forces have been found to destroy the roughening transition [272]. The role of strong single-ion anisotropy in random field dipolar spin glasses has been studied in [273]. We conclude by mentioning some recent theoretical studies which especially include the effects of a random field [274–277].

We conclude this section by noting that disordered itinerant magnetic systems and related GM singularities have been studied in several interesting papers [278–281]; we refer to the review article [152] for relevant discussions.

IV. RELATED MODELS WITH FRUSTRATION

In this section, we shall study variants of TIMs in the presence of regular frustration, for example, models with competing nearest-neighbor and next-nearest-neighbor interaction or long-range antiferromagnetic interactions. The discussion will point to the fact that even the phase diagram of the model with minimal frustration is not yet fully understood.

(A). Quantum ANNNI model

The classical axial next-nearest-neighbor Ising (ANNNI) model was introduced by Fisher and Selke [282] to simulate the spatially modulated structures observed in magnetic and ferroelectric systems (for reviews see [283, 284]). The

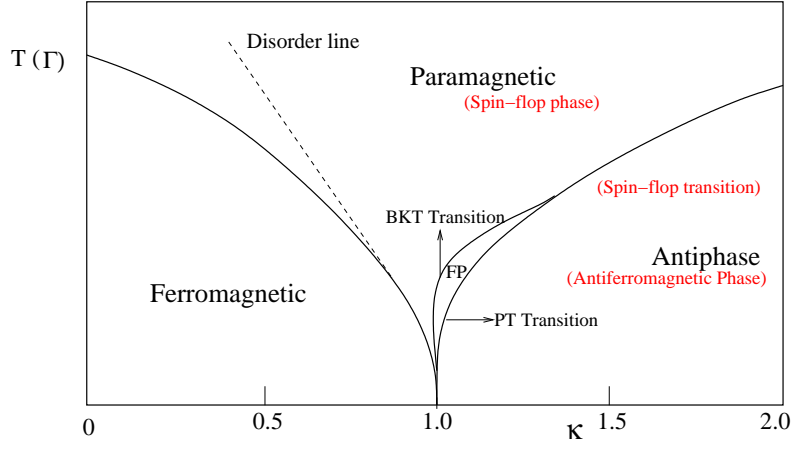


FIG. 8: (Color online) The phase diagram of a two-dimensional classical ANNNI model ($\tilde{J}_0 = \tilde{J}_1$) (58) and one-dimensional transverse ANNNI model (59) with x -axis as $\kappa = |\tilde{J}_2|/|\tilde{J}_1|$ or $\kappa = |J_2|/J_1$, respectively. The y axis denotes thermal fluctuations (T) for the $2d$ classical model and quantum fluctuations induced by the transverse field Γ for the $1d$ quantum model. As discussed in the text, the dual model (60) is expected to show an identical phase diagram but the corresponding phases are different and are shown in parenthesis in red. A bosonization study of (60) suggests that the quantum transition from the antiferromagnetic to the spin-flop phase far away from the multicritical point ($\kappa = 1$) is a spin-flop transition and there is no intermediate gapless floating phase.

model is described by a system of Ising spins with nearest-neighbor FM interactions in all directions as well as a competing next-nearest-neighbor antiferromagnetic interaction along one axis which leads to frustration in the model. The Hamiltonian for a two-dimensional system is

$$H = -\tilde{J}_0 \sum_{i,j} S_{i,j}^z S_{i,j+1}^z - \tilde{J}_1 \sum_{i,j} S_{i,j}^z S_{i+1,j}^z + \frac{\tilde{J}_2}{2} \sum_{i,j} S_{i,j}^z S_{i+2,j}^z, \quad (58)$$

where the $S_{i,j}$'s are binary classical variables with values ± 1 , i labels the layers perpendicular to the axial direction, \tilde{J}_0 denotes nearest-neighbor FM interactions within a layer, and \tilde{J}_1 and \tilde{J}_2 respectively denote ferromagnetic nearest-neighbor and antiferromagnetic next-nearest-neighbor interactions along the axial direction. The model given by (58) has been studied extensively over nearly three decades [283–288]. The phase diagram of the model obtained via analytical and numerical studies is presented in Fig. 8 with $\tilde{J}_0 = \tilde{J}_1$. It consists of a FM phase, a PM phase and an antiphase (with a modulated $++--$ structure with period 4) and a floating phase (FP) with incommensurate modulation where the spin-spin correlations decay algebraically separating the PM phase from the antiphase. The multicritical point at $\kappa = |\tilde{J}_2|/|\tilde{J}_1| = 1$ is infinitely degenerate with the degeneracy being equal to $[(1 + \sqrt{5})/2]^N$ for a system of N spins. A disorder line starts from this point and touches the temperature axis asymptotically; it divides the PM phase in two regions such that on the large κ side the exponential decay of correlations is modulated by periodic oscillations. The antiphase and the modulated phase are separated by a line corresponding to the Pokrovsky-Talapov (PT) transition [289–291] between a commensurate and an incommensurate phase, while the transition from the gapless modulated phase to the gapped PM phase is a BKT transition [104, 292]. There is probably a Lifshitz point at which the three phases, modulated, para and antiphase, meet.

We will review here some recent studies of the one-dimensional quantum ANNNI model [288, 293–296] in a transverse field which is related to the two-dimensional classical ANNNI model through the τ -continuum formalism [297–300]; hence they belong to the same universality class and a similar phase diagram is expected. The Hamiltonian is given by

$$H_A = \sum_i \left[-\frac{J_1}{2} \mu_i^x \mu_{i+1}^x + \frac{J_2}{4} \mu_i^x \mu_{i+2}^x + \frac{\Gamma}{4} \mu_i^y \right], \quad (59)$$

where the μ_i^α are Pauli matrices, and J_1 and J_2 are nearest-neighbor FM and next-nearest-neighbor antiferromagnetic Ising interactions, respectively, and Γ is the transverse magnetic field. The ground state is exactly solvable on the disorder line $\Gamma/J_1 = \kappa - 1/4\kappa$, [301–303], and is given by a direct product of certain spin configurations on each of the sites, i.e., is a matrix product state.

Although large parts of the phase diagram of this model are well established, the width of the floating phase shown in the above phase diagram for a quantum ANNNI chain (59) (and equivalently for the $2d$ classical ANNNI model in (58)) has been a subject of serious debate over last three decades. Analytical [13, 284, 286, 287, 291, 293] and numerical [304–308] studies of the phase diagrams of the two-dimensional classical ANNNI model and the one-dimensional quantum ANNNI model provide contradictory results about the extent of the floating phase. While some of these studies indicate that the floating phase, if it exists at all, is restricted to only a line [294, 305], other studies showed that the floating phase has a finite width [293, 306, 307]. We will address this particular issue in the present section.

The Hamiltonian in (59) has been studied using bosonization and the RG in recent years [293, 294]. Dutta and Sen [294] studied the dual Hamiltonian

$$H_D = \sum_i \left[\frac{J_2}{4} \sigma_i^x \sigma_{i+1}^x + \frac{\Gamma}{4} \sigma_i^y \sigma_{i+1}^y - \frac{J_1}{2} \sigma_i^x \right], \quad (60)$$

to address the issue of the width of the floating phase. Here, the σ_i^α are Pauli matrices dual to μ_i^α (for instance, $\sigma_i^x = \mu_i^x \mu_{i+1}^x$ and $\mu_i^y = \sigma_{i-1}^y \sigma_i^y$). Scaling this Hamiltonian by an appropriate factor gives

$$H = \sum_i \left[\frac{1+a}{4} \sigma_i^x \sigma_{i+1}^x + \frac{1-a}{4} \sigma_i^y \sigma_{i+1}^y + \frac{J_z}{4} \sigma_i^z \sigma_{i+1}^z - \frac{h}{2} \sigma_i^x \right], \quad (61)$$

where the parameters in Eqs. (60) and (61) are related as $a = J_2 - \Gamma/J_2 + \Gamma$, $h = 2J_1/J_2 + \Gamma$, and $J_z = 0$. The Hamiltonian in (61) describes a spin-1/2 XYZ chain with a magnetic field applied along one of the three directions; a non-zero value of J_z allows for the study of a more general model than the one in (60). We will assume that $-1 \leq a, J_z \leq 1$, $|J_z| < 1 \pm a$, and $h \geq 0$; it then turns out that the critical behavior of the Hamiltonian in (61) does not depend on J_z because, as discussed below, the Luttinger parameter K (which is a function of J_z) changes very little under the RG flows.

The model in (61) can be bosonized as described in Appendix C. For $a = h = 0$, the bosonic theory is governed by a parameter K given by (C28), namely, $1/K = 1 + (2/\pi) \arcsin(J_z)$. Up to second order, one finds the RG equations [294, 309–311],

$$\begin{aligned} \frac{dh}{dl} &= (2 - K - \frac{1}{4K})h - \frac{1}{K}ah - 4Kbh, \\ \frac{da}{dl} &= (2 - \frac{1}{K})a - (2K - \frac{1}{2K})h^2, \\ \frac{db}{dl} &= (2 - 4K)b + (2K - \frac{1}{2K})h^2, \\ \frac{dK}{dl} &= \frac{a^2}{4} - K^2b^2, \end{aligned} \quad (62)$$

where l denotes the logarithm of the length scale, and b is a coupling generated in the process of renormalization. Noting that K renormalizes very little, one finds remarkably that Eqs. (62) have a non-trivial fixed point (FP) given by

$$\begin{aligned} h^* &= \frac{\sqrt{2K^*(2 - K^* - 1/(4K^*))}}{2K^* + 1}, \\ a^* &= (K^* + \frac{1}{2}) h^{*2}, \quad \text{and} \quad b^* = \frac{a^*}{2K^*}. \end{aligned} \quad (63)$$

For $K^* = 1$ (corresponding to $J_z = 0$), the FP is at $(a^*, b^*, h^*) = (1/4, 1/8, 1/\sqrt{6})$. Fig. IV (A) shows the numerically obtained RG flows in (62) projected on to the $a-h$ plane with $b = 0$, $K = 1$ and a, h chosen to be very small initially; the flow of K has been ignored [294].

The non-trivial FP has two stable directions, one unstable direction and one marginal direction; the last one corresponds to changing K^* and simultaneously a^* , b^* and h^* to maintain the relations in Eqs. (63). The presence of two stable directions implies that there is a two-dimensional surface of points, in the space of parameters (a, b, h) , which flows to this FP; the system is gapless on that surface. A perturbation in the unstable direction produces a gap in the spectrum. A small perturbation of size δa at the FP with $(K^*, a^*, b^*, h^*) = (1, 1/4, 1/8, 1/\sqrt{6})$ in that direction will produce a gap in the spectrum which scales as $\Delta E \sim |\delta a|^{1/1.273} = |\delta a|^{0.786}$; the correlation length is then given by $\xi \sim 1/\Delta E \sim |\delta a|^{-0.786}$. In the gapped regions A ($\delta a > 0$) and B ($\delta a < 0$), the RG flows are towards $a = \infty$ and $a, h \rightarrow -\infty$, respectively.

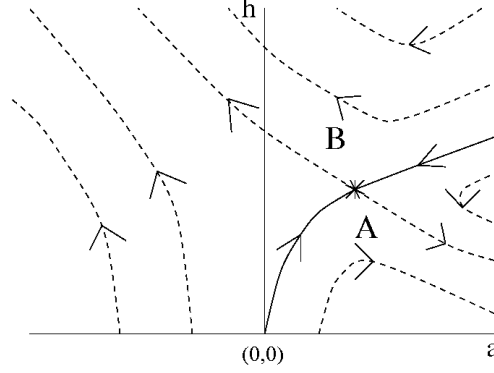


FIG. 9: RG flow diagram in the (a, h) plane of a XYZ model where a is the anisotropy and h is the longitudinal field. The solid line shows the set of points which flow to the FP at $a^* = 0.246$, $h^* = 0.404$ marked by an asterisk. The dotted lines show the RG flows in the gapped phases A and B (see text). The dual version of the ANNNI model shows a similar RG flow in the bosonization picture. (After Dutta and Sen, 2003).

To distinguish between the phases A and B we introduce an order parameter, namely, the staggered magnetization in the \hat{y} direction, defined in terms of a ground state expectation value as $m_y = [\lim_{i \rightarrow \infty} (-1)^i \langle S_0^y S_i^y \rangle]^{1/2}$. This is zero in phase A; hence the Z_2 symmetry is unbroken. In phase B, m_y is non-zero, and the Z_2 symmetry is broken. The scaling of m_y with the perturbation δa can be found as follows [312, 313]. At $a = h = 0$, the leading term in the long-distance equal-time correlation function of σ^y is given by $\langle \sigma_0^y \sigma_i^y \rangle \sim (-1)^n / |i|^{1/2K}$ giving the scaling dimension of σ_i^y to be $1/(4K)$. In a gapped phase in which the correlation length is much larger than the lattice spacing, m_y will therefore scale with the gap as $m_y \sim (\Delta E)^{1/(4K)}$. If we assume that the scaling dimension of σ_i^y at the non-trivial FP remains close to $1/(4K)$, then the numerical result quoted above for $K = 1$ implies that $m_y \sim |\delta a|^{0.196}$ for δa small and negative.

The bosonization study is valid only if a, h are small, i.e., if J_2/J_1 is large, and it predicts a vanishingly small width of the FP in the phase diagram in (8). At $J_2/J_1 \simeq 1$, the situation is quite different for the following reason. Exactly at $\kappa = 1$ and $\Gamma = 0$, the Hamiltonian in (60) is $H_{MC} = (J_2/4) \sum_i (\sigma_i^x - 1)(\sigma_{i+1}^x - 1)$. This is a multicritical point with a ground state degeneracy growing exponentially with the system size, since any state in which every pair of neighboring sites $(i, i+1)$ has at least one site with $\sigma^x = 1$ is a ground state. For $J_2 - J_1$ and Γ non-zero but small, one can argue, using lowest order perturbation theory within the large space of degenerate states [284, 286–288, 291], that the low-energy properties of the model in (60) do not change if $\Gamma \sigma_i^y \sigma_{i+1}^y$ is replaced by $(\Gamma/2)(\sigma_i^y \sigma_{i+1}^y + \sigma_i^z \sigma_{i+1}^z)$.¹⁰ Thus the fully anisotropic model in (60) becomes equivalent to a different model which is invariant under the $U(1)$ symmetry of rotations in the $y - z$ plane. The $U(1)$ symmetric model has been studied earlier using bosonization which shows a finite width of the gapless region separating two gapped phases [309, 314]; in the bosonization study by Dutta and Sen [294], the symmetry away from the MCP is Z_2 which reduces this region to a line.

To summarize, the transition from phase A to phase B can occur either through a gapless line (if a, h are small), or through a gapless phase of finite width (if a, h are large). The complete phase diagram of the ground state of the dual model in (60) is shown in Fig. 8 incorporating all the possibilities discussed above where different phases are shown in parenthesis. The three major phases are distinguished by the following properties of the expectation values of the different spin components. In the antiferromagnetic phase, the spins point alternately along the \hat{x} and $-\hat{x}$ directions. In the spin-flop phase, they point alternately along the \hat{y} and $-\hat{y}$ directions, with a uniform tilt towards the \hat{x} direction. In the FM phase, all the spins point predominantly in the \hat{x} direction. The antiferromagnetic and spin-flop phases are separated by a floating phase of finite width for κ close to 1, and by a spin-flop transition line for large values of κ . It has been conjectured that the floating phase and the spin-flop transition line are separated by a Lifshitz point as indicated in Fig. 8. We note that in terms of the original quantum Hamiltonian in (59), the antiphase is in fact the antiferromagnetic phase while the PM phase is the spin-flop phase in the dual model in (60).

Taking the classical limit ($S \rightarrow \infty$) [315, 316] of (61) and minimizing the ground state energy, one finds a phase

¹⁰ This is because the difference between the two kinds of terms is given by operators which, acting on one of the degenerate ground states, take it out of the degenerate space to an excited state in which a pair of neighboring sites have $\sigma^x = -1$.

transition line $h^2 = 4a$. This denotes a spin-flop transition from a phase with an antiferromagnetic alignment of the spins with respect to the y -axis (with a small tilt towards the x -axis if h is small) to an antiferromagnetic alignment of the spins with respect to the x -axis. Moreover the symmetry is enhanced from a Z_2 symmetry away from the line to a $U(1)$ symmetry (of rotations in the $x - y$ plane) on the line. One therefore expects a gapless mode in the excitation spectrum corresponding to the Goldstone mode of the broken continuous symmetry which can be found explicitly by going to the next order in a $1/S$ expansion [316]. It may be mentioned here that spin-flop transitions in one-dimensional spin-1/2 systems have been studied earlier [317–319].

The corresponding numerical studies need to be mentioned here. A study based on the cluster heat bath algorithms [304] points to a finite width of the gapless phase in the finite temperature phase diagram of the two-dimensional classical ANNNI model. In contrast, a subsequent study based on the non-equilibrium relaxation method [305] showed that its width is infinitesimally small and the correlation length diverges in a power-law fashion as this line is approached from the antiphase side. The one-dimensional quantum ANNNI model has been studied using the density matrix renormalization group technique [320]; while no evidence of the floating phase is found for $\kappa < 1$ [321], the floating phase with a finite width seems to exist for $\kappa > 1$ and extends for very large $\kappa \simeq 5$ [306]. A very recent study [322] which uses finite entanglement scaling of the matrix product state in the one-dimensional quantum ANNNI system seems to corroborate the findings of Beccaria *et al.* [306]. The discussion above shows that even after thirty years of exploration, the phase diagram of a quantum ANNNI chain is not yet fully understood.

The model in (61) with $a = 0$ has been studied theoretically in [312, 313, 323, 324]. A number of phases have been found as a function of J_z and h , including Neel and FM order along the z axis (depending on the magnitude and sign of J_z), Neel order along the y axis (the spin-flop phase), and a phase with no long-range order. Experimentally, a system with $a = 0$ and magnetic fields along both \hat{x} and \hat{z} directions has been studied in [325], where the two Neel phases and the spin-flop phase have been found.

An n -component quantum rotor model (see (21)) with ANNNI-like regular frustration in some of the spatial directions given by the Hamiltonian

$$H_R = \frac{g}{2} \sum_i \hat{L}_i^2 - J_1 \sum_{\langle ij \rangle} \hat{x}_i \cdot \hat{x}_j + J_2 \sum_{\langle\langle ij \rangle\rangle} \hat{x}_i \cdot \hat{x}_j, \quad (64)$$

where $\langle\langle \dots \rangle\rangle$ denotes next-nearest-neighbor interaction, has been studied in recent years [326, 327]. In this model, in addition to the nearest-neighbor FM interactions J_1 , there exists a next-nearest-neighbor antiferromagnetic interaction J_2 along m of the d spatial directions. The zero-temperature phase diagram of the model shows the existence of a (d, m) quantum Lifshitz point (QLP) [326, 328, 329] where the FM, PM and helically ordered phases meet; this is a quantum generalization of a classical Lifshitz point [330–332]. The QPT at a QLP is an example of an anisotropic QCP with correlation time $\xi_\tau \sim \xi_{||}^{z_{||}} \sim \xi_{\perp}^{z_{\perp}}$ where $\xi_{||}$ (ξ_{\perp}) is the spatial correlation length in m ($d - m$) directions with (without) frustration. Using the Gaussian propagator, it can be shown [326] that $z_{||} = 2z_{\perp} = 2$, $2\nu_{||} = \nu_{\perp} = 1/2$ for an anisotropic QLP with $m < d$, with the upper critical dimension being $d_u^c = 3 + m/2$. We note that the scaling valid close to a QLP has been observed experimentally. The magnetic fluctuations in $\text{CeCu}_{6-x}\text{Au}_x$, which has a QCP at $x = 0.1$ separating a heavy fermion paramagnet from an antiferromagnet, has been studied using inelastic neutron scattering [333]. The form of the susceptibility so obtained has been explained in terms of a QLP and the value of $2/z_{||}$ is found to be 0.8 in contrast to the mean field prediction $2/z_{||} = 1$.

(B). Models with long-range antiferromagnetic interactions

In this section, we discuss the properties of the long-range transverse Ising antiferromagnet (LRTIAF) with a disorder in the cooperative interactions superposed on it [334–338]. The general model one studies is given by the Hamiltonian

$$H = - \frac{1}{N} \sum_{ij(j>i)} J_{ij} \sigma_i^x \sigma_j^x - h \sum_i \sigma_i^z, \quad (65)$$

where one assumes that the pairwise interactions J_{ij} 's are chosen from a Gaussian distribution, $P(J_{ij}) = \exp[-(J_{ij} - J_0)^2/2\tilde{J}^2]/\sqrt{2\pi}\tilde{J}$, and $J_0 (< 0)$ is the parameter controlling the strength of the antiferromagnetic bias. We thus recover the 'pure' antiferromagnetic Ising model with infinite range interactions when we consider the disorder-free limit $\tilde{J} \rightarrow 0$. The model with $J_0 > 0$ and $h = 0$ is identical to the classical SK model [168].

In the mean field limit, one can derive an effective single site Hamiltonian [163]

$$H = \vec{h}_{\text{eff}} \cdot \sum_{i=1}^N \vec{\sigma}_i \quad \text{where} \quad \vec{\sigma}_i = \sigma_i^z \hat{z} + \sigma_i^x \hat{x}, \quad (66)$$

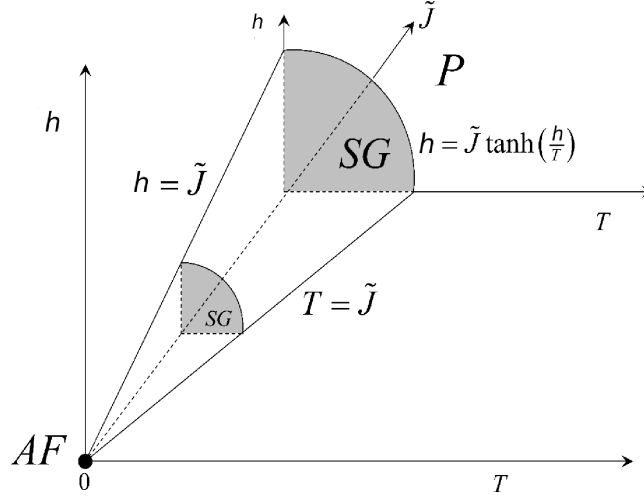


FIG. 10: Schematic phase diagram for the quantum system given in (65). The antiferromagnetic order (AF) exists if and only if we set $h = T = \tilde{J} = 0$. As \tilde{J} decreases, the spin glass (SG) phase gradually shrinks to zero and eventually ends up at an antiferromagnetic phase at its vertex (for $h = T = \tilde{J} = 0$). The phase boundary between the spin-glass and paramagnetic (P) phase is $h = \tilde{J} \tanh(h/T)$ as obtained from mean field theory. (After Chandra *et al.*, 2010).

and $\vec{h}_{\text{eff}} = (J_0 m + \tilde{J} \sqrt{q} y) \hat{z} + h \hat{x}$; we can then calculate the magnetization $m \equiv N^{-1} \sum_i \langle \sigma_i^x \rangle$ and spin-glass order parameter $q \equiv N^{-1} \sum_i \langle \sigma_i^x \rangle^2$ in a self-consistent manner. In the disorder-free case with $h = 0$, one observes indications of a very unstable quantum antiferromagnetic (AF) phase (50% spins up and 50% spins down without any sub-lattice structure) which gets destabilized by both infinitesimal thermal (classical) as well as quantum fluctuations induced by h . In the presence of spin glass-like disorder the AF phase is destabilized and a spin glass order sets in; this eventually gets destroyed as the thermal or quantum fluctuations increase beyond their threshold values and a transition to a para phase occurs. This mean field calculations are supported by numerical simulations although the replica symmetric solution indicates some corrections.

The resulting mean field phase diagrams for the quantum model is presented in Fig. 10; we find that an infinitesimal disorder is enough to induce a stable glass order which eventually gets destroyed due to thermal or quantum fluctuations leading to a transition to the para phase. As shown in Fig. 10, the antiferromagnetic phase of the LRTIAF (occurring only at $h = T = \tilde{J} = 0$) can get ‘frozen’ into a spin glass phase if a little SK-type disorder is added ($\tilde{J} \neq 0$). It is noteworthy that the degeneracy factor of $e^{0.693N}$ for the ground state of the LRTIAF with $h = 0$ is much larger than the factor of $e^{0.199N}$ for the classical SK model. Hence, because of the presence of full frustration, the LRTIAF possesses a surrogate incubation property of a stable spin glass phase which can be induced by the addition of a small amount of disorder. However, the effect of replica symmetry breaking on these phases is yet to be explored.

V. THEORETICAL STUDIES OF QUANTUM PHASE TRANSITION AND INFORMATION

In this section, our main focus is on the connection between QPTs in transverse spin models and quantum information theory [339–343]. Quantum information theoretic measures like the concurrence, fidelity, entanglement entropy, etc., are able to capture the ground state singularities associated with a QPT. More importantly, as we shall discuss below, these measures show interesting scaling behavior close to the QCP which is given in term of some of the quantum critical exponents. We shall also show how the integrability of the transverse Ising/ XY chains and the qubit form of the ground state as given in (30) turn out to be extremely useful for studying quantum information theoretic measures [344–346].

(A). Entanglement

We start our discussion with a brief review on the behavior of concurrence close to the QCP of transverse spin models.

(a). Concurrence

The knowledge of pairwise entanglement in a quantum many-body system can provide a characterization of the ground state wave function close to a QCP. In fact, non-analyticities characterizing a QPT are in general directly related to the bipartite entanglement measures [347]. The concurrence, which is one of the measures of pairwise entanglement between two spins separated by n lattice spacings in a spin-1/2 chain, is defined as [343, 348, 349]

$$C^n = \max\{\sqrt{\lambda_1^n} - \sqrt{\lambda_2^n} - \sqrt{\lambda_3^n} - \sqrt{\lambda_4^n}, 0\}, \quad (67)$$

where the λ_i^n 's are the eigenvalues of the positive Hermitian matrix $\sqrt{\rho^n} \tilde{\rho}^n \sqrt{\rho^n} = \sqrt{\rho^n} (\sigma^y \otimes \sigma^y) \rho^{n*} (\sigma^y \otimes \sigma^y) \sqrt{\rho^n}$ in decreasing order [348, 349], and ρ^n is the two-spin density matrix for two sites i and $j = i + n$, which is obtained by integrating the total density matrix over all the other spins; the eigenvalues λ_i are invariant under unitary transformations of the two qubits which implies that they are independent of the basis. The case $C^n = 1$ corresponds to maximum entanglement between the two spins while $C^n = 0$ denotes the absence of entanglement. For the transverse field spin chains, the density matrix ρ^n can be expressed in terms of different correlators [350]:

$$\rho^n = \begin{pmatrix} a_+^n & 0 & 0 & b_1^n \\ 0 & a_0^n & b_2^n & 0 \\ 0 & b_2^{n*} & a_0^n & 0 \\ b_1^{n*} & 0 & 0 & a_-^n \end{pmatrix}, \quad (68)$$

where the matrix elements are given in terms of the two-spin correlation functions as follows:

$$a_{\pm} = \left\langle \frac{1}{4} (1 \pm \sigma_i^z) (1 \pm \sigma_{i+n}^z) \right\rangle, \quad (69)$$

$$a_0^n = \left\langle \frac{1}{4} (1 \pm \sigma_i^z) (1 \mp \sigma_{i+n}^z) \right\rangle, \quad (70)$$

$$b_{1(2)}^n = \langle \sigma_i^- \sigma_{i+n}^{-(+)} \rangle. \quad (71)$$

The other correlators such as $\langle \sigma_i^{\pm} (1 \mp \sigma_{i+n}^z) \rangle$, and hence the other matrix elements of ρ^n , vanish if there is a symmetry under $\sigma_i^x \rightarrow -\sigma_i^x$, $\sigma_i^y \rightarrow -\sigma_i^y$ and $\sigma_i^z \rightarrow \sigma_i^z$, as is true for the transverse XY Hamiltonian. Using the available analytical results [22, 31, 56], the above correlators and hence the entanglement of the ground state can be obtained exactly.

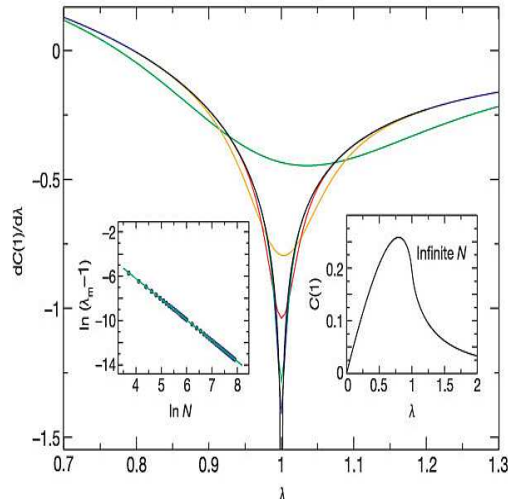


FIG. 11: (Color online) In the figure $C(1) = C^1$ and $\lambda = h$. For a transverse Ising chain, the minima gets pronounced with increasing system size (top to bottom) and also the position of the minima approaches the value $\lambda_c = h_c = 1$ (left inset). The right inset shows the variation of $C(1)$ as a function of λ for a thermodynamic system (After Osterloh *et al.*, 2002).

The pairwise entanglement can be used to indicate the proximity to a QCP as has been shown for the transverse Ising chain in (9) [351, 352]. The concurrence tends to vanish in the limits when the transverse field $h \rightarrow 0$ and $h \gg h_c = 1$

(choosing $J_x = 1$) since the ground of the system is then fully polarized along the \hat{x} and \hat{z} directions, respectively. It has also been observed that the concurrence is practically zero unless two sites are at most next-nearest neighbors even at the QCP where the correlation length diverges in the thermodynamic limit; the next-nearest-neighbor concurrence is smaller by one order of magnitude than the nearest-neighbor value [351]. This observation signifies that the non-local quantum part of the two-point correlations is indeed short-ranged.

The nearest-neighbor concurrence C^1 is a smooth function of the field h showing a maximum close to QCP (see Fig. 11), while the next-nearest-neighbor concurrence is maximum at the QCP. The derivative of C^1 captures the signature of criticality and diverges as

$$\frac{\partial C^1}{\partial h} \sim \frac{8}{3\pi^2} \ln |h - h_c|, \quad h_c = 1, \quad (72)$$

in the thermodynamic limit ($L \rightarrow \infty$) on approaching the QCP. Eq. (72) yields a quantitative measure of the non-local correlations in the quantum critical region. For a finite system, one can use the finite size scaling theory [96] which predicts that in the vicinity of the transition point, the concurrence scales with the combination $L^{1/\nu}(h - h_m)$, where $h_m(L)$ is the value of h where the derivative $\partial C^1/\partial h$ is minimum for a system of size L . For a logarithmic divergence, the scaling ansatz is of the form

$$\partial_h C^1(L, h) - \partial_h C^1(L, h_0) \sim Q[L^{1/\nu}(h - h_m)] - Q[L^{1/\nu}(h_0 - h_m)], \quad (73)$$

where $\partial_h \equiv \partial/\partial h$ and h_0 is some non-critical value. The scaling function goes as $Q(x) \sim Q(\infty) \ln x$ for large x . The critical value scales as $h_m(L) \sim h_c + L^{-1.86}$, while the derivative satisfies the scaling form

$$\partial_h C^1(L, h_m) = -0.2702 \ln L + \text{constant}. \quad (74)$$

The ratio of prefactors of the logarithms in Eqs. (72) and (74) yields the critical exponent $\nu(= 1)$ of the transverse Ising chain; this suggests that although the concurrence describes short-range properties, it is able to capture the scaling behavior of a QCP.

For a transverse XY chain, the above scaling relation has been verified [352] for the Ising transition with $0 < \gamma < 1$ (Fig. 12). However, the range of entanglement is not universal and tends to infinity as $\gamma \rightarrow 0$. The total entanglement $\sum_n C^n$ is found to be weakly dependent on γ . Studies of the entanglement in the transverse XY chain in the presence of a single defect [353] and many defects [354] show that the finite size scaling of the concurrence is drastically modified in the presence of disorder, and strong disorder eventually kills the critical behavior.

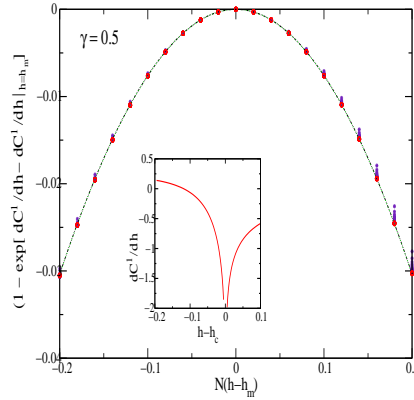


FIG. 12: (Color online) The universality hypothesis for the entanglement is verified in transverse XY chain with $\gamma = 0.5$ and N ranging from 41 up to 401. Data collapse shows that $\nu = 1$ for the Ising transition. The inset shows the divergence at the critical point for the infinite system. (After Osterloh *et al.*, 2002).

The transverse Ising and XY chains have been extremely useful for studying thermal entanglement [351], localizable entanglement [355], macroscopic multi-species entanglement [356], and the propagation and dynamics of entanglement [357–359]. We refer the reader to [344], for an extensive discussion. We note that usually a continuous QPT is associated with a singularity in the derivative of the ground state concurrence while a first order QPT shows discontinuities in the ground state concurrence [360–362].

In conclusion, we would like to point out that a quantum critical environment can also induce entanglement between two qubits which are coupled to it. Coupling two spin-1/2's initially in a separable state to a transverse XY chain which is initially in the ground state, one can calculate the reduced density matrix and hence the concurrence of the central system as a function of time. At a fixed time, one observes a sharp decay of the concurrence on the anisotropic critical line (see Fig. 2) as $\gamma = J_x - J_y \rightarrow 0$ and $-(J_x + J_y) \leq h \leq J_x + J_y$, whereas the concurrence can become nearly unity away from the QCP [363].

Another commonly used measure of entanglement between two spin-1/2 objects is called negativity $\mathcal{N}(\rho)$ [364, 365]. This will be discussed in Sec. VI(J) (a); see (154). To calculate negativity, one takes a partial transpose (ρ^T) of a bipartite mixed state described by ρ ; the negativity $\mathcal{N}(\rho)$ is then given by the sum of the absolute values of the negative eigenvalues of ρ^T . If the two objects are entangled $\mathcal{N} > 0$.

(b). *Entanglement entropy*

Motivated by the works of Fiola *et al.* [366], and Holzhey *et al.* [128], in the context of black hole physics, another important measure of entanglement was introduced in which a composite system (which is in a pure state) is partitioned into two distinct sub-systems A and B . The entanglement between A and B is measured by the von Neumann entropy associated with the reduced density matrix of one of the subsystems; this is called the entanglement entropy [129, 367]; for a review, see [368]. The entropy is invariant under local unitary transformations, and is continuous and additive in the sense that for a direct product state $|\psi\rangle \otimes |\phi\rangle$, $S(|\psi\rangle \otimes |\phi\rangle) = S(|\psi\rangle) + S(|\phi\rangle)$. For a quantum spin chain with N spins with the ground state $|\psi_0\rangle$, the reduced density matrix of a block of l neighboring spins is $\rho_l = \text{tr}_{N-l} |\psi_0\rangle\langle\psi_0|$ (i.e., $N-l$ spins of the environment are integrated out). Then the entanglement entropy of the block with the rest of the system is given by $S_l = -\text{tr}(\rho_l \log_2 \rho_l)$ [129]. For a translationally invariant ground state, S_l is a concave function of l , i.e., $S_l \geq (S_{l-m} + S_{l+m})/2$ where $l = 0, \dots, N$, and $m = 0, \dots, \min\{N-l, l\}$.

According to the area law [369], the entropy S_l depends only on the surface of separation between the two regions A and B . In a d -dimensional system, this implies that $S_l \sim l^{d-1}$ [368, 370]. Therefore, the entanglement entropy for systems with one spatial dimension should be independent of the block size which is indeed the case when the system is off-critical (gapped). However, in the gapless (critical) case, S_l diverges logarithmically with the block size, with the prefactor of the logarithmic term being universal and related to the central charge c of the underlying conformal field theory [128], i.e., $S_l \sim (c/3) \log_2(l/a)$, where a is the lattice spacing. Away from the critical point, when the system has a finite correlation length $\xi \gg a$, the block entropy saturates to a value $S_l \sim (c/3) \log_2(\xi/a)$ for $l \rightarrow \infty$. The above result was extended at the critical point of the thermodynamic system; for example, with periodic boundary conditions, one gets [128] $S_l \sim (c/3) \log_2[(N/\pi a) \sin(\pi l/N)]$. At finite temperature, one gets [371, 372]

$$S_l = \frac{c}{3} \log_2 \left[\frac{\beta}{\pi a} \sinh\left(\frac{\pi \beta}{l}\right) \right] + A,$$

where $\beta = 1/(k_B T)$ and A is some non-universal constant. Of course, a finite temperature block entropy is not unexpected because the initial state is necessarily mixed.

The entanglement between two halves of an infinitely long chain close to a QCP that is described by a conformal field theory has also been studied [371]; it is given by $S \sim (c/6) \log_2 \xi$ and $\sim (c/3) \log_2 \xi$ for open and periodic boundary conditions, respectively; this is because in the periodic boundary condition, the contribution comes from two boundaries. This result can be generalized as follows. If an infinitely long system consists of a finite subsystem A which has n disjoint blocks, each of which has a length much larger than ξ , the entanglement entropy of A with the rest of the system is given by $(c/3)n \log_2 \xi$ [371]. In the opposite case of a critical system ($\xi = \infty$) with n disjoint blocks, the form of the entanglement entropy is much more complicated and has been studied in [373] and [374].

(i) Pure systems:

The entanglement entropy of transverse Ising/ XY spin chains has been studied extensively in recent years [129, 375–378]. Using the mapping to Majorana fermions, it has been shown that on the anisotropic critical line with $\gamma = 0$ (Fig. 2), $S_l = 1/3 \log_2 l + b$, where b is a constant close to $\pi/3$ [129, 375]. This is in agreement with the conformal field theory prediction noting that the central charge for the underlying CFT is $c = 1$ (see Sec. II(B)). On the Ising critical line, on the other hand, one gets a logarithmic scaling with the coefficient $1/6$ which is expected since the central charge $c = 1/2$. Hence, for a one-dimensional TIM ($J_y = 0$), one gets $S_l = 1/6 \log_2 l + b$.

We mention here some interesting work on the scaling of the entanglement entropy near the critical point of the transverse XY chain [62, 63]. Let us ask how well the matrix product approximation for the ground state of a critical system can reproduce the entanglement entropy between two halves of a system. If the matrices A_i in (6) are D -dimensional, it is clear that their information content can increase with increasing D . We therefore expect that

the matrix product form may be able to correctly reproduce the properties of a critical system (whose correlation length ξ is infinitely large) if we take the limit $D \rightarrow \infty$. Let us therefore make the ansatz that there is a matrix product state with D -dimensional matrices which has the same properties as the ground state of a system with a large correlation length ξ if these scale with each other as $\xi \sim D^\kappa$ for $\xi \rightarrow \infty$ [62, 63]. It is then found that this ansatz reproduces the entanglement entropy of two halves of an infinitely long system, $S = (c/6) \log_2 \xi = (c\kappa/6) \log_2 D$, if κ is related to the central charge c of the critical system as

$$\kappa = \frac{6}{c(1 + \sqrt{12/c})}. \quad (75)$$

A generalized version of the entanglement entropy between a part A of a system with the rest of the system is given by the Renyi entropies [379, 380]

$$S_\alpha = \frac{1}{1-\alpha} \log_2 \text{Tr}(\rho_A)^\alpha. \quad (76)$$

Note that the limit of S_α as $\alpha \rightarrow 1$ gives the von Neumann entropy; in principle, a knowledge of S_α for all values of α allows us to infer the complete spectrum of eigenvalues of ρ_A . In a critical one-dimensional system with central charge c , the Renyi entropies of a block of length l lying in the middle of the system are given by

$$S_\alpha = \frac{c}{6} \left(1 + \frac{1}{\alpha}\right) \log_2 l \quad (77)$$

plus non-universal constant terms. For a Tomonaga-Luttinger liquid (see Appendix C) with Fermi momentum k_F and Luttinger parameter K , there are subleading corrections to (77) which are of the form $\cos(2k_F l)/(2l \sin k_F)^{2K/\alpha}$ with non-universal coefficients [379]. We note that the entanglement entropy has also been studied for a two-dimensional quantum model belonging to the Lifshitz universality class with $z = 2$ [381]. The experimental observation of entangled states of magnetic dipoles will be discussed in Sec. 7 [345].

(ii) Random systems:

In Sec. III (B), we have discussed that the QCPs associated with a random transverse Ising spin chain is an IRFP. In the presence of infinitesimal randomness, the RG flow is from the pure fixed point to the IRFP. According to the c -theorem [382] if the RG flow is from the critical point A to B , then the associated central charges satisfy the relation, $c_A \geq c_B$. The possibility of a pure-random c -theorem in random Ising spin chains has been explored using the entanglement entropy as a measure. In [155, 383], the entanglement entropy of a segment of l spins of such a chain given in (53) has been studied at the QCP. Exploiting the properties of the IRFP, it has been shown that the universal logarithmic scaling still holds though conformal invariance is lost. One can argue that for a segment of length l embedded in an infinite chain, the frozen clusters which are totally inside or outside the segment l do not affect the total entanglement. The only contribution comes from the number of decimated clusters which cross the two edges. Each of such clusters contribute $\ln 2$ to the entropy resulting in $S_L \sim 2p \ln 2 \langle D \rangle_l$, where $\langle D \rangle_l$ is the average number of decimations that occur at the edge, and p is the probability that a field is decimated instead of a coupling; the self-duality of the model yields $p = 1/2$, and using the properties of the IRFP in a random Ising chain it can be shown that $\langle D \rangle_l \sim (1/3) \log_2 l$. We eventually get $S_L^{\text{dis}} \sim \frac{\ln 2}{6} \log_2 l + \kappa_1$; for a random XY chain with $\gamma = 0$, one gets $S_L^{\text{dis}} \sim \frac{\ln 2}{3} \log_2 l + \kappa_2$, where κ_1 and κ_2 are non-universal constants. Comparison with the pure system leads to following observations: (i) there is a loss of entropy due to randomness, and (ii) the effective central charges of the random chain are related to those of the pure chain as $c^{\text{dis}} = \ln 2 \times c^{\text{pure}}$; $c^{\text{pure}} = 1/2$ for the Ising transition. These charges determine the universality class of the associated IRFP. For this spin chain, disorder is a relevant perturbation and the RG flow is from the pure fixed point to the IRFP. Hence, the observation $c^{\text{pure}} > c^{\text{dis}}$ is consistent with the c -theorem [382].

The above study has been extended to generalized random chains with Z_q symmetry [227] given in (54) with $\alpha_n = \sin(\pi/q)/\sin(\pi n/q)$. The entanglement entropy is found to be $S_l = \frac{\ln q}{6} \log_2 l$ so that the effective central charge is $c_q^{\text{dis}} = \frac{\ln q}{6}$; comparing with the central charge of the pure chain $c_q^{\text{pure}} = 2(q-1)/(q+2)$, one finds an increase of the effective central charge at the IRFP for $q > 41$ which apparently rules out the possibility of a pure-to-random c -theorem mentioned above. However, an intermediate disorder critical line separating weak and strong disorder phase may exist in these models, as discussed in Sec. III (B) and one therefore, can not conclusively rule out the possibility of a pure-random c -theorem [155].

The logarithmic dependence of S_l^{dis} has been verified numerically for random XY (with $\gamma = 0$) [384] and Heisenberg chains [385]. Generalizing the strong disorder RG to $d = 2$, for a random transverse Ising model, a double logarithmic correction to the area law was pointed out in contrast to the $d = 1$ case [386, 387].

(B). Quantum discord

A different and significant measure of quantum correlations between two spins other than entanglement, namely “quantum discord” was introduced in [388], (see also [389]) which exploits the fact that different quantum analogs of equivalent classical expressions can be obtained because of the fact that a measurement perturbs a quantum system. While the concurrence is a measure of quantum correlations based on separability of states, the discord, on the other hand, is a measurement based measure of the same. There are quantum states which are completely separable but the discord (and hence the quantum correlation) is not necessarily zero.

The information associated with a classical system is quantified in terms of the Shannon entropy $H(p)$ where p is the probability distribution of the system. If the system comprises two subsystems A and B , the mutual information is defined as $I(p) = H(p^A) + H(p^B) - H(p)$, where $H(p^i)$, $i = A, B$, stands for the entropy associated with the subsystem i ; this can alternatively be expressed as $J(p) = H(p^A) - H(p|p^B)$, where $H(p|p^B) = H(p) - H(p^B)$ is the conditional entropy. In the classical context, $I(\rho) = J(\rho)$.

In the quantum context, the classical Shannon entropy functional gets replaced by the quantum von Neumann entropy expressed in terms of the density matrix ρ acting on the composite Hilbert space. The natural quantum extension of the mutual information is given by

$$I(\rho) = s(\rho^A) + s(\rho^B) - s(\rho). \quad (78)$$

The conditional entropy derived through local measurements however alters the system. A local measurement is of the von Neumann type defined by a set of one-dimensional projectors $\{\hat{B}_k\}$ which sum up to identity. Following a local measurement only on the subsystem B , the final state ρ_k of the composite system is given by $\rho_k = (1/p_k)(\hat{I} \otimes \hat{B}_k)\rho(\hat{I} \otimes \hat{B}_k)$, with the probability $p_k = \text{tr}(\hat{I} \otimes \hat{B}_k)\rho(\hat{I} \otimes \hat{B}_k)$ where \hat{I} is the identity operator for the subsystem A . The quantum conditional entropy can be defined as $s(\rho|\{\hat{B}_k\}) = \sum_k p_k s(\rho_k)$, such that the measurement based quantum mutual information takes the form $J(\rho|\{\hat{B}_k\}) = s(\rho^A) - s(\rho|\{\hat{B}_k\})$. This expression maximized based on the local measurement gives the classical correlation [390, 391]. Hence we have

$$C(\rho) = \max_{\{\hat{B}_k\}} J(\rho|\{\hat{B}_k\}). \quad (79)$$

We arrive at two quantum analogs of the classical mutual information: the original quantum mutual information $I(\rho)$ (78) and the measurement induced classical correlation (79). As introduced by Olliver and Zurek [388], the difference between these two, i.e.,

$$Q(\rho) = I(\rho) - C(\rho) \quad (80)$$

is the quantum discord which, being the difference between total information (correlation) I and the classical correlation C , measures the amount of quantumness in the state; a non-zero Q implies that all the information about the correlation between A and B cannot be extracted by local measurement on B .

The studies of quantum discord for spin systems close to QCPs have established a natural connection between QPTs and quantum information theories [388, 392–398]. The Z_2 symmetry of the one-dimensional transverse Ising chain in (9) enables us to write the density matrix for two spins separated by a lattice spacing n given in (68) and thereby to calculate quantum discord. The total correlation I is calculated using the eigenvalues of the reduced density matrices for subsystems A and B , while the classical correlations are derived by introducing a set of projection operators for part B parametrized on the Bloch sphere and optimizing for the polar and azimuthal angles [392–394].

Quantum discord is also able to capture the QPT occurring at transverse field $h = h_c = 1$ ($J_x = 1$). For a chain of length L , one finds the following.

- (i) The derivative of the nearest-neighbor classical correlation with respect to h shows a pronounced minimum at h_m which approaches $h_c = 1$ as $L \rightarrow \infty$. The derivative at h_m shows a logarithmically divergence with L . This behavior surprisingly resembles that of the behavior of nearest-neighbor concurrence shown in Fig. 11.
- (ii) In contrast, the first derivative of the nearest-neighbor quantum discord, $\partial Q/\partial h$, has a point of inflection at h_m while the second derivative has a pronounced maximum that shows a quadratic logarithmic divergence in the thermodynamic limit. This observation leads to the conclusion that near a QCP, Q and the concurrence show quite different scaling behaviors. Although the study of discord in quantum critical systems is in its infancy, an experimental study to measure quantum discord using an NMR set up has already been reported [399].

(C). Quantum fidelity

In this section, we will study an information theoretic measure known as the quantum fidelity which is able to capture ground state singularities associated with a QPT. In the present context, fidelity is defined as the overlap

between the ground states of a quantum Hamiltonian calculated for two different values of some external tunable parameter, e.g., the transverse field in TIMs. The study of quantum fidelity dates back to 1967 when P. W. Anderson showed that the ground state fidelity for a system of N fermions vanishes in the thermodynamic limit $N \rightarrow \infty$ [400]. This phenomenon is shared by many other quantum many body systems (see e.g., [401, 402]) and is known as the Anderson orthogonality catastrophe. Quantum fidelity is currently being studied extensively as an indicator of a QPT without making reference to an order parameter [403]; for a review see [404].

The ground state fidelity between two ground states of a d -dimensional quantum mechanical Hamiltonian $H(\lambda)$ described by parameters λ and $\lambda + \delta$ is defined as

$$F(\lambda, \delta) = |\langle \psi_0(\lambda) | \psi_0(\lambda + \delta) \rangle|. \quad (81)$$

For small system sizes, the overlap is usually expected to be close to unity if the two states are very close to each other in the parameter space. In contrast, the fidelity should vanish in the limit in which the states are orthogonal which is the case close to a QCP where the fidelity shows a sharp dip (see Fig. 13). We emphasize that in the limit $N \rightarrow \infty$, the fidelity vanishes irrespective of the proximity to a QCP even though a sharper decay in the fidelity is expected close to a QCP [403].

Let us consider a Hamiltonian of the form

$$H(\lambda) = H_0 + \lambda H_I \quad (82)$$

which satisfies the eigenvalue equation

$$H(\lambda) |\psi_m(\lambda)\rangle = E_m(\lambda) |\psi_m(\lambda)\rangle, \quad (83)$$

where $m = 0, 1, 2, \dots$. Let H_0 describe a QCP while H_I is a driving term which does not commute with H_0 .

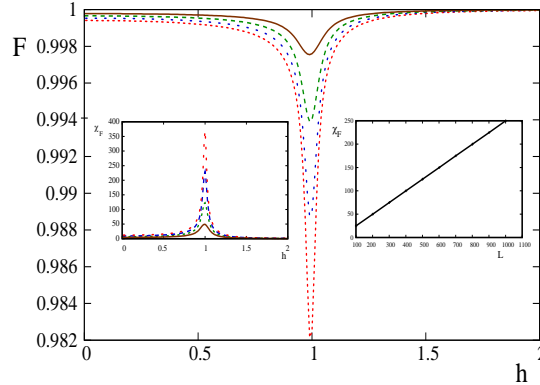


FIG. 13: (Color online) The fidelity between two ground states of a transverse Ising chain with transverse fields h and $h + \delta$, with $\delta = 0.1$, is plotted as a function of h for small system sizes. The fidelity shows a dip around the QCP at $h = 1$ ($J_x = 1$). One observes a sharper decay at the QCP when the system size increases. Left inset shows the divergence of the fidelity susceptibility which again becomes prominent with increasing system size. Right inset shows the scaling $\chi_F \sim L$ at the QCP.

When $\delta \rightarrow 0$, the overlap $\langle \psi_0(\lambda) | \psi_0(\lambda + \delta) \rangle$ between two ground states infinitesimally separated in the parameter space can be expanded using a Taylor expansion,

$$\langle \psi_0(\lambda) | \psi_0(\lambda + \delta) \rangle = 1 + \delta \langle \psi_0(\lambda) | \frac{\partial}{\partial \lambda} | \psi_0(\lambda) \rangle + \frac{\delta^2}{2} \langle \psi_0(\lambda) | \frac{\partial^2}{\partial \lambda^2} | \psi_0(\lambda) \rangle + \dots \quad (84)$$

The term linear in δ is the Berry connection term which gives rise to the Pancharatnam-Berry phase [405, 406].

(i) Fidelity susceptibility

We now introduce the concept of fidelity susceptibility valid in the limit $\delta \rightarrow 0$ [28, 407–418]. We can use the expansion

$$|\psi_0(\lambda + \delta)\rangle \simeq |\psi_0(\lambda)\rangle + \delta \sum_{n \neq 0} \frac{\langle \psi_n(\lambda) | H_I | \psi_0(\lambda) \rangle |\psi_n(\lambda)\rangle}{E_n - E_0} + \dots$$

to express the fidelity in the form

$$F(\lambda, \delta) = 1 - \frac{1}{2}\delta^2 L^d \chi_F(\lambda) + \dots, \quad (85)$$

where the term linear in δ vanishes due to the normalization condition of the wave function, and L is the linear dimension of the system. The quantity $\chi_F = -(2/L^d) \lim_{\delta \rightarrow 0} (\ln F)/\delta^2 = -(1/L^d)(\partial^2 F/\partial \delta^2)$ is called the fidelity susceptibility (FS) and is given by

$$\chi_F(\lambda) = \frac{1}{L^d} \sum_{m \neq 0} \frac{|\langle \psi_m(\lambda) | H_I | \psi_0(\lambda) \rangle|^2}{[E_m(\lambda) - E_0(\lambda)]^2}. \quad (86)$$

It is useful to compare the form of χ_F with the ground state specific heat density given by

$$\chi_E = -\frac{1}{L^d} \frac{\partial^2 E_0}{\partial \lambda^2} = -\frac{2}{L^d} \sum_{m \neq 0} \frac{|\langle \psi_m(\lambda) | H_I | \psi_0(\lambda) \rangle|^2}{E_m(\lambda) - E_0(\lambda)}, \quad (87)$$

which diverges at the QCP following the scaling relation $|\lambda|^{-\alpha}$. We note that Eq. (85), defined for a fixed system size $N = L^d$, describes a situation where the fidelity is close to unity even at the critical point; however, as we will show below, the scaling of the FS is dictated by some of the quantum critical exponents.

Using the scaling relation $\chi_E \sim |\lambda|^{-\alpha}$ along with the hyperscaling relation $2 - \alpha = \nu(d + z)$ valid below the upper critical dimension, the scaling relation of the FS close to the QCP can be readily obtained [419, 420]. One finds that $\chi_F \sim |\lambda|^{\nu d - 2}$ away from the QCP ($|\lambda|^{-\nu} \ll L$), while close to the QCP ($|\lambda|^{-\nu} \gg L$), finite size scaling [96] yields a modified scaling relation $\chi_F \sim L^{2/\nu - d}$. Therefore, we conclude that χ_F diverges when $\nu d < 2$. For $\nu d > 2$, although the FS appears to vanish at $\lambda = 0$ in the thermodynamic limit, a non-zero value of the FS is expected due to non-universal high-energy modes which are insensitive to the presence of a QCP [419].

These scaling relations have been verified for the transverse Ising model on a square lattice using extensive Monte Carlo simulations [420]. Very recently, the above scaling has been generalized to the case of an anisotropic QCP [421] as is seen at a semi-Dirac band crossing point [422]. At an anisotropic QCP, characterized by critical exponents ν_1 in m spatial directions and ν_2 in the other $(d - m)$ directions, $\chi_F \sim L^{2/\nu_1 - \nu_1/\nu_2(d - m) - m}$ which reduces to the conventional scaling when $\nu_1 = \nu_2$. Also the finite size scaling of the bipartite entanglement and the ground state fidelity have been used to study the QCP in the one-dimensional Bose-Hubbard model [423].

The FS can be related to the connected imaginary time ($\bar{\tau}$) correlation function of the perturbation $H_I(\bar{\tau})$ using the relation [407, 410]

$$\chi_F(\lambda) = \int_0^\infty d\bar{\tau} \bar{\tau} \langle H_I(\bar{\tau}) H_I(0) \rangle_c, \quad (88)$$

where we define $H_I(\bar{\tau}) = \exp(H\bar{\tau})H_I \exp(-H\bar{\tau})$, $\bar{\tau}$ being the imaginary time, and $\langle H_I(\bar{\tau}) H_I(0) \rangle_c = \langle H_I(\bar{\tau}) H_I(0) \rangle - \langle H_I(\bar{\tau}) \rangle \langle H_I(0) \rangle$. Assuming $H_I = \sum_{\vec{r}} V(\vec{r})$ and using the scaling $r' = br$, $\bar{\tau}' = b^z \bar{\tau}$ and $V(r') = b^{-\Delta_V} V(r)$ for a change of length scale by a factor b , one finds from (88) that the scaling dimension of χ_F is given by $\dim[\chi_F] = 2\Delta_V - 2z + d$, i.e., $\chi_F \sim L^{2z + d - 2\Delta_V}$ at the QCP; away from the QCP ($L > \xi \sim \lambda^{-\nu}$), $\chi_F \sim \lambda^{-\nu(2z + d - 2\Delta_V)}$. A marginal or relevant perturbation H_I (so that λH_I scales as the energy, $\lambda H_I \sim \lambda^{\nu z}$) allows us to make an additional simplification coming from the fact that the scaling dimension of H_I is $\Delta_{H_I} = z - 1/\nu$ [418, 419], so that $\chi_F \sim L^{2/\nu - d}$ at $\lambda = 0$ as derived previously.

For the transverse XY chain in (10), the ground state can be written in a direct product form for a chain of L sites (spins) (see (30)). One then finds that the fidelity between neighboring states is given by $F = \prod_{k>0} \cos(\theta_k - \theta'_k)$ [403]. Now, under a change in the transverse field from h to $h + dh$, the FS can be derived by writing the fidelity in the form $F \simeq \exp(-\delta^2 L^d \chi_F/2)$ as

$$\chi_F = \frac{1}{L} \sum_{k>0} \left(\frac{\partial \theta_k}{\partial h} \right)^2 = \frac{1}{L} \sum_{k>0} \frac{\gamma^2 \sin^2 k}{[(h + \cos k)^2 + \gamma^2 \sin^2 k]^2}, \quad (89)$$

where we have set $J_x + J_y = 1$. At the Ising critical point ($\lambda = h - 1 = 0$), one obtains using the continuum limit

$$\chi_F \sim \int_{-\frac{\pi}{L}}^{\frac{\pi(L-1)}{L}} dk \frac{\gamma^2 k^2}{\gamma^4 k^4} \sim L, \quad (90)$$

where $\pi - k \rightarrow k$. This is consistent with the scaling $\chi_F \sim L^{2/\nu-d}$ noting that the Ising critical exponents $\nu = z = 1$ and $d = 1$ [403] (see the right inset of Fig. 13). On the other hand, away from the critical point, i.e., $\lambda \gg L^{-1}$ when one can essentially assume k to be continuous, we get

$$\chi_F \sim \int_0^\infty \frac{dk}{2\pi} \frac{\gamma^2 k^2}{((\lambda + \frac{k^2}{2})^2 + \gamma^2 k^2)^2} \sim \lambda^{-1}, \quad (91)$$

which is again in agreement with the proposed scaling $\chi_F \sim \lambda^{\nu d - 2}$.

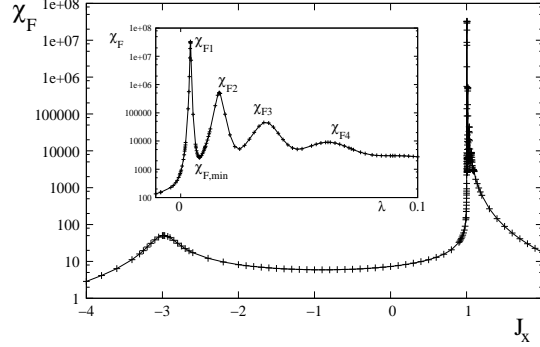


FIG. 14: The variation of χ_F with J_x , as obtained numerically, for a system size of $L = 100$. We have fixed $h = 2J_y = 2$. The peak near the Ising critical point $J_x = -3$ scales as L , whereas the peak near the MCP at $J_x = 1$ shows a L^5 divergence. Inset: The oscillatory behavior of the FS is a signature of the presence of the quasicritical modes. Each of the maxima, denoted by χ_{Fj} , $j = 1, 2, \dots$, scales as L^5 . (After Mukherjee *et al.*, 2010).

While the FS close to a QCP satisfies the conventional scaling relations proposed above, surprises emerge when the same is calculated close to a quantum multicritical point. One finds remarkable features like oscillations in FS and its anomalous scaling with the system size. To illustrate these, let us consider the case $J_y = 2h$ and calculate the overlap by changing the parameter J_x so that the chain is at a critical point for $J_x = -3J_y$ and at a multicritical point (MCP) for $J_x = J_y$ [424] (see Fig. 21). The FS ($\chi_F = (1/L) \sum_k (\partial\theta_k/\partial J_x)^2$) is then found to be

$$\chi_F = \frac{1}{L} \sum_k \frac{(J_y \sin k + 2J_y \sin 2k)^2}{[(h + (J_x + J_y) \cos k)^2 + ((J_x - J_y) \sin k)^2]^2}. \quad (92)$$

As expected from the scaling relation given above, one finds that $\chi_F \sim L$ at the Ising critical point ($h = -3J_y$). However, close to the quantum MCP ($J_x = J_y$), one finds a stronger divergence of the maximum value of FS given by $\chi_F^{\max} \sim L^5$ (see Fig. 14); this cannot be explained using standard scaling relations because the critical exponents associated with the MCP are $\nu_{mc} = 1/2$ and $z_{mc} = 2$. Also, oscillations of the FS are observed close to the quantum MCP. This observation can be attributed to the existence of quasicritical points close to the MCP. For a finite chain, these quasicritical points are points of local minima of energy (also see Sec. VI (E)) which lie on the FM side of the MCP. The exponents associated with these quasicritical points appear in the scaling relation of the maximum value of the FS, i.e., $\chi_F^{\max} \sim L^{2/\nu_{qc}-d}$; for the present model it can be easily shown that $\nu_{qc} = 1/3$. As we move away from the MCP, the FS oscillates and attains a maximum whenever a quasicritical point is hit. As we approach the thermodynamic limit, these quasicritical points approach the MCP.

We now consider studies of the FS for a path defined in a multidimensional parameter space [410, 414] when more than one parameter is varied; such a situation arises in the transverse XY model when the MCP is approached by simultaneously tuning the transverse field and the anisotropy γ [424]. Motivated by the geometrical interpretation of fidelity which is in fact the angle between two vectors in the Hilbert space, one can define a measure known as the Fubini-Study distance, d_{FS} , given by [414, 425]

$$d_{FS} = \cos^{-1} F(|\psi_0\rangle, |\psi_0 + \delta\psi_0\rangle). \quad (93)$$

Here $|\psi_0\rangle$ and $|\psi_0 + \delta\psi_0\rangle$ represent two ground states infinitesimally spaced in the parameter space so that F is close to unity, allowing for the expansion $d_{FS}^2 \simeq 2(1 - F)$. We consider a M -dimensional parameter space spanned by λ_a , $a = 1, 2, \dots, M$, with Hamiltonian given by $H = H_0 + \sum_a \lambda_a H_a^q$; the QCP is at $\lambda_i = 0$ for all $i = 1, 2, \dots, M$. Using a Taylor expansion, $\delta\psi_0 = \sum_a \partial_a \psi_0 d\lambda^a$ where $\partial_a \psi_0 \equiv \partial\psi_0/\partial\lambda_a$, one obtains $d_{FS}^2(|\psi_0\rangle, |\psi_0 + \delta\psi_0\rangle) = L^d \sum_{a,b} g_{ab} d\lambda_a d\lambda_b$.

Consequently, the fidelity is given by

$$F = 1 - \frac{L^d}{2} \sum_{ab} g_{ab} d\lambda_a d\lambda_b. \quad (94)$$

In (94), g_{ab} stands for the FS and is the real part of a complex geometric tensor given by [410]

$$\begin{aligned} Q_{ab} &= \frac{1}{L^d} [\langle \partial_a \psi_0 | \partial_b \psi_0 \rangle - \langle \partial_a \psi_0 | \psi_0 \rangle \langle \psi_0 | \partial_b \psi_0 \rangle] \\ &= \frac{1}{L^d} \sum_{n \neq 0} \frac{\langle \psi_0(\lambda) | \partial_a H | \psi_n(\lambda) \rangle \langle \psi_n(\lambda) | \partial_b H | \psi_0(\lambda) \rangle}{[E_n - E_0]^2}. \end{aligned} \quad (95)$$

The imaginary part of Q_{ab} gives the curvature two-form of the geometric phase. Using a similar scaling analysis of the connected correlation function defined in a M -dimensional space as shown above, we can readily show that $Q_{ab} \sim L^{2z+d-\Delta_a-\Delta_b}$ at the QCP, where Δ_a is the scaling dimension of the operator $H_I^a = \partial H / \partial \lambda_a|_{\lambda_i=0}$, for $i = 1, 2, \dots, M$. Using the relevant or marginal nature of the driving operators, this scaling can be recast into the form $Q_{ab} \sim L^{1/\nu_a+1/\nu_b-d}$, where ν_a is the correlation length exponent associated with the perturbation λ_a ; the scaling reduces to the simple form $\chi_F \sim L^{2/\nu-d}$ for a path with $\lambda_a = \lambda_b = \lambda$. In this connection, it has recently been shown that the geometric phase (GP) shows an interesting scaling behavior close to the QCP of the transverse XY chain (10) given by some of the quantum critical exponents [426–432]; we present a note on these studies in Appendix D.

The FS approach has been implemented to identify the quantum phase transition from a gapless to a gapped phase in the Kitaev model [433] when the interaction J_3 is varied; at the QCP at which the system enters the gapless phase (see Fig. 6), $\chi_F \sim L^{1/2}$. This can be explained noting the anisotropic nature of the associated critical point with $\nu_1 = 1/2, \nu_2 = 1, d = 2$ and $m = 1$ [150]. Moreover, in the gapless phase $\chi_F \sim \ln L$, while no such scaling is observed inside the gapped phase [434]. The phase transition in the Kitaev model has also been studied using the fidelity per site approach [435].

Finally, we recall the extended Ising model in (11) with a matrix product ground state. One can find the fidelity between two ground states with parameters $g_1 = g + \delta$ and $g_2 = g - \delta$ for a spin chain of length L [28, 64], given by

$$F = \frac{[(1 + \sqrt{g_1 g_2})^L + (1 - \sqrt{g_1 g_2})^L]}{[\sqrt{(1 + g_1)^L + (1 - g_1)^L} \sqrt{(1 + g_2)^L + (1 - g_2)^L}]}, \quad (96)$$

which shows that F is symmetric in both g and δ . The fidelity in (96) decays exponentially if the two states are in the same phase, but shows a strong oscillatory behavior with an exponentially decaying envelope for two states in different phases [64]. At the QCP ($\lambda = g = 0$), the FS scales as L which is consistent with the scaling $L^{2/\nu-d}$ with $\nu = d = 1$; similarly, away from the QCP, $\chi_F \sim g^{-1}$ in agreement with the scaling $\chi_F \sim \lambda^{\nu d-2}$ [28]. In the thermodynamic limit [436] for $|\delta| \ll |g| \ll 1$, the fidelity takes the form $F \simeq \exp(-\delta^2 L/2|g|)$.

We conclude with a brief note on random spin chains. The scaling of the FS can also be useful for determining the critical point and GM singularities (see Sec. III (B)) in a disordered transverse XY chain [437]; this can be mapped to quasi-free fermions using the JW transformation although the system is not reducible to decoupled 2×2 problems due to the loss of translational invariance. The results derived using the FS approach predicts the presence of Griffiths singular regions in the vicinity of the Ising and anisotropic transition lines (see Fig. 2). Moreover, the scaling analysis of the FS shows a complete disappearance of the anisotropic transition (for some disorder distributions) and the emergence of a GM phase; this is in congruence with the previous study of the same model based on a mapping to Dirac fermions with random mass [124].

(ii) Fidelity per site and fidelity in the thermodynamic limit:

The advantage of using the FS approach is that the parameter δ gets factored out in the Taylor expansion rendering the FS dependent on λ alone; however this approach fails to describe the Anderson orthogonality catastrophe. In an alternative approach [64, 438, 439], the ground state fidelity per site, defined as $\mathcal{F}(\lambda, \delta) = \lim_{N \rightarrow \infty} F^{1/N}(\lambda, \delta)$, $N = L^d$ or $\ln \mathcal{F} = \lim_{N \rightarrow \infty} \ln F(\lambda, \delta)/N$, is calculated in the large system limit with an arbitrary δ , in contrast to the FS approach in which N is small and $\delta \rightarrow 0$. As a result, the fidelity differs significantly from unity. It has been shown that \mathcal{F} is able to detect QPTs in the transverse XY chain and the Kitaev model on the hexagonal lattice. In particular, using the direct product form of the ground state in (30) for an anisotropic transverse XY chain, \mathcal{F}

between two ground states with transverse fields h and h' is given by

$$\begin{aligned}\ln \mathcal{F}(h, h') &= \lim_{L \rightarrow \infty} \frac{1}{L} \sum_{k>0} \ln [\cos(\theta_k - \theta'_k)] \\ &= \frac{1}{2\pi} \int_0^\pi \ln [\cos(\theta_k - \theta'_k)] dk.\end{aligned}\quad (97)$$

Numerical studies show that the first derivative of $\mathcal{F}(h, h')$ shows a logarithmic divergence of the form $\partial \mathcal{F}(h, h')/\partial h \sim \kappa_1 \ln |h - h_c|$ as $h \rightarrow h_c = J_x + J_y = 1$, in the thermodynamic limit. On the other hand, $(\partial \mathcal{F}(h, h')/\partial h)|_{h_m} \sim \kappa_2 \ln L$, where h_m , as defined previously, is the effective critical point at which $\partial \mathcal{F}(h, h')/\partial h$ shows a pronounced maximum for large L . The ratio of the non-universal coefficients yields the exponent ν ; $\nu = |\kappa_1/\kappa_2| \approx 1$ [439].

As seen from Eq. (85) and also the preceding discussion, the knowledge of χ_F should be sufficient to draw conclusions about the behavior of F and the associated QCP for small system sizes and in the limit $\delta \rightarrow 0$ ($\delta^2 L^d \chi_F/2 \ll 1$). However, in the thermodynamic limit ($L \rightarrow \infty$ at fixed δ), the expansion in Eq. (85) up to the lowest order becomes insufficient. Recently, Rams and Damski [436] have proposed a generic scaling relation valid in the thermodynamic limit given by

$$\ln F(\lambda - \delta, \lambda + \delta) \simeq -L^d |\delta|^{\nu d} A\left(\frac{\lambda}{|\delta|}\right), \quad (98)$$

where A is a scaling function; this relation interpolates between the fidelity susceptibility approach and the fidelity per site approach. In deriving the scaling relation in Eq. (98), it is assumed that the fidelity per site is well behaved in the limit $L \rightarrow \infty$, the QCP is determined by a single set of critical exponents, and $\nu d > 2$ so that non-universal corrections are subleading [419]. In particular, at the critical point $\lambda = 0$, the fidelity, measured between the ground states at $+\delta$ and $-\delta$, is non-analytic in δ and satisfies the scaling $\ln F \sim -L^d |\delta|^{\nu d}$. On the other hand, away from the QCP, i.e., for $|\delta| \ll |\lambda| \ll 1$, the scaling gets modified to $\ln F \sim -L^d \delta^2 |\lambda|^{\nu d - 2}$. This scaling has been verified for an isolated quantum critical point using one-dimensional transverse Ising and XY Hamiltonians [436]. Moreover, near a QCP a cross-over has been observed from the thermodynamic limit ($L|\delta|^\nu \gg 1$) to the non-thermodynamic (small system) limit ($L|\delta|^\nu \ll 1$) where the concept of fidelity susceptibility becomes useful. We note that Eq. (98) is an example of the Anderson orthogonality catastrophe [400] which states that the overlap of two states vanishes in the thermodynamic limit irrespective of their proximity to a QCP. For the transverse Ising chain with $h \neq h_c$, it was found that $F(g, \delta) \simeq \exp(-L\delta^2/16|h - h_c|)$ which reduces to the result derived above for the FS when the argument of the exponent is small and at the same time provides a new result when the lowest order Taylor expansion is insufficient; one finds no non-analyticity in δ as we are away from the critical point. The scaling in (98) has recently been generalized to a massless Dirac fermions and the two-dimensional Kitaev model [150].

(iii) Other fidelity measures:

So far, our discussion has been limited to pure states. The concept of fidelity has been generalized to mixed states through a measure known as the reduced fidelity [440, 441] in which the two ground states in a fidelity analysis are replaced with two states differing slightly in the driving parameter and describing only a local region A of the system of interest. The reduced fidelity between two states described by reduced density matrices $\rho_A(\lambda)$ and $\rho_A(\lambda')$ for two parameters λ and λ' is defined as

$$F(\lambda, \lambda') = \text{Tr} \sqrt{\sqrt{\rho_A(\lambda')} \rho_A(\lambda) \sqrt{\rho_A(\lambda')}}. \quad (99)$$

The states under consideration describe a subsystem A ; ρ_A , obtained by tracing out the rest of the system from the total density matrix, usually describes a mixed state. In contrast, for a pure state, $\rho_A = |\psi\rangle\langle\psi|$ and $F(\lambda, \lambda')$ reduces to the modulus of the overlap $|\langle\psi(\lambda')|\psi(\lambda)\rangle|$. Denoting $\lambda' = \lambda + \delta\lambda$ and taking the limit $\delta\lambda \rightarrow 0$, we can define a FS analogous to the pure state case as $\chi_F = -2 \lim_{\delta\lambda \rightarrow 0} \ln F/(\delta\lambda)^2$. In the context of a QPT, the reduced fidelity has been introduced in connection to fidelity per site and renormalization flows [442]. Even though the reduced fidelity encodes local properties of a quantum system, surprisingly it is also able to capture the signature of both order-disorder [443–448] and topological [449] QPTs. For a transverse Ising chain the susceptibility associated with the reduced fidelity diverges logarithmically as $\chi_F(h) \sim \ln^2 |h - h_c|$ as $h \rightarrow h_c = 1$ which is a slower divergence in comparison to the global fidelity case [449].

The notion of reduced fidelity for mixed states can be further generalized to finite temperatures using thermal mixed states $\rho = (1/\mathcal{Z}) \sum_n \exp(-\beta E_n) |\psi_n\rangle\langle\psi_n|$, where the canonical partition function $\mathcal{Z} = \sum_n \exp(-\beta E_n)$ [450].

To define the mixed state fidelity of two thermal states with small perturbations in the inverse temperature β and driving parameter λ , we rewrite (99) in the form

$$F(\beta_0, \lambda_0; \beta_1, \lambda_1) = \text{Tr} \sqrt{\sqrt{\rho_0} \rho_1 \sqrt{\rho_0}}, \quad (100)$$

where $\rho_\alpha = \exp(-\beta_\alpha H(\lambda_\alpha)) / \mathcal{Z}(\beta_\alpha, \lambda_\alpha)$ with $\alpha = 0, 1$; we consider the limit $\beta_1 = \beta + \delta\beta$ and $\lambda_1 = \lambda_0 + \delta\lambda$ where perturbation theory is applicable. In the limit $\beta_0, \beta_1 \rightarrow \infty$, (100) reduces to the ground state fidelity. When $\delta\lambda = 0$ and $\lambda_0 = \lambda$, one can define the thermal fidelity which can be simplified to the form

$$F_\beta(\beta_0, \beta_1, \lambda) = \frac{\mathcal{Z}\left(\frac{\beta_0 + \beta_1}{2}, \lambda\right)}{\sqrt{\mathcal{Z}(\beta_0, \lambda) \mathcal{Z}(\beta_1, \lambda)}}.$$

F_β can be related to well-known thermodynamic quantities [407, 414, 433, 451], e.g., the FS defined as $\chi_F = -2 \ln F / (\delta\beta)^2|_{\delta\beta \rightarrow 0}$ can be shown to be proportional to the specific heat, and has been useful for studying the classical phase transition at a finite temperature [452, 453]. On the other hand, $F(\lambda, \lambda + \delta\lambda, \beta)$ defined at a fixed β has been employed to detect the finite temperature signature of a QPT as occurs in the transverse Ising chain [450, 454]. It has been found that although there is a decay in the fidelity right at the QCP at low temperatures, the sharpness diminishes with increasing temperatures and the decay is eventually wiped out at high temperatures.

(D). Quantum critical environment: decoherence and Loschmidt echo

In recent years, there has been great interest in studies of decoherence, namely, the quantum-classical transition by a reduction from a pure state to a mixed state [389, 455–457], specially from the viewpoint of quantum measurements and computations when a quantum system or qubit is coupled to a macroscopic environment. In connection to the quantum-classical transition in quantum chaos, the concept of Loschmidt echo (LE) has been proposed to describe the hyper-sensitivity of the time evolution of the system to the perturbations experienced by the surrounding environment [458–461]. Zurek and Paz [462] argued that for a quantum system with a classically chaotic Hamiltonian, the rate at which the environment loses information about the initial state (e.g., the rate of production of von Neumann entropy calculated using the reduced density matrix of the system) is independent of the coupling strength between the system and the environment and is governed by the classical Lyapunov exponent for a wide window of the coupling strength.

The measure of the LE is the overlap between two states that evolve from the same initial state $|\psi_0\rangle$ under the influence of two Hamiltonians H_0 and $H_0 + V$, where V is a perturbation; the mathematical expression is

$$L(t) = |\langle \psi_0 | e^{i(H_0+V)t} e^{-iH_0 t} | \psi_0 \rangle|^2. \quad (101)$$

In some of the recent works, attempt has been made to connect these two fields by studying the behavior of the LE close to a QCP as a probe to detect the quantum criticality. In this section, we will study the dynamics of a central spin coupled to a spin system (environment) and discuss that the decay of the Loschmidt echo can indicate the proximity to a QPT in the surrounding spin chain [463]. In the process, we shall also point out the close connection between quantum fidelity and the echo.

We consider the central spin model in which a central spin-1/2 (qubit) is coupled to the environment which is chosen to be a transverse XY chain in (10) with N spins. Denoting the ground state and excited wave functions of the central spin as $|g\rangle$ and $|e\rangle$, respectively, one can write the Hamiltonian incorporating the interaction between the central spin and all the spins of the chain as [463]

$$H = - \sum_{i=1}^{N-1} (J_x \sigma_i^x \sigma_{i+1}^x + J_y \sigma_i^y \sigma_{i+1}^y) - h \sum_{i=1}^N \sigma_i^z - \delta(J_x + J_y) \sum_{i=1}^N |e\rangle\langle e| \sigma_i^z, \quad (102)$$

where the spin chain couples to only the excited state $|e\rangle$ of the central spin. One assumes that the central spin is in a pure state $|\phi_s(t=0)\rangle = c_e|e\rangle + c_g|g\rangle$ with $|c_e|^2 + |c_g|^2 = 1$. If the spin chain is initially prepared in the ground state $|\psi_0\rangle$, then the evolution of the spin chain gets split into two branches $|\psi_\alpha(t)\rangle = \exp(-iH_\alpha t)|\psi_0\rangle$, with $\alpha = g, e$; the total wave function is $\psi_T = c_g|g\rangle \otimes |\psi_g(t)\rangle + c_e|e\rangle \otimes |\psi_e(t)\rangle$. We note that H_α , for $\alpha = g$ and e , represents XY chains with transverse fields h and $h + \delta(J_x + J_y)$, respectively. Therefore the coupling between the central spin and the environmental spin chain provides two channels of evolution of the spin chain with two different Hamiltonians. This leads to the decay of the Loschmidt echo defined as $L(J_x, J_y, \gamma, t) = |\langle \psi_g(t) | \psi_e(t) \rangle|^2$.

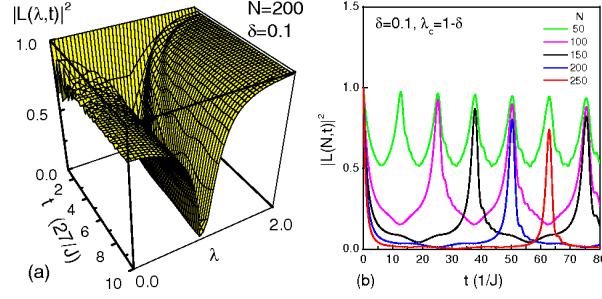


FIG. 15: (Color online) In the figure $\lambda = h$. Left panel: Three-dimensional (3d) diagram of the LE, $|L(\lambda, t)|^2$, as a function of λ and t for a system with $N = 200$. The valley around the critical point $\lambda_c = 1$ indicates that the decay of the LE is enhanced by the QPT. Right panel: The cross section of the 3d plot for different system sizes and $\lambda = \lambda_c - 0.1 = 0.9$. It shows that the period of the LE depends on the size of the surrounding spin chain. (After Quan *et al*, 2006).

Using the JW and Bogoliubov transformations (see Sec. II (A)), one can derive the exact analytical expression for the Ising case ($J_x = 1$ and $J_y = 0$),

$$L(t) = \prod_{k>0} G_k = \prod_{k>0} [1 - \sin^2(2\alpha_k) \sin^2(\omega_k^e t)], \quad (103)$$

where $\alpha_k = [\theta_g^k - \theta_e^k]/2$ with $\theta_g^k = \arctan(-\sin k/(\cos k - h))$ and $\theta_e^k = \arctan(-\sin k/(\cos k - (h + \delta)))$, and ω_k^e is the excitation energy for the transverse field $h + \delta$. Defining a cut-off wave vector k_c , it has been shown [463] that $L(t) \simeq \exp(-\Gamma t^2)$ as $h \rightarrow h_c = 1$, where $\Gamma = \delta^2 E(k_c)/(1 - h)^2$, $E(k_c) = 4\pi^2 N_c(N_c + 1)(2N_c + 1)/6N^2$, and N_c is the integer closest to $n\pi k_c/(Na)$ with a being the lattice spacing; hence one may expect an exponential decay of $L(t)$ in the vicinity of h_c when N is large. Numerical studies for a finite system ($N = 50$ to 250 and $\delta = 0.1$) show (i) a highly enhanced decay of L at a fixed time around the critical point of the surrounding system, and (ii) collapses and revivals of $L(t)$ as a function of time if $h + \delta = 1$, the period of the revival being proportional to N , i.e., the size of the surrounding system as shown in Fig. 15. The decay and revival of the echo is an indicator of a QPT. The present study has been generalized to the XY spin chain [464, 465], where it has also been shown that the ground state geometric phase of the central spin and its derivative with h have a direct connection to the QPT of the surrounding system as discussed in Sec. V (C). The decay parameter γ is found to scale as $1/N^{2z}$ which is verified close to the quantum MCP of the XY spin chain [466].

Rossini *et al* [467], studied a generalized central spin model in which the qubit interacts with a single spin of the environmental transverse Ising spin chain and it has been shown that the decay of the LE at short time is given by the Gaussian form $\exp(-\Gamma t^2)$ where the decay rate Γ depends on the symmetries of the phases around the critical point and the critical exponents. For instance, for such systems with local coupling, it has also been reported that Γ has a singularity in its first derivative as a function of the transverse field at the QCP [467]. In a subsequent work [468], the LE has been used as a probe to detect QPTs experimentally; at the same time, using a perturbative study in the short-time limit, the scaling relation $\Gamma \sim (\lambda)^{-2z\nu}$ valid close to a QCP (at $\lambda = 0$) has been proposed. In contrast to these studies where the coupling between the qubit and the environment is chosen to be weak, it has been shown that in the limit of strong coupling the envelope of the echo becomes independent of the coupling strength which may arise due to a quantum phase transition in the surrounding [469, 470].

At this point, it is natural to seek a connection between the dynamical LE approach and the geometrical fidelity approach discussed in Sec. V (C). In this regard, one defines a projected density of state function $D(\omega; \lambda, \lambda') = \langle \psi_0(\lambda') | \delta(\omega - H(\lambda)) | \psi_0(\lambda) \rangle$ which is related to the square of the overlap as $|\langle \psi_0(\lambda) | \psi_0(\lambda') \rangle|^2 = 1 - \int_{E_1}^{\infty} D(\omega) d\omega$, where E_1 is the first excited energy. One can further show that $L(\lambda, t) = |\int_{-\infty}^{+\infty} D(\omega) \exp(-i\omega t) d\omega|^2$. These relations show that if the ground states are significantly different, the overlap tends to vanish leading to a broader $D(\omega)$ and hence a faster decay of the LE [403].

Let us now indicate how the LE can be shown to be related to the decoherence (decay of the off-diagonal terms) of the two-level reduced density matrix of the central spin. More precisely, one defines a quantity called purity $P = \text{Tr}_S(\rho_S)^2$ where ρ_S is the reduced density matrix of the central spin [460]. One can show that $P = 1 - 2|c_g c_e|^2(1 - L(t))$ (in fact, $L(t)$ appears in the off-diagonal term of ρ_s [471]); therefore the central spin transits from the initial pure state to a mixed state due to the enhanced decay of the LE around the QCP.

VI. NON-EQUILIBRIUM DYNAMICS ACROSS QUANTUM CRITICAL POINTS

In this section, we will review recent studies of non-equilibrium dynamics of transverse field spin systems. The non-equilibrium dynamics of a transverse XY spin chain was first investigated in a series of papers [55–57] where the time evolution of the model was studied in the presence of various time-dependent magnetic fields and the non-ergodic behavior of the magnetization was pointed out. A similar result was also obtained in [472].

There is a recent upsurge in studies of non-equilibrium dynamics of a quantum system swept across a QCP. These studies are important to explore the universality associated with quantum critical dynamics. Moreover, recent experiments with ultracold atomic gases [1, 473–475] have stimulated numerous theoretical studies. The main properties of these atomic gases are low dissipation rates and phase coherence over a long time so that the dynamics is well described by the usual quantum evolution of a closed system.

In the subsequent sections, we shall discuss that when a quantum system is driven across a QCP, the dynamics fails to be adiabatic however slow be the change in parameter of the Hamiltonian be. This is due to the divergence of the characteristic time scale of the quantum system, namely, the relaxation time close to the QCP. This non-adiabaticity results in the occurrence of defects in the final state of the quantum Hamiltonian. Interestingly, the defect density scales in a power-law fashion with the rate of quenching, when a parameter of the Hamiltonian is changed linearly in time, with the exponent given in terms of some of the critical exponents associated with the QCP. This implies that even after a non-equilibrium quench across a QCP, the scaling of defect density is given in terms of some of the equilibrium quantum critical exponents. We shall discuss slow dynamics across quantum critical and multicritical points and shall comment on their relevance in adiabatic quantum dynamics. We shall also discuss how the quantum information theoretic measures discussed in Sec. 5 scale following such a quench. In all these studies, the transverse Ising/ XY spin chains and the two-dimensional Kitaev model play a crucial role because of their integrability and the direct product form of the ground state.¹¹ However, in Appendix H, we incorporate a brief discussion on the quenching of Tomonaga-Luttinger liquids, and we discuss some other interesting and related developments in Appendix F and G. Our focus will be mainly limited to systems at zero-temperature although we shall briefly comment on the role of quantum quenching at a finite temperature.

We note that TIMs have been studied in the presence of a time-varying and periodic transverse [476–478] and the dynamics of domain walls has been examined [479]. For a recent mean field study of hysteresis in a TIM in a time varying longitudinal field, we refer to [480].

(A). Rapid quenching through a QCP

Let us first discuss what happens when a parameter in the Hamiltonian of a system is suddenly changed so as to take the system across a QCP [481]. We assume that the system is in its ground state before the quench. Immediately after the quench, the system will be in the same state; however, it will then start evolving in time since it is no longer an eigenstate of the new Hamiltonian. Our aim is to understand how quantities such as the order parameter change under this time evolution.

Das *et al.* [84] studied quenching dynamics of an infinite range ferromagnetic spin-1/2 Ising model in a transverse field (see (15) with $\sigma^x \rightarrow \sigma^z$, $\sigma^z \rightarrow \sigma^x$ and $\gamma = 0$) due to a sudden variation of the transverse field across the QCP (at $h_c = J/2$) from an initial value $h_i \gg h_c$ to a final value h_f . The dynamics of the equal-time order parameter correlation function (EOC) (defined as $\langle (S_z)^2 \rangle / S^2$, where $S_z = \sum_i \sigma_i^z$) has been studied. Expressing the initial ground state of the system in terms of the eigenstates $|n\rangle$ of the new Hamiltonian $|\psi\rangle = \sum_n c_n |n\rangle$, one obtains

$$\langle \psi(t) | (S_z)^2 / S^2 | \psi(t) \rangle = \sum_{m,n} c_n c_m \cos[(E_n - E_m)t] \langle m | (S_z)^2 / S^2 | n \rangle. \quad (104)$$

A numerical solution of (104) shows that the amplitude of oscillations is maximum when h_f is near h_c [84]. The long-time averaged value, given by $O = \lim_{T \rightarrow \infty} \langle \langle (S_z)^2(t) \rangle \rangle_T / S^2 = \frac{1}{S^2} \sum_n c_n^2 \langle n | (S_z)^2 | n \rangle$, peaks around $h_f/J = 0.25$ ($= h_c/2$), and the peak height decreases slowly with increasing S (see Fig. 16).

To understand the above findings, we consider the thermodynamic limit which is equivalent to the $S \rightarrow \infty$ (classical) limit for this model. One can study the classical equations of motion for $\mathbf{S} = S(\cos \phi \sin \theta, \sin \phi \sin \theta, \cos \theta)$ using the

¹¹ To be more precise, integrability means that the system has so many conserved operators that the eigenstates of the Hamiltonian can be completely distinguished from each other by the eigenvalues of those operators. States with different eigenvalues of those operators do not mix under the dynamics. This makes such systems easier to study, but it also implies that such systems are not ergodic and do not equilibrate in the same way as non-integrable systems.

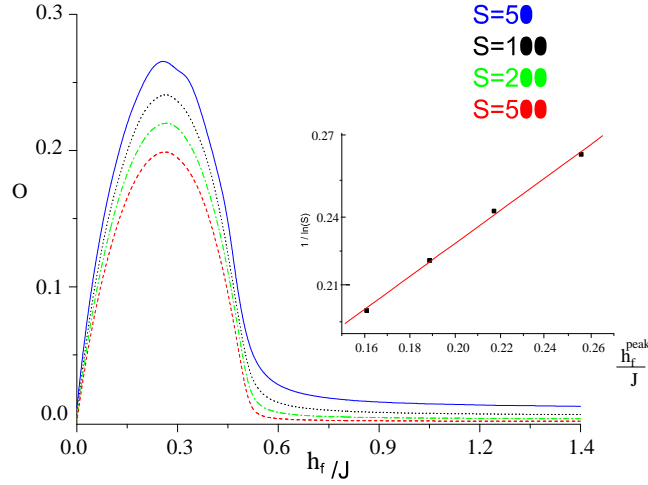


FIG. 16: (Color online) Plot of the long-time average O as a function of h_f/J for different S . The solid (blue), dotted (black), dash-dotted (green) and the dashed (red) lines represent respectively the results for $S = 50, 100, 200$ and 500 . O peaks around $h_f/J = 0.25$, and the peak value decreases with increasing S ; $h_i/J = 2$ for all the plots. Inset shows the plot of the maximum peak height O_{\max} of the long-time average of the EOC as a function of $1/\ln(S)$. The straight line shows a linear fit. (After Das *et al.*, 2006).

Lagrangian [482] $L = -S [1 - \cos \theta] d\phi/dt - H[\theta, \phi]$, with the initial condition $\theta = \pi/2 - \epsilon$, $\phi = \epsilon$, where ϵ is an arbitrarily small constant so that $S_x \approx S$ at $t = 0$. Since the motion occurs on a constant energy surface after the quench has taken place, one gets $h_f = (J/4) \cos^2 \theta + h_f \sin \theta \cos \phi$. The equation of motion for θ then gives

$$\begin{aligned} \langle \cos^2 \theta \rangle_T &= \mathcal{N}/\mathcal{D}, \\ \text{where } \mathcal{N} &= \int_{\theta_1}^{\theta_2} d\theta \frac{\cos^2 \theta}{f(\theta)} = 4\sqrt{8h_f(J - 2h_f)/J}, \\ \text{and } \mathcal{D} &= \int_{\theta_1}^{\theta_2} d\theta \frac{1}{f(\theta)}, \end{aligned} \quad (105)$$

where $d\theta/dt = (\sqrt{h_f^2 \sin^2 \theta - [h_f - J/4(\cos^2 \theta)]^2})/\sin \theta \equiv f(\theta)$, and $\theta_1 = \sin^{-1}(|1 - 4h_f/J|)$ and $\theta_2 = \pi/2$ are the classical turning points obtained from the equation of motion of θ . Regularizing the end-point singularity in \mathcal{D} at θ_2 , by a cut-off η so that $\theta_2 = \pi/2 - \eta$, one finds that $\mathcal{D} = -J \ln(\eta)/\sqrt{h_f(J - 2h_f)/2}$. Note that η is a measure of how close to the point $\theta = \pi/2$ we can get and must be of the order of $1/\sqrt{S}$. One finally gets

$$\langle \cos^2 \theta \rangle_T = \frac{16h_f(J - 2h_f)}{J^2 \ln(S)}. \quad (106)$$

Equation (106) demonstrates that the long-time average of the EOC must be peaked at $h_f/J = 0.25$ which agrees perfectly with the quantum mechanical numerical analysis leading to Fig. 16. Moreover, it provides an analytical understanding of the S (and hence system size) dependence of the peak values of h_f/J . A plot of the peak height of O as a function of $1/\ln(S)$ indeed fits a straight line as shown in the inset of Fig. 16.

The issue of thermalization after a rapid quench has been studied considering the non-equilibrium dynamics of a one-dimensional Ising model in a transverse field where the system is prepared in the ground state corresponding to h_0 [483, 484]. At $t = 0$, the field is suddenly changed to h so that the system is no longer in the ground state and hence relaxes in some fashion. The situation is equivalent to studying the temporal evolution of the correlation functions starting from a state which is not an eigenstate of the Hamiltonian [485]. The decay with time of the autocorrelation function defined as

$$C_{zz}(t) = \langle 0_i | \sigma_i^z(t) \sigma_i^z(0) | 0_i \rangle = \langle 0_i | e^{iH_f t} \sigma_i^z e^{-iH_f t} \sigma_i^z | 0_i \rangle,$$

where $|0_i\rangle$ is the initial ground state and H_f is the final Hamiltonian, has been studied. As we have seen before in Sec. II (A), σ_i^x is non-local in terms of the fermions while σ_i^z is quadratic in the fermions; this leads to completely different asymptotic behaviors of their autocorrelation functions. The order parameter autocorrelation function $C_{xx}(t)$

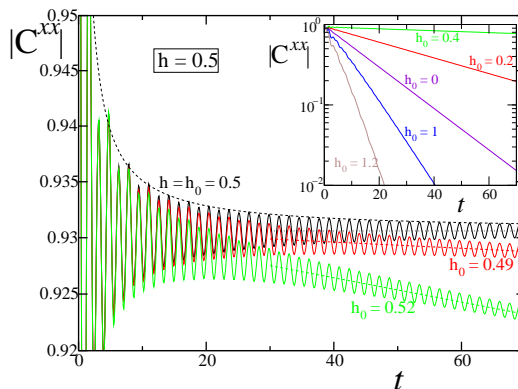


FIG. 17: (Color online) The exponential decay of correlators for different values of initial transverse field with final transverse field set equal to 0.5. In the main frame, the solid curve corresponds to equilibrium: the horizontal dotted line indicates the asymptotic value of $\langle \sigma^x \rangle^2$, while the dashed line denotes the power-law envelope t^{-1} . The inset shows data for strong quenches to show the exponential decay clearly. (After Rossini *et al.*, 2009).

shows an effective thermal behavior, decaying exponentially in time even though the underlying Hamiltonian is integrable; the decay time depends on the initial and final values of the field. In an integrable system, the states can be classified into a number of sectors defined by the eigenvalues of a large number of conserved operators. States lying in different sectors do not mix under the dynamics; this prevents the system from equilibrating as completely as non-integrable systems. The effective temperature can be deduced in two ways: from the decay time at finite temperatures, and from the excess energy $\langle 0_i | H_f | 0_i \rangle - E_{0f}$, where E_{0f} is the ground state energy of the final Hamiltonian. The autocorrelation $C_{zz}(t)$, on the other hand, does not show thermalization and decays only as a power-law with the exponent given by 1, 3/2 and 2 for $g_f < 0$, $= 0$, and > 0 , respectively. The exponential decay of $C_{xx}(t)$ when the quench is in the FM region is shown in Fig. 17. This problem has been revisited from the point of view of the fluctuation-dissipation relations in a recent work [486].

A proposal has been made [487] to exploit rapid quenching dynamics in spin chains for generating distant entanglement and quantum teleportation [488].

The results discussed in this section can be tested in two kinds of experimental systems. One class of systems are those with long-range dipole-dipole interactions such as KH_2PO_4 or $\text{Dy}(\text{C}_2\text{H}_5\text{SO}_4)_3 \cdot 9\text{H}_2\text{O}$ (see Sec. VII (B)) which exhibit order-disorder transitions driven by tunneling fields. The other class of systems are two-component Bose-Einstein condensates where the inter-species interaction is strong compared to the intra-species interaction; the relative strengths of these interactions can be changed by tuning the system to be near a Feshbach resonance as discussed for the $^{41}\text{K} - ^{87}\text{Rb}$ system in [489–493]. The quench dynamics that we have discussed can be realized by applying a radio frequency pulse to the system and suddenly changing the frequency of the pulse.

(B). Defect generation: Kibble-Zurek (KZ) scaling

Recently a remarkable intersection of the fields of cosmology and condensed matter systems has caught the attention of physicists [494, 495]. In general, a symmetry breaking phase transition produces some defects. For example, when water freezes into ice below a critical temperature, the rotational symmetry is broken by the choice of the orientation of the crystal of ice. The crystalline ordering sometimes fails especially in regions where one crystal meets another. In a similar spirit, Kibble in 1976 [495, 496] proposed that in the early universe too, symmetry breaking phase transitions might have led to the formation of topological defects, e.g., point-like monopoles, linear cosmic strings or planar domain walls.

Later in 1985, Zurek pointed out that some of the low-temperature phase transitions occurring in condensed matter systems can be used to mimic the formation of cosmic strings in the laboratory, for example, the vortices formed in the normal to superfluid transition in liquid helium [497–499]. Zurek argued that in a continuous phase transition, a power-law relation exists between ξ (the typical distance between two cosmic strings or defects) and the time taken by the system to pass through the phase transition. This power-law relation has been tested numerically [500] and experimentally in various systems, such as non-linear optical systems made up of liquid crystals [501–503], annular Josephson junctions [504], and superfluids [505]. Even though most of the experimental data are in agreement with the theoretical predictions, the situation in liquid He^4 is not clear [506, 507].

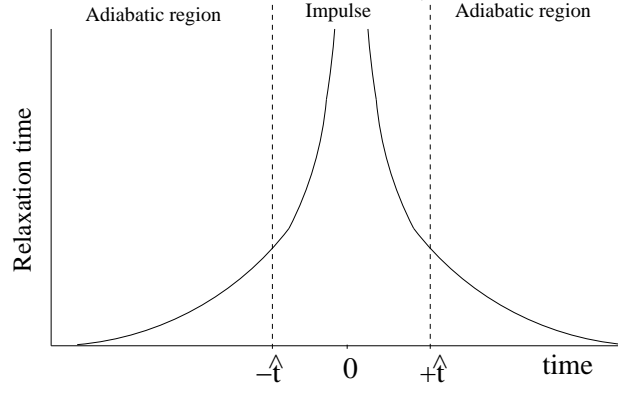


FIG. 18: Kibble-Zurek argument: the division of the entire time evolution into three regions. For $t < |\hat{t}|$, the system is in the impulse region, whereas for $t < -\hat{t}$ and $t > \hat{t}$, it is in the adiabatic region. (After Damski and Zurek, 2006).

The Kibble-Zurek scaling proposed for second order CPTs has recently been generalized to the quantum case independently by Zurek, Dorner and Zoller [508] and by Polkovnikov [509]. To present the KZ argument extended to the quantum scenario, we note that according to the adiabatic theorem [510, 511], if the time scale associated with the minimum gap between the two states of a two-level system is sufficiently larger than the rate at which a parameter of the two-level Hamiltonian is varied (called the adiabatic condition), the system remains in its initial state. If the gap between the two levels is smaller than the rate at which the parameter is varied, we have a non-adiabatic process which leads to excitations.

In a driven quantum many-body system, the characteristic time scale is the relaxation time (inverse of the minimum gap) which diverges at the critical point. If the relaxation time of the system is smaller than the time scale on which the Hamiltonian is changed, the system is able to respond to the changes in the Hamiltonian and it remains in the ground state. Clearly, the adiabatic condition is satisfied when the system is far away from the critical point. Near the critical point, the relaxation time is large and the system is no longer able to follow the change in the Hamiltonian and hence non-adiabatic excitations appear. The time \hat{t} at which the behavior of the system changes from adiabatic to non-adiabatic can be obtained as follows. Let us assume that the parameter g is varied such that it approaches the critical point g_c as t/τ , or $\lambda = g - g_c = t/\tau$, such that the QCP occurs at $t = 0$. As explained before, at \hat{t} , the relaxation time ξ_τ of the system is of the order of the time scale at which the Hamiltonian is changed; hence

$$\left| \frac{\lambda}{\dot{\lambda}} \right|_{\hat{t}} = \hat{t} = \xi_\tau|_{\hat{t}}. \quad (107)$$

This relaxation time diverges as $\xi_\tau \sim |g - g_c|^{-\nu z}$ which leads to

$$\begin{aligned} \hat{t} &\sim (g - g_c)^{-\nu z}|_{\hat{t}} \sim \left(\frac{\hat{t}}{\tau} \right)^{-\nu z}, \\ \text{implying } \hat{t} &\sim \tau^{\nu z/(\nu z + 1)}. \end{aligned} \quad (108)$$

The times $\pm \hat{t}$ divide the entire evolution into three regions as shown in Fig. 18.

According to the above argument, if the ground state wave function at $-\hat{t}$ is $\psi(-\hat{t})$, the system does not evolve at all in the impulse region and hence remains in the same state $\psi(-\hat{t})$ at time $+\hat{t}$ also [512, 513]; thus it loses track of the instantaneous ground state which leads to excitations. For large τ or slow variation of g , this argument is only valid for the low-energy modes, while the high-energy modes do evolve adiabatically. Combining $\hat{t} \sim \xi_\tau$ (see (107)) and the healing length $\hat{\xi} \sim \xi_\tau^{1/z}$, and assuming that there is one defect per unit domain size of linear dimension $\hat{\xi}$, the density of defects n is found to be

$$n \sim \frac{1}{\hat{\xi}^d} \sim \tau^{-d\nu/(\nu z + 1)}, \quad (109)$$

where d is the dimensionality of the system. Thus the Kibble-Zurek scaling (KZS) connects the equilibrium quantum critical exponents to the non-equilibrium dynamics and points towards universality even in the case of non-equilibrium dynamics through a QCP. The scaling in (109) was independently derived in [509], using adiabatic perturbation theory,

and the existence of an upper critical dimension $d_u^c = 2z + 2/\nu$ was pointed out where the exponent of the scaling saturates to 2 with possible logarithmic corrections to the scaling. For $d > d_u^c$, the KZS breaks down and one gets $n \sim 1/\tau^2$; the main contribution to the defects then comes from the high-energy modes.

The KZS is also relevant to adiabatic transitions in a finite system of linear dimension L . In this case, the healing length ξ is limited by L and one therefore gets a minimum value of $\tau = \tau_0 \sim L^{(1+\nu z)/\nu}$ such that for slower quenches ($\tau \gg \tau_0$), one can achieve a perfect adiabatic transition [508, 514]. It is in fact the finite energy gap at the QCP for a finite system that suppresses any excitation exponentially.

The KZS can also be arrived at using a phase space argument [509]. Let us assume that the system is described by the Hamiltonian $H(\lambda(t))$, and the time evolution of the parameter $\lambda(t) = \lambda_0(t/\tau)$ takes the system through the critical point $\lambda = 0$ at $t = 0$. In the limit of large τ , a non-vanishing probability of excitations requires the non-adiabaticity condition [509, 515] $\partial\Delta(\vec{k}, t)/\partial t \sim \Delta^2$, where Δ is the characteristic energy-scale near the QCP scaling as $\Delta \sim \lambda^{z\nu}$. Using $\partial\Delta(t)/\partial t = [\partial\Delta(\lambda)/\partial\lambda]\tau^{-1}$, the non-adiabaticity condition can be rewritten as $\Delta^2 \sim \tau^{-1}\lambda^{z\nu-1}$. Near a QCP, we generally expect $\Delta \sim k^z$ and $\lambda \sim k^{1/\nu}$; the non-adiabaticity condition then yields $k \sim \tau^{-\nu/(z\nu+1)}$ leading to a scaling of the gap as $\Delta \sim \tau^{-z\nu/(z\nu+1)}$. The available phase space for quasiparticle excitations is given by $\Omega \sim k^d \sim \Delta^{d/z} \sim \tau^{-\nu d/(z\nu+1)}$ which is directly proportional to the defect density n , thus yielding the KZS.

We will briefly discuss some interesting generalizations of the KZS to different quenching schemes in the following. (i) *A non-linear variation of the quenching parameter* [516, 517]: The quenching parameter $\lambda(t)$ varies as $\lambda_0|t/\tau|^r \text{sign}(t)$, where r denotes the power-law exponent and sign denotes the sign function. We consider the case when the critical point is crossed at time $t_0 = 0$; the case $t_0 \neq 0$ requires special attention [516, 518]. Following the same line of arguments as in the linear case, we get $\hat{t} = \tau^{r\nu z/(1+r\nu z)}$ which leads to

$$n \sim \tau^{-r\nu d/(1+r\nu z)}. \quad (110)$$

Thus the non-linearity exponent r seems to renormalize the critical exponent ν to $r\nu$ which can also be seen employing the phase space argument discussed above.

(ii) *Quenching across a $(d - m)$ -dimensional gapless surface* [145, 519]: Let us consider a d -dimensional quantum system quenched across a $(d - m)$ -dimensional critical hyperspace on which the energy gap vanishes. We then find that the phase space available for excitations gets modified to $\Omega \sim k^m$ which leads to a modified KZS given by

$$n \sim \tau^{-m\nu/(1+\nu z)}. \quad (111)$$

For $m = d$ the standard KZS in (109) is retrieved.

(iii) *Quenching through an anisotropic quantum critical point*: The phase space argument can be extended to a (d, m) anisotropic QCP [147, 520] which is defined by $\Delta \sim k_i^{z_1}$ for m momentum components while $\Delta \sim k_i^{z_2}$ for the remaining $d - m$ momentum components, with $z_2 > z_1$. For a non-linear quenching, one uses the relations $\Delta \sim \tau^{-\alpha\nu z/(1+r\nu z)}$ and the phase space available for quasiparticle excitations, $\Omega = \prod_i k_i$. Since different momentum components scale differently with energy, one gets the scaling of the defect density given by [147]

$$n \sim \tau^{-[m+(d-m)z_1/z_2]\nu_1\alpha/(1+\alpha\nu_1 z_1)}, \quad (112)$$

where $d = m$ is the standard KZS. The possibility of verifying the scaling relation in (112) for quenching through gapless Dirac points as observed in the low-energy properties of graphene [521], semi-Dirac [422] and quadratic band crossing points [522] has been proposed in [520]. The quench dynamics and scaling of defect density in monolayer and bilayer graphene have also been studied in recent years [523, 524]. The feasibility of studying graphene physics experimentally by loading ultracold fermionic atoms in a two-dimensional optical lattice has been reported [525].

We have discussed above the KZS when the quenching parameter varies in time. One may wonder what happens when it varies in space. We defer this discussion to Appendix F. In Appendix G, on the other hand, we discuss how topology influences the traditional KZS given in Eq. (109).

We should note here that it is sometimes convenient to discuss the residual energy per site, e_r , rather than the defect density n . The residual energy is defined as the difference between the expectation value of the final Hamiltonian in the state which is reached after the quench and the ground state energy of the final Hamiltonian. Although e_r and n are often related to each other and scale in the same way with the quenching time τ , there are situations where they scale differently; this happens for disordered systems as we will discuss in Sec. VI(H).

Contrary to the classical result, the KZS at quantum critical points is relatively new and has not been verified experimentally till now, although the possibility of verification in cold atom systems has been proposed [473, 475]. The formation of topological defects in the form of spin vortices in a quantum system following a rapid quench across a QCP has already been reported [473] using ^{87}Rb spinor condensates. The Hamiltonian of $F = 1$ ^{87}Rb spinor gases has two terms (here F is the sum of electronic and nuclear spin angular momenta), namely, $c_2 n^2 \langle \vec{J} \rangle^2 + q \langle J_z^2 \rangle$. The first term (which is proportional to the square of the density of atoms, n) favors a FM phase with broken symmetry,

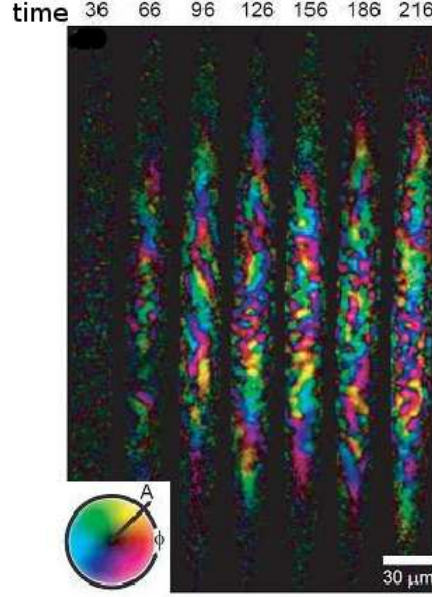


FIG. 19: (Color online) Ferromagnetic domains shown at different times after a quench (time in ms). The maximum brightness, shown by the color wheel on the left, corresponds to full magnetization of the condensate center. Near the center of the condensate, one can see small magnetic domains divided by domain walls with zero magnetization (After Sadler *et al.*, 2006).

whereas the second term (which depends quadratically on a magnetic field applied in the \hat{z} direction, $q \sim B_z^2$) favors a phase with $J_z = 0$; a quantum phase transition between the two phases occurs at some critical field. After preparing optically trapped BECs in the phase with $J_z = 0$ at a high field, the magnitude of the field is ramped down to a small value so that the FM phase becomes favorable. The formation of small FM domains is observed throughout the condensate divided by unmagnetized domain walls as shown in Fig. 19. The different domains correspond to different orientations of $\langle \vec{J} \rangle$ in the $x - y$ plane; the domains grow with time which is indicated at the top of the figure in ms . This experiment demonstrated for the first time the formation of topological defects in a system undergoing a quantum phase transition.

Following the prediction of the KZS, there have been a number of studies exploring the non-equilibrium dynamics of various quantum many-body systems [526–534] using various quenching protocol, for example, Rosen-Zener quenching [535, 536]. We limit our discussions mainly to studies related to transverse field spin systems, and refer to the review articles, [21, 419, 537–542], for transverse field models as well as more generic quantum many-body systems. We present a note on the quenching of Tomonaga-Luttinger liquids in Appendix H.

(C). Adiabatic perturbation theory: Slow and Sudden Quenches

Let us briefly discuss the adiabatic perturbation theory with which one can rederive the KZS [509] given in (109) for a slow quenching across a QCP. Following that we shall consider the limit of sudden quenching and review the concept of a generalized fidelity susceptibility that leads to the scaling of defects in the slow as well as the sudden limit.

We consider a Hamiltonian $H(\lambda) = H_0 + \lambda(t)H_I$ with a linear variation of λ which goes through a QCP at $t = 0$. The wave function $|\psi(t)\rangle$ at any time t can be expanded in its instantaneous (adiabatic) basis $|q(t)\rangle$ as

$$|\psi(t)\rangle = \sum_q a_q(t) |q(t)\rangle.$$

The Schrödinger equation can be written as

$$i \frac{\partial a_p}{\partial t} + i \sum_q a_q(t) \langle p | \frac{\partial}{\partial t} | q \rangle = \epsilon_p(t) a_p(t), \quad (113)$$

where $\epsilon_p(t)$ is the instantaneous eigenvalue in the basis $|p(t)\rangle$. Performing a unitary transformation

$$a_p(t) = \tilde{a}_p(t) e^{-i \int^t \epsilon_p(\lambda(t)) dt} = \tilde{a}_p(\lambda) e^{-i \tau \int^\lambda \epsilon_p(\lambda) d\lambda}, \quad (114)$$

and assuming that the system is prepared in the ground state $|0\rangle$ of the initial Hamiltonian so that only the term with $q = 0$ contributes to the total sum in Eq. 113, the total density of excitations at final time $t = +\infty$ is given by

$$n \approx \sum_{p \neq 0} |a_p(\infty)|^2 \approx \sum_{p \neq 0} \left| \int_{-\infty}^{\infty} d\lambda \langle p | \frac{\partial}{\partial \lambda} | 0 \rangle e^{i \tau \int^\lambda (\epsilon_p(\lambda') - \epsilon_0(\lambda')) d\lambda'} \right|^2. \quad (115)$$

Assuming that the system is translationally invariant, the above equation can be rewritten in momentum space k replacing the summation by an integration as follows:

$$n \approx \int \frac{d^d k}{(2\pi)^d} \left| \int_{-\infty}^{\infty} d\lambda \langle k | \frac{\partial}{\partial \lambda} | 0 \rangle e^{i \tau \int^\lambda (\epsilon_k(\lambda') - \epsilon_0(\lambda')) d\lambda'} \right|^2. \quad (116)$$

Near a quantum critical point, the excitation energy can be written using a scaling function $F(x)$ as

$$\epsilon_k - \epsilon_0 \sim \lambda^{z\nu} F(k/\lambda^\nu), \quad (117)$$

such that for $x \gg 1$, $F(x) \propto x^z$ and for $x \rightarrow 0$, $F(x) \rightarrow \text{constant}$ giving the correct scalings as required. To analyze Eq. (116), we introduce the following scaling ansatz for the matrix element given by

$$\langle k | \frac{d}{d\lambda} | 0 \rangle \sim \frac{1}{\lambda} G(k/\lambda^\nu), \quad (118)$$

where $G(x)$ is another scaling function. The form of this scaling function can be obtained by the following argument: for small λ^ν/k , the matrix element should be independent of λ , i.e., $G(x) \propto x^{-1/\nu}$ for $x \gg 1$. Redefining $\lambda = \zeta \tau^{-1/(z\nu+1)}$ and $k = \mu \tau^{-\nu/(z\nu+1)}$, we get

$$n \sim \int \frac{d^d k}{(2\pi)^d} |\tilde{a}_k|^2 = \tau^{-\frac{d\nu}{z\nu+1}} \int \frac{d^d \mu}{(2\pi)^d} |\tilde{a}(\mu)|^2, \quad (119)$$

$$\text{where } \tilde{a}(\mu) = \int_{\zeta_i}^{\zeta_f} \frac{d\zeta}{\zeta} G\left(\frac{\mu}{\zeta^\nu}\right) \exp \left[i \int_{\zeta_i}^{\zeta_f} d\zeta_1 \zeta_1^{z\nu} F(\mu/\zeta_1^\nu) \right]. \quad (120)$$

Thus we have rederived the KZS using adiabatic perturbation theory. Let us study the convergence behavior of the above integrals carefully. The integral over ζ is always convergent because of the fast oscillating function at large ζ and the absence of singularities at small ζ . We now need to check the convergence of the integral over μ at large μ . If this integral converges, one gets KZS, but if it does not, the defect density is dominated by the high energy modes and is given by τ^{-2} thereby destroying the KZ universality. Using explicit asymptotics of the scaling functions $F(x)$ and $G(x)$ at large x ($\mu \gg \zeta^\nu$), it can be shown that

$$\alpha(\mu) \propto \frac{1}{\mu^{z+1/\nu}}.$$

This shows that there is a crossover from the low-dimensional universal KZS to a τ^{-2} scaling at a critical dimension given by $d_c = 2z + 2/\nu$. For a detailed discussion, we refer to [509].

So far our discussion has been limited to slow quenching across a QCP. Let us now define a variation of a parameter λ in some fashion starting from the critical point ($\lambda = 0$) at $t = 0$ to a final value λ_f at time $t = t_f$; the system is initially in the ground state. If $|t_f| < |\hat{t}|$ (defined in (107)), we are dealing with a sudden quench in the sense that the wave function is frozen in this region if we consider the low-energy modes only. For sudden quenching, the response of the system depends on the final value of λ_f but not on the protocol of changing λ ; this is in contrast to the slow quenching ($t_f > \hat{t}$) discussed so far for which the system is sensitive to the quenching protocol but is independent of λ_f . The question one would like to address is whether there is a KZS for such a sudden quenching of parameters.

The defect density and heat density (Q) following a sudden quench have been studied in recent years [419, 515]; the heat density is the excess energy above the new ground state. The advantage of using the heat density is that it can be computed even for non-integrable systems. But for an integrable system with non-interacting quasiparticles, it is more useful to define the defect density, which is a measure of the density of excited quasiparticles generated in the system. When λ is suddenly increased from $\lambda = 0$ to its final value λ_f , all the momentum modes $k \lesssim k_0 \sim \lambda_f^\nu$ get excited with

unit probability having excitation energy $\sim \lambda_f^{\nu z}$ for each mode. This gives the defect density $n \sim k_0^d \sim \lambda_f^{d\nu}$ and an excess energy density or heat density of the form $Q \sim \lambda_f^{\nu z} k_0^d \sim \lambda_f^{\nu(d+z)}$. The defect density is related to the probability of excitations, which in turn can be expressed in terms of the FS (see Sec. V (C)). From adiabatic perturbation theory [419, 434, 515, 543] one finds that $n \sim \lambda_f^2 \chi_F \sim \lambda_f^{\nu d}$.

The concept of a generalized FS has been introduced in [515], using a generic quench from a QCP at time $t = 0$ given by

$$\lambda(t) = \delta \frac{t^l}{l!} \Theta(t), \quad (121)$$

where δ is a small parameter, and Θ is the step function. The case $l = 0$ denotes a rapid quench of amplitude δ , the case $l = 1$ implies a slow linear quench with a rate δ , and so on. In all these cases the limit $\delta \rightarrow 0$ signifies a slow adiabatic time evolution. If the system is initially in the ground state, the transition probability to the instantaneous excited state as obtained from the adiabatic perturbation theory is given by

$$P_{ex} = \delta^2 \sum_{n \neq 0} \frac{|\langle \psi_n | \frac{\partial H}{\partial \lambda} | \psi_0 \rangle|^2}{(E_n - E_0)^{2l+2}} = \delta^2 L^d \chi_{2l+2}, \quad (122)$$

where we have defined a generalized fidelity susceptibility χ_m given by

$$\chi_m = \frac{1}{L^d} \sum_{n \neq 0} \frac{|\langle \psi_n | \frac{\partial H}{\partial \lambda} | \psi_0 \rangle|^2}{(E_n - E_0)^m}. \quad (123)$$

From (123), one finds that χ_1 stands for the specific heat density χ_E , while χ_2 is the fidelity susceptibility χ_F ; χ_4 , on the other hand, yields the excitation probability following a slow linear quench starting from a QCP.

In the same spirit as in (88), χ_m can also be expressed in terms of a time-dependent connected correlation function in imaginary time ($\bar{\tau}$) given by

$$\chi_m = \frac{1}{L^d (m-1)!} \int_0^\infty d\bar{\tau} \bar{\tau}^{m-1} \langle H_I(\bar{\tau}) H_I(0) \rangle_c. \quad (124)$$

Now, using $\lambda \sim L^{-1/\nu}$ and $\bar{\tau} \sim L^z$ in Eq. (121) leads to the scaling relation $L \sim \delta^{-\nu/(1+\nu z l)}$. One can further conclude (using the relevance or marginality of H_I) that $H_I \sim \lambda^{\nu z - 1} \sim \delta^{(\nu z - 1)/(1+\nu z)}$, and $\bar{\tau} \sim L^z \sim \delta^{-\nu z/(1+\nu z l)}$. Substituting for L , H_I and $\bar{\tau}$ in (124) with $m = 2l + 2$ one gets

$$\begin{aligned} \chi_{2l+2} &\sim \delta^{(\nu d - 2 - 2\nu z l)/(1+\nu z l)} \sim L^{2z l + 2/\nu - d}, \\ P_{ex} &\sim \delta^2 L^{2/\nu + 2z l}, \end{aligned} \quad (125)$$

where we have assumed $d\nu < 2(1 + \nu z l)$. The expression for P_{ex} defined above is valid in the limit $\delta \ll L^{1/\nu + z l}$ which ensures that $P_{ex} \ll 1$. One can therefore derive the scaling of the defect density given by $n \sim \delta^2 L^{(2/\nu - d + 2z l)}$ for $|\delta| L^{1/\nu + z l} \gg 1$ and $n \sim \delta^{d\nu/(z\nu l + 1)}$ in the opposite limit. With $l = 0$ and $\delta = \lambda_f$, we retrieve the results for the sudden quench $n \sim \lambda_f^{\nu d}$. For $l = 1$ and $\delta = 1/\tau$, we get back the scaling relation $n \sim \tau^{-\nu d/(\nu z + 1)}$, while for $l > 2$, the scaling of the defect density for non-linear quench is obtained. Similarly, one can derive the scaling of the heat density $Q \sim \lambda^{\nu z + \nu d}$ for $\delta \gg L^{1/\nu + z l}$. We reiterate that the scaling relations presented above are valid as long as the corresponding exponents do not exceed 2. Otherwise contributions from short wavelength modes become dominant and hence the low-energy singularities associated with the critical point become subleading [419, 515]. Very recently, a study of the influence of the geometric phase on the non-equilibrium dynamics of a quantum many-body system has been reported [544]; it has been shown that for fast driving the GP strongly affects transitions between levels, and the possibility of the emergence of a dynamical transition due to a competition between the geometrical and dynamical phases has been pointed out.

(D). Linear and non-linear slow evolution through critical points

In this section and also in subsequent sections, we shall mainly focus on slow quenching dynamics (defined through a rate of quenching) across critical and multicritical points.

Let us first illustrate the KZS taking the example of the XY spin-1/2 chain in a transverse field to calculate the defect density produced when the spin chain is driven through critical points. Using the 2×2 form of the Hamiltonian

(26), one use the Landau-Zener (LZ) transition probability to calculate the probability of non-adiabatic transition and hence the defect density. We refer to Appendix E for a detailed discussion of the LZ transition formula.

If the transverse field of the XY chain in (10) is linearly quenched as t/τ [545], where t is varied from $-\infty$ to $+\infty$, the system crosses the two Ising critical lines ($h = \pm(J_x + J_y)$) shown in the phase diagram in Fig. 2. For $J_y = 0$ this reduces to the quenching of a transverse Ising chain [509, 512, 514]. We have shown in Sec. II (A) that the many-particle Hamiltonian decouples in Fourier space into 2×2 matrices H_k for each mode k . Therefore, if the system starts in the state $|0\rangle$, the dynamics takes place only between the two basis states $|0\rangle$ and $|k, -k\rangle$ such that the time evolved state $|\psi(t)\rangle$ at time t is a superposition given by $|\psi(t)\rangle = C_{1k}(t)|0\rangle + C_{2k}(t)|k, -k\rangle$. We arrive at the following evolution equation for $C_{1k}(t)$ and $C_{2k}(t)$,

$$i \begin{pmatrix} \dot{C}_{1k} \\ \dot{C}_{2k} \end{pmatrix} = \begin{pmatrix} h(t) + J \cos k & i\gamma \sin k \\ -i\gamma \sin k & -h(t) - J \cos k \end{pmatrix} \begin{pmatrix} C_{1k} \\ C_{2k} \end{pmatrix}, \quad (126)$$

where $J = J_x + J_y$ and $\gamma = J_x - J_y$.

For $h = t/\tau$ for $-\infty < t < \infty$, the system starts in the state $|C_{1k}(-\infty)|^2 = 1$ and $|C_{2k}(-\infty)|^2 = 0$ and crosses the two Ising critical lines at $t = \pm t_0 = \pm\tau(J_x + J_y)$. The excitation energy of the system vanishes for the critical modes $k = 0, \pi$, and the relaxation time diverges at $-t_0$ and $+t_0$, respectively; thus the system loses adiabaticity close to $t = -t_0$ (i.e., close to the QCP) no matter how slow the rate of variation of h may be. The system starts from the ground state $|\dots \downarrow\downarrow\downarrow\downarrow \dots\rangle$ (i.e., $\sigma_z = -1$ for all i) which corresponds to the zero fermion state $|0\rangle$, whereas the final state should be $|\dots \uparrow\uparrow\uparrow\uparrow \dots\rangle$ if adiabaticity is followed throughout the quenching. On the other hand, due to the reasons mentioned above, the system cannot follow the instantaneous ground state close to the critical point and hence gets excited. The final state therefore has a structure such as $|\dots \uparrow\uparrow\uparrow\uparrow\downarrow\uparrow\uparrow\uparrow\downarrow\uparrow\uparrow\uparrow \dots\rangle$, where the density of down spins corresponds to defects.

The Hamiltonian in (126) resembles the LZ Hamiltonian as discussed in Appendix H. For convenience, let us first denote the off-diagonal elements of the matrix in (126) by Δ_k and Δ_k^* , and the diagonal elements by $\epsilon_k(t)$ and $-\epsilon_k(t)$. This equation then corresponds to the Schrödinger equation of a two-level system where two levels with energies $E_{1,2} = \pm\sqrt{\epsilon_k(t)^2 + |\Delta_k|^2}$ approach each other linearly with a rate $1/\tau$. Physically, the two energy levels $E_{1,2}$ approach each other from $t \rightarrow -\infty$ till some time t^* where the energy gap is minimum ($= 2|\Delta_k|$) which occurs when $\epsilon_k(t^*) = 0$. For $t > t^*$, the energy levels start moving away from each other. If the system is initially ($t \rightarrow -\infty$) prepared in the ground state of the two-level system, the LZ transition formula yields the probability of the system being in the excited state at the final time $t \rightarrow +\infty$. The Schrödinger equation of such a two-level system can be solved by mapping it to the standard Weber equation with the above mentioned initial conditions [511, 546–548] (see Appendix E). The probability of excitations thus obtained at the final time is given by (see Eq. (127))

$$p_k = e^{-2\pi|\Delta_k|^2/[d(\epsilon_k - (-\epsilon_k))/dt]} = e^{-\pi\tau|\Delta_k|^2}, \quad (127)$$

where we have used $d\epsilon_k/dt = 1/\tau$.

Substituting $|\Delta_k| = \gamma \sin k$ appropriately, the probability of excitations for each k mode following the quenching in (126) is given by (127) and we get

$$p_k = |C_{1k}(+\infty)|^2 = e^{-\pi\tau\gamma^2 \sin^2 k}. \quad (128)$$

Fig. 20 shows the variation of p_k with k for the transverse field quenching. The critical modes at $k = 0$ and $k = \pi$ for which the gap vanishes get excited with probability 1, while the modes close to the critical modes have probability close to 1. The density of defects is obtained by integrating p_k over all the modes in the Brillouin zone,

$$\begin{aligned} n_h &= \int_{-\pi}^{\pi} \frac{dk}{2\pi} p_k = \frac{1}{\pi} \int_0^{\pi} dk e^{-\pi\tau\gamma^2 \sin^2 k} \\ &\simeq \frac{1}{\pi} \left[\int_0^{\infty} dk e^{-\pi\tau\gamma^2 k^2} + \int_{-\infty}^0 dk e^{-\pi\tau\gamma^2 (\pi-k)^2} \right] \\ &= \frac{1}{\pi\gamma\sqrt{\tau}}. \end{aligned} \quad (129)$$

The subscript h in n_h denotes the quenching of the transverse field. In deriving (129), we have expanded p_k around the critical modes $k = 0$ and π where the contributions to the defect density are peaked in the limit of large τ ; this allows us to extend the limits of integration to $\pm\infty$. The density of defects is the fraction of spins which could not accomplish the reversal, i.e., the density of wrongly oriented spins in the final state. Noting that the critical exponents of the Ising transition are $\nu = z = 1$, the $1/\sqrt{\tau}$ behavior in (129) for the density of defects is in perfect agreement

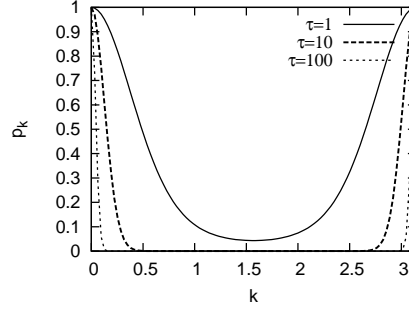


FIG. 20: Variation of probability of excitations p_k with k for different τ as given in (128). For the modes $k=0$ and π , $p_k=1$ showing that these modes do not evolve. For large τ , only modes close to these critical modes contribute to the defect.

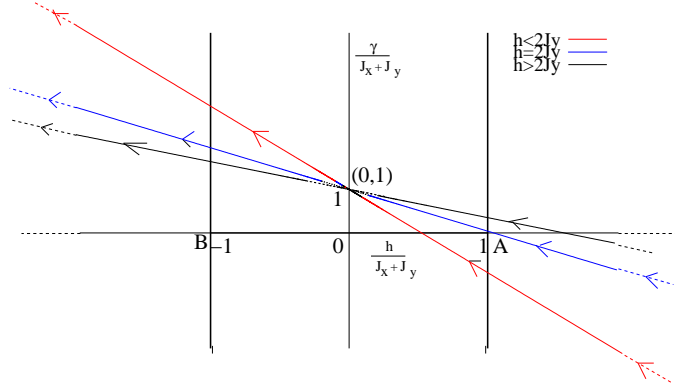


FIG. 21: (Color online) The anisotropic quenching path for three different cases as discussed in the text: $h < 2J_y$, $h = 2J_y$ and $h > 2J_y$ shown in the phase diagram in Fig. (2). All the quenching paths cross the point $(0, 1)$ at $t \rightarrow \pm\infty$.

with KZS noting that $d = 1$ and $\nu = z = 1$ for the Ising transition. The n_h obtained by numerically integrating the Schrödinger equation also exhibits the predicted $1/\sqrt{\tau}$ scaling. For a finite chain, one can naively argue that the $|\Delta_k|^2$ appearing in (128) scales as $1/L^2$ at the QCP so that one arrives at the condition $\tau \gg L^2$ for the transition in a finite chain to be adiabatic.

In the anisotropic quenching scheme, $J_x = t/\tau$ goes from $-\infty$ to $+\infty$ with J_y and h fixed [549] (see Fig. 21). If $h < 2J_y$, the system crosses the two Ising critical lines ($h = \pm(J_x + J_y)$) and also the anisotropic transition line ($J_x = J_y$); for $h > 2J_y$ it crosses the two Ising critical lines only. At a critical point on the anisotropic critical line, the critical mode with wave vector $k_0 = \cos^{-1}(h/2J_y)$ (see (31)) gets excited with unit probability. Performing a unitary transformation to a basis which are the eigenstates of the initial and final time Hamiltonians defined by [549]

$$|e_{1k}\rangle = \sin(k/2)|0\rangle + i \cos(k/2)|k, -k\rangle,$$

$$|e_{2k}\rangle = \cos(k/2)|0\rangle - i \sin(k/2)|k, -k\rangle,$$

one can rewrite the reduced 2×2 Hamiltonian (26) H_k in the form

$$\begin{pmatrix} J_x + J_y \cos 2k + h \cos k & J_y \sin 2k + h \sin k \\ J_y \sin 2k + h \sin k & -(J_x + J_y \cos 2k + h \cos k) \end{pmatrix}.$$

In the process, the time dependence of the off-diagonal terms in (126) gets shifted to only the diagonal terms of the transformed Hamiltonian so that the Landau-Zener expression becomes applicable. After expanding about all the three critical modes for $h < 2J_y$, we get

$$n_{jx} = n_1 + n_2 \simeq \frac{4J_y}{\pi\sqrt{\tau} (4J_y^2 - h^2)}. \quad (130)$$

For $h > 2J_y$, the total density of defects will be simply given by $n_{jx}/2$ as the system does not cross the anisotropic transition line. For $h = 2J_y$, the system crosses the MCP during the evolution when (130) is not valid; we will discuss this special case in the next section.

We recall the one-dimensional transverse Ising Hamiltonian in a longitudinal field (32) which is non-integrable for $h_L \neq 0$. For $h_L = 0$, the system is at the QCP at $h_c = 1$ if $J_x = 1$, which is described by a Lorentz invariant theory (see Sec. II (B)) with $z = 1$. In contrast, the correlation length exponent ν depends on how the theory is perturbed from the QCP. If the transverse field h is perturbed then $\nu = 1$. But if the longitudinal field h_L is perturbed, the exponent $\nu_L = 8/15$. This can be shown as follows. The scaling of the magnetization near the QCP, $\langle \sigma_z \rangle \sim (h-1)^{1/8}$, yields the scaling dimension of σ_z to be $[\sigma_z] = 1/8$. Consequently, we must have $[h_L] = 15/8$ so that the change in the imaginary time action in the continuum limit, $\partial S = \int dx \int dt h_L \sigma_z(x, t)$, is dimensionless. Defining the correlation length ξ_L corresponding to a perturbation in the longitudinal field as $h_L \sim 1/\xi_L^{15/8}$ leads to $\xi_L \sim h_L^{-8/15}$ as $h_L \rightarrow 0$ (QCP); hence $\nu_L = 8/15$. Therefore, if the critical point is crossed by linearly varying $h_L = t/\tau$, the defect density is expected to scale as $n \sim \tau^{-\nu_L d/(\nu_L z + 1)} \sim \tau^{-8/23}$, since $d = z = 1$ and $\nu_L = 8/15$. If we quench through the QCP in a generic direction by varying both transverse and longitudinal fields as $h - 1 = h_L = t/\tau$, the defect density will have terms scaling as $\tau^{-1/2}$ and $\tau^{-8/23}$, respectively; the latter dominates in the limit $\tau \rightarrow \infty$. If one considers the Hamiltonian [550]

$$H = - \sum_i [\sigma_i^x \sigma_{i+1}^x + \sigma_i^z + g(\cos \phi \sigma_i^z + \sin \phi \sigma_i^x)], \quad (131)$$

and g is varied as t/τ across the QCP at $t = 0$, the defect density n is expected to scale as $\tau^{-1/2}$ if $\phi = 0$ or π but as $\tau^{-8/23}$ for any other value of ϕ . This predictions are numerically verified in [550].

Finally, let us comment on the non-linear quenching when the transverse field is quenched as $h(t) - J = |t/\tau|^r \text{sign}(t)$ so that the system crosses the Ising critical point at $t = 0$. In this case, the probability cannot be evaluated by directly applying the LZ transition formula (127) which is valid only for linear variation. However, using an appropriate scaling of the Schrödinger equation, it can be shown that the excitation probability $p_k = f(k^2 \tau^{2r/(r+1)})$, i.e., it is only a function of the dimensionless combination $k^2 \tau^{2r/(r+1)}$; in the $\tau \rightarrow \infty$ limit, one can then readily show that $n_h \sim \tau^{-r/(r+1)}$ [516] which is in agreement with (110). In contrast, if one employs the quenching scheme $h(t) = |t/\tau|^r \text{sign}(t)$, the minimum energy gap that contributes maximally to the defect production does not occur at $t = 0$, rather occurs at the instant $t = t_0$ such that $|t_0/\tau|^r \text{sign}(t) + J \cos k = 0$. Linearizing the Hamiltonian H_k around $t = t_0$, we get

$$H_k = \frac{t - t_0}{\tau_{\text{eff}}} \sigma^z + k \sigma^x, \quad (132)$$

where we have expanded around the critical mode $k = \pi$ (with relabeling $\pi - k$ as k) and $\tau_{\text{eff}} = \tau/r$ so that one can now use the LZ formula.

(E). Quenching through multicritical points

As pointed out in the previous section, the density of defects given by (130) is not valid when the system is quenched through the multicritical point (MCP), implying that the standard KZS need not be valid [551]. Let us employ a quenching scheme in which both the transverse field and the anisotropy vary with time as $h - 1 = \gamma = t/\tau$, so that the system hits the MCP at $t = 0$. Using an appropriate unitary transformation and with $J_x + J_y = 1$, we can recast the two-level problem into the form

$$H_k(t) = \begin{bmatrix} t/\tau + k^2 & -k^3 \\ -k^3 & -(t/\tau + k^2) \end{bmatrix}, \quad (133)$$

where we have expanded close to the critical mode $k = \pi$. Applying the Landau-Zener formula, we find the defect density $n \sim \tau^{-1/6}$ which is not consistent with (109) if one substitutes $d = 1$, $z_{mc} = 2$ and $\nu_{mc} = 1/2$. Divakaran *et al.* [551] proposed a generalized scaling $n \sim \tau^{-d/(2z_{qc})}$, where z_{qc} is determined by the off-diagonal term of the two-level Hamiltonian which scales as $k^{z_{qc}}$ close to the multicritical point; for the transverse XY chain $z_{qc} = 3$.

Let us first qualitatively analyze the reason behind this anomaly before venturing into the technical details provided below. We have already discussed in the previous section that the low-energy modes (modes close to the critical mode) contribute to the density of defect in the limit of large τ . It can be shown that the minimum gap point is not at the MCP, but rather at some special points close to it (on the ferromagnetic side); these are the so-called quasicritical points. The exponents associated with the low-energy excitations above these quasicritical points in fact appear in the scaling of the defect density which in turn becomes different from the predicted KZS.

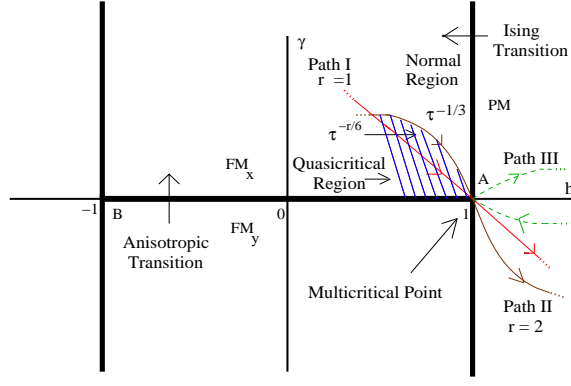


FIG. 22: (Color online) The phase diagram of the one-dimensional XY model in a transverse field. The multicritical points are shown by points A ($h = 1, \gamma = 0$) and B ($h = -1, \gamma = 0$). Different quenching paths corresponding to different values of r are shown; path I (path II) is for $r = 1$ ($r = 2$). Path III corresponds to a quenching scheme in which the system is always in the PM phase and touches the MCP at $t = 0$. The shaded region corresponds to a continuously varying exponent for the defect density, while for $r \geq 2$, n scales as $n \sim \tau^{-1/3}$. (After Mukherjee and Dutta, 2010).

Let us elaborate on the argument provided above. Deng *et al.* [552] attributed this anomalous KZS (for the quenching scheme $h - 1 = \gamma = t/\tau$, as discussed above), to the presence of some special quasicritical points mentioned above; they proposed a generic KZS involving the exponents ν_{mc} , z_{mc} and $\nu_{qc} = \nu_{mc} z_{mc} / z_{qc}$ associated with these quasicritical points [552]. For the transverse XY spin chain, it can be shown that $z_{qc} = 1/\nu_{qc} = 1/3$ using Eq. (133); the energy gap is minimum at $t + k^2 = 0$ (rather than at the MCP at $t = 0$) where the excitations scale as k^3 yielding $z_{qc} = 3$.

To illucidate the notion of these quasicritical points, Mukherjee and Dutta, proposed a quenching scheme $h(t) = 1 + |\gamma|^r \text{sign}(t)$, $r > 0$ and $\gamma = -t/\tau$, as t goes from $-\infty$ to $+\infty$, which enables the system to hit the MCP along different directions characterized by the parameter r [553] (see Fig. 22). Here the case $r = 1$, refers to the situation studied in [552]. The Eq. (132) turns out to be extremely useful in this case. One finds that $\tau_{\text{eff}} = \tau k^{-2(r-1)/r}$ which leads to $\tau_{\text{eff}} = \tau$ for $r = 1$. The higher order terms lead to faster decay of the defect density and hence linearization is a valid approximation for large τ . For $r < 1$, $\tau_{\text{eff}} \rightarrow 0$ as $k \rightarrow 0$, rendering the linearization method inappropriate. The effective dynamical exponent, obtained via linearization method, $z_{qc} = 2/r + 1$, turns out to be a function of r up to a critical value of $r = r_c = 2$, for $r > r_c$, it saturates at a constant value of $z_{qc} = z_{mc} = 2$; for $r = 1$, we get $z_{qc} = 3$ and $\nu_{qc} = 1/3$. The value $\nu_{qc} = 1/3$ as has already been used in explaining the scaling of the FS near the MCP in Sec. V (C).

Linearizing the equations of motion around a quasicritical point and using the Landau-Zener formula, it can be shown that for a path passing through the quasicritical region (i.e., for $r < 2$), the defect density varies continuously with r as

$$n \sim \tau^{-r/6} \quad \text{for } 1 < r < 2. \quad (134)$$

However, for $r \geq 2$, the system passes through a normal region, devoid of any quasicritical points, and hits the multicritical point vertically; this yields the same results as obtained by Divakaran *et al.*, 2008, (Sec. VI (G)) for a slow quench along the gapless line $h = J_x + J_y = 1$ (see Fig. 2), given by $n \sim \tau^{-1/3}$ for $r \geq 2$.

Quenching along a special path (path III in Fig. 22), characterized by $h(t) = 1 + |\gamma|^r$ with $\gamma = t/\tau$, which lies entirely in the PM region and touches the quantum multicritical point at $t = 0$ [552, 553] leads to some unexpected results. For this path, one finds using linearization, $n \sim \tau^{-(4-r)/(2(1+r))}$ for $r < 2$, while for $r \geq 2$, the scaling $n \sim \tau^{-1/3}$ is retrieved. This was explained in terms of the shift in the center of the impulse region which leads to a dimensional shift ($d \rightarrow d + d_0$) [552] in the KZS, where $d_0(r) = 2(2 - r)/r$ and varies continuously with r for $r < 2$. Using adiabatic perturbation theory [509], a KZS for a generic MCP has been proposed [520, 552] though the results for quenching through a MCP is still far from being fully understood and whether the scenario based on the assumption of the existence of quasicritical points is a valid description close to a generic MCP is still an open question. A recent study of thermalization behavior in a transverse XY chain following a sudden quench towards the MCP has also pointed out the anomalous behavior close to it [554].

A similar behavior is observed for the FS (see Sec. V (C)) close to the MCP for a generic path with $\lambda_1 = h - 1 = \gamma^r$ ($\lambda_1 = \gamma = 0$ at the MCP) [424]. One finds that the maximum of χ_F scales as $\chi_F^{\text{max}} \sim L^{2/\nu_{qc}-d}$, where $\nu_{qc} = (2/r + 1)^{-1}$ for $r < 2$, while for $r > 2$, it saturates to $\chi_F^{\text{max}} \sim L^4$ which is the expected scaling of the χ_F at the MCP when

approached along the Ising critical line $\lambda_1 = 0$.

(F). Generalized quenching schemes

In this section, we discuss defect generation in quenching schemes where the quenching parameter is varied in a non-monotonic fashion.

Let us first consider the effect of reversal of the quenching parameter right at the critical point [146]. To study this, we choose the one-dimensional Kitaev model in (42) and quench the anisotropy parameter $J_- = J_1 - J_2$ linearly as $J_- = -|t/\tau|$, for $-\infty < t < \infty$. This implies that the spin chain initially prepared in the ground state is driven by increasing J_- up to the quantum critical point at $t = 0$, after which J_- is decreased at the same rate to its initial value. The advantage of choosing the Kitaev model is that we can choose the parameter variation in such a way that the minimum gap for all the modes occurs at the same time which makes the analytical calculations simpler. Solving the Schrödinger equation exactly with the reversal of the parameter (see (44)), the probability of excitations is found to be

$$p_k(t \rightarrow \infty) = \frac{1}{4}(1 - e^{-2\pi\alpha}) \left| \frac{\Gamma(1 - i\alpha/2)}{\Gamma(1 + i\alpha/2)} + i \frac{\Gamma(1/2 - i\alpha/2)}{\Gamma(1/2 + i\alpha/2)} \right|^2, \quad (135)$$

where $\alpha = \tau \cos^2(k)/|\sin(k)|$ and $\Gamma(x)$ is the Γ -function. The density of defects obtained by numerically integrating this expression appears to be one-half of the defects generated in the conventional quenching without any reversal, i.e., for forward quenching ($-\infty < J_- < +\infty$) when p_k can be derived by using the LZ formula appropriately in (44).

We now consider a similar problem where the parameter J_- is varied linearly up to the critical point at which the variation is stopped for some time t_w [555]. After this waiting time t_w , the variation is once again resumed in the forward direction. Although one cannot use the LZ formula in the present case, the probability of excitations can be exactly obtained by considering the effect of time reversal on the Schrödinger equation which allows us to relate the time evolution from $t = 0$ to ∞ to the evolution from $t = 0$ to $-\infty$. In the limit $t_w/\sqrt{\pi\tau} \ll 1$, the residual energy e_r is found to be [555]

$$e_r \simeq \frac{0.32}{\sqrt{\tau}} [1 + 0.37 e^{-2.3t_w/\sqrt{\tau}}]. \quad (136)$$

Interestingly, one finds that the residual energy decreases with increasing waiting time t_w . The analytical calculations for the two quenching schemes above are apparently not applicable for a transverse XY spin chain because the minimum gap for different modes occurs at different times given by the vanishing diagonal term in (26). However, it can be proved that in the limit $\tau \rightarrow \infty$, the time of occurrence of the minimum gap for all k modes approaches the time at which the minimum of the critical mode occurs; hence the above calculations valid for the Kitaev model should also hold good for the transverse XY spin chain.

Mukherjee *et al.*, 2008, considered the effect of linearly varying the transverse field in a XY chain from a large negative value to a large positive value and then bringing it back to its initial large negative value repeatedly l times, in the process crossing the critical points many times [556]. Here, $l = 1$ corresponds to a variation from $-\infty$ to $+\infty$ which is the usual case, while bringing the system back to its initial value implies $l = 2$. It has been shown that for a general l , the probability of excitations varies as

$$p_k(l) = \frac{1}{2} - \frac{(1 - 2e^{-\pi\tau\gamma^2 \sin^2 k})^l}{2}, \quad (137)$$

which is derived using the generalized form of the Landau-Zener formula for an arbitrary initial condition [556]. For $l = 1$, we retrieve the excitation probability in (128) for the transverse quenching across the Ising critical point. The defect density for an arbitrary l is given by

$$n(l) = \frac{1}{2\pi\gamma\sqrt{\tau}} \sum_{w=1}^{l+1} \frac{l!}{w!(l-w)!} \frac{2^w}{\sqrt{w}} (-1)^{w+1}. \quad (138)$$

As $l \rightarrow \infty$, $p_k(l) \rightarrow 1/2$, i.e., after many oscillations, each spin has an equal probability of being in the up or down state. The expression for the defect density suggests that $n(l+1) < n(l)$ for small values of τ and odd l . This indicates some sort of corrective mechanism in the reverse path. On the other hand, $n(l+1) \rightarrow n(l)$ for large l (irrespective of whether it is even or odd) in the limit of large τ . One striking observation is that for odd l , the kink density $n(l)$

decreases monotonically with τ , while for even l , $n(l)$ attains a maximum around some characteristic value of τ . In the limit $\tau \rightarrow \infty$, $n(l)$ decays as $1/\sqrt{\tau}$ for all l in agreement with the KZS.

Mukherjee and Dutta, 2009, studied the quenching dynamics of a transverse XY spin chain using a time-dependent oscillatory transverse field h given by $h(t) = h_0 \cos \omega t$, with $|h_0| \gg J_x + J_y = J$. They obtained the scaling of defects for a single crossing through the QCP ($h(t) = J$) for evolution from $t = -\pi/\omega$ to $t = 0$, using linearized dynamical equations close to the gapless point. The excitation probability is given by $p_k = \exp(-\pi\gamma^2 \sin^2 k/\omega \sqrt{h_0^2 - J^2 \cos^2 k})$. In deriving p_k through linearization, one defines an effective inverse quenching rate $\tau_{\text{eff}} = 1/(2\omega \sqrt{h_0^2 - J^2 \cos^2 k})$; therefore the limits $\omega \rightarrow 0$ and $h_0 \gg J$ refer to the slow quenching limit where the KZS is applicable. For a single crossing, the defect density is found to scale as $n \sim 1/\sqrt{\omega}$. On the other hand, for two successive crossings of the gapless point, i.e., with $0 \leq t < 2\pi/\omega$, the interference effects were found to play a major role [557–561]. The probability of non-adiabatic transition, Q_{2k} , is given by [562]

$$Q_{2k} = 4p_k(1 - p_k) \sin^2 \left(\frac{2h_0 + J\pi \cos k}{\omega} + \frac{\pi}{4} \right). \quad (139)$$

In the limit $\omega \rightarrow 0$, Q_{2k} oscillates rapidly; one can coarse grain over a small range of k to obtain $Q_k \approx 2p_k(1 - p_k)$ which is the excitation probability following a repeated linear quench [556] obtained by setting $l = 2$ in (137).

Similar studies of multiple crossings [559, 560] reveal the presence of some special momentum modes, given by $2J \cos k/\omega = m$, m being an integer [559, 562], for which the non-adiabatic transition probabilities vary periodically with the number of full cycles; the other modes do not participate in the dynamics. The resultant kink density and entropy density also show an oscillatory dependence on the number of full cycles. These studies have been generalized in recent years from the point of view of dynamical freezing [478] and using the Floquet approach [563].

(G). Quenching through gapless phases

In the quenching processes discussed in previous sections, the initial and final phases are gapped while the spectrum is gapless at the QCP or quantum MCP that the system crosses. However, there are examples in which the system traverses along a gapless line or surface during the process of quenching [71, 145, 519, 564].

Quenching along an infinitely long gapless line can be achieved by varying the anisotropy $\gamma = J_x - J_y = t/\tau$ along the Ising critical line $h = J_x + J_y$ (set = 1) in a spin-1/2 XY chain in a transverse field; see Fig. 2. The two-level Hamiltonian gets modified to

$$H_k(t) = \begin{bmatrix} kt/\tau & k^2 \\ k^2 & -kt/\tau \end{bmatrix}. \quad (140)$$

An application of the Landau-Zener formula leads to the scaling $n \sim \tau^{-1/3}$. Using adiabatic perturbation theory [509], a generalized scaling of the following form has been proposed as [555] $n \sim \tau^{-d/(2a-z)}$, where $\epsilon_k = \gamma(t)k^z + \delta k^a$, where z is the dynamical exponent associated with gapless line (i.e., Ising critical line in the present example) and δ is a time-independent constant which depends on the other parameters of the Hamiltonian. The scaling relation presented here is applicable when the system is quenched across the MCP.

Recalling the phase diagram in Fig. 3 of the transverse XY spin chain with an alternating transverse field (14), we find that the phase boundary given by $h^2 = \delta^2 + J^2$, with γ arbitrary and J held fixed, defines a critical surface in the parameter space spanned by h , δ and γ . If γ is quenched linearly the system traverses a gapless line in the parameter space. Divakaran *et al.* [71] mapped that problem into an equivalent two-level system and the scaling $n \sim \tau^{-1/3}$ was again reproduced. When the transverse field h and the alternating term δ are quenched linearly with $\gamma = 0$, the system again traverses a gapless line and a scaling $n \sim \tau^{-1/2}$ was obtained. This observation brought in the concept of a dominant critical point [70]; the exponents associated with the dominant critical point appear in the KZS in quenching across a gapless line in some situations. In the present case, the dominant critical point is the point $h = \delta = 0$ with critical exponents $\nu = z = 1$.

Another situation arises when the system has a gapless line which has a finite length in parameter space. As pointed out earlier, this occurs in the two-dimensional Kitaev model on a hexagonal lattice [519] (see Fig. 6). As J_3 is linearly quenched from $-\infty < t < \infty$ (i.e., $J_3 = t/\tau$), the system first passes through a gapped region, then through a gapless region, and finally ends in a gapped region. In the limit $\tau \rightarrow \infty$, using the Landau-Zener transition formula in (47), one finds the probability of ending up in the excited state given by $p_{\vec{k}} = \exp(-2\pi\tau[J_1 \sin(\vec{k} \cdot \vec{M}_1) - J_2 \sin(\vec{k} \cdot \vec{M}_2)]^2)$. In the limit $\tau \rightarrow \infty$ when only modes close to the gapless modes contribute, the defect density is found to scale as $1/\sqrt{\tau}$. This is consistent with the scaling relation in (111) for quenching through a gapless surface since $d = 2$ and $m = \nu = z = 1$ in the present case.

Pellegrini *et al.* [564] looked at a similar finite region in a gapless model given by the one-dimensional XXZ chain with the Hamiltonian

$$H = - \sum_i^{N-1} [\sigma_i^x \sigma_{i+1}^x + \sigma_i^y \sigma_{i+1}^y + J_z(t) \sigma_i^z \sigma_{i+1}^z]. \quad (141)$$

The low-lying excitations of the model have a gap $\Delta E = 4J(J_z - 1)$ which closes for $J_z \rightarrow 1^+$. In the whole region $-1 \leq J_z \leq 1$, the spectrum is gapless in the thermodynamic limit. For finite N , the gap vanishes as $1/N$ for $-1 \leq J_z < 1$, whereas it vanishes as $1/N^2$ at $J_z = 1$. The point $J_z = -1$ corresponds to a BKT transition point and for $J_z < -1$, the system is in the antiferromagnetic Neel phase with the energy gap being exponentially small in the system size.

For evolution from the antiferromagnetic ground state with an initial value of the anisotropy $J_z^i \ll -1$ to the ferromagnetic region at a final value of $J_z^f \gg 1$ using a linear variation $J_z(t) = t/\tau$, the time-dependent density matrix renormalization group studies show that the residual energy follows a power law $1/\tau^{1/4}$; this is in agreement with the Kibble-Zurek prediction since the minimum gap, relevant in the $\tau \rightarrow \infty$ limit, scale as $1/N^2$ and N scales as $N \sim \tau^{\nu d/(\nu z + 1)} \sim \sqrt{\tau}$. For a quench starting from $J_z = 0$ and ending deep inside the Neel phase, the residual energy shows a power-law scaling with τ but with an exponent 0.78 ± 0.02 which cannot be explained by a LZ treatment or the KZ argument.

The quenching dynamics of a XY spin chain including multispin interactions and a staggered transverse magnetic field [565, 566], which shows a special QPT between two gapless phases involving doubling of the number of Fermi points [567, 568], has been studied [569]. It is found that for a linear quenching of the transverse field, the defect density in the final state decays exponentially with the inverse rate τ even after passage through gapless phases for models in which the interactions between the two sublattices are not symmetric. This happens because the term that drives the QPT does not participate in the quench dynamics.

(H). Quenching of a disordered chain

The quenching dynamics of a disordered transverse Ising chain cannot be mapped to decoupled 2×2 matrices due to the loss of translational invariance [570, 571]; hence the study of quenching dynamics becomes much more complicated. The disordered Hamiltonian considered in [571], is that of a one-dimensional random transverse field Ising model defined by

$$H = - \sum_i J_i \sigma_i^x \sigma_{i+1}^x - \Gamma(t) \sum_i h_i \sigma_i^z.$$

The parameter $\Gamma(t)$ is quenched as $-t/\tau$ for $-\infty < t \leq 0$, so that the Hamiltonian at $t = 0$ reduces to a classical disordered Ising model. The random couplings J_i, h_i are chosen from a uniform distribution between 0 and 1. The Schrödinger equation given in terms of the fermions c_i by time-dependent Bogoliubov theory is numerically solved [222]. The numerically obtained scaling of the residual energy (e_r) and the defect density (n) averaged over different realizations of randomness can be summarized as follows:

$$\begin{aligned} n &\sim (\log \tau)^{-2}, \\ e_r &\sim (\log \tau)^{-3.4}. \end{aligned} \quad (142)$$

The logarithmic scaling behavior shows that n decays very slowly with τ in the random case in contrast to the power-law decay in pure systems. It is noteworthy that the scaling of the residual energy and defect density are different from each other; this is because the defects are formed more easily near the bonds which are weaker (i.e., where J_i is smaller), which implies that the energy cost of the defects (which is proportional to the values of J_i at those bonds) goes to zero faster than the number of defects as τ becomes large. We also note that this logarithmic scaling is an artifact of the activated quantum dynamics of a disordered chain discussed in Sec. III (B).

(I). Quenching with coupling to a bath

We now discuss the quenching dynamics of a system which is weakly coupled to a thermal bath as studied in [572, 573]. The transverse Ising chain is initially in equilibrium with a bath whose temperature T is kept constant during a linear quench of the transverse field, $h(t) = -t/\tau$. The quench of a parameter of the Hamiltonian takes the

system through the quantum critical region at a finite T . Assuming that the total density of excitations n is obtained by adding up the contributions from the Kibble-Zurek scaling at $T = 0$ (n_{kz}) and the thermally induced incoherent defects at finite T (n_{th}), the total defect density n can be written as

$$n = n_{kz} + n_{th}. \quad (143)$$

The decoupling of the thermal and Kibble-Zurek contributions is justified by the assumption that the system is weakly coupled to the bath. Let us assume that the relaxation time ξ_τ for the excitations varies with the temperature T as $\xi_\tau^{-1} \propto \alpha T^\theta$, where α is the system-bath coupling constant. Then the scaling of incoherent defects is given by

$$n_{th} \propto \frac{\alpha}{\tau} T^{\theta+(d\nu+1)/(z\nu)}. \quad (144)$$

For quenching times smaller than a critical $\tau = \tau_c$ (obtained by equating the KZ and thermal contributions), the KZ contribution dominates, whereas for quenching times larger than τ_c , the incoherent thermal contribution is more important as the system spends more time within the quantum critical region.

In another series of works by Polkovnikov *et al.*, the authors studied a system which is prepared in an initial state in thermal equilibrium at a temperature T after which the dynamics is started [515, 532, 540, 543]. Once the variation of the parameter of the Hamiltonian begins, no effect from the bath is considered. They show that at finite temperatures, the statistics of the low-energy quasiparticles plays an important role; if one considers the quenching of free massive bosons and fermions¹², the number of quasiparticles excited to the momentum k is different in the two cases depending on the statistics.

The effect of the environment on the quenching dynamics of a spin chain has also been studied in recent years [574–576]. Mostame *et al.*, 2007, considered a global interaction between the transverse field of (9) and the environment of the form $R \sum_i \sigma_i^z$, where R is the Hermitian operator describing the environment; the model is solvable due to the global nature of the interactions and it has been showed that the decoherence increases the defect density.

Cincio *et al.*, 2009, studied the linear quenching of the transverse field of the Ising chain in (9) coupled to a static environment through the interaction $V = -\sum_{m,n} \sigma_m^z V_{mn} \mu_n^z$, where the μ_n 's are the static spins describing the environment. If the dynamics starts from a pure state when the system and the environment are uncoupled, it can be shown that the static environment generates a random transverse field in the spin Hamiltonian. The original problem of quench in a pure Ising system gets mapped to an average over quenches in an isolated Ising model in a random transverse field; the quenching dynamics then can be solved by numerically diagonalizing the Schrödinger equation. The KZS for the isolated system predicts that for an adiabatic evolution $\tau \sim L^2$, while in the model of decoherence, as is expected from the mapping to the dynamics of a disordered chain of size L (compare with the result of the previous section), $\tau \sim \exp(\sqrt{L})$ which is non-polynomial in L ; hence we have an upper bound on the system size that can be quenched adiabatically by coupling to a static bath. Assuming that influence of a random field is negligible, the dynamics becomes non-adiabatic when $t \sim \hat{t}$; KZS predicts a defect density scaling as $1/\sqrt{\tau}$. On the other, a perturbation expansion in the strength of the disorder (h_0) predicts a defect density $\sim h_0^2$. We therefore get an additional condition for adiabatic evolution $1/\sqrt{\tau} \gg h_0^2$ or $L \ll 1/h_0^2$.

(J). Quenching and quantum information

We have seen that slow and sudden quenches across a QCP lead to defects in the final state of the quantum Hamiltonian. These defects influence the scaling behavior of different quantum information theoretic measures discussed in Sec. 5, e.g., the concurrence and negativity show an identical scaling relation as that of the defect density. We start the discussion focussing on the von Neumann entropy density generated following a linear quench across the Ising critical point.

(a). Slow quenches

(i) Decohered density matrix, von Neumann entropy density and correlation functions

The quenching dynamics of the spin models considered so far is governed by the Schrödinger equation and is unitary. Therefore, the final state following a quench must be a pure state. However, it is expected to have a fairly complicated

¹² These are actually two limits of the sine-Gordon model [543] (see Appendix H and Eq. (H1)).

local structure; a sweep through a critical point generates defects which in turn lead to intrinsic decoherence and a local entropy which we discuss below [545].

Following an evolution from $-T < t < T$ of the transverse Ising chain, the final state is described by a density matrix of the product form $\rho = \bigotimes \rho_k$, where ρ_k is given by

$$\begin{bmatrix} p_k & q_k \\ q_k^* & 1 - p_k \end{bmatrix}. \quad (145)$$

with p_k is the excitation probability and $q_k = C_{1k}(T)C_{2k}^*(T)$ (see the discussion around Eq. (126)). In the thermodynamic limit, the correlation functions for any local observable are calculated by expressing them in terms of the 2×2 matrix of pair correlators and taking a trace over (i.e., integrating over k) the above density matrix. The diagonal elements of the reduced 2×2 density matrix are smooth functions of k and are independent of the total quenching time $T (\gg \sqrt{\tau})$, whereas the off-diagonal terms are rapidly oscillating functions of both k and T . In the limit $T \rightarrow \infty$, the phase of the off-diagonal term varies rapidly; as a result the integral of q_k over k vanishes.

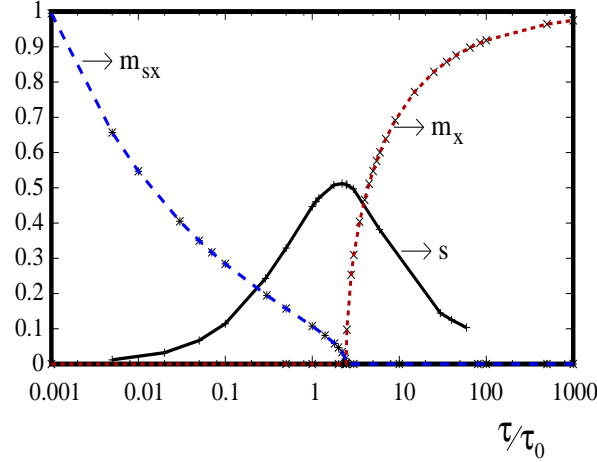


FIG. 23: (Color online) Variation of von Neumann entropy density s , staggered magnetization m_{sx} and magnetization m_x as a function of τ/τ_0 , for $J_y = 1$ and $h = 0.2$. (After Mukherjee *et al.*, 2007).

The final state may therefore be viewed locally as a mixed state described by a decohered reduced density matrix ρ_D given by

$$\begin{bmatrix} p_k & 0 \\ 0 & 1 - p_k \end{bmatrix}. \quad (146)$$

To quantify the amount of information lost in the decoherence process, we consider the von Neumann entropy density of the system, $s = -\text{tr}(\rho_D \ln \rho_D)$, namely,

$$s = - \int_0^\pi \frac{dk}{\pi} [p_k \ln(p_k) + (1 - p_k) \ln(1 - p_k)]. \quad (147)$$

The von Neumann entropy density shows an interesting dependence on the inverse quenching rate τ for both transverse and anisotropic quenching in a transverse XY spin chain [545, 549]. For sufficiently small τ , the final state is very close to the initial state, while for $\tau \rightarrow \infty$, the dynamics is nearly adiabatic and the system almost reaches the final ground state. In both these limits, the final state is almost pure and the entropy density tends to vanish; it attains the maximum value at an intermediate value of $\tau \sim \tau_0$, for which $p_k = 1/2$ for the wave vector $k = k_0$ corresponding to the critical mode. Moreover, for the anisotropic quenching [549] in the limit $\tau \rightarrow 0$, the final state is antiferromagnetically ordered in the \hat{x} direction with a non-zero staggered magnetization m_{sx} , and is ferromagnetically ordered ($m_x \neq 0$) for large τ . The entropy density attains a maximum close to the value of τ for which the magnetic order of the final state changes from antiferromagnetic to ferromagnetic as shown in Fig. 23.

Following a transverse quenching, we can calculate the correlation functions in the final state from the decohered density matrix using the notation introduced in Eqs. (68-71) [577]. We note that the correlation functions such as $\langle \sigma_i^\pm \sigma_{i+n}^z \rangle = 0$ due to a Z_2 symmetry of the Hamiltonian. The non-zero correlation functions can be computed using

the method developed in [545], introducing a quantity $\alpha_n = \int_0^\pi (dk/\pi) p_k \cos(nk)$; $\alpha_n = 0$ for odd n as p_k is invariant under $k \rightarrow \pi - k$. In terms of α_n , the diagonal correlation functions are given by

$$\langle \sigma_i^z \rangle = 1 - 2\alpha_0 \quad \text{and} \quad \langle \sigma_i^z \sigma_{i+n}^z \rangle = \langle \sigma_i^z \rangle^2 - 4\alpha_n^2. \quad (148)$$

Thus, for any two spins separated by an odd number of lattice spacings, $\langle \sigma_i^z \sigma_{i+n}^z \rangle = \langle \sigma_i^z \rangle^2$ [545]. The off-diagonal correlators $\langle \sigma_i^a \sigma_{i+n}^b \rangle$ (where a, b can take the values $+, -$) can also be computed in terms of α_n .

For the correlation functions appearing in Eqs. (71), we find that $\langle \sigma_i^\pm \sigma_{i+n}^\pm \rangle = b_1^n = 0$ for all n since these involve correlations between two fermionic annihilation/creation operators and hence vanish. Further, $\langle \sigma_i^\pm \sigma_{i+n}^\mp \rangle = b_2^n = 0$ for all odd n since these are odd under the transformation $\sigma_n^x \rightarrow (-1)^n \sigma_n^x$, $\sigma_n^y \rightarrow (-1)^n \sigma_n^y$, $\sigma_n^z \rightarrow \sigma_n^z$ which changes the signs of the couplings J_x and J_y but leaves p_k invariant. For even $n \leq 6$, we find

$$\begin{aligned} \langle \sigma_i^+ \sigma_{i+2}^- \rangle &= \alpha_2 \langle \sigma_i^z \rangle, \\ \langle \sigma_i^+ \sigma_{i+4}^- \rangle &= (\alpha_4 \langle \sigma_i^z \rangle - 2\alpha_2^2) \langle \sigma_i^z \sigma_{i+2}^z \rangle, \\ \langle \sigma_i^+ \sigma_{i+6}^- \rangle &= \left[\alpha_6 \langle \sigma_i^z \sigma_{i+2}^z \rangle + 4\alpha_2(\alpha_2^2 + \alpha_4^2 - \alpha_4 \langle \sigma_i^z \rangle) \right] \times \\ &\quad \left[\langle \sigma_i^z \rangle [\langle \sigma_i^z \sigma_{i+2}^z \rangle - 4(\alpha_2^2 + \alpha_4^2)] + 16\alpha_2^2 \alpha_4 \right]. \end{aligned} \quad (149)$$

We will use these correlators to calculate the concurrence and negativity below. We note that the correlation function can also be calculated in a similar way when the transverse field of a transverse Ising chain is quenched from $-\infty$ to 0 [578].

For quenching through the gapless phase of the two-dimensional Kitaev model (see Sec. VI(G)), it can be shown that the defect density is related to certain spin correlation functions. Let us consider a two-fermion operator

$$O_{\vec{r}} = ib_{\vec{n}} a_{\vec{n}+\vec{r}}, \quad (150)$$

where $b_{\vec{n}}$ and $a_{\vec{n}}$ are Majorana operators. In terms of the spin operators, $O_{\vec{r}=\vec{0}}$ is equal to $\sigma_{j,l}^z \sigma_{j,l+1}^z$, i.e., a product of σ^z 's for two spins connected by a vertical bond. For $\vec{r} \neq \vec{0}$, $O_{\vec{r}}$ can be written as a product of spin operators going from a b site at \vec{n} to an a site at $\vec{n} + \vec{r}$ along with a string of σ^z 's in between. In momentum space, we have

$$O_{\vec{r}} = \frac{4i}{N} \sum_{\vec{k}} [b_{\vec{k}}^\dagger a_{\vec{k}} e^{i\vec{k} \cdot \vec{r}} - a_{\vec{k}}^\dagger b_{\vec{k}} e^{-i\vec{k} \cdot \vec{r}}], \quad (151)$$

where N is the number of sites. We then find that on quenching J_3 from $-\infty$ to ∞ as Jt/τ (holding J, J_1, J_2 fixed), the expectation value of $O_{\vec{r}}$ in the final state is given by

$$\langle O_{\vec{r}} \rangle = -\delta_{\vec{r},\vec{0}} + \frac{2}{A} \int d^2 \vec{k} p_{\vec{k}} \cos(\vec{k} \cdot \vec{r}), \quad (152)$$

where the integral over momentum runs over half the Brillouin zone with area $A = 4\pi^2/(3\sqrt{3})$, and the excitation probability $p_{\vec{k}} = e^{-2\pi\tau [J_1 \sin(\vec{k} \cdot \vec{M}_1) - J_2 \sin(\vec{k} \cdot \vec{M}_2)]^2}$ as given by the LZ formula. For an adiabatic quench ($\tau \rightarrow \infty$), $p_{\vec{k}} = 0$ for all \vec{k} ; Eq. (152) then shows that only the on-site fermion correlation ($\vec{r} = \vec{0}$) is non-zero. But if the quench is non-adiabatic, then longer-range correlations become non-zero; these have an interesting and highly non-anisotropic dependence on the separation \vec{r} [145].

(ii) Concurrence and negativity

Sengupta and Sen [577], studied concurrence and negativity as measures of the two-spin entanglement in the final state of the transverse Ising chain in (9) following a linear quench of the transverse field $h = t/\tau$ as t goes from $-\infty$ to ∞ . As seen in the case of the von Neumann entropy, the entanglement is expected to vanish in both the limits $\tau \rightarrow 0$ and $\tau \rightarrow \infty$, when the system only retains information about the initial and final ground states, respectively. However, for a finite quenching time τ , the defects generated in the process of quenching across the QCP lead to a non-zero value of the two-spin entanglement [577].

To compute the concurrence and negativity, we use the expressions given in Eqs. (68-71) and the correlation functions given in Eqs. (148-149). For $n \leq 6$, we find (see (67)) that $\sqrt{\lambda_i^n}$ are given by $\sqrt{a_+^n a_-^n}$ (appearing twice), and $a_0^n \pm |b_2^n|$. Thus the spin chain has a non-zero concurrence given by

$$C^n = \max \{0, 2(|b_2^n| - \sqrt{a_+^n a_-^n})\}. \quad (153)$$

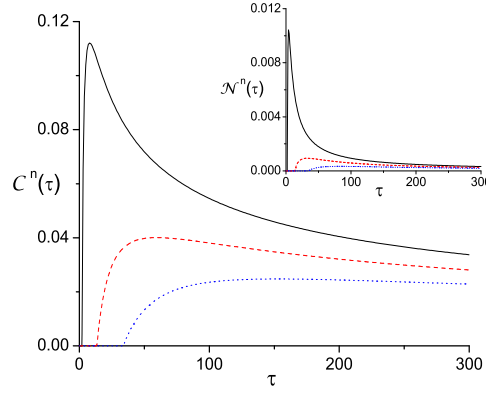


FIG. 24: (Color online) Plots of C^n as a function of τ for $n = 2$ (black solid line), $n = 4$ (red dashed line) and $n = 6$ (blue dotted line). The inset shows analogous plots for \mathcal{N}^n . (After Sengupta and Sen, 2009).

To compute the negativity \mathcal{N}^n , we need to take a partial transpose of ρ^n with respect to the labels corresponding to the site $j = i + n$ in (68) [364]. This interchanges $b_1^n \leftrightarrow b_2^n$; the eigenvalues of the resultant matrix $\bar{\rho}^n$ are given by $\tilde{\lambda}_0^n = a_0^n$ (appearing twice), and $\tilde{\lambda}_{\pm}^n = (1/2)[a_+^n + a_-^n \pm \sqrt{(a_+^n - a_-^n)^2 + 4|b_2^n|^2}]$ of which only $\tilde{\lambda}_-^n$ can become negative. This happens when $|b_2^n| > \sqrt{a_+^n a_-^n}$ and yields

$$\mathcal{N}^n = \max\{0, \tilde{\lambda}_-^n\}. \quad (154)$$

Eqs. (153) and (154) lead to several interesting findings [577]. First, it can be easily shown that both C^n and \mathcal{N}^n vanish when n is odd, i.e., the quench generates entanglement only between the even neighbor sites. Second, for large τ and $n \ll \sqrt{\tau}$, one finds that $C^n \sim \sqrt{1/\tau}$ and $\mathcal{N}^n \sim 1/\tau$. Thus, for slow quenches, C^n (\mathcal{N}^n) scales with the same (twice the) universal exponent as the defect density [508, 509]. Third, both the concurrence and the negativity become non-zero for a *finite critical quench rate* $(\tau_c^n)^{-1}$ above which there is no entanglement between a site and its n^{th} neighbor. Numerical studies for $n = 2, 4$ and 6 indicate that τ_c^n scales as n^2 for large n . Figure 24 shows plots of C^n and \mathcal{N}^n as functions of τ for $n = 2, 4, 6$; we see that C^n and \mathcal{N}^n become non-zero between $\tau = \tau_c^n$ and ∞ . Further, the ratios C^4/C^2 or $\mathcal{N}^4/\mathcal{N}^2$ can be selectively tuned between zero and 1 by tuning τ . The maximum values of both C^n and \mathcal{N}^n decrease rapidly with n . For large $n \gg \sqrt{\tau}$, using the properties of Toeplitz determinants used to compute the spin correlators in these systems, it can be shown that $\langle \sigma_i^+ \sigma_{i+n}^- \rangle \sim \exp(-n/\sqrt{\tau})$ [545]. Thus one expects the entanglement to vanish exponentially for $n \gg \sqrt{\tau}$.

(iii) Entanglement entropy

The defects generated by a quantum quench lead to a non-zero entanglement entropy between two parts of the final state of the system. When a one-dimensional chain is quenched linearly across the QCP with $z = 1$, the KZS provides the scaling of the healing length given by $\hat{\xi} \sim \tau^{\nu/(\nu+1)}$ which also determines the entanglement entropy. For an open chain, one gets the entanglement entropy (see Sec. V (A) (b)) $S_{\text{quench}} = c\nu/6(\nu+1) \log_2 \tau$. For quenching of a transverse Ising chain by linearly varying a generic magnetic field (see (131)), one gets $\nu = 1$ for $\phi = 0$ and π , and $\nu = 8/15$ otherwise, while the central charge $c = 1/2$ [550].

Cincio *et al.*, 2007, studied the linear quenching of a transverse Ising chain in (9) with $h(t) = t/\tau$, where t changes from $-\infty$ to 0 so that the system is expected to reach the Ising ferromagnetic ground state. The entanglement entropy of a block of l spins which is coupled to the rest of the system saturates to $S_l = 1/6 \log_2 \hat{\xi}$ which is in complete agreement with the argument provided above. However, this saturation is found to occur when the block size $l \gg l_0 = \sqrt{\tau} \ln \tau$. This secondary length scale l_0 is argued to develop as a result of a dephasing process which is in fact the dynamical equivalent of the classical phase-ordering process [579].

The geometric phase [580], quantum discord [581] and generalized entanglement [582] in the final state of a quantum XY chain following a quench across the QCP or the quantum MCP have been studied in recent years. Cincio *et al.* [578] calculated the fidelity between the final state reached through quenching the transverse field of the transverse field Ising model as $h = t/\tau$, and the ground state of the final Hamiltonian at $t = 0$, given by $F = \prod_{k>0} (1 - p_k)$, where p_k is the excitation probability calculated in previous sections. In the limit $\tau \gg 1$, one finds that

$$\ln F \simeq \frac{L}{\pi} \int_0^\pi dk \ln(1 - p_k) \sim -1.3 n L \quad (155)$$

for a chain of length L . In deriving the above equation, one assumes that $N \gg \hat{\xi}$ and uses the excitation probability $p_k = \exp(-2\pi\tau k^2)$ and the density of excitations n . Eq. (155) shows that the fidelity decays exponentially with the system size L over a length scale determined by the healing length $\hat{\xi} \sim 1/n$.

Let us now address the question of dynamical generation of decoherence; this has been studied by measuring the LE within the central spin model introduced in Sec. V(D). Damski *et al.*, studied the decoherence of a single qubit (spin-1/2) coupled to all the spins of a transverse Ising chain with the transverse field being quenched linearly across the QCP as t/τ [471]. At the initial time $t \rightarrow -\infty$, the qubit is chosen to be in a pure state which is a superposition of up and down states, and the spin chain is in the ground state. By calculating the reduced density matrix of the qubit as a function of time, it has been shown that the decoherence is dramatically increased (i.e., the modulus of the off-diagonal term of the reduced density matrix shows a sharp decay) when the surrounding spin chain is close to the QCP. Moreover the logarithmic of the LE or the decoherence factor that appears in the off-diagonal term of the reduced density matrix is found to scale in an identical fashion to that of the defect density when the environmental spin chain is quenched across isolated critical [471] and multicritical points; the scaling is not identical when the spin chain is quenched across a gapless critical line (for example for quenching along the Ising critical line through the MCP of Fig. (2)) [583]. Whether the decoherence factor satisfies a universal scaling relation for such a non-equilibrium quenching of the environment is still an open question. It has also been observed that a sudden quenching of the environment increases the decoherence of the central spin [584].

(b). Sudden quenches

The time evolution of the entanglement entropy in a quantum spin chain following a sudden quench of a parameter λ from an initial value λ_i to a final value λ_f , where the initial state is the ground state for the parameter λ_i and the final Hamiltonian is critical has been studied recently [585, 586]. If the Hamiltonian is held fixed after the quench, it was found using both CFT and exactly solvable models that

$$\begin{aligned} S_L(t) &\sim t \quad \text{for } t \leq t^*, \\ &\sim L \quad \text{for } t \geq t^*, \end{aligned} \tag{156}$$

where t^* is of the order of $L/2$. A similar crossover is also seen for quenching to a non-critical final Hamiltonian as seen from numerical studies of the transverse Ising chain (with initial and final transverse field both greater than h_c) [585]. This can be understood as follows. Following the sudden quench, pairs of entangled quasiparticles are produced at different points of the chain and propagate in opposite directions with a velocity which is set equal to 1. The entanglement entropy receives a contribution from those pairs for which one quasiparticle lies inside the block while the other lies outside; hence the entropy increases linearly in time till it saturates when all the pairs which started inside the block reach its boundary.

However, following a slow quench in the generic transverse Ising Hamiltonian in (131) (with $\phi = 0$) from $g = g_i$ to $g_f = -g_i$ through the critical point at $g = 0$, if the system is allowed to evolve with the final Hamiltonian, one finds that the entanglement entropy S oscillates as a function of time around a linearly increasing mean (Fig. 25) [550]. This can be explained in terms of the Loschmidt echo (see Sec. V(D)) for an integrable system which can be written as a product of two-level systems parametrized by the wave vector k (e.g., for the transverse Ising and XY spin chains). Let us assume that in one of the subsystems, the probabilities of being in the ground and excited states following the quench are $1 - p_k$ and p_k , respectively; these states evolve in time with the final Hamiltonian. Assuming the energy difference between these two levels to be ΔE_k , one can calculate the overlap between the state $|\psi_k(0)\rangle$ immediately after the quench and the state $|\psi_k(t)\rangle$ after an additional time t , given by

$$\langle \psi_k(0) | \psi_k(t) \rangle = \begin{pmatrix} \sqrt{p_k} & \sqrt{1-p_k} \end{pmatrix} \begin{pmatrix} \sqrt{p_k} \\ \sqrt{1-p_k} e^{-i\Delta E_k t} \end{pmatrix}. \tag{157}$$

Hence, the overlap for the total wave function is

$$\begin{aligned} |\langle \psi(0) | \psi(t) \rangle|^2 &= \bigotimes_k |\langle \psi_k(0) | \psi_k(t) \rangle|^2 \\ &= \exp \left[-L \int \frac{dk}{2\pi} \log \left[1 - 4p_k(1-p_k) \sin^2 \left(\frac{\Delta E_k t}{2} \right) \right] \right]. \end{aligned}$$

The mode for which $p_k = 1/2$, gives rise to the cusp in the above equation whenever $\sin^2(\Delta E_k t/2) = 1$. This oscillation does not occur if the system is non-integrable ($\phi \neq 0$ or π in (131)).

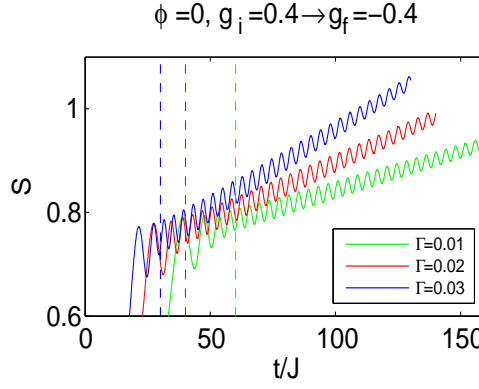


FIG. 25: (Color online) Entanglement entropy as a function of time for a sweep of the Hamiltonian in (131) with $\phi = 0$ from $g_i = 0.4$ to $g_f = -0.4$. The dashed lines indicate the time at which the final value of $g_f = -0.4$ has been reached, and the Hamiltonian remains unchanged thereafter. Here, Γ is the inverse rate $1/\tau$. (After Pollmann *et al*, 2010).

Venuti and Zanardi studied a sudden quench of small amplitude around a QCP and showed that a generic observable does not equilibrate in the sense that its distribution is not peaked around the mean [587]. Moreover the distribution function is found to assume a universal, bistable form rather than the generic Gaussian form. The essential point is that the overlap $c_n = \langle \psi_n | \psi_0 \rangle$, where ψ_0 is the initial state and ψ_n is the eigenstate of the final Hamiltonian with eigenvalue E_n , decays very rapidly ($c(E) \sim E^{-1/(z\nu)}$) near the QCP; this in turn implies a power-law double-peaked distribution. This prediction has been verified for the quantum ANNNI chain in (59) with $\kappa < 1$.

(K). Local quenching processes

Another interesting problem going in parallel with global quenches is local quenches [588]. As the name suggests, in local quenches, a parameter of the Hamiltonian H_0 is changed only locally, say at site r or in a small region R . The system which is prepared in the ground state $|\psi_0\rangle$ of H_0 is now in the excited state corresponding to the locally disturbed Hamiltonian H . One can then look at the evolution of the average values of various quantities like the entanglement entropy [589–591], correlation function and magnetization [590, 592], Loschmidt echo and light cone effects [593]. Experimentally, this type of situation corresponds to the X-ray absorption problem in metals where the creation of a hole plays the role of a local defect which is then removed by filling a conduction electron.

Eisler *et al.* numerically studied the evolution of the entanglement entropy S in a critical XX chain expressed in terms of non-interacting fermions hopping between neighboring sites when the hopping parameter is changed at a particular site [589]. In global quenches, S exhibits the scaling given in (156). In contrast, for local quenches where the defect is at the center of a system of size L , S does not change till time $t = L/2$ after which there is a sudden jump followed by a slow relaxation towards the value in the homogeneous system of size L as shown in Fig. 26. They looked at the effect of various defect positions and defect strengths on the evolution of S . These observations were analytically justified using conformal field theory by Calabrese and Cardy [590]; they also looked at the evolution of the correlation function and magnetization after such a local quench in a system consisting of two disconnected (but individually critical) parts for $t < 0$ which are suddenly joined together at $t = 0$. They showed that the correlation function, like the entanglement entropy, shows a horizon effect, i.e., it remains in its initial value till some time t , which depends upon the defect position. After this time t , the correlation function shifts towards its equilibrium value corresponding to the homogeneous system.

Let us consider a local quench of a critical transverse Ising model where the interaction term connecting two sites at the center of the chain is suddenly increased from zero to the homogeneous value $J_x (= h_c)$ (see (9)). If the two sites between which the correlations are measured are on the same side of the defect (where the local quench is performed) such that r_2 is the distance of the defect from the closer reference point and r_1 is the distance from the farther point, with $r_2 < r_1$, then the correlation function $\langle \psi_0 | \sigma^x(r_1, t) \sigma^x(r_2, t) | \psi_0 \rangle$ for $t < r_2$ behaves as

$$C_t(r_1, r_2) = \left(\frac{(r_1 + r_2)^2}{4r_1 r_2 (r_1 - r_2)^2} \right)^x F \left(\frac{4r_1 r_2}{(r_1 + r_2)^2} \right), \quad (158)$$

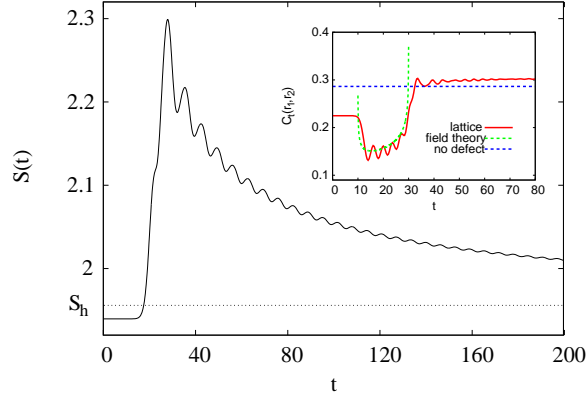


FIG. 26: (Color online) Time evolution of entanglement entropy for a subsystem of $L=40$ sites with a central defect. A sudden jump is followed by a slow relaxation towards the homogeneous value S_h (After [589]). Inset shows the time evolution of the correlation function after a local quench comparing the numerical and field theory results (After [592]).

where x is the scaling dimension of the operator σ^x , and the function F has the form

$$F(\eta) = \frac{\sqrt{1+\sqrt{\eta}} - \sqrt{1-\sqrt{\eta}}}{\sqrt{2}}. \quad (159)$$

Clearly, the correlations for $t < r_2$ do not depend on the time since the signal traveling at unit velocity from the defect located outside the two reference points will not arrive at the closer reference point till $t = r_2$. As the signal reaches the first reference point, the correlation changes to

$$C_t(r_1, r_2) = \left(\frac{(r_1 + r_2)(r_2 + t)\epsilon}{(r_1 - r_2)(r_1 - t)4r_1(t^2 - r_2^2)} \right)^x F\left(\frac{2r_1(r_2 + t)}{(r_1 + r_2)(r_1 + t)} \right), \quad (160)$$

where ϵ is the regularization parameter used as a damping factor in conformal field theory calculations. Finally, at $t = r_1$, the second reference point also receives the signal from the defect and the system recognizes the presence of the enlarged system. The correlation saturates to the equilibrium value corresponding to the homogeneous system of size L and is given by $C_t(r_1, r_2) \propto |r_1 - r_2|^{-2x}$. The expression for C_t is different when the reference points are located on opposite sides of the defect.

These results have been numerically verified by Divakaran *et al.* [592]. They numerically studied the evolution of the magnetization and correlation functions of the transverse Ising model in the critical system where the conformal theory predictions were successfully verified and also discussed some results when the final Hamiltonian is in the ferromagnetic and PM phases. The numerically obtained results along with the conformal field theory results for the evolution of correlation functions is shown in the inset of Fig. 26 for comparison. The non-zero correlations can be explained using the quasiparticle picture [594, 595]; in this framework, kink like excitations (a pair of quasiparticles with opposite momenta) are created at the defect which move semi-classically with a momentum dependent velocity. Since these quasiparticles are emitted only at the site of defect, they are quantum entangled causing correlations between the two reference points. This is contrary to the picture of global quenches where the quasiparticles are emitted at all the sites [483, 484, 596].

(L). Thermalization

In the major part of this section, we have studied what happens immediately after a parameter in the Hamiltonian of a many-body system is varied so as to take it across a QCP. We typically find that starting with the ground state of the initial Hamiltonian H_i , we end in a state which is *not* the ground state of the final Hamiltonian H_f . For instance, for a slow quench, the final state reached differs from the ground state of H_f by a finite density of defects.

One can then ask: what would now happen if the Hamiltonian is held fixed at H_f and the many-body system is allowed to evolve further in time? The problem of ergodicity and thermalization following a quantum quench [485, 572, 597–600] has been of great interest following the experimental observations with cold atoms [1, 473]. We will not discuss this important problem here, and we refer the reader to recent review articles [537, 542].

(M). KZ mechanism and adiabatic evolution

The defect generation following a passage through a QCP is relevant in the context of adiabatic quantum computation [601], where the adiabatic evolution of a system from an initial state to a computationally non-trivial state is explored. When a QCP is encountered during the evolution, the defects are inevitably generated according to the KZS. Considering a non-linear quenching of the driving parameter $\lambda \simeq \lambda_0 |t/T|^r \text{sign}(t)$, where $-T < t < T$ and T is the characteristic passage time which is held fixed, we note that a large number of excitations are produced for both $r \rightarrow 0$ and $r \rightarrow \infty$. To minimize defect production, one therefore needs to find an optimized value of r and check whether this optimal value is determined by some universal properties of the associated QCP.

Using adiabatic perturbation theory for the above mentioned quenching scheme, Barankov and Polkovnikov [517] found that the defect density $n \sim (r\delta)^{dr\nu/(r\nu+1)}$ where $\delta = 1/(T\Delta_0)$ and Δ_0 is the lowest excitation energy at $\lambda = \lambda_0$, i.e., the final value of the coupling at $t = T$. We note that an identical exponent for the scaling of the defect density was also derived by Sen *et al.* [516] (see Sec. VI(B)), although the dependence on the parameter δ through $r\delta$ was not included. Optimizing n with respect to r , one finds that minimum excitation occurs at $r_{\text{opt}}\delta \simeq \exp(-r_{\text{opt}}z\nu)$. For a transverse Ising chain with $z = \nu = 1$, one finds $n \simeq [A(r)\delta]^{r/(r+1)}$ where $A(r)$ scales linearly with r ; hence the optimal condition gets modified to $r_{\text{opt}} \simeq -\ln[(\delta/C)\ln(C/\delta)]$ with the non-universal constant $C = 14.7$ [517]. In the context of a power-law sweep of the confining potential of a trapped system, the above study has been further generalized to the case where the quenching potential varies both in space and time as $\lambda(x, t) \simeq \lambda_0(t)|x|^w$, where the QCP is at $x = t = 0$; the amplitude $\lambda_0(t) \sim |t/\tau|^r$ [602] for $-T < t < T$ (see also Sec. F). It has been shown that the mean excitation density follows an algebraic law as a function of the sweeping rate with an exponent that depends on the space-time properties of the potential.

In relation to the generalized quenching schemes (see Sec. VI(F)), the concept of a quench echo has been introduced to test the adiabaticity of quantum dynamics [603]. In this approach, one calculates the fidelity between the initial ground state and the final evolved state following a slow quench in which the final Hamiltonian of the quantum system happens to be the same as the initial one. For example, for a transverse Ising chain of finite length, one can define a quenching protocol for the transverse field h ,

$$\begin{aligned} h(t) &= h_0 - \frac{t}{\tau} \quad \text{for } 0 < t < (h_0 - h_T)\tau, \\ &= 2h_T - h_0 + \frac{t}{\tau} \quad \text{for } (h_0 - h_T)\tau < t < 2(h_0 - h_T)\tau. \end{aligned} \quad (161)$$

Namely, the system is initially prepared in the ground state of h_0 . Then h is first ramped in the forward direction from $h = h_0$ to $h = h_T$, and is then reversed from h_T to h_0 , where h_T is the turnaround point. The idea is that if τ is so large that the system is protected against excitations due to a finite gap at $h = h_c = 1$ (for $J_x = 1$), both forward and reverse evolutions are adiabatic, and the fidelity between the initial and final state is close to unity. The advantage of the quench echo approach is that no prior knowledge of the eigenstates or eigenvalues of the Hamiltonian is necessary.

In another approach, the adiabaticity is tested locally in time during the evolution and the local speed is adjusted accordingly so that the system stays close to the instantaneous ground state though the energy gap may be unknown [604]. Similarly, for a local Hamiltonian like the transverse Ising chain, the linear evolution from an initial to a final Hamiltonian can be replaced by a series of straight-line interpolations, along which the fundamental energy gap is always greater than a constant independent of the system size; this enables a very efficient and adiabatic preparation of a highly entangled ground state [605]. We note that the role of quenching protocol has also been studied in [606].

(N). A brief note on quantum annealing

In this section, we will include a brief note on the optimization method known as quantum annealing which is also related to the adiabatic evolution; for an extensive review we refer to [607, 608]. In this method, one attempts to find the ground state of a random classical Hamiltonian (or a multivariate cost function viewed as the same). To achieve this, a (non-commuting) quantum kinetic term (e.g., a transverse field term in a classical random Ising Hamiltonian) is added. The kinetic term is initially set at a value much higher than all the interaction terms so that the initial ground state is trivially known. The kinetic term is then reduced to zero slowly following some protocol. If the dynamics is completely adiabatic, one is expected to reach the ground state of the classical random Hamiltonian at the final time. Of course, one assumes that there is no crossing of energy levels with the ground state in the course of evolution. The quantum annealing is meaningful for finding the ground state of classical Ising SK spin glass where, as mentioned already, ergodicity is broken at $T = 0$ and barriers between neighboring local minima become proportional to system size. We have already mentioned that quantum fluctuations may induce tunneling between these minima

and the ergodicity may get restored [182]. However, in the presence of disorder extended states in a quantum system may get localized [609].

Let us clarify quantitatively in what sense one believes that quantum annealing may be more efficient than thermal annealing. In fact, if two local minima of the free energy landscape are separated by a barrier of height l and width w , the classical escape rate at a finite temperature T is given by $\exp(-l/T)$. On the other hand, the quantum tunneling probability induced by the transverse field h is approximately given by $\exp(-(\sqrt{l}w)/h)$, ensuring the clear advantage of quantum tunneling when $w \ll \sqrt{l}$ [610, 611]. Recent numerical studies clearly demonstrate that quantum annealing can occasionally help reaching the ground state of a complex glassy system much faster than could be done using thermal annealing. Following the pioneering demonstrations, theoretically in the references [601, 612–615], and experimentally by Brooke *et al.*, 1999 and Aeppli and Rosenbaum, 2005, the quantum annealing technique has now emerged as a successful technique for optimization of complex cost functions (see Sec. VII (E)). (For a mathematical discussion on the bounds and schedule strategies for quantum annealing see the ref. [616].)

However, it needs to be mentioned that recent studies show that the possibility of Anderson localization [617], and also of first order phase transitions [618, 619] with exponentially small gaps [620, 621] may lead to an exponential complexity in quantum adiabatic algorithms. These studies raise some concerns regarding the prospect of quantum annealing in searching for efficient solutions (bounded in time by a polynomial in the size of the problem) of computationally hard problems for which classical algorithms take a time which is exponential in the problem size. However the typical problems of quantum annealing, arising due to the exponential decay (in the problem size) of the minimum energy gap and the consequent failure of the adiabatic theorem, may not pose a serious threat to the efficiency of quantum annealing. It has recently been demonstrated that a suitable design of the tunable quantum driving term in the Hamiltonian may remove the difficulty [622].

VII. EXPERIMENTAL REALIZATIONS OF TRANSVERSE FIELD ISING SYSTEMS

(A). Singlet ground state magnets

In a crystalline lattice, the crystal fields often take a form such that the ground states of magnetic ions are singlets separated from the higher lying spin multiplets. Sufficiently strong magnetic dipolar or exchange couplings between different sites can mix the singlets with the multiplets enough so as to induce non-zero expectation values for the magnetic dipoles at individual sites. Examples of this phenomenon are generally found among metals and insulators based on rare earths. Such metals were a subject of extensive research in the 1960's and 1970's, and the book by MacKintosh and Jensen [623] gives an excellent account of both the data as well as mean field approaches. With respect to insulating materials, LiTbF_4 emerged as a model system in the 1970's. It is an example of an ideal Ising dipolar coupled ferromagnet; here the long-range nature of the dipolar interactions leads to an upper critical dimension d_u^c [3] (at which mean field theory with logarithmic corrections calculable using RG methods becomes an exact description of thermal phase transitions) of three rather than four.

LiTbF_4 belongs to the LiREF_4 isostructural series of ionic salts. Li and F carry valences +1 and -1 respectively, leaving RE, which can be any rare earth atom or the nonmagnetic element Y, with a valence of +3. Figure 27 shows the body-centered tetragonal crystal structure for the family. The underlying LiF_4^{-3} lattice together with the number of f -electrons (i.e., the position in the RE row of elements) determine the magnetic crystal field levels for the RE ions. Because the RE ions have compact f orbitals with little site-to-site overlap, the dominant magnetic interactions are dipolar. The early work of Luttinger and Tisza [624] then shows that the ground state (ferromagnetic or antiferromagnetic) for pure compounds in this series of salts is entirely determined by the identity of the rare earth ion, leading to, for example, ferromagnetism with a Curie temperature $T_c = 1.53$ K for RE=Ho, with a non-Kramers doublet ground state, and antiferromagnetism with a Neel temperature $T_N \sim 0.4$ K for RE=Er [625, 626]. The lowest lying crystal field states for RE=Tb are actually two singlets, separated by a splitting $\Delta = 1$ K. There is a strong Ising character to the dipole matrix elements connecting them, and because the dipolar interactions between ions are actually larger than Δ , the outcome is again a ferromagnet, but with the more convenient T_c of 3.5 K. Figure 28 [627] shows what is most relevant for this review: upon substitution of Y for Tb at a fraction $1 - p$ of the RE sites to produce $\text{LiTb}_p\text{Y}_{1-p}\text{F}_4$, T_c does not follow the classical mean field prediction $T_c(p) = pT_c(p = 1)$. Instead, it is well-described by the mean field form taking single site quantum mixing into account, with a quantum critical point where the dipolar interaction ceases to be strong enough to yield the quantum mixing needed to produce magnetic moments. The reason for the deviation of $T_c(p)$ from this form, represented by the solid line, below the quantum critical concentration $p \sim 0.2$ in Fig. 28 is the nuclear hyperfine interaction which continues to mix the singlets and thereby restores the dipole moments on the Tb ions. Such effects are discussed in more detail in the context of LiHoF_4 below.

A key feature of transverse field Ising systems is the mode softening which occurs on approaching the quantum

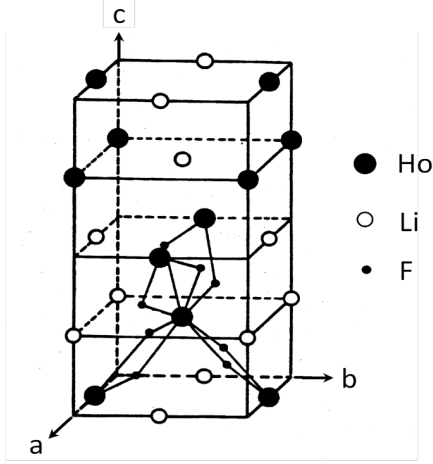


FIG. 27: Crystal structure for LiHoF_4 , one of the series of rare earth tetrafluorides that illustrates the physics of three dimensional Ising model in a transverse field.

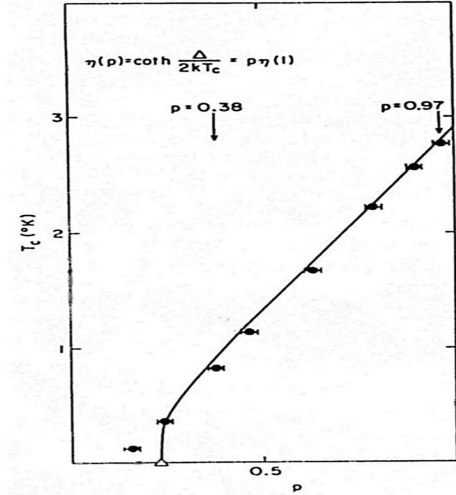


FIG. 28: (Color online) Phase diagram for the dipolar-coupled Ising ferromagnet LiTbF_4 as a function of substitution of magnetic Tb with non-magnetic Y (denoted by p). (After Youngblood *et al.*, 1982.)

critical point where fluctuations become pronounced and long-ranged. Figure 29 shows this phenomenon in the form of inelastic neutron scattering data for $\text{LiTb}_{0.38}\text{Y}_{0.62}\text{F}_4$. The observed magnetic excitation has the required dispersion, but there is both considerable damping of the excitation and strong quasielastic scattering. There is also no trace of the excitation for the pure compound LiTbF_4 , and all the spectral weight seems to be concentrated in quasielastic scattering.

(B). Order/disorder transitions in hydrogen-bonded and other ferro/antiferroelectric systems

In hydrogen-bonded systems, it is quite common for there to be two possible sites which any H ion can occupy. An electric field could bias the ions towards particular site occupancy patterns, and this field could be internally generated via the electric charges of the protons themselves. We therefore have a situation very much analogous to that for the singlet ground state magnets discussed above, and indeed much of the same physics is observed. The ferroelectricity

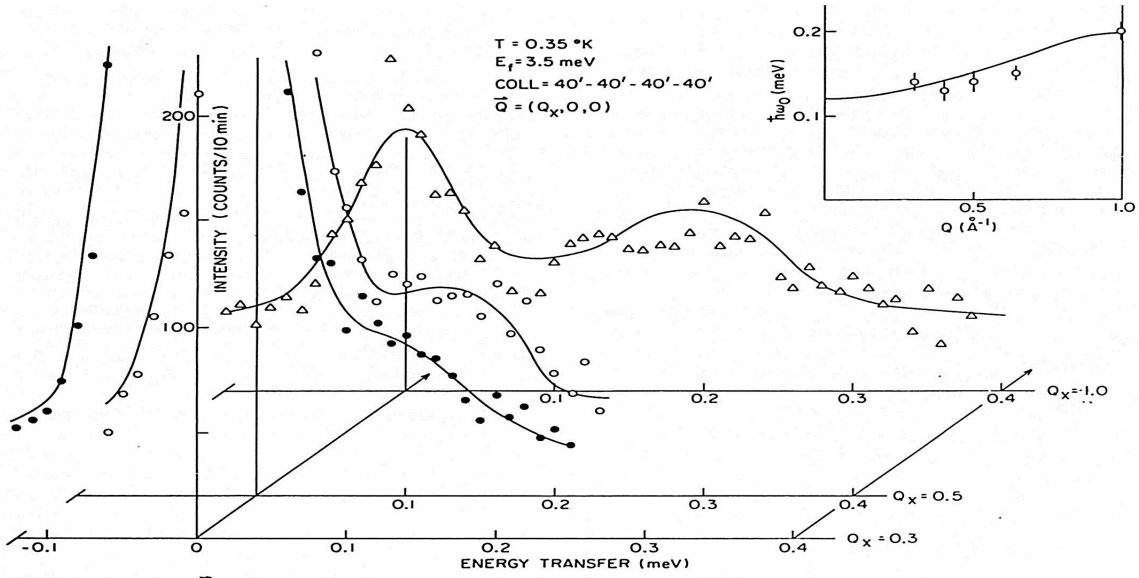


FIG. 29: Magnetic excitons in $\text{LiTb}_p\text{Y}_{1-p}\text{F}_4$ at $p = 0.38$ in the ferromagnetic phase; solid line corresponds to the theoretical line shape fitted to the data. Inset compares the theoretical dispersion curve for excitons (solid line) and fitted value of the exciton energies. (After Youngblood *et al.*, 1982.)

of potassium dihydrogen phosphate (KH_2PO_4) and isomorphous systems and their order-disorder transition behavior were satisfactorily explained employing transverse Ising models [34, 628]. The hydrogen ion (proton) in the O-H-O bond linking the PO_4 tetrahedra on the three-dimensional lattice is in a symmetric double well potential provided by the pair of oxygen ions at each lattice site. An asymmetric position of the proton in any of these wells would induce a tiny electrical dipole moment and these local dipole moments at different sites would interact (ferroelectrically in the case of KH_2PO_4) and induce order at low temperatures in the absence of any quantum tunneling across the double wells. However, since the oxygen-oxygen double well at each site has a finite width and finite height of the barrier separating the individual wells, quantum tunneling of the proton can take place (with a probability dependent on the proton mass and the well structure or lattice constant), thereby inducing quantum relaxation that thwarts the development of order.

In a transverse Ising model of such ferro- or antiferroelectric systems, the degenerate (double well minima) proton states at each site can be represented by Ising spin states ($\sigma_i^z = \pm 1$), interacting with each other through long-range dipole-dipole interactions J . The quantum tunneling field h (which couples to σ_i^x , inducing transitions from one Ising spin state to the other) is determined by the mass of the proton or deuteron (in the case of KD_2PO_4) or the pressure induced changes in the lattice constants. For low values of the tunneling field h , the dipolar interactions J induce order (ferro or antiferro type, depending on the sign of J), while if the value of the field is higher than a certain threshold (which depends on the magnitude of J and the lattice structure), one gets a disordered (paraelectric) phase. The resulting analysis of the static and dynamic behavior across such order-disorder transitions of the ferro-/antiferroelectric systems have been very satisfactory and well-accepted in the literature (see e.g., Blinc and Zeks, 1987). Solid state mixtures of ferroelectric and antiferroelectric components induce glassy behavior, where the tunneling of protons dominates the low temperature relaxation and can be related directly to the quantum mechanical action [629].

(C). Low-dimensional magnetic realizations of the transverse field Ising model

Because of the analytic tractability of one-dimensional systems, there is a long history of experiments on magnetic chain compounds, and there has been a correspondingly large body of reviews. Even so, it is only within the last year that a definitive experiment on the one-dimensional transverse field Ising model has been performed [25]. The material for this study is CoNb_2O_6 , whose crystal structure is illustrated in Fig. 30. The building blocks are ferromagnetic zig-zag chains of edge sharing CoO_6 octahedra; this is in contrast to the linear chains of apex sharing NiO_6 octahedra in the model $S = 1$ antiferromagnet, YBaNiO_5 [630] which are arranged so as to be coupled antiferromagnetically. In an external field transverse to the “easy” spin axis, the ordering along the easy axis is destroyed at a QPT due

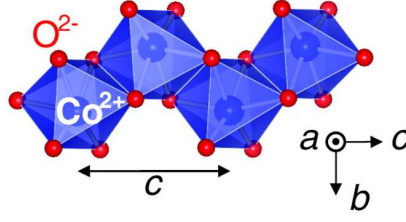


FIG. 30: (Color online) Structure of CoNb_2O_6 .

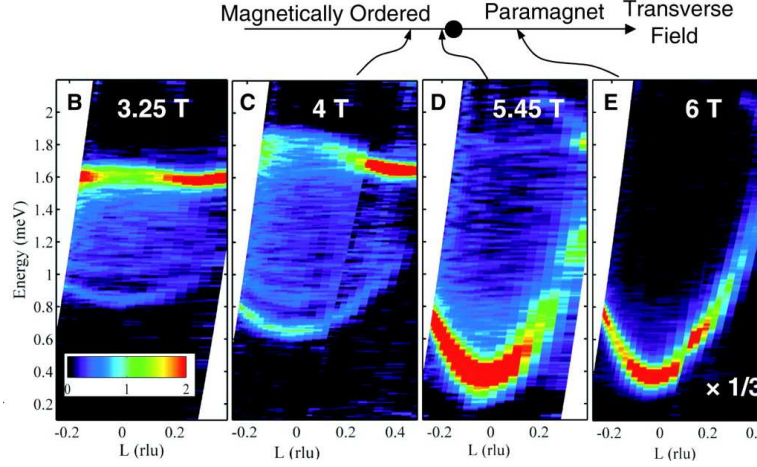


FIG. 31: (Color online) Magnetic spectra in CoNb_2O_6 for transverse fields above and below QCP. In the ordered phase [(B) and (C)], excitations form a continuum due to scattering by pairs of kinks; in the paramagnetic phase (E), a single dominant sharp mode occurs, due to scattering by a spin-flip quasiparticle. Near the critical field (D), the two types of spectra tend to merge into one another. (After Coldea *et al.*, 2010).

to delocalized domain walls, sometimes referred to as kinks or solitons. The associated magnetic Bragg reflections, resulting from the full three-dimensional order, disappear at the quantum critical field $h = 5.5T$. There will be a related mode softening, where the frequency of the zone center excitation vanishes at the quantum critical field. The zone center is where three-dimensional order appears among the weakly coupled chains; elsewhere, the softening is incomplete. Fig. 31 displays the corresponding inelastic neutron scattering data for transverse fields near, at and above the critical transverse field. The dominant feature in the ordered state is a domain wall pair continuum split into discrete levels due to the longitudinal field h_L derived from neighboring chains, which results in an attraction between domain walls rising linearly with their separation (because the number of spins misoriented relative to the molecular field in the ordered state is equal to the separation between walls); this is very similar to the confining potential for quarks in high energy physics. As the quantum critical point is approached and $h_L \rightarrow 0$, an exact scattering matrix analysis predicts that a scaling regime should be entered where the Lie algebra of E_8 accounts for eight bound states with energies such that the ratio of the lowest two are given by the golden mean [130] (see also Sec. II (B)).

Experimental results for CoNb_2O_6 , reproduced in Fig. 32, bear out this prediction. For $h > h_c$, the spectrum is dominated by single spin flips instead of domain wall pairs, with the result that the continuum is replaced by a dispersing magnetic excitation (see Fig. 31). The experiments on CoNb_2O_6 are important not only because of the many exact theoretical results tested so far, but also because they suggest new avenues for research. In particular, we look forward to experiments dealing with magnetic and non-magnetic impurities substituted for Co to parse the effects of disorder and chemical doping on the statics and dynamics of transverse Ising models in reduced dimensions. Furthermore, pressure could regulate the interchain coupling, thus modifying the bound state spectra.

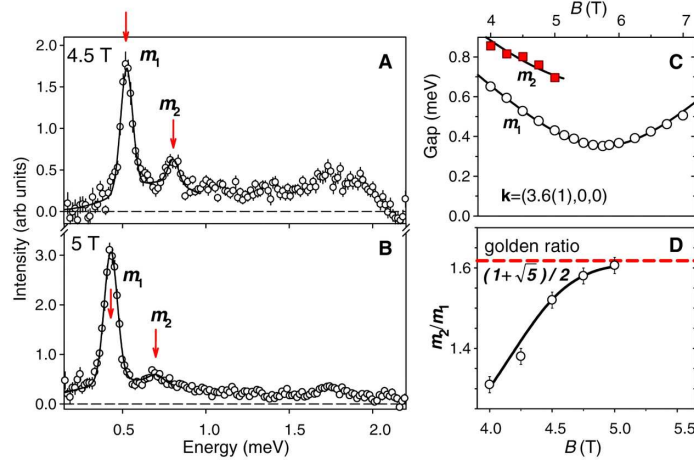


FIG. 32: (Color online) Scaling regime for QCP in CoNb_2O_6 . (A) and (B): Energy scan at zone centers at 4.5 and 5T with two peaks m_1 and m_2 . (C) Softening of two energy gaps near the critical field. (D) The ratio m_2/m_1 approaches the E_8 golden ratio just below the critical field. (After Coldea *et al.*, 2010).

(D). Ising doublets in external magnetic fields in three-dimensions

The system for which the most data are available is LiHoF_4 , from the LiREF_4 family already introduced in Sec. VII (A). The ground state term is a non-Kramers doublet with strong anisotropy, implying effective Ising spins with angular momentum $J = 8$ along the tetragonal c -axis. External magnetic fields can mix this term with the excited states at energies of ~ 1 meV and above. Of particular interest are laboratory fields applied perpendicular to the c -axis, which split the degenerate ground state into two terms with $\langle J_z \rangle = 0$. The splitting of the ground state doublet in a transverse field, Γ , is even in the external field because it is generated via mixing, implying that to lowest order a transverse Ising model representation of the system with an effective transverse field $h \sim \Gamma \sim H_t^2$. Here H_t is the laboratory magnetic field applied transverse to the Ising axis. Figure 33 A displays the field-temperature phase diagram [113, 631] for LiHoF_4 , with a boundary between Ising ferromagnetism and paramagnetism terminating at the classical phase transition for $H_t = 0$ and a quantum critical point at $H_t = 5T$. The dashed line corresponds to the mean field expression for the boundary where the nuclear spins ($I = 7/2$) are ignored. The solid line takes into account the nuclear hyperfine coupling, and provides a good description of the data; the bulge setting in below $0.7K$ means that the nuclear spins inhibit the electronic quantum fluctuations, i.e., produce composite electro-nuclear degrees of freedom with effectively higher and more classical spin, and therefore raise the critical field from $4T$ to $5T$. This correction notwithstanding, LiHoF_4 , with its crystalline and chemical perfection, represents an excellent venue for a quantitative examination of quantum critical phenomena, in the same way that it and more prominently LiTbF_4 previously served as testbeds for the RG theory of classical critical behavior. Figure 34 shows the divergence of the bulk susceptibility as the quantum critical point is approached along thermal and field trajectories.

The important result is that they are both described by exponents indistinguishable from unity, which is what is also anticipated based on mean field theory which should be valid given that d_c^u is already 3 for the classical system, and is reduced by z , the dynamical critical exponent which will be a positive number, for the quantum phase transition. Inelastic neutron scattering measurements show that the nuclear spins also affect the quantum critical dynamics strongly [113, 632]. In particular, the magnetic excitation which dominates the inelastic neutron scattering data in Fig. 35 undergoes incomplete softening at the quantum phase transition. What accounts for the diverging susceptibilities seen in the bulk measurements (Fig. 34) is then the quasielastic peak which appears near zero frequency in the images of Fig. 35 is due to the mixing of electronic and nuclear degrees of freedom.

(E). Disorder and the transverse field Ising model

The $\text{LiTb}_x\text{Y}_{1-x}\text{F}_4$ and $\text{K}(\text{H}_x\text{D}_{1-x})_2\text{PO}_4$ series of compounds are naturally disordered materials where the mean transverse fields are scanned by changing the composition variables x . Because of localization and random field effects naturally associated with disorder, it would obviously be useful to scan the transverse field and disorder separately. This is achieved for $\text{LiHo}_x\text{Y}_{1-x}\text{F}_4$ in a transverse external field. As the Ho sublattice is diluted by non-magnetic

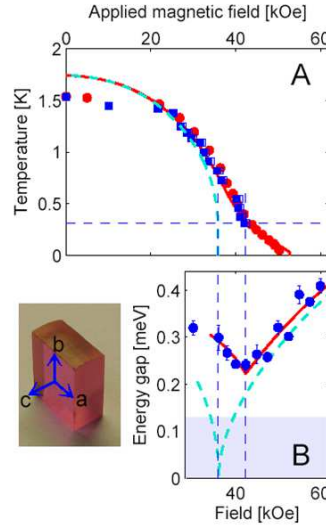


FIG. 33: (Color online) Phase diagram of LiHoF₄ shown in (A). In (B), we show the field dependence of the lowest excitation energy. (After Ronnow *et al.*, 2005.)

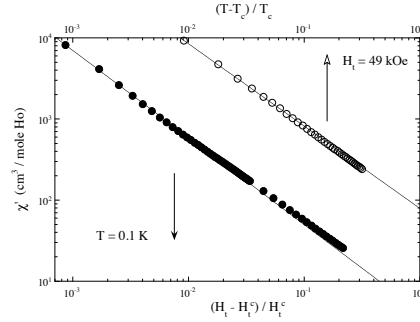


FIG. 34: Divergence of magnetic susceptibility on approaching QCP in LiHoF₄. (After Bitko *et al.*, 1996).

Y, the fact that the dipolar interaction is ferromagnetic between Ising spins with separation vector parallel to the Ising axis and antiferromagnetic between spins separated by a vector orthogonal to the Ising axis becomes highly relevant in that it will introduce numerous antiferromagnetically correlated spins into the (classical) ground state of the system. Furthermore, a very long time ago, Aharony and Stephens predicted that this would lead to a spin glass ground state for any $x > 0$. Initial experiments [633, 634] focused on the zero field phase diagram, shown in Fig. 36 along with its analogue in transverse field [635]. For $x > 0.4$, the dominant feature is a para-ferromagnetic transition located along the straight line $T_c = xT_c(x = 1)$ given by the most simple effective medium theory. For $x < 0.4$, the transition is clearly below this line, and the signatures of ferromagnetism apparently disappear entirely below $x \sim 0.2$, where there is first a low-temperature state displaying glassy behavior, which persists at least to $x \sim 0.1$.

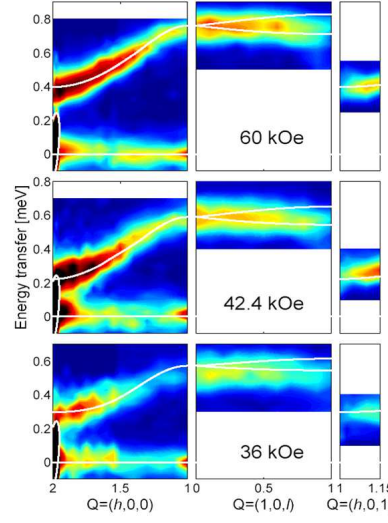


FIG. 35: (Color online) Incomplete mode softening on passing through QPT in LiHoF₄. Figure shows pseudocolor representation of the inelastic neutron scattering intensity of LiHoF₄ at $T = 0.31$ K observed along the reciprocal space trace $(2, 0, 0) \rightarrow (1, 0, 0) \rightarrow (1, 0, 1) \rightarrow (1.15, 0, 1)$. (After Ronnow *et al.*, 2005).

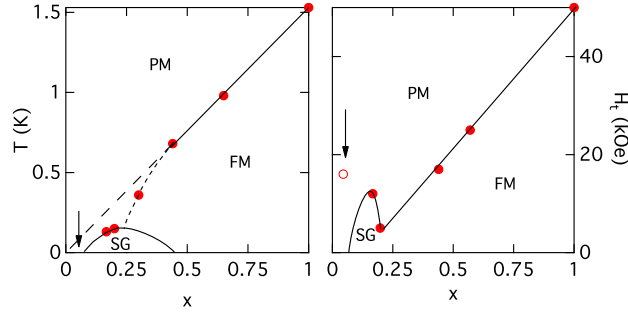


FIG. 36: Dilution of the dipolar-coupled, Ising ferromagnet LiHo_xY_{1-x}F₄. Left panel: magnetic phases in the $x - T$ plane. Arrow denotes spin liquid “antiglass” phase. Right panel: Magnetic phases in $x - H_t$ plane where H_t is the field applied transverse to the Ising axis. Open circle shows the peak in susceptibility for the anticlass. (After Ancona-Torres *et al.*, 2008)

We note parenthetically that there has been some controversy [636] surrounding this spin glass state, but this has died away in view of the agreement between the two groups [53, 635, 637] which probed it using low fields and low frequencies; the seemingly different results were obtained under the very different experimental circumstances of dc SQUID magnetometry performed with rapid sweep rates to high fields.

For $x < 0.1$, there are reports of both continued spin glass behavior [637, 638] as well as a novel antiglass state [639], so named because a reduction in the temperature lead to a reduction of the width of the distribution of barriers to relaxation rather than the conventional increase. The antiglass state is marked by strongly entangled spins, analogous to the Bhatt-Lee state [640] found below the insulator-metal transition in doped silicon, and indeed, a decimation calculation [345] which ignores nuclear spin degrees of freedom but takes into account both the diagonal and off-diagonal dipolar couplings between Ho³⁺ ions (the latter providing the necessary quantum mixing), gives a remarkably good description of the magnetic susceptibility in the limit of small frequencies. An additional astonishing effect (Fig. 37) is spectral hole burning [641], the acoustic frequency analog to optical experiments where the frequency(f)-dependent small signal response $\chi(f)$ is measured in the presence of a large pump signal at fixed frequency f_o . Very sharp minima at f_o are induced in $\chi(f)$, indicating the decoupling of low frequency magnetic excitations from each other; these experiments motivated a successful search for similar behavior in the classic geometrically frustrated system Gadolinium Gallium Garnet (Gd₃Ga₅O₁₂ or GGG) [642].

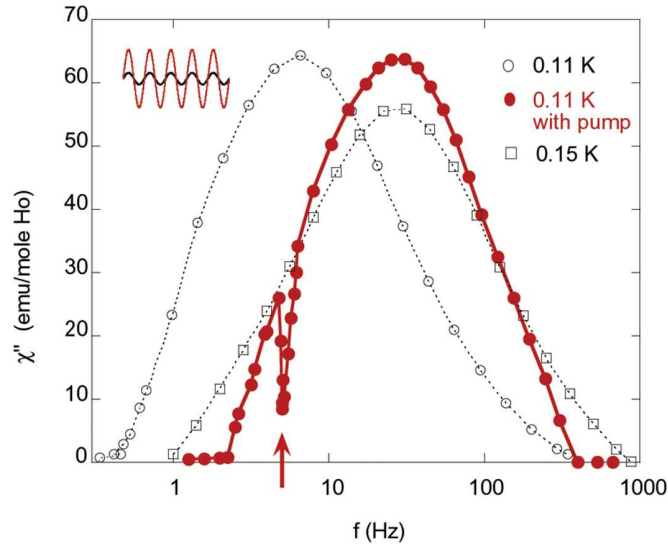


FIG. 37: (Color online) The presence of a sharp minimum is indicative of spectral hole burning in $\text{LiRE}_x\text{Y}_{1-x}\text{F}_4$ with $\text{RE}=\text{Ho}$ and $x = 0.046$. (After Ghosh *et al.*, 2002).

The antiglass regime remains a highly active area of contemporary research, both for the fundamental reason that it seems an excellent venue for probing non-equilibrium quantum effects in macroscopic systems of strongly coupled degrees of freedom, but also on account of the divergent claims based on different experiments. The differing claims are made for samples of nominally the same composition ($x = 0.046$), but mounted in radically different ways in the measuring cryostat. The discrepancy is real and interesting: trivial aspects of thermalization cannot account for the differing results because in both sets of measurements, cooling the cryostats towards their base temperatures does result in monotonic changes in properties. It is worth adding that the different measuring apparatuses (superconducting SQUID and ac induction coils) used by the two groups involved similar measuring fields and frequencies, and are therefore unlikely to be responsible for the different results. For the lowest concentrations, the magnetic behavior is dominated by single ions and the occasional pairs of ions, and SQUID magnetometry shows the hysteresis loops characteristic of single molecule magnets, including quantum tunneling effects [643]. Transverse fields H_t applied to $\text{LiHo}_x\text{Y}_{1-x}\text{F}_4$ lead to three important families of phenomena.

1. The transverse field induces a random field via the off-diagonal terms of the dipolar interaction, which have non-zero expectation values due to the lower local symmetries [277, 644] resulting from random substitution of Y for Ho. This is manifested in a hardening of the (longitudinal field-induced) magnetization loops on application of the transverse field for T near $T_c(x)$ [645], as well as different critical exponents for the longitudinal susceptibility as a function of transverse field for $T = T_c(x)$ in the cases where $x = 0.44$ and $x = 1$, respectively [646]. In particular, the divergence of the longitudinal susceptibility at the classical critical point is defined by the exponent $1/\delta$ in

$$\chi' = \frac{dM_z}{dh_z}(H_t)|_{T=T_c(H_t=0)} \sim \frac{1}{|H_t|^{1/\delta}}.$$

The experiment shows that for ordered, pure LiHoF_4 , $1/\delta = 2$, while for the disordered $x = 0.46$ compound $\delta = 1$, where all of the data in the PM phase are described by the form

$$\chi' = \frac{C}{\alpha' \nu_B |H_t| + (T - T_c) + \gamma T}. \quad (162)$$

The power law seen at T_c is remarkable enough, but the accuracy of (162) is even more so, especially because it is non-analytic as $H_t \rightarrow 0$, encapsulating the singular nature of the magnetic response above T_c , and the corresponding experiments represent a particularly clear manifestation of the Griffiths phenomenon, where singular behavior inherited from rare fluctuations towards higher x is visible in a thermodynamic quantity. In spite of the simplicity of the data and phenomenology for small H_t for T near T_c , there is no analytical theory accounting for the observed effects, although much less finely grained numerical data for the phase diagram are consistent with (162), which entails a linear approach of the critical temperature towards T_c as $H_t \rightarrow 0$ [277].

2. For low temperatures, the principal effect of the transverse field H_t is to facilitate quantum fluctuations. The dc magnetization experiments [645] show a monotonic narrowing of the magnetic hysteresis loops with increasing H_t , and

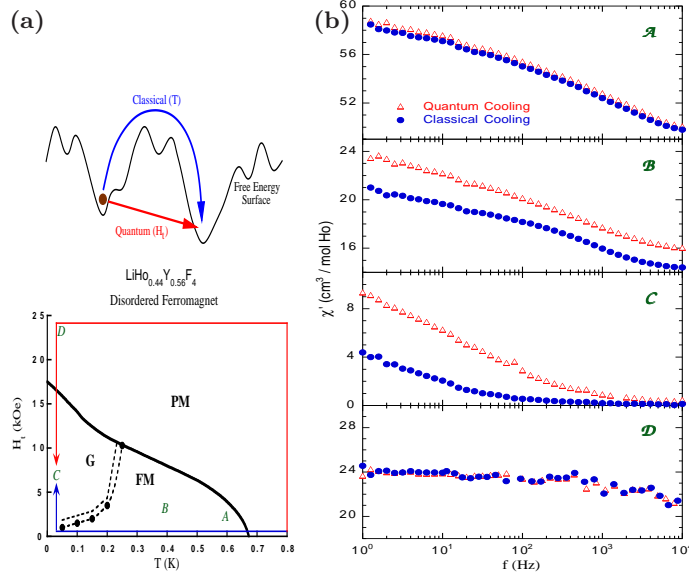


FIG. 38: (Color online) Left panel: Top: The schematic picture of quantum annealing. Bottom: The phase diagram of the disordered Ising magnet $\text{LiHo}_{0.44}\text{Y}_{0.56}\text{F}_4$ in a transverse field. The quantum (red) and classical (blue) annealing protocols provide different pathways for the free-energy minima. Right panel: Spectroscopy of the material at points A to D after quantum and classical computations. (After Brooke *et al.*, 1999).

ac susceptibility data [647] show a speed-up of the magnetic response well described by a WKB model of domain wall tunneling, where the transverse field controls the mass of the domain walls (M^*) which play the role of the particles in the model. Pinning sites provide confining potential barriers, whose magnitudes are established independently from the Arrhenius behavior observed in the thermal activation regime at higher temperatures. M^* was measured to be of order $10^4 m_e$ (where m_e is the electron mass), consistent with coherent tunneling of wall segments containing 10 spins and the magnitude of the magnetic dipole coupling between Ho^{3+} moments. The control of the tunneling by an external transverse field enabled the first experimental exploration of quantum annealing (or ‘adiabatic quantum computation’) in 1999 [648]. The computational problem was that of finding the low-lying states of the disordered magnet with the impurity configuration of the particular $x = 0.44$ sample used. The readout was achieved simply by measuring the frequency-dependent magnetic susceptibility $\chi(\omega)$ along the Ising axis, and different trajectories in the $H_t - T$ plane were used as ‘programs’ for finding optimal states. The experiments (see Fig. 38) established that quantum and thermal protocols give rise to states characterized by visibly different properties. The principal effect seems to be that reaching low H_t and T via the quantum route of reducing H_t results in a state with more rapid small amplitude fluctuations than that reached via a thermal route. Indeed, quantum annealing moves $\chi(\omega)$ towards higher frequencies in such a way that the $\log \omega$ behavior of χ' , corresponding to a marginally stable ferromagnetic state, is apparent. Because more rapid small amplitude fluctuations are associated with sharper free energy minima, the experiments show that quantum annealing uncovers less gentle minima than thermal annealing. In addition, if there is some scale invariant distribution of minima curvatures, as suggested by the $\log \omega$ decay of χ' , quantum annealing has proven its value by virtue of revealing this behavior over easily reachable frequencies. Notwithstanding this result, the question of which state has lower free energy has yet to be answered by careful thermodynamic measurements.

3. The phase boundaries in the $H_t - T$ plane, which bound a ferromagnetic phase for $x > x_c \sim 0.2$ and a spin glass-like phase for $x < x_c$, do not scale as simply as one might expect. In particular, neither the laboratory quantum critical field H_t^c nor the effective transverse field Δ scale as T_c . There is even a minimum in the critical field at x_c , which represents evidence for the very different nature of the spin glass-like and disordered ferromagnetic ground states. Also, as we pass from the pure to the disordered samples with $x \sim 0.5$, the shape of the phase boundary in the $H_t - T$ plane also changes from being highly curved near $T = T_c(x)$ to much more linear. In the spin glass regime, the phase boundary between the PM and spin-glass states is established by looking for the vanishing of the power law α in the fluctuation spectrum $\chi(\omega) \sim \omega^\alpha$ [53]. This is correlated with the (analysis-free) observation of the onset of a plateau in $\chi(\omega)$ for suitably low, fixed ω , as a function of H_t , and it yields a very well-defined phase boundary. There was also an examination [54, 635] of the non-linear susceptibility along this phase boundary, and its behavior was consistent with divergence near $T_g(H_t = 0)$. The associated critical exponent, however, was anomalously

small, and as $T \rightarrow 0$ and $H_t \rightarrow H_t^c$ it becomes smaller as the singularity is washed out, even as the signal for the phase boundary becomes sharper in $\chi(\omega)$. There is also a theoretical puzzle coming from the knowledge that H_t also induces internal random fields, and should, according to classical theory, eliminate phase transitions at finite H_t . The resolution for this as well as an explanation of the various peculiar observations is likely to lie in the fact that the classical theory does not consider a quantum glass with entangled spin pairs and the associated distribution of level crossing resonances. The configurational entropy of the glass state can be due to a near degeneracy of the quantum pairing of spins rather than the relative orientation of classical spins; we look forward to a theory of this approach to provide a better understanding of the experiments.

VIII. CONCLUDING REMARKS

In this review, we have discussed quantum phase transitions in transverse field Ising and XY models in one and higher dimensions. Quantum phase transitions for pure models as well as models with random interactions or random fields have been discussed. As mentioned earlier, these models were introduced in the early 1960's in the context of order-disorder ferroelectric systems. Our review focuses on the salient issues for which these models continue to be important and interesting even fifty years after their inception.

On the theoretical side, the integrability of the transverse field Ising/ XY models in one dimension has provided an ideal testing ground for field theoretical and information theoretical studies. Numerous predictions of theoretical studies have been verified experimentally in recent years. [25]. The one-dimensional models have been extremely useful in studying information theoretic measures like concurrence, entanglement entropy, fidelity and fidelity susceptibility, and also the scaling of the defect density generated by quantum critical and multicritical quenches, namely, the Kibble-Zurek scaling. These models have played a crucial role in the development of quantum annealing techniques and adiabatic quantum algorithms. The equilibration or thermalization following quantum quenches have been studied using variants of transverse field models.

An advantageous feature of transverse field Ising models is the quantum-classical mapping which renders these models ideally suited for quantum Monte Carlo studies for $d > 1$. One can study the QPTs in these models, both pure and random, by investigating the thermal phase transitions of equivalent classical Ising models in higher dimensions (see for example, Sec. III). We have also discussed Griffiths-McCoy singularities and activated quantum critical dynamics associated with low-dimensional random quantum transitions.

On the experimental side, the discovery of LiHoF_4 systems and their disordered versions has opened up new vistas in the studies of transverse field Ising models. The experiments have established the existence of both quantum phase transitions and quantum glassy states. Unique phenomena like “spectral hole burning” and the existence of “antiglass states” and “entangled quantum states of magnetic dipoles” have emerged from these experimental studies. More importantly, we have discussed the possibility of realizing quantum annealing in these systems*. We have also pointed out some experimental observations which do not have any theoretical explanations to date. In short, the transverse field models have played a crucial role in the understanding of quantum phase transitions, and we believe that they will continue to remain important for future theoretical and experimental research.

* Note added: After this review was originally prepared, a realization of the transverse field Ising model for an eight-qubit chain using tunable Josephson junctions was implemented. This represents a significant breakthrough because it also permits experimental examination of quantum annealing (adiabatic quantum computation) with unprecedented detail [649].

Acknowledgments

We thank M. Acharyya, C. Ancona-Torres, J. Axe, G. Baskaran, D. P. Belanger, J. K. Bhattacharjee, D. Bitko, C. Broholm, J. Brooke, E. Bucher, A. Chakrabarti, A. Chandra, Y. Chen, R. Chitra, R. Coldea, P. Coleman, A. Das, W. DeGottardi, J. F. DiTusa, B. Elluman, C. D. Frost, S. Ghosh, J. Griffin, H. J. Guggenheim, J.-I. Inoue, T. Ito, J. Jensen, M. Kenzelmann, C. Kraemer, H. R. Krishnamurthy, D. F. McMorrow, S. Mondal, V. Mukherjee, T. Nag, K. Oka, R. Parthasarathy, S. Pati, A. Polkovnikov, S. Ramasesha, R. Ramazasvilli, S. Rao, P. Ray, D. H. Reich, H. Rieger, H. M. Ronnow, D. Samanta, G. Santoro, A. Schröder, P. Sen, K. Sengupta, R. Shankar, S. Sharma, D. Silevitch, R. R. P. Singh, Y.-A. Soh, R. B. Stinchcombe, H. Takagi, M. Thakurathi, S. Vishveshwara, W. Wu, G. Xu, and P. Youngblood for collaborations and discussions on the many works presented in this review. We specially thank V. Mukherjee for immense help in preparing the manuscript. AD acknowledges CSIR, India, for financial support, UD acknowledges AV Humboldt foundation for financial support and CSIR, India, for research associateship, DS acknowledges DST, India for Project SR/S2/JCB-44/2010, TR acknowledges DOE BES Grant No. DE-FG02-99ER45789, and GA thanks the Wolfson Foundation and the UK ESPRC for support.

Appendix A: Large spin limits: transverse XY spin chain

We have already discussed the exact solution of the spin-1/2 transverse XY model (10) in Sec. II (A). In this Appendix, we shall study the model in the large spin limit ($S \rightarrow \infty$). This method sometimes turns out to be useful for a given quantum spin Hamiltonian. In this limit, the spins become classical objects whose components commute with each other. Quantum fluctuations can then be studied by going to the first order in the small parameter $1/S$ using the Holstein-Primakoff transformation which maps the spin operators at site n to the raising and lowering operators of a simple harmonic oscillator at the same site [40–42]. To illustrate this, let us consider the Hamiltonian of the XY spin chain in a transverse magnetic field,

$$H = - \sum_n [J_x S_n^x S_{n+1}^x + J_y S_n^y S_{n+1}^y + h S_n^z], \quad (\text{A1})$$

where $\tilde{S}_n^2 = S(S+1)$; we have introduced a factor of S in the last term in Eq. (A1) so that all the terms scale as S^2 in the limit $S \rightarrow \infty$. Let us assume that $|J_x| \geq |J_y|$. We can ensure that $J_x, h \geq 0$ by performing unitary transformations if necessary. In the limit $S \rightarrow \infty$, let us assume that the spins point in the direction given by (θ, ϕ) in polar coordinates, namely, $(S^x, S^y, S^z) = S(\sin \theta \cos \phi, \sin \theta \sin \phi, \cos \theta)$ at all sites n . Eq. (A1) then implies that the energy per site, e_0 , is given by

$$e_0 = -S^2(J_x \sin^2 \theta \cos^2 \phi + J_y \sin^2 \theta \sin^2 \phi + h \cos \theta). \quad (\text{A2})$$

Minimizing this as a function of θ and ϕ gives $\phi = 0$ if $J_x > |J_y|$. Further, we find that $\theta = 0$ if $h \geq 2J_x$ while $\theta = \cos^{-1}(h/2J_x)$ lies between 0 and $\pi/2$ if $h < 2J_x$. We will now consider these two cases in turn.

(i) For $h \geq 2J_x \geq 2|J_y|$, the spins point along the z direction. The Holstein-Primakoff transformation then takes the form

$$\begin{aligned} S_n^z &= S - a_n^\dagger a_n, \\ S_n^x + i S_n^y &= (2S - a_n^\dagger a_n)^{1/2} a_n, \\ S_n^x - i S_n^y &= a_n^\dagger (2S - a_n^\dagger a_n)^{1/2}. \end{aligned} \quad (\text{A3})$$

In the large S limit, we expand the square roots in Eq. (A3) to the lowest order to obtain

$$\begin{aligned} S_n^x &= (S/2)^{1/2} (a_n + a_n^\dagger), \\ S_n^y &= -i (S/2)^{1/2} (a_n - a_n^\dagger). \end{aligned} \quad (\text{A4})$$

Keeping terms up to order S , the Hamiltonian in Eq. (A1) takes the form

$$H = E_0 + S \sum_n \left[h a_n^\dagger a_n - \frac{J_x + J_y}{2} (a_n^\dagger a_{n+1} + a_{n+1}^\dagger a_n) - \frac{J_x - J_y}{2} (a_n a_{n+1} + a_{n+1}^\dagger a_n^\dagger) \right], \quad (\text{A5})$$

where $E_0 = -NS^2h$ is the classical ground state energy which is of order S^2 . Here N denotes the number of sites and we assume periodic boundary conditions; we will eventually take the limit $N \rightarrow \infty$. The remaining terms in (A5) can be analyzed by Fourier transforming from a_n to $a_k = (1/\sqrt{N}) \sum_n a_n e^{-ikn}$, where $-\pi < k < \pi$. These terms then take the form

$$H = S \sum_{0 < k < \pi} \left[(a_k^\dagger a_k + a_{-k}^\dagger a_{-k})(h - (J_x + J_y) \cos k) + (a_k a_{-k} + a_{-k}^\dagger a_k^\dagger)(J_y - J_x) \cos k \right]. \quad (\text{A6})$$

This can be diagonalized using a bosonic Bogoliubov transformation of the form $b_k = \cosh \alpha a_k + \sinh \alpha a_{-k}^\dagger$ and $b_{-k} = \cosh \alpha a_{-k} + \sinh \alpha a_k^\dagger$. We then obtain

$$\begin{aligned} H &= \sum_{0 < k < \pi} \omega_k (b_k^\dagger b_k + b_{-k}^\dagger b_{-k}), \\ \omega_k &= hS \left[\left(1 - \frac{2J_x}{h} \cos k\right) \left(1 - \frac{2J_y}{h} \cos k\right) \right]^{1/2}. \end{aligned} \quad (\text{A7})$$

We see that the excitation spectrum is gapped unless $h = 2J_x$ in which case the gap vanishes at $k = 0$.

(ii) For $2J_x \geq h \geq 0$ and $J_x \geq |J_y|$, the spins lie in the $z - x$ plane and point in a direction which makes an angle $\theta = \cos^{-1}(h/2J_x)$ with the z axis. The Holstein-Primakoff transformation then takes the form

$$\begin{aligned} S_n^z \cos \theta + S_n^x \sin \theta &= S - a_n^\dagger a_n, \\ S_n^x \cos \theta - S_n^z \sin \theta + iS_n^y &= (2S - a_n^\dagger a_n)^{1/2} a_n, \\ S_n^x \cos \theta - S_n^z \sin \theta - iS_n^y &= a_n^\dagger (2S - a_n^\dagger a_n)^{1/2}. \end{aligned} \quad (\text{A8})$$

Expanding the square roots in Eq. (A8) to the lowest order and keeping terms up to order S , the Hamiltonian in Eq. (A1) takes the form

$$\begin{aligned} H = E_0 + S \sum_n & [(h \cos \theta + 2J_x \sin^2 \theta) a_n^\dagger a_n - \frac{J_x \cos^2 \theta + J_y}{2} (a_n^\dagger a_{n+1} + a_{n+1}^\dagger a_n) \\ & - \frac{J_x \cos^2 \theta - J_y}{2} (a_n a_{n+1} + a_{n+1}^\dagger a_n^\dagger)], \end{aligned} \quad (\text{A9})$$

where $E_0 = -NS^2[J_x + h^2/(4J_x)]$ is the classical ground state energy. After doing Fourier and Bogoliubov transformations, the remaining terms in (A9) take the form

$$\begin{aligned} H &= \sum_{0 < k < \pi} \omega_k (b_k^\dagger b_k + b_{-k}^\dagger b_{-k}), \\ \omega_k &= 2J_x S \left[\left(1 - \frac{h^2}{4J_x^2} \cos k\right) \left(1 - \frac{J_y}{J_x} \cos k\right) \right]^{1/2}. \end{aligned} \quad (\text{A10})$$

The excitation spectrum is gapped unless $J_y = J_x$ (or $-J_x$) in which case the gap vanishes at $k = 0$ (or π).

Putting together the above conditions for gaplessness of the spectrum, we find the following critical lines in terms of the parameters J_x , J_y and h . Let us scale these parameters simultaneously so as to make $J_x + J_y = 1$. Then in terms of the variables $\gamma = J_x - J_y$ and h , we find that the critical lines correspond to: (i) $-2 \leq h \leq 2$ and $\gamma = 0$, (ii) $h \geq 1$ and $\gamma = \pm(h-1)$, and (iii) $h \leq -1$ and $\gamma = \pm(h+1)$. Here (i) corresponds to the anisotropic phase transition, while (ii) and (iii) correspond to the Ising transition. These may be compared with the critical lines of the spin-1/2 model shown in Fig. 2. We note that the large-spin method has been useful study other quantum models like the quantum ANNNI chain [315, 650] and the Kitaev model [651].

Appendix B: Derivation of a matrix product Hamiltonian

In this Appendix, we will show how the Hamiltonian in Eq. (11) can be derived [26] given that its ground state has a matrix product form with two 2×2 matrices $A_1 = \begin{pmatrix} 0 & 0 \\ 1 & 1 \end{pmatrix}$ and $A_2 = \begin{pmatrix} 1 & g \\ 0 & 0 \end{pmatrix}$. Note that since there is a matrix $X = \begin{pmatrix} 0 & g \\ 1 & 0 \end{pmatrix}$ such that $X^{-1}A_1X = A_2$ and $X^{-1}A_2X = A_1$, we expect the Hamiltonian H to be Z_2 symmetric. To derive H , we observe that the matrix product structure involving A_1 and A_2 is such that if the values of σ^z at two next-nearest-neighbor sites $i-1$ and $i+1$ are given, this uniquely fixes the state at the site i which lies in between. There are four possibilities as follows.

(i) $\sigma_{i-1}^z = +1$ and $\sigma_{i+1}^z = +1$ goes with a normalized state at site i given by

$$|\psi_{i,++}\rangle = \frac{1}{\sqrt{1+g^2}} \begin{pmatrix} 1 \\ g \end{pmatrix}. \quad (\text{B1})$$

(ii) $\sigma_{i-1}^z = +1$ and $\sigma_{i+1}^z = -1$ goes with a state at i given by

$$|\psi_{i,+-}\rangle = \frac{1}{\sqrt{2}} \begin{pmatrix} 1 \\ 1 \end{pmatrix}. \quad (\text{B2})$$

(iii) $\sigma_{i-1}^z = -1$ and $\sigma_{i+1}^z = +1$ goes with a state at i given by

$$|\psi_{i,-+}\rangle = \frac{1}{\sqrt{2}} \begin{pmatrix} 1 \\ 1 \end{pmatrix}. \quad (\text{B3})$$

(iv) $\sigma_{i-1}^z = -1$ and $\sigma_{i+1}^z = -1$ goes with a state at i given by

$$|\psi_{i,-,-}\rangle = \frac{1}{\sqrt{1+g^2}} \begin{pmatrix} g \\ 1 \end{pmatrix}. \quad (\text{B4})$$

Now, a state $|\psi_i\rangle$ will be the ground state (with zero energy) of a Hamiltonian h_i if we choose h_i to be the projection operator to the state orthogonal to $|\psi_i\rangle$, i.e., if $h_i = I - |\psi_i\rangle\langle\psi_i|$. Hence the four possibilities listed above show that the Hamiltonian h_i should be chosen to be

$$\begin{aligned} h_i = & \frac{I + \sigma_{i-1}^z}{2} \frac{I + \sigma_{i+1}^z}{2} (I - |\psi_{i,++}\rangle\langle\psi_{i,++}|) \\ & + \frac{I - \sigma_{i-1}^z}{2} \frac{I + \sigma_{i+1}^z}{2} (I - |\psi_{i,-+}\rangle\langle\psi_{i,-+}|) \\ & + \frac{I + \sigma_{i-1}^z}{2} \frac{I - \sigma_{i+1}^z}{2} (I - |\psi_{i,+-}\rangle\langle\psi_{i,+-}|) \\ & + \frac{I - \sigma_{i-1}^z}{2} \frac{I - \sigma_{i+1}^z}{2} (I - |\psi_{i,--}\rangle\langle\psi_{i,--}|) \end{aligned} \quad (\text{B5})$$

in order to make the matrix product state the ground state of h_i for all possible values of σ_{i-1}^z and σ_{i+1}^z . This gives

$$h_i = \frac{1}{4(1+g^2)} [(g^2 - 1)(\sigma_{i-1}^z \sigma_i^z + \sigma_i^z \sigma_{i+1}^z) - (1+g)^2 \sigma_i^x + (g-1)^2 \sigma_{i-1}^x \sigma_i^x \sigma_{i+1}^z + 2(1+g^2)]. \quad (\text{B6})$$

This in turn implies that the matrix product state is the ground state (with zero energy) of $H = \sum_i h_i$. We see that this is identical to Eq. (11) up to an overall factor of $4(1+g^2)$ and a constant $-\sum_i 2(1+g^2)$ which is the ground state energy of Eq. (11).

Appendix C: From Jordan-Wigner to bosonization

Before discussing bosonization, let us briefly consider systems of interacting fermions in one dimension. It turns out that many such systems are described by Tomonaga-Luttinger liquid (TLL) theory [88, 652–661] in contrast to interacting fermionic systems in three dimensions which are usually well described by Fermi liquid (FL) theory. Let us assume for the moment that we are considering gapless systems in which no symmetry is spontaneously broken; for instance, we are not considering charge/spin density waves and superconductors. Then the main differences between FLs and TLLs are as follows.

In a FL, the low-energy excitations are quasiparticles which are fermions; they do not have a one-to-one relationship between energy and momentum. There are also low-energy bosonic excitations consisting of particle-hole pairs which can be thought of as sound modes. The one-particle momentum distribution function $n(\vec{k})$, obtained by Fourier transforming the one-particle equal-time correlation function, has a finite discontinuity at the Fermi surface; this is called the quasiparticle renormalization factor $z_{\vec{k}}$, and it lies in the range $[0, 1]$ (for a non-interacting system, $z_{\vec{k}} = 1$). Finally, the various correlation functions decay asymptotically at long distances as power laws, where the powers are independent of the strength of the interactions and are therefore universal.

In a TLL, on the other hand, there are no quasiparticle excitations. All the low-energy excitations consist of particle-hole pairs. The one-particle renormalization factor $z_{\vec{k}}$ therefore vanishes, and the momentum distribution function $n(\vec{k})$ has no discontinuity at the Fermi surface (in one dimension this usually consists of two points), although it has a cusp of the form

$$n(k) = n(k_F) + c \operatorname{sign}(k - k_F) |k - k_F|^\beta, \quad (\text{C1})$$

where $\operatorname{sign}(x) \equiv 1$ if $x > 0$, -1 if $x < 0$, and 0 if $x = 0$, and c is some constant. The exponent β is a positive number whose value depends on the strength of the interactions. For a non-interacting system, $\beta = 0$ and $n(k)$ has a discontinuity at k_F , but for $\beta > 0$ there is no such discontinuity. Finally, the various correlation functions decay asymptotically at long distances as power laws, but the powers now depend on the strength of the interactions and are therefore not universal.

We now turn to bosonization. This is a very useful field theoretic technique which can be used to study a variety of quantum systems in one dimension including TLLs [655–667]. Bosonization allows us to map fermionic operators into bosonic ones, and then use whichever set of operators is easier to compute with. This technique is most directly applied

to translation invariant and gapless systems of fermions in which the low-energy excitations have a linear energy-momentum dispersion ($z = 1$). As we will see below, bosonization can also be used to study various perturbations from gapless systems of the above type, and it can be applied to systems such as a chain of spin-1/2 objects which can be mapped to fermions using the JW transformation.

Although the dispersion relation is generally not linear for all the modes of a given system, it may happen that the low-energy and long-wavelength modes can be studied using bosonization. For a fermionic system in one dimension, these modes are usually the ones lying close to the two Fermi points with momenta $\pm k_F$ respectively. One can then define right- and left-moving second quantized fields ψ_R and ψ_L , which vary slowly on the length scale $1/k_F$, as

$$\psi(x) = \psi_R(x) e^{ik_F x} + \psi_L(x) e^{-ik_F x}. \quad (C2)$$

Assuming that the system is on a line of length L with periodic boundary conditions, we define the Fourier expansion of the fermionic fields as

$$\begin{aligned} \psi_R(x) &= \frac{1}{\sqrt{L}} \sum_{k=-\infty}^{\infty} c_{R,k} e^{ikx}, \\ \psi_L(x) &= \frac{1}{\sqrt{L}} \sum_{k=-\infty}^{\infty} c_{L,k} e^{-ikx}, \end{aligned} \quad (C3)$$

where $k = 2\pi n_k/L$ is now being measured with respect to $\pm k_F$ (so that the Fermi momentum is at $k = 0$), and $n_k = 0, \pm 1, \pm 2, \dots$. Further,

$$\{c_{\nu,k}, c_{\nu',k'}\} = 0 \quad \text{and} \quad \{c_{\nu,k}, c_{\nu',k'}^\dagger\} = \delta_{\nu\nu'} \delta_{kk'}, \quad (C4)$$

where $\nu = R, L$.

Next, let us consider a model of bosons with the right- and left-moving fields being denoted by ϕ_R and ϕ_L respectively. These fields have the Fourier expansion

$$\begin{aligned} \phi_R(x) &= \frac{i}{2\sqrt{\pi}} \sum_{q>0} \frac{e^{-\alpha q/2}}{\sqrt{n_q}} [b_{R,q} e^{iqx} - b_{R,q}^\dagger e^{-iqx}], \\ \phi_L(x) &= -\frac{i}{2\sqrt{\pi}} \sum_{q>0} \frac{e^{-\alpha q/2}}{\sqrt{n_q}} [b_{L,q} e^{-iqx} - b_{L,q}^\dagger e^{iqx}], \end{aligned} \quad (C5)$$

where $q = 2\pi n_q/L$, and $n_q = 0, \pm 1, \pm 2, \dots$. Further,

$$[b_{\nu,q}, b_{\nu',q'}] = 0 \quad \text{and} \quad [b_{\nu,q}, b_{\nu',q'}^\dagger] = \delta_{\nu\nu'} \delta_{qq'}, \quad (C6)$$

where $\nu = R, L$. In (C5), we have introduced a cut-off α in order to ensure that the contributions from high-momentum modes do not produce divergences when computing various commutators and correlation functions; α will often be of the same order as $1/k_F$. [In writing (C5), we have ignored the zero modes. The interested reader may find discussions of these in the references on bosonization [88, 652–661]].

The bosonization formulae allow us to write the bosonic operators in terms of the fermionic ones and vice versa. For instance, we find that the creation/annihilation operators in momentum space are related as

$$\begin{aligned} b_{\nu,q}^\dagger &= \frac{1}{\sqrt{n_q}} \sum_{k=-\infty}^{\infty} c_{\nu,k+q}^\dagger c_{\nu,k}, \\ b_{\nu,q} &= \frac{1}{\sqrt{n_q}} \sum_{k=-\infty}^{\infty} c_{\nu,k-q}^\dagger c_{\nu,k}, \end{aligned} \quad (C7)$$

where $q = 2\pi n_q/L$ and $\nu = R, L$ as before. Eq. (C7) shows that a bosonic excitation is generally a superposition of an infinite number of fermionic particle-hole pairs. On the other hand, the fermionic operators can be written as exponentials of the bosonic operators as follows:

$$\begin{aligned} \psi_R(x) &= \frac{1}{\sqrt{2\pi\alpha}} \eta_R e^{-i2\sqrt{\pi}\phi_R(x)}, \\ \psi_L(x) &= \frac{1}{\sqrt{2\pi\alpha}} \eta_L e^{i2\sqrt{\pi}\phi_L(x)}. \end{aligned} \quad (C8)$$

The unitary operators η_R and η_L are called Klein factors, and they are required to ensure that the field operators given in (C8) anticommute with each other at two different spatial points.

It is convenient to define the two bosonic fields

$$\begin{aligned}\phi &= \phi_R + \phi_L, \\ \theta &= -\phi_R + \phi_L.\end{aligned}\tag{C9}$$

Eq. (C7) then implies that

$$\psi_R^\dagger \psi_R + \psi_L^\dagger \psi_L = -\frac{1}{\sqrt{\pi}} \frac{\partial \phi}{\partial x}.\tag{C10}$$

The fermionic density is given by

$$\rho - \rho_0 = \psi^\dagger \psi = \psi_R^\dagger \psi_R + \psi_L^\dagger \psi_L + e^{-i2k_F x} \psi_R^\dagger \psi_L + e^{i2k_F x} \psi_L^\dagger \psi_R,\tag{C11}$$

where ρ_0 is the background density, and we have written the density fluctuation around ρ_0 in terms of fermionic fields. Ignoring the last two terms in (C11) which vary rapidly (since their length scale of variation is $1/k_F$), we see that

$$\rho - \rho_0 = -\frac{1}{\sqrt{\pi}} \frac{\partial \phi}{\partial x} + \frac{1}{\sqrt{2\pi\alpha}} [\eta_R^\dagger \eta_L e^{i2\sqrt{\pi}\phi - i2k_F x} + \eta_L^\dagger \eta_R e^{-i2\sqrt{\pi}\phi + i2k_F x}].\tag{C12}$$

The formalism outlined so far does not explicitly refer to any particular dynamics of the bosonic or fermionic system. Let us now introduce some dynamics by specifying appropriate Hamiltonians. We first consider a system of non-interacting fermions; let us assume that the velocity of the modes described by $\psi_{R,L}$ is given by $(dE_k/dk)_{k=k_F} = -(dE_k/dk)_{k=-k_F} = v_F$, where v_F is called the Fermi velocity. The Hamiltonian for such a system is given by

$$H_0 = -v_F \int dx [\psi_R^\dagger(x) i \partial_x \psi_R(x) - \psi_L^\dagger(x) i \partial_x \psi_L(x)],\tag{C13}$$

where $\partial_x \equiv \partial/\partial x$. Let us now add to this a short-range density-density interaction of the form

$$V = \frac{1}{2} \int dx [2g_2 \rho_R(x) \rho_L(x) + g_4 (\rho_R^2(x) + \rho_L^2(x))],\tag{C14}$$

where $\rho_R = \psi_R^\dagger \psi_R$ and $\rho_L = \psi_L^\dagger \psi_L$. Physically, we may expect an interaction term like $g\rho^2$, so that $g_2 = g_4 = g$. However, we will allow g_2 to differ from g_4 for the sake of generality. Then the Hamiltonians for the corresponding bosonic systems are as follows. The non-interacting Hamiltonian in (C13) maps to

$$H = \frac{v_F}{2} \int dx [(\partial_x \theta)^2 + (\partial_x \phi)^2],\tag{C15}$$

while the Hamiltonian for the interacting fermion system $H = H_0 + V$ maps to the bosonic Hamiltonian

$$H = \frac{v}{2} \int dx [K(\partial_x \theta)^2 + \frac{1}{K}(\partial_x \phi)^2],\tag{C16}$$

where

$$\begin{aligned}v &= \left[\left(v_F + \frac{g_4}{2\pi} - \frac{g_2}{2\pi} \right) \left(v_F + \frac{g_4}{2\pi} + \frac{g_2}{2\pi} \right) \right]^{1/2}, \\ K &= \left[\left(v_F + \frac{g_4}{2\pi} - \frac{g_2}{2\pi} \right) / \left(v_F + \frac{g_4}{2\pi} + \frac{g_2}{2\pi} \right) \right]^{1/2}.\end{aligned}\tag{C17}$$

This describes bosonic modes with an energy $E_q = v|q|$. Note that the interaction has changed the velocity from v_F to v , and has also given rise to a parameter K which is called the Luttinger parameter. We observe here that this analysis breaks down if $g_2 > 2\pi v_F + g_4$ since K and v then become imaginary numbers.

An important use of bosonization is that one can easily compute certain correlation functions using the bosonic theory which would be very difficult to compute in an interacting fermionic theory. Eq. (C5) can be used to show that the equal-time correlation functions of the fields ϕ and θ are given by

$$\begin{aligned}\langle 0 | \phi(x) \phi(0) | 0 \rangle &= -\frac{K}{2\pi} \ln \left(\frac{|x|}{\alpha} \right), \\ \langle 0 | \theta(x) \theta(0) | 0 \rangle &= -\frac{1}{2\pi K} \ln \left(\frac{|x|}{\alpha} \right),\end{aligned}\tag{C18}$$

for $|x| \gg \alpha$. (In (C18), we have not written the time coordinates for the fields since these are equal). Let us now consider an exponential operator of the form

$$O_{m,n} = e^{i2\sqrt{\pi}(m\phi+n\theta)}. \quad (\text{C19})$$

Eq. (C18) can then be used to derive the following result for the equal-time correlation function

$$\langle 0|O_{m,n}(x)O_{m',n'}^\dagger(0)|0\rangle \sim \delta_{mm'}\delta_{nn'} \left(\frac{\alpha}{|x|}\right)^{2(m^2K+n^2/K)}, \quad (\text{C20})$$

where K is the Luttinger parameter. Note that the correlation function decays as a power law, but the power law depends on K and is therefore not universal. In the language of the RG, the scaling dimension of $O_{m,n}$ can be read off from (C20) as $m^2K + n^2/K$.

We can now study a quantum spin chain using bosonization. Let us consider the XXZ spin-1/2 chain in a magnetic field which is described by the Hamiltonian

$$H = \sum_{n=1}^{N-1} \left[\frac{J}{2} (\sigma_n^+ \sigma_{n+1}^- + \sigma_n^- \sigma_{n+1}^+) + \frac{J_z}{4} \sigma_n^z \sigma_{n+1}^z \right] - \frac{h}{2} \sum_{n=1}^N \sigma_n^z, \quad (\text{C21})$$

where $\sigma_n^+ = (1/2)(\sigma_n^x + i\sigma_n^y)$ and $\sigma_n^- = (1/2)(\sigma_n^x - i\sigma_n^y)$ are the spin raising and lowering operators, h denotes the strength of the magnetic field, and we assume that $J > 0$. (We will eventually be interested in the thermodynamic limit $N \rightarrow \infty$). Note that the model has a $U(1)$ invariance, namely, rotations about the z axis. When $J_z = J$ and $h = 0$, the $U(1)$ invariance is enhanced to an $SU(2)$ invariance, because at this point the model can be written as $H = (J/4) \sum_n \vec{\sigma}_n \cdot \vec{\sigma}_{n+1}$. Although the model in (C21) can be exactly solved using the Bethe ansatz [668], and one has the explicit result that the model is gapless for a certain range of values of J_z/J and h/J (see [314]), it is not easy to explicitly compute correlation functions in that approach. We will therefore use bosonization to study this model.

Using the JW transformations (24), (C21) can be written as

$$H = \sum_n \left[-\frac{J}{2} (c_n^\dagger c_{n+1} + H.c.) + J_z c_n^\dagger c_n c_{n+1}^\dagger c_{n+1} - h c_n^\dagger c_n \right], \quad (\text{C22})$$

where we have ignored some constants. We see that the spin-flip operators S_n^\pm lead to hopping terms in the fermionic Hamiltonian, whereas the $S_n^z S_{n+1}^z$ interaction term leads to an interaction between fermion densities on adjacent sites.

Let us first consider the non-interacting case given by $J_z = 0$. By Fourier transforming the fermions, $c_k = \sum_n c_n e^{-ikna}/\sqrt{N}$, where a is the lattice spacing and the momentum k lies in the first Brillouin zone $-\pi/a < k \leq \pi/a$, we find that the Hamiltonian is given by

$$H = \sum_k \omega_k c_k^\dagger c_k, \quad (\text{C23})$$

where $\omega_k = -J \cos(ka) - h$.

The ground state of this system is one in which all the single-particle states with $\omega_k < 0$ are occupied, and all the states with $\omega_k > 0$ are empty. If we set the magnetic field $h = 0$, the magnetization per site $m \equiv \sum_n \sigma_n^z/N$ will be zero in the ground state; equivalently, in the fermionic language, the ground state is half-filled. Thus, for $m = 0$, the Fermi points lie at $ka = \pm\pi/2$ where $\omega_k = 0$; hence $k_F a = \pi/2$. Let us now add the magnetic field term. In the fermionic language, this is equivalent to adding a chemical potential term which couples to ρ_n . Now the ground state no longer has $m = 0$ and the fermion model is no longer half-filled. The Fermi points are then given by $\pm k_F$, where

$$k_F a = \frac{\pi}{2} (m + 1). \quad (\text{C24})$$

It turns out that this relation between k_F (which governs the oscillations in the correlation functions as discussed below) and the magnetization m continues to hold even if we turn on the interaction J_z , although the simple picture of the ground state (with states being occupied below some energy and empty above some energy) no longer holds in that case.

In the linearized approximation, the modes near the two Fermi points have the velocities $d\omega_k/dk = \pm v$, where v is some function of J , J_z and h . Let us define the continuum fermionic field $\psi(x) = c_n$ where $x = na$. We introduce the slowly varying fermionic fields ψ_R and ψ_L as defined in (C2), and then bosonize these fields. The spin fields can be

written in terms of either the fermionic or the bosonic fields. For instance, σ^z is given by the fermion density as in (24) which then has a bosonized form given in (C12). Similarly,

$$\begin{aligned} \sigma^+(x) &= (-1)^{x/a} [e^{-ik_F x} \psi_R^\dagger(x) + e^{ik_F x} \psi_L^\dagger(x)] \\ &\times [e^{i\pi \int_{-\infty}^x dx' (\psi^\dagger(x')\psi(x') + 1/2a)} + H.c.], \end{aligned} \quad (C25)$$

where $(-1)^{x/a} = \pm 1$ since x/a is an integer. This can now be written entirely in the bosonic language; the term in the exponential is given by

$$\int_{-\infty}^x dx' \psi^\dagger(x')\psi(x') = -\frac{1}{\sqrt{\pi}} \int_{-\infty}^x dx' \frac{\partial \phi}{\partial x'} = -\frac{1}{\sqrt{\pi}} [\phi_R(x) + \phi_L(x)], \quad (C26)$$

where we have ignored the contribution from the lower limit at $x' = -\infty$.

We can now use these bosonic expressions and Eq. (C20) to compute the two-spin, equal-time correlation functions $G^{ab}(x) \equiv \langle 0 | \sigma^a(x) \sigma^b(0) | 0 \rangle$. We find that

$$\begin{aligned} G^{zz}(x) &= m^2 + \frac{c_1}{x^2} + c_2 \frac{\cos(2k_F x)}{x^{2K}}, \\ G^{+-}(x) + G^{-+}(x) &= c_3 \frac{(-1)^{x/a}}{x^{1/(2K)}} + c_4 \frac{(-1)^{x/a} \cos(2k_F x)}{x^{2K+1/(2K)}}, \end{aligned} \quad (C27)$$

where c_1, \dots, c_4 are some constants. The parameter K in (C27) is a function of J_z/J and h/J as discussed in [314]. For $h = 0$, K is given by the expression

$$\frac{1}{K} = 1 + \frac{2}{\pi} \sin^{-1} \left(\frac{J_z}{J} \right). \quad (C28)$$

Note that at the $SU(2)$ invariant and isotropic antiferromagnetic point, $J_z = J$ and $h = 0$, we have $m = 0$, $k_F a = \pi/2$ and $K = 1/2$, and the two correlations G^{zz} and G^{+-} have the same forms, as expected; since the terms which decay the slowest do so as $1/x$, we conclude that σ^x , σ^y and σ^z all have the scaling dimension equal to $1/2$ at the isotropic point. Two other points of interest are given by $J_z = 0$ where $K = 1$ (non-interacting fermions), and $J_z \rightarrow -J$ (the isotropic ferromagnetic point) where $K \rightarrow \infty$. In general, $J_z > (<) 0$ corresponds to fermions with repulsive (attractive) interactions and $K < (>) 1$ respectively.

We can compute the exponent β appearing in the momentum distribution function $n(k)$ in (C1). In terms of the parameter K , we find that $\beta = (1 - K)^2/(2K)$. This is always positive except for the special case of non-interacting fermions where $K = 1$.

In addition to providing a convenient way of computing correlation functions, bosonization also allows us to study the effects of small perturbations. We will consider a few examples here.

A physically important perturbation is a dimerizing term

$$V = \delta \sum_n (-1)^n \left[\frac{J}{2} (\sigma_n^+ \sigma_{n+1}^- + \sigma_n^- \sigma_{n+1}^+) + \frac{J_z}{4} \sigma_n^z \sigma_{n+1}^z \right], \quad (C29)$$

where δ is the strength of the perturbation. Upon bosonizing and ignoring terms which oscillate on the scale of the lattice spacing a or $1/k_F$ (and which therefore integrate to zero on length scales much larger than a), we find that the slowly varying terms are proportional to $e^{\pm i 2\sqrt{\pi}\phi}$. Eq. (C20) then implies that the scaling dimension of these terms is K . Namely, under an RG flow, the effective length-scale dependent dimerization parameter $\delta(L)$ satisfies the equation

$$\frac{d\delta}{d \ln L} = (2 - K)\delta \quad (C30)$$

to first order in δ . Hence this perturbation is relevant, irrelevant and marginal for $K < 2$, > 2 and $= 2$ respectively. If $K < 2$, a small value of δ at the microscopic length scale a will grow to be of order 1 at a length scale L_0 given by $L_0/a \sim 1/(\delta(a))^{1/(2-K)}$. This implies that the two-point correlation function will decay exponentially at large separations with a correlation length of order L_0 . To put it differently, this perturbation produces an energy gap in the system which scales with $\delta(a)$ as

$$\Delta E \sim (\delta(a))^{1/(2-K)}. \quad (C31)$$

For an isotropic antiferromagnet with $K = 1/2$, we see that $\Delta E \sim \delta^{2/3}$. This kind of phenomenon occurs in spin-Peierls systems such as CuGeO_3 ; below a transition temperature T_{sp} , such a system goes into a dimerized phase which has a gap [669].

Another interesting perturbation is to consider the spin-1/2 XYZ chain where the x and y couplings are slightly different from each other. (This is a generalization of the “anisotropic transition” discussed in Sec. II(A) where we had taken $J_z = 0$ and therefore K was equal to 1). Namely, we consider the Hamiltonian

$$H = \frac{1}{4} \sum_n [J_x S_n^x S_{n+1}^x + J_y S_n^y S_{n+1}^y + J_z S_n^z S_{n+1}^z]. \quad (\text{C32})$$

Let us denote $J = (J_x + J_y)/2$, and $\gamma = (J_x - J_y)/(J_x + J_y)$. The JW transformation turns this Hamiltonian into

$$H = \sum_n \left[-\frac{J}{2} \{c_n^\dagger c_{n+1} + H.c. + \gamma(c_n^\dagger c_{n+1}^\dagger - c_n c_{n+1})\} + J_z c_n^\dagger c_n c_{n+1}^\dagger c_{n+1} \right]. \quad (\text{C33})$$

Upon bosonizing and ignoring terms which oscillate on the scale of the lattice spacing, we find that the slowly varying terms are proportional to $e^{\pm i2\sqrt{\pi}\theta}$. Eq. (C20) then implies that the scaling dimension of these terms is $1/K$. Using RG arguments similar to those given above, we conclude that this perturbation will lead to the opening of an energy gap which scales as

$$\Delta E \sim \gamma^{1/(2-1/K)}. \quad (\text{C34})$$

Another important perturbation is a weak coupling between two isotropic antiferromagnetic spin-1/2 chains (with the spin variables in the two chains being denoted by $\vec{\sigma}_n^{(1)}$ and $\vec{\sigma}_n^{(2)}$) given by

$$V = J' \sum_n \vec{\sigma}_n^{(1)} \cdot \vec{\sigma}_n^{(2)}. \quad (\text{C35})$$

We saw above that for a single isotropic chain, the scaling dimension of the spin operators is equal to $1/2$; hence the perturbation $\vec{\sigma}^{(1)} \cdot \vec{\sigma}^{(2)}$ has the scaling dimension 1. Hence this perturbation is relevant, and it produces an energy gap which scales as $\Delta E \sim J'$. This has been confirmed by numerical calculations [670].

Finally, let us consider a spin-1/2 chain with both nearest- and next-nearest-neighbor isotropic antiferromagnetic interactions governed by the Hamiltonian

$$H = J_1 \sum_n \vec{\sigma}_n \cdot \vec{\sigma}_{n+1} + J_2 \sum_n \vec{\sigma}_n \cdot \vec{\sigma}_{n+2}. \quad (\text{C36})$$

This is called a frustrated system since the classical ground states of the J_1 and J_2 pieces of the Hamiltonian are in conflict with each other; the first term has a classical ground state of the Neel form $\uparrow\downarrow\uparrow\downarrow \dots$ while the second term has a period-4 ground state of the form $\uparrow\uparrow\downarrow\downarrow \dots$. Since the spin-1/2 chain is a quantum system, the effect of frustration is not as easy to visualize here as in a classical spin system. A field theoretic study indicates that the model makes a transition from a gapless phase to a gapped and spontaneously dimerized phase when $J_2/J_1 \gtrsim 1/6$ [671]. Numerical calculations show that the spin-1/2 chain is gapless and in a Neel state for $0 < J_2/J_1 \lesssim 0.241$, gapped and in a spontaneously dimerized Neel state for $0.241 \lesssim J_2/J_1 < 1/2$, and gapped and in a spiral state for $1/2 < J_2/J_1$ [672–678]. Here, the words Neel and spiral refer to ground states in which the structure factor $S(q)$, given by the Fourier transform of the equal-time two-spin correlation function $\langle 0 | \vec{\sigma}_0 \cdot \vec{\sigma}_n | 0 \rangle$, has peaks at $q = \pi$ and $q < \pi$ respectively. The point $J_2/J_1 = 1/2$ is called the Majumdar-Ghosh point; the ground states are doubly degenerate and exactly solvable there. The two ground states are given by a product of singlets in which each spin on an even numbered sites forms a singlet with its neighbor either to its left or to its right [679]. An interesting perturbation to consider now is to study what happens when J_2 crosses the critical value $J_{2c} \simeq 0.241$. This turns out to be a marginal perturbation (i.e., the scaling dimension is 2), so that in the RG equation one has to go to the second order in the perturbing parameter $J_2 - J_{2c}$. One finds eventually that for $J_2 > J_{2c}$, an energy gap opens up with an essential singularity of the form $\Delta E \sim \exp[-c/(J_2 - J_{2c})]$, where c is a constant [672].

Appendix D: Scaling of the geometric phase close to a QCP

When the Hamiltonian of a system changes adiabatically in time in the parameter space, then in addition to the usual dynamical phase, there is a phase that arises purely due to the geometry of the parameter space. This is

known as the Pancharatnam-Berry phase or geometric phase (GP) [405, 406]; this phase is non-zero only if there is a degeneracy inside the circuit enclosed. At a QCP, the energy gap between the ground and the first excited state vanishes, i.e., there is a degeneracy which is expected to lead to a non-zero GP. In this section, we shall briefly note the scaling of the GP (which is also the imaginary part of the geometric tensor defined in Sec. V (C)) close to the QCP of a transverse XY spin chain [426–432].

The GP is estimated introducing a new family of Hamiltonians which is generated by rotating every spin of Hamiltonian (10) by an angle ϕ around the \hat{z} direction. The direct product ground state in (30) then takes the form

$$|\psi_0(\gamma, h)\rangle = \bigotimes_{k>0} (\cos \theta_k |0\rangle + i e^{2i\phi} \sin \theta_k |k, -k\rangle), \quad (\text{D1})$$

where θ_k is defined in (28); the energy spectrum and hence the critical exponents remain unaltered under this rotation. The GP of the ground state is given by $\beta_g = (\pi/L) \sum_{k>0} (1 - \cos 2\theta_k)$. Carollo and Pachos [427] studied the behavior of the GP close to the anisotropic critical point in a transverse XY chain (Fig. 2) and showed that a non-contractible geometric phase difference between the ground state and the first excited state exists when the Hamiltonian encounters a critical point while passing through an adiabatic cycle¹³. In subsequent work [426], it was shown that the ground state GP is non-analytic along the Ising critical line; the derivative $d\beta_g/dh$ shows a peak at the Ising critical point when plotted as a function of h and diverges logarithmically with the chain length. From the scaling relations $d\beta_g/dh \sim \kappa_1 \ln L + C_1$ at the effective critical point $h_m(L)$ where the peak occurs for large L , and $d\beta_g/dh \sim \kappa_2 \ln |h - h_c| + C_2$ in the thermodynamic limit as $h \rightarrow h_c = J_x + J_y = 1$ (where C_1 and C_2 are non-universal constants), the critical exponent ν can be obtained from the relation $\nu = \kappa_2/\kappa_1 = 1$. On the anisotropic critical line ($\gamma = 0$), the GP is given by $\beta_g = 2\pi - 2\cos^{-1}(h)$ in the thermodynamic limit, and $d\beta_g/dh \sim (1 - h)^{-1/2}$ for $h \rightarrow 1^-$ which provides the correct exponent $\nu_{mc} = 1/2$, associated with the MCP. Close to the multicritical point, the derivative of the GP shows an oscillatory behavior due to the presence of quasicritical points as seen in the FS and exhibits a power-law divergence with the system size with an exponent that depends on the path of approach to the MCP [680]. Recently a NMR interferometry study which exploits the geometric phase as a probe of quantum transitions of the ground state in a spin-1/2 transverse XY models has been reported [681].

Appendix E: Landau-Zener tunneling

We present here an outline of the calculational details leading to an exact solution for the conventional Landau-Zener-Stueckelberg-Majorana-Stueckelberg problem [682–685]. Let us first consider a general Hamiltonian in the basis $|1\rangle$ and $|2\rangle$ as shown below [511, 513, 683]

$$H(t) = \begin{bmatrix} \epsilon_1(t) & \Delta(t) \\ \Delta^*(t) & \epsilon_2(t) \end{bmatrix},$$

where ϵ_1 and ϵ_2 are the two bare energy levels (diagonal elements) varying as $\sim t/2\tau$ and $-t/2\tau$ respectively. If $|\psi(t)\rangle = c_1(t)|1\rangle + c_2(t)|2\rangle$, then the Schrödinger equation for $c_1(t)$ and $c_2(t)$ is

$$i \frac{d}{dt} \begin{pmatrix} c_1 \\ c_2 \end{pmatrix} = \begin{bmatrix} \epsilon_1(t) & \Delta(t) \\ \Delta^*(t) & \epsilon_2(t) \end{bmatrix} \begin{pmatrix} c_1 \\ c_2 \end{pmatrix}. \quad (\text{E1})$$

The wave function $\psi(t)$ can be analytically obtained at any instant t when ϵ_1 and ϵ_2 vary linearly in time and Δ is time-independent. If the off-diagonal term is time-dependent, in some cases one can use a unitary transformation to shift the time-dependence entirely to the diagonal terms to find an exact solution [549]. We now redefine $c_1(t)$ and $c_2(t)$ as follows

$$c_1(t) = \tilde{c}_1(t) e^{-i \int_{-\infty}^t \epsilon_1(t') dt'} \quad \text{and} \quad c_2(t) = \tilde{c}_2(t) e^{-i \int_{-\infty}^t \epsilon_2(t') dt'}.$$

¹³ The geometric phase depends on the path over which the Hamiltonian is traversed. If one considers a loop and tries to find the net GP accumulated, then there can be two cases. If the enclosed region does not include any critical point, the loop can be continuously deformed to a point and hence produces a zero GP. On the other hand, if a critical point is enclosed in the loop, then one finds a finite GP even when the loop is contracted to a point. The GP is non-contractible in the sense that even when one deforms the loop, it always encloses the critical point and thus has a associated non-zero phase associated with the critical point.

The Schrödinger equation for \tilde{c}_2 is

$$i\frac{\partial}{\partial t}\tilde{c}_2(t) = \Delta^*\tilde{c}_1(t)e^{-i\int_{-\infty}^t(\epsilon_1(t')-\epsilon_2(t'))dt'}. \quad (\text{E2})$$

Replacing $\tilde{c}_2(t)$ by $U_2(t)$ defined as

$$\tilde{c}_2(t) = e^{-\frac{i}{2}\int_{-\infty}^t(\epsilon_1-\epsilon_2)dt'}U_2(t), \quad (\text{E3})$$

followed by a change of variable given by

$$z = \frac{t}{\sqrt{\tau}}e^{-i\pi/4},$$

the Schrödinger equation can be re-written as

$$\frac{\partial^2}{\partial z^2}U_2(z) + (m + \frac{1}{2} - \frac{z^2}{4})U_2(z) = 0, \quad (\text{E4})$$

where $m = i\Delta^2\tau$ (where $\Delta^2 = \Delta\Delta^*$) and $\epsilon_1 - \epsilon_2 = t/\tau$. By all these transformations, we are able to recast the Schrödinger equation E1 in the form of the Weber differential equation whose solutions are linear combination of well known Weber functions $D_{-m-1}(iz)$ and $D_{-m-1}(-iz)$ i.e., $U_2(z) = aD_{-m-1}(iz) + bD_{-m-1}(-iz) = \tilde{c}_2(t)e^{\frac{it^2}{4\tau}}$, or, going back to the notation of $\tilde{c}_1(t)$ and $\tilde{c}_2(t)$,

$$\begin{aligned} |\psi(t)\rangle &= \frac{i}{\Delta}[\partial_t - \frac{it}{2\tau}] [aD_{-m-1}(iz) + bD_{-m-1}(-iz)] |1\rangle \\ &+ [aD_{-m-1}(iz) + bD_{-m-1}(-iz)] |2\rangle. \end{aligned} \quad (\text{E5})$$

The initial condition demands that at $t \rightarrow -\infty$, $|\psi(t)\rangle \sim |1\rangle$ which implies $\tilde{c}_2(-\infty)=0$. This forces $\tilde{c}_2(t)$ or $U_2(z)$ to be a function of only $D_{-m-1}(-iz)$ as $D_{-m-1}(-iz)$ goes to zero at $t \rightarrow -\infty$ but $D_{-m-1}(iz)$ does not. This can be shown as follows. The asymptotic forms of the Weber functions are

$$\lim_{z \rightarrow +\infty} D_n(z) \sim e^{-\frac{1}{4}z^2} z^n - \frac{\sqrt{2\pi}}{\Gamma(-n)} e^{n\pi i r} e^{\frac{1}{4}z^2} z^{-n-1} \quad \text{for} \quad \frac{\pi r}{4} < \arg(z) < \frac{5\pi r}{4}, \quad (\text{E6})$$

where r is either 1 or -1 , and

$$\lim_{z \rightarrow +\infty} D_n(z) \sim e^{-\frac{1}{4}z^2} z^n \quad \text{for} \quad |\arg(z)| < \frac{3\pi}{4}. \quad (\text{E7})$$

The $t \rightarrow -\infty$ ($z \rightarrow -\infty$) form of the two Weber functions $D_{-m-1}(iz)$ and $D_{-m-1}(-iz)$ is

$$\begin{aligned} \lim_{z \rightarrow -\infty} D_{-m-1}(iz) &= \lim_{R \rightarrow +\infty} D_{-m-1}(Re^{-i3\pi/4}) \\ &\sim \frac{\sqrt{2\pi}}{\Gamma(m+1)} e^{i7\pi m/4} e^{iR^2/4} R^{m+1}. \end{aligned} \quad (\text{E8})$$

and,

$$\lim_{z \rightarrow -\infty} D_{-m-1}(-iz) = \lim_{R \rightarrow +\infty} (Re^{i\pi/4}) = 0. \quad (\text{E9})$$

where $R = |t|/\sqrt{\tau}$.

Since at $t \rightarrow -\infty$, $\tilde{c}_2 = 0$, and $D_{-m-1}(iz)$ does not go to zero, we must have $a = 0$ whereas the form of b can be obtained by these asymptotic forms along with the initial condition as follows: Putting $a = 0$, we have

$$\tilde{c}_2(t) = e^{-\frac{it^2}{4\tau}} b D_{-m-1}(-iz).$$

Expanding Eq. (E2) after substituting $\tilde{c}_2(t)$ as given above, we get

$$\begin{aligned} \Delta\tilde{c}_1(t)e^{-\frac{it^2}{2\tau}} &= \frac{bt}{2\tau}e^{-\frac{it^2}{4\tau}} \left[e^{-\frac{iR^2}{4}} R^{-k-1} e^{-\frac{\pi(k+1)i}{4}} \right] \\ &+ bie^{-\frac{it^2}{4\tau}} \frac{dR}{dt} \left[\frac{d}{dR} e^{-iR^2/4} R^{-k-1} e^{-\frac{\pi(k+1)i}{4}} \right]. \end{aligned}$$

Neglecting the second term and substituting $c_1(-\infty) = 1$ gives

$$b = \Delta \sqrt{\tau} e^{-\frac{\pi}{4} \Delta^2 \tau}.$$

Once we know the value of b with the given initial conditions, it is easy to obtain the excitation probability at $t \rightarrow +\infty$ which is simply given by $p = |c_1|^2 = 1 - |c_2|^2$, where

$$|c_2(t \rightarrow +\infty)|^2 = |b \lim_{z \rightarrow +\infty} D_{-m-1}(-iz)|^2. \quad (\text{E10})$$

Substituting the expression of b obtained along with the asymptotic form of $D_{-m-1}(-iz)$ when $z \rightarrow +\infty$ which is the same as given in Eq. (E8), we get

$$p = e^{-2\pi\tau\Delta^2}. \quad (\text{E11})$$

This can be generalized to finite coupling duration [546], and the LZ transition times have been calculated in diabatic and adiabatic limits [547]. We note that this problem has recently been extended to various other situations [513, 686] and to many particle systems [687, 688].

Appendix F: KZ mechanism in space

In Sec. VI, we have considered different quenching schemes (except in Sec. VI (K)) where the quenching parameter is homogeneous throughout the system. This is to some extent an idealized situation; for example, in ultracold atom gases confined in magnetic/optical traps, the trapping potential results in an inhomogeneous density of atoms and the critical point depends on the local density of atoms. In this context, the notion of a symmetry breaking (inhomogeneous) QPT in space has been introduced [575, 689–692]. For a classical phase transition, spatial inhomogeneities influence the critical behavior if the resulting perturbation is relevant in the sense of the RG; for a review, see [693]. Also, the critical behavior of a Bose condensate in a trapped potential has recently been studied, and a power-law scaling of the correlation length with the trap size has been proposed [694].

Let us define the driving parameter $\lambda(\vec{r})$ as follows. The part of the system where $\lambda(\vec{r}) > 0$ is in a different phase than the region in which $\lambda(\vec{r}) < 0$; a phase transition between the two phases occurs at the critical surface $\lambda(\vec{r}) = 0$. We consider the variation of λ along the \hat{x} direction and linearize near the critical point x_c ($\lambda(x_c) = 0$); this gives $\lambda \simeq \lambda_0(x - x_c)/\alpha_x$, where $1/\alpha_x = (\partial\lambda/\partial x)_{x_c}$. The system is in the symmetry broken phase for $x < x_c$ while in the symmetric phase for $x > x_c$. Within the local density approximation (LDA) which assumes that the system is locally uniform, the order parameter vanishes as $(x_c - x)^\beta$ as $x \rightarrow x_c^-$. However, the LDA breaks down in the vicinity of x_c due to the diverging healing length $\hat{\xi} \sim |x - x_c|^{-\nu}$ which is the only characteristic length as $x \rightarrow x_c$. We now encounter a situation analogous to that which appeared in deriving (107); in a similar spirit we argue that if $\lambda(x)$ is varied linearly through $x = x_c$, the LDA must break down when the local correlation length $\xi \sim [(x - x_c)/\alpha_x]^{-\nu}$ is of the order of the distance from the critical point $|x - x_c|$. We define a length scale \hat{x} where the healing length $\hat{\xi}$ becomes of the order of the length scale associated with the spatial driving $\lambda/(d\lambda/dx)$ at which the adiabatic to non-adiabatic transition occurs, given by $\hat{x} \sim \alpha_x^{\nu/(\nu+1)}$. The above equation is very similar to that of \hat{t} in (108) showing a striking resemblance between the temporal and spatial quenches.

The KZ mechanism in space predicts that the order parameter is frozen in x in the impulse region given by $-(x - x_c) < \hat{x} < x - x_c$; it penetrates into the disordered symmetric phase up to the length \hat{x} which is given in terms of the quantum critical exponent ν , i.e., the QCP is rounded off on the scale \hat{x} . Consequently, the energy gap is finite at $x = x_c$ and scales as $\hat{x}^{-z} \sim \alpha_x^{-\nu z/(\nu+1)}$ which vanishes only in the limit $\alpha_x \rightarrow \infty$. The scaling can be easily generalized to non-linear quenching by renormalizing $\nu \rightarrow r\nu$ (see Sec. VI (B)). This prediction has been verified for an Ising chain in an inhomogeneous transverse field $h(x) - 1 = x/\alpha_x$ with an open boundary condition; the gap was found to scale as $\alpha_x^{-1/2}$ and $\hat{x} \sim \alpha_x^{1/2}$ which is expected since $\nu = z = 1$ [689, 690]. On the other hand, when the MCP of the transverse XY chain (Fig. 2) is approached along a linear path varying both $h - 1$ and γ , the gap scales as $\alpha_x^{-3/4}$ because the quasicritical exponents $\nu_q = 1/3$ and $z_q = 3$ [695].

The situation has been further generalized to study an inhomogeneous phase transition that takes place both in space and time [695, 696]; here the driving parameter can be linearized close to the QCP as $\lambda(x, t) = (x - vt)/\alpha_x$, where α_x and v denote the inhomogeneity and the speed of the critical front $\lambda(x, t) = 0$, respectively. At a fixed point in space, this represents a homogeneous temporal quenching discussed in previous sections with $\tau = \alpha_x/v$. The part of the system for which $x < vt$ is in the symmetry broken phase and the orientation of the order parameter cannot propagate with velocity exceeding the critical speed $\hat{v} = \hat{\xi}/\hat{t}$; with $\hat{t} \sim \tau^{\nu z/(z\nu+1)}$ and $\hat{\xi} \sim \tau^{\nu/(z\nu+1)}$, one finds

$\hat{v} \sim \tau^{\nu(1-z)/(z\nu+1)}$ or, equivalently, $\hat{v} \sim \alpha_x^{\nu(1-z)/(z\nu+1)}$ as $\tau = \alpha_x/v$. If $v < \hat{v}$, one expects the final state to have fewer excitations than predicted by the KZS. One can equivalently find an optimal rate which scales with the inhomogeneity parameter α_x as $\tau_{\text{opt}} \sim \alpha_x^{(z\nu+1)/(1+\nu)}$; for $\tau \gg \tau_{\text{opt}}$, inhomogeneities become relevant and fewer defects are produced. In the homogeneous limit, $\alpha_x \rightarrow \infty$ and hence $\tau_{\text{opt}} \rightarrow \infty$. For a transverse XY chain, the \hat{x} and $\hat{\tau}$ has been derived analytically for the Ising transition as well as the transition across the MCP ($z = 2$) [695, 696].

Appendix G: Effect of topology on quantum quenching

In certain models, it turns out that topology can have an important effect on defect production by quenching through a QCP. We will briefly discuss two such models here both of which have the form of a two-legged ladder.

Bermudez *et al.*, 2009, considered a two-legged ladder with spinless electrons hopping between nearby sites on both legs. In addition, there is a magnetic flux through each plaquette; as this flux is varied over one period (given by the flux quantum), there is one point where the system becomes gapless. With open boundary conditions, the model contains states which are localized either in the bulk or at the ends. If the system is initialized so that only a bulk-localized state is occupied by an electron, a quantum quench (which consists of slowly varying the magnetic flux over one period) leads to a defect density given by the KZ power-law $\tau^{-1/2}$. But if the system is initialized so as to occupy only an end-localized state, a quantum quench leads to a defect density which was numerically found to scale as $\tau^{-1.35}$. So far there is no analytical understanding of this unusual power law [530]. In another paper, Bermudez *et al.*, 2010, showed that when a Majorana chain with open boundary conditions is quenched across a QCP, an initial Majorana edge state gives rise to a density of excitations which scales as τ^0 , i.e., the density does not go to zero as $\tau \rightarrow \infty$. This again differs from the KZ power-law. The reason for this anomalous behavior is that at the QCP, the edge state gets completely delocalized and mixes with all the bulk excitations [531].

Sen and Vishveshwara, 2010, considered a two-legged ladder version of the Kitaev model in which there are spin-1/2's at each site which are coupled to nearest neighbors on both legs. The model has a Z_2 -valued invariant on each plaquette; hence the system decouples into 2^N sectors for a system with N sites. Denoting the coupling between the two legs by J_3 , it turns out that $J_3 = 0$ is a QCP for every sector. The effect of quenching $J_3 = t/\tau$ from $-\infty$ to ∞ was studied in a number of sectors in which the Z_2 invariants form a periodic pattern. It was found that in one class of sectors, the quenching leads to a defect density or residual energy which scales as $\tau^{-1/2}$. However, in another class of sectors, these quantities were found to scale as $\tau^{-2/3}$. This can be analytically understood as follows. In the first class of sectors, close to the QCP the system decouples into subsystems (parametrized by a wave number k as usual) in which two states lie close to zero energy and are directly coupled by terms proportional to J_3 . A Landau-Zener derivation of the excitation probability followed by an integration over k then leads to the standard $\tau^{-1/2}$ scaling of the defect density since $d = \nu = z = 1$. However, in the second class of sectors, close to the QCP the system decouples into a set of subsystems in which two states again lie close to zero energy. However, there is now no direct coupling between these two states; rather, they are coupled through some intermediate high-energy states. Eliminating the high-energy states using second order perturbation theory, one obtains an effective coupling between the two low-energy states which is of the order of $J_3^2 = t^2/\tau^2$. Hence the quenching in such sectors effectively has the non-linear form discussed around Eq. (110), and one gets a defect density scaling as $\tau^{-2/3}$ since $r = 2$ [697]. These arguments were developed further in Thakurathi *et al.*, 2012, which considered a spin-1/2 chain with equal xx and yy couplings and a periodically varying magnetic field in the \hat{z} direction with period $2q$, where q is a positive integer. When the strength of the magnetic field is linearly quenched at a rate $1/\tau$ across a quantum critical point, it was found that the density of defects produced scales as $1/\tau^{q/(q+1)}$ [698]. This behavior could be understood by mapping the low-energy physics of the model to a set of fermionic two-level systems in which the two states are coupled at q -th order in perturbation theory. Hence these systems effectively undergo a non-linear quench in which a parameter in the Hamiltonian varies with time as $(t/\tau)^q$; this explains the defect scaling of the form $1/\tau^{q/(q+1)}$ since $d = \nu = z = 1$ and $r = q$ (see Eq. (110)).

Appendix H: Studies of Tomonaga-Luttinger liquids

In this appendix, we will briefly mention some recent studies of Tomonaga-Luttinger liquids (TLLs) from the perspective of quenching dynamics and quantum information. The loading of interacting bosons onto a one-dimensional optical lattice provides an example of quenching in a TLL [699]. Suppose that the periodic potential of the optical lattice is changed in time as $V(x, t) = V(t) \cos(2\pi x/a)$, where the lattice spacing a is commensurate with the bosonic density. The potential couples the right and left moving particles leading to a mass term. The action in terms of the

bosonic field variables $\phi(x, t)$ can be written in the sine-Gordon form

$$S = \int dx dt \left[\frac{1}{v} \left(\frac{\partial \phi}{\partial t} \right)^2 - v \left(\frac{\partial \phi}{\partial x} \right)^2 + V(t) \cos(2\sqrt{\pi K} \phi) \right], \quad (\text{H1})$$

where K and v are as defined in Appendix C. The Luttinger parameter K is governed by the interaction strength; $K \rightarrow 1$ is the limit of strongly repulsive interactions (note that bosons with very strongly repulsive interactions are equivalent to weakly interacting fermions in one dimension), while $K \rightarrow \infty$ is the weakly interacting limit. The scaling dimension of the cosine term can be read off from the equal-time correlation function $\langle \cos(2\sqrt{\pi K} \phi(x, 0)) \cos(2\sqrt{\pi K} \phi(0, 0)) \rangle \sim 1/|x|^{2K}$ leading to the scaling dimension $[\cos(2\sqrt{\pi K} \phi(x, 0))] = K$. Therefore the mass term generated by the cosine term satisfies the relation $V(t) \sim m^{2-K}$ so that the correlation length $\xi \sim 1/m \sim V(t)^{1/(2-K)}$; hence the correlation length exponent is $\nu = 1/(2-K)$. If one considers a linear ramp $V(t) = t/\tau$, with $d = z = 1$, the number of excitations will be given by the KZS in (109), $n \sim \tau^{-1/(3-K)}$ for $0 < K < 2$. For $K > 2$, the cosine term is irrelevant and one gets $n \sim \tau^{-1}$ as there are contributions from the high-energy modes also [540, 699]. $K = 2$ is the BKT transition point.

A quench of the interaction strength in a TLL from zero to a finite value has been studied in [700]. It was shown that the residual energy goes as $\ln \tau/\tau^2$ in the limit $\tau \rightarrow \infty$. Further, the space-time dependent one-particle density matrix and the time-dependent momentum distribution exhibit crossovers between sudden quench, adiabatic and Fermi liquid behaviors as functions of the spatial (or momentum) coordinate, time and τ .

The ground state FS of a one-dimensional gapless model has also been studied using the TLL Hamiltonian in (C16) [433, 701]. The fidelity between two ground states with Luttinger parameters K and K' , respectively, is found to be $F(K, K') = \prod_{k \neq 0} 2/(\sqrt{K/K'} + \sqrt{K'/K})$, so that the fidelity is unity when $K \rightarrow K'$; one can then show that for a large system, the fidelity decays very fast as K separates from K' . For the XXZ chain in (C21) with $h = 0$, the parameter K is related to the zz coupling J_z through the relation (C28); one then finds the FS to be $\chi_F = 1/[4(\pi - \arccos(J_z))^2(1 - J_z^2)]$ [433]. Therefore, the fidelity susceptibility is able to detect the BKT transition at $J_z = 1$.

-
- [1] M. Greiner, O. Mandel, T. Esslinger, T. W. Hansch, and I. Bloch, *Nature (London)* **415**, 39 (2002).
 - [2] H. E. Stanley, *Introduction to Phase Transitions and Critical Phenomena* (Oxford University Press, Oxford, 1987).
 - [3] P. Chaikin and T. Lubensky, *Principles of Condensed Matter Physics* (Cambridge University Press, Cambridge, 1995).
 - [4] N. Goldenfeld, *Lectures on Phase transitions and renormalization group* (Addison-Wesley, Reading, Massachusetts, 1992).
 - [5] J. Cardy, *Scaling and Renormalization in Statistical Physics* (Cambridge University Press, Cambridge, 1996).
 - [6] S. K. Ma, *Modern theory of critical phenomena* (Benjamin, Reading, Massachusetts, 1976).
 - [7] G. Mussardo, *Statistical Field Theory* (Oxford University Press, Oxford, 2010).
 - [8] H. Nishimori and G. Ortiz, *Elements of Phase Transitions and Critical Phenomena* (Oxford University Press, Oxford, 2010).
 - [9] D. J. Amit, *Field theory, renormalization group and critical phenomena* (World Scientific, Singapore, 1984).
 - [10] J. Jinn-Zustin, *Quantum field theory and critical phenomena* (Clarendon Press, Oxford, 1989).
 - [11] K. G. Wilson and J. B. Kogut, *Physics Reports* **12C**, 75 (1974).
 - [12] G. Parisi, *Statistical Field theory* (Addison-Wesley, Reading, Massachusetts, 1988).
 - [13] B. K. Chakrabarti, A. Dutta, and P. Sen, *Quantum Ising Phases and Transitions in Transverse Ising models* (Springer-Verlag, Berlin, 1996).
 - [14] S. Sachdev, *Quantum Phase Transitions* (Cambridge University Press, Cambridge, 1999).
 - [15] S. L. Sondhi, S. M. Girvin, J. P. Carini, and D. Shahar, *Rev. Mod. Phys.* **69**, 315 (1997).
 - [16] M. Vojta, *Rep. Prog. Phys.* **66**, 2069 (2003).
 - [17] M. Continentino, *Quantum Scaling in many body systems* (World Scientific, Singapore, 2001).
 - [18] D. Belitz and T. Kirkpatrick, *J. Low Temp. Phys.* **126**, 1107 (2002).
 - [19] D. Belitz and T. R. Kirkpatrick, in *Dynamics: Models and Kinetic Methods for Non-Equilibrium Many Body Systems* (Kluwer, Dordrecht, 2000, p. 399).
 - [20] D. Belitz, T. R. Kirkpatrick, and T. Vojta, *Rev. Mod. Phys.* **77**, 579 (2005).
 - [21] L. D. Carr, ed., *Understanding Quantum Phase Transitions* (Taylor and Francis, Boca Raton, Florida, 2010).
 - [22] E. Lieb, T. Schultz, and D. Mattis, *Ann. Phys. (NY)* **16**, 407 (1961).
 - [23] S. Katsura, *Phys. Rev* **127**, 132 (1962).
 - [24] P. G. de Gennes, *Solid State Comm.* **1**, 132 (1963).
 - [25] R. Coldea, D. A. Tennant, E. M. Wheeler, E. Wawrzynska, D. Prabhakaran, M. Telling, K. Habicht, P. Smeibidl, and K. Kiefer, *Science* **327**, 177 (2010).
 - [26] M. M. Wolf, G. Ortiz, F. Verstraete, and J. I. Cirac, *Phys. Rev. Lett.* **97**, 110403 (2006).

- [27] I. Affleck, T. Kennedy, E. H. Lieb, and H. Tasaki, *Comm. Math. Phys.* **115**, 477 (1988).
- [28] M. Cozzini, R. Ionicioiu, and P. Zanardi, *Phys. Rev. B* **76**, 104420 (2007).
- [29] A. Y. Kitaev, *Ann. Phys. (NY)* **303**, 2 (2003).
- [30] C. Castelnovo, S. Trebst, and M. Troyer, in *Understanding Quantum Phase Transitions* (Taylor and Francis, Boca Raton, Florida, 2010).
- [31] P. Pfeuty, *Ann. Phys. (N.Y.)* **57**, 79 (1970).
- [32] R. Blinc, *J. Phys. Chem. Solids* **13**, 204 (1962).
- [33] R. Brout, K. A. Muller, and H. Thomas, *Solid State Comm.* **4**, 507 (1966).
- [34] R. B. Stinchcombe, *J. Phys. C* **4**, 124 (1963).
- [35] R. J. Elliott, *Phys. Rev.* **124**, 346 (1961).
- [36] M. E. Fisher, *J. Phys. Math.* **4**, 124 (1963).
- [37] K. Kim, M.-S. Chang, S. Korenblit, R. Islam, E. E. Edwards, J. K. Freericks, G.-D. Lin, L.-M. Duan, and C. Monroe, *Nature* **465**, 590 (2010).
- [38] E. J. S. Lage and R. B. Stinchcombe, *J. Phys. C* **9**, 3295 (1976).
- [39] B. K. Chakrabarti and A. Das, in *Quantum Annealing and Related Optimization Methods: Lecture Notes in Physics Vol. 679* (Springer, Heidelberg, 2005).
- [40] T. Holstein and H. Primakoff, *Phys. Rev.* **58**, 1098 (1940).
- [41] P. W. Anderson, *Phys. Rev.* **86**, 694 (1952).
- [42] R. Kubo, *Phys. Rev.* **87**, 568 (1952).
- [43] H. A. Kramers and G. H. Wannier, *Phys. Rev.* **60**, 252 (1941).
- [44] E. Fradkin and L. Susskind, *Phys. Rev. D* **17**, 2637 (1978).
- [45] J. B. Kogut, *Rev. Mod. Phys.* **51**, 659 (1979).
- [46] K. K. Kobayashi, *J. Phys. Soc. Japan* **24**, 497 (1968).
- [47] I. P. Kaminow and T. C. Damen, *Phys. Rev. Lett.* **20**, 1105 (1968).
- [48] W. Cochran, *Adv. Phys.* **18**, 157 (1969).
- [49] G. A. Samara, *Phys. Rev. Lett* **27**, 103 (1971).
- [50] K. A. Gehring, A. P. Malozemoff, W. Staude, and R. N. Tyte, *Sol. State. Comm.* **9**, 511 (1971).
- [51] R. J. Elliott, G. A. Gehring, A. P. Malozemoff, S. R. P. Smith, W. Staude, and R. N. Tyte, *J. Phys. C* **4**, L179 (1971).
- [52] R. Pirc, B. Tadic, and R. Blinc, *Z. Phys. B* **65**, 69 (1985).
- [53] W. Wu, B. Ellman, T. F. Rosenbaum, G. Aeppli, and D. H. Reich, *Phys. Rev. Lett* **67**, 2076 (1991).
- [54] W. Wu, D. Bitko, T. F. Rosenbaum, and G. Aeppli, *Phys. Rev. Lett.* **74**, 3045 (1993).
- [55] E. Barouch, B. M. McCoy, and M. Dresden, *Phys. Rev. A* **2**, 1075 (1970).
- [56] E. Barouch and B. M. McCoy, *Phys. Rev. A* **3**, 786 (1971).
- [57] E. Barouch and B. M. McCoy, *Phys. Rev. A* **3**, 2137 (1971).
- [58] M. Suzuki, *Prog. Theor. Phys.* **46**, 1337 (1971).
- [59] P. W. Anderson, *Phys. Rev* **112**, 1900 (1958).
- [60] K. Damle and S. Sachdev, *Phys. Rev. Lett.* **76**, 4412 (1996).
- [61] D. M. Greenberger, M. A. Horne, and A. Zeilinger, in *Bell's Theorem, Quantum Theory and Conceptions of the Universe* (Kluwer Academics, Dordrecht, The Netherlands, 1989).
- [62] L. Tagliacozzo, T. R. de Oliveira, S. Iblisdir, and J. I. Latorre, *Phys. Rev. B* **78**, 024410 (2008).
- [63] F. Pollmann, S. Mukerjee, A. M. Turner, and J. E. Moore, *Phys. Rev. Lett.* **102**, 255701 (2009).
- [64] H.-Q. Zhou and J. P. Barjaktarevic, *J. Phys. A: Math. Theor.* **41**, 412001 (2008).
- [65] A. Kopp and S. Chakravarty, *Nat. Phys.* **1**, 53 (2005).
- [66] J. E. Hirsch and G. F. Mazenko, *Phys. Rev. B* **19**, 2656 (1979).
- [67] U. Divakaran and A. Dutta, *J. Stat. Mech.* P11001 (2007).
- [68] J. H. H. Perk, H. W. Capel, and M. J. Zuilhof, *Physica A* **81**, 319 (1975).
- [69] K. Okamoto and K. Yasumura, *Physica A* **59**, 993 (1990).
- [70] S. Deng, G. Ortiz, and L. Viola, *Eurphys. Lett.* **84**, 67008 (2008).
- [71] U. Divakaran, A. Dutta, and D. Sen, *Phys. Rev. B* **78**, 144301 (2008).
- [72] H. J. Lipkin, N. Meshkov, and A. J. Glick, *Nucl. Phys.* **62**, 188 (1965).
- [73] R. Botet, R. Jullien, and P. Pfeuty, *Phys. Rev. Lett.* **49**, 478 (1982).
- [74] P. Ribeiro, J. Vidal, and R. Mosseri, *Phys. Rev. Lett.* **99**, 050402 (2007).
- [75] S. Dusuel and J. Vidal, *Phys. Rev. Lett.* **93**, 237204 (2004).
- [76] S. Dusuel and J. Vidal, *Phys. Rev. B* **71**, 224420 (2005).
- [77] J. Vidal, R. Mosseri, and J. Dukelsky, *Phys. Rev. A* **69**, 054101 (2004).
- [78] J. Vidal, G. Palacios, and J. Aslangul, *Phys. Rev. A* **70**, 062304 (2004).
- [79] T. Barthel, S. Dusuel, and J. Vidal, *Phys. Rev. Lett.* **97**, 220402 (2006).
- [80] H. Wichterich, J. Vidal, and S. Bose, *Phys. Rev. A* **81**, 032311 (2010).
- [81] H.-M. Kwok, W.-Q. Ning, S.-J. Gu, and H.-Q. Lin, *Phys. Rev. E* **78**, 032103 (2008).
- [82] T. Caneva, R. Fazio, and G. E. Santoro, *Phys. Rev. B* **78**, 104426 (2008).
- [83] R. Botet and R. Jullien, *Phys. Rev. B* **28**, 3955 (1983).
- [84] A. Das, K. Sengupta, D. Sen, and B. K. Chakrabarti, *Phys. Rev. B* **74**, 144423 (2006).
- [85] R. P. Feynmann, *Statistical Mechanics* (Addison-Wesley, Reading, Massachusetts, 1972).
- [86] A. P. Young, *J. Phys. C* **8**, L309 (1975).

- [87] J. A. Hertz, Phys. Rev. B **14**, 1163 (1975).
- [88] G. D. Mahan, *Many-Particle Physics* (Kluwer Academic/Plenum Publishers, New York, 2000).
- [89] M. Suzuki, Prog. Theor. Phys. **56**, 1454 (1976).
- [90] M. Suzuki, in *Quantum Monte Carlo Methods*, edited by M. Suzuki (Springer, Heidelberg, 1986).
- [91] R. J. Elliott, P. Pfeuty, and C. Wood, Phys. Rev. Lett. **36**, 856 (1970).
- [92] A. Dutta, B. K. Chakrabarti, and R. B. Stinchcombe, J. Phys. A **29**, 5285 (1996).
- [93] H. Rieger and N. Kawashima, Eur. Phys. J. B **9**, 233 (1999).
- [94] B. M. McCoy and T. T. Wu, Phys. Rev. **176**, 631 (1968).
- [95] T. D. Schultz, D. C. Mattis, and E. Lieb, Rev. Mod. Phys. **36**, 856 (1964).
- [96] M. Barber, Phase Transitions and Critical Phenomena **8**, 209 (1983), edited by C. Domb and J. L. Lebowitch.
- [97] A. J. Leggett and S. Chakravarti, Rev. Mod. Phys. **59**, 1 (1987).
- [98] U. Weiss, *Quantum Dissipative Systems* (World Scientific, Singapore, 1999).
- [99] N. V. Prokof'ev and P. C. E. Stamp, Rep. Prog. Phys. **63**, 669 (2000).
- [100] M. E. Fisher, S. K. Ma, and B. G. Nickel, Phys. Rev. Lett. **29**, 917 (1972).
- [101] A. Dutta and J. K. Bhattacharjee, Phys. Rev. B **64**, 184106 (2001).
- [102] J. M. Kosterlitz, Phys. Rev. Lett. **37**, 1577 (1976).
- [103] J. Bhattacharjee, S. Chakravarty, J. L. Richardson, and D. J. Scalapino, Phys. Rev. B **24**, 3862 (1981).
- [104] J. M. Kosterlitz and D. J. Thouless, J. Phys. C **6**, 1181 (1973).
- [105] R. Bulla, N. H. Tong, and M. Vojta, Phys. Rev. Lett. **91**, 170601 (2003).
- [106] M. Vojta, R. Bulla, and N. H. Tong, Phys. Rev. Lett. **94**, 070604 (2005).
- [107] A. Winter, H. Rieger, M. Vojta, and R. Bulla, Phys. Rev. Lett. **102**, 030601 (2009).
- [108] A. Alvermann and H. Fehske, Phys. Rev. Lett. **102**, 150601 (2009).
- [109] S. Kirchner, K. Ingersent, and Q. Si, Phys. Rev. B **85**, 051113 (2012).
- [110] S. Florens, D. Venturelli, and R. Narayanan, in *Quantum Quenching, Annealing and Computation: Lecture Notes in Physics, Vol. 802*, edited by A. Das, A. K. Chandra, and B. K. Chakrabarti (Springer, Heidelberg, 2010).
- [111] S. Florens, A. Freyn, D. Venturelli, and R. Narayanan, Phys. Rev. B **84**, 155110 (2011).
- [112] P. Werner, K. Volker, M. Troyer, and S. Chakravarty, Phys. Rev. Lett. **94**, 047201 (2005).
- [113] H. M. Ronnow, R. Parthasarathy, J. Jensen, G. Aeppli, T. F. Rosenbaum, and D. F. McMorrow, Science **308**, 389 (2005).
- [114] S. Chakravarty, B. I. Halperin, and D. R. Nelson, Phys. Rev. B **39**, 2344 (1989).
- [115] N. Nagaosa, *Quantum field theory in condensed matter physics* (Springer, Heidelberg, 1999).
- [116] M. Wallin, E. Sorensen, S. M. Girvin, and A. P. Young, Phys. Rev. B **49**, 12115 (1994).
- [117] T. Vojta, Phys. Rev. B **53**, 710 (1996).
- [118] T. H. Berlin and M. Kac, Phys. Rev. **86**, 821 (1952).
- [119] J. Ye, S. Sachdev, and N. Read, Phys. Rev. Lett. **70**, 4011 (1993).
- [120] N. Read, S. Sachdev, and J. Ye, Phys. Rev. B **52**, 384 (1995).
- [121] S. Sachdev, N. Read, and R. Oppermann, Phys. Rev. B **52**, 10286 (1995).
- [122] T. Vojta and M. Schreiber, Phys. Rev. B **53**, 8211 (1996).
- [123] A. Dutta and J. K. Bhattacharjee, Phys. Rev. B **58**, 6378 (1998).
- [124] J. E. Bunder and R. H. McKenzie, Phys. Rev. B **60**, 344 (1999).
- [125] C. Itzykson, H. Saleur, and J.-B. Zuber, *Conformal invariance and applications to statistical mechanics* (World Scientific, Singapore, 1988).
- [126] H. W. J. Blöte, J. L. Cardy, and M. P. Nightingale, Phys. Rev. Lett. **56**, 742 (1986).
- [127] I. Affleck, Phys. Rev. Lett. **56**, 746 (1986).
- [128] C. Holzhey, F. Larsen, and F. Wilczek, Nucl. Phys. B **424**, 443 (1994).
- [129] G. Vidal, J. I. Latorre, E. Rico, and A. Kitaev, Phys. Rev. Lett. **90**, 227902 (2003).
- [130] A. B. Zamolodchikov, Int. J. Mod. Phys. A **4**, 4235 (1989).
- [131] G. Delfino and G. Mussardo, Nucl. Phys. B **455**, 724 (1995).
- [132] G. Delfino, G. Mussardo, and P. Simonetti, Nucl. Phys. B **473**, 469 (1996).
- [133] P. Fonseca and A. Zamolodchikov, arXiv:hep-th/0612304 (2006).
- [134] I. Affleck, Nature **464**, 362 (2010).
- [135] J. A. Kjäll, F. Pollmann, and J. E. Moore, Phys. Rev. B **83**, 020407 (2011).
- [136] B. M. McCoy, E. Barouch, and D. B. Abraham, Phys. Rev. A **4**, 2331 (1971).
- [137] T. T. Wu, Phys. Rev. **149**, 380 (1966).
- [138] B. M. McCoy and T. T. Wu, *Two Dimensional Ising Models* (Harvard University Press, Cambridge, Massachusetts, 1973).
- [139] J. J. H. Perk and H. Au-Yang, J. Stat. Phys. **135**, 599 (2009).
- [140] A. Kitaev, Ann. Phys. **321**, 2 (2006).
- [141] X. Y. Feng, G. M. Zhang, and T. Xiang, Phys. Rev. Lett. **98**, 087204 (2007).
- [142] Z. Nussinov and G. Ortiz, arXiv:0812.4309 (2008) (unpublished).
- [143] H. D. Chen and Z. Nussinov, J. Phys. A **41**, 075001 (2008).
- [144] D. H. Lee, G.-M. Zhang, and T. Xiang, Phys. Rev. Lett. **99**, 196805 (2007).
- [145] S. Mondal, D. Sen, and K. Sengupta, Phys. Rev. B **78**, 045101 (2008).
- [146] U. Divakaran and A. Dutta, Phys. Rev. B **79**, 224408 (2009).
- [147] T. Hikichi, S. Suzuki, and K. Sengupta, Phys. Rev. B **82**, 174305 (2010).

- [148] H. W. Capel and J. H. H. Perk, *Physica A* **87**, 211 (1977).
- [149] J. H. H. Perk, H. W. Capel, and T. J. Siskens, *Physica A* **89**, 304 (1977).
- [150] V. Mukherjee, A. Dutta, and D. Sen, *Phys. Rev. B* **85**, 024301 (2012).
- [151] F. Igloi and C. Monthus, *Phys. Reports* **412**, 277 (2005).
- [152] T. Vojta, *J. Phys. A* **39**, R143 (2006).
- [153] R. N. Bhatt, in *Spin Glasses and Random Fields* (World Scientific, Singapore, 1998).
- [154] H. Rieger and A. P. Young, in *Complex Behavior of Glassy Systems: Lecture Notes in Physics Vol. 492* (Springer-Verlag, Heidelberg, 1997).
- [155] G. Refael and J. E. Moore, *J. Phys. A: Math. Theor.* **42**, 504010 (2009), special Issue “Entanglement Entropy in Extended Quantum Systems” edited by P. Calabrese, J. Cardy and B. Doyon.
- [156] A. B. Harris, *J. Phys. C* **7**, 1671 (1974).
- [157] G. Grinstein and A. Luther, *Phys. Rev. B* **13**, 1329 (1976).
- [158] J. T. Chayes, L. Chayes, D. S. Fisher, and T. Spencer, *Phys. Rev. Lett.* **57**, 2999 (1986).
- [159] F. Pazmandi, R. T. Scalettar, and G. T. Zimanyi, *Phys. Rev. Lett.* **79**, 5130 (1997).
- [160] A. B. Harris, *J. Phys. C* **7**, 3082 (1974).
- [161] D. Boyanovski and J. Cardy, *Phys. Rev. B* **27**, 5557 (1983).
- [162] S. F. Edwards and P. W. Anderson, *J. Phys. F* **5**, 965 (1975).
- [163] K. Binder and A. P. Young, *Rev. Mod. Physics* **58**, 801 (1986).
- [164] D. Chowdhury, *Spin Glass and other frustrated systems* (World Scientific, Singapore, 1986).
- [165] K. Fischer and J. Hertz, *Spin Glasses* (Cambridge University Press, Cambridge, 1991).
- [166] T. Castelloni and A. Cavagna, *J. Stat. Mech.* **81**, P05012 (2005).
- [167] C. D. Dominicis and I. Giardinà, *Random Fields and Spin Glasses* (Cambridge University Press, Cambridge, 2006).
- [168] D. Sherrington and S. Kirkpatrick, *Phys. Rev. Lett.* **35**, 1792 (1975).
- [169] J. R. L. de Almeida and D. J. Thouless, *J. Phys. A* **11**, 983 (1978).
- [170] G. Parisi, *Phys. Lett. A* **73**, 203 (1979).
- [171] G. Parisi, *Phys. Rev. Lett.* **43**, 1754 (1978).
- [172] G. Parisi, *J. Phys. A* **13**, 1101 (1980).
- [173] G. Parisi, *Phys. Rev. Lett.* **50**, 1946 (1983).
- [174] C. D. Dominicis and I. Kondor, *Phys. Rev. B* **27**, 606 (1983).
- [175] M. Talagrand, *J. Phys. A: Math. Gen.* **13**, 1101 (1980).
- [176] A. J. Bray and M. A. Moore, *J. Phys. C* **17**, L463 (1984).
- [177] D. S. Fisher and D. A. Huse, *Phys. Rev. B* **38**, 386 (1988).
- [178] A. P. Young and H. J. Katzgraber, *Phys. Rev. Lett.* **93**, 207203 (2004).
- [179] H. J. Katzgraber, D. Larson, and A. P. Young, *Phys. Rev. Lett.* **102**, 177205 (2009).
- [180] B. K. Chakrabarti, *Phys. Rev. B* **24**, 4062 (1981).
- [181] H. Ishii and T. Yamamoto, *J. Phys. C* **18**, 6225 (1985).
- [182] P. Ray, B. K. Chakrabarti, and A. Chakrabarti, *Phys. Rev. B* **39**, 11828 (1989).
- [183] D. Thirumalai, Q. Li, and T. R. Kirkpatrick, *J. Phys. A* **22**, 3339 (1989).
- [184] Y. Y. Goldschmidt and P. Y. Lai, *Phys. Rev. Lett.* **64**, 2497 (1990).
- [185] G. Buttner and K. D. Usadel, *Phys. Rev. B* **41**, 428 (1990).
- [186] T. K. Kopec, *J. Phys. A* **21**, 297 (1988).
- [187] T. K. Kopec, *J. Phys. A* **21**, 6053 (1988).
- [188] A. J. Bray and M. Moore, *J. Phys. C* **13**, L655 (1980).
- [189] K. D. Usadel and B. Schmitz, *Solid State Commun.* **64**, 975 (1987).
- [190] J. Miller and D. Huse, *Phys. Rev. Lett.* **70**, 3147 (1993).
- [191] G. Aeppli and T. F. Rosenbaum, in *Quantum Annealing and Related Optimization Methods: Lecture Notes in Physics Vol. 679* (Springer, Heidelberg, 2005).
- [192] H. Rieger and A. P. Young, *Phys. Rev. Lett.* **72**, 4141 (1994).
- [193] M. Guo, R. N. Bhatt, and D. A. Huse, *Phys. Rev. Lett.* **72**, 4137 (1994).
- [194] A. Dutta, *Phys. Rev. B* **65**, 224427 (2002).
- [195] G. Kotliar, P. W. Anderson, and D. L. Stein, *Phys. Rev. B* **27**, 602 (1983).
- [196] A. J. Bray, M. A. Moore, and A. P. Young, *Phys. Rev. Lett.* **56**, 2641 (1986).
- [197] M. J. Thill and D. Huse, *Physica A* **214**, 321 (1995).
- [198] R. B. Griffiths, *Phys. Rev. Lett.* **23**, 17 (1969).
- [199] A. J. Bray and M. A. Moore, *J. Phys. C* **15**, L765 (1982).
- [200] B. M. McCoy, *Phys. Rev. Lett.* **23**, 383 (1969).
- [201] B. M. McCoy, *Phys. Rev.* **188**, 1014 (1969).
- [202] R. Shankar and G. Murthy, *Phys. Rev. B* **35**, 3671 (1987).
- [203] R. Shankar and G. Murthy, *Phys. Rev. B* **36**, 536 (1987).
- [204] M. Randeria, J. P. Sethna, and R. G. Palmer, *Phys. Rev. Lett.* **54**, 1321 (1985).
- [205] A. J. Bray, *Phys. Rev. Lett.* **59**, 586 (1987).
- [206] D. Dhar, M. Randeria, and J. P. Sethna, *Phys. Rev. Lett.* **5**, 485 (1988).
- [207] D. S. Fisher, *Phys. Rev. Lett.* **69**, 534 (1992).
- [208] D. S. Fisher, *Phys. Rev. B* **50**, 3799 (1994).

- [209] D. S. Fisher, Phys. Rev. B **51**, 6411 (1995).
- [210] D. S. Fisher, Physica A **263**, 222 (1999).
- [211] D. S. Fisher and A. P. Young, Phys. Rev. B **58**, 9131 (1998).
- [212] C. Dasgupta and S. K. Ma, Phys. Rev. B **22**, 1305 (1980).
- [213] O. Motrunich, S.-C. Mau, D. A. Huse, and D. S. Fisher, Phys. Rev. B **61**, 1160 (2000).
- [214] Y. C. Lin, N. Kawashima, F. Igloi, and H. Rieger, Prog. Theor. Phys. Supp. **138**, 479 (2000).
- [215] A. P. Young and H. Rieger, Phys. Rev. B **53**, 8486 (1996).
- [216] J. Kisker and A. P. Young, Phys. Rev. B **58**, 14397 (1998).
- [217] A. P. Young, Phys. Rev. B **56**, 11691 (1997).
- [218] A. Weinrib and B. I. Halperin, Phys. Rev. B **27**, 413 (1983).
- [219] H. Rieger and F. Igloi, Phys. Rev. Lett. **83**, 3741 (1999).
- [220] F. Igloi and H. Rieger, Phys. Rev. Lett. **78**, 2473 (1997).
- [221] H. Rieger and F. Igloi, Phys. Rev. B **57**, 11404 (1998).
- [222] H. Rieger and A. P. Young, Phys. Rev. B **54**, 3328 (1996).
- [223] M. Guo, R. N. Bhatt, and D. A. Huse, Phys. Rev. B **54**, 3336 (1996).
- [224] C. Pich, A. P. Young, H. Rieger, and N. Kawashima, Phys. Rev. Lett. **81**, 5196 (1998).
- [225] K. Damle and D. A. Huse, Phys. Rev. Lett. **99**, 205303 (2002).
- [226] P. Mohan, R. Narayanan, and T. Vojta, Phys. Rev. B **81**, 144407 (2010).
- [227] R. Santacharia, J. Stat. Mech. **L06002** (2006).
- [228] F. Y. Wu, Rev. Mod. Phys. **54**, 235 (1982).
- [229] J. Jose, L. P. Kadanoff, S. Kirkpatrick, and D. R. Nelson, Phys. Rev. B **16**, 1217 (1977).
- [230] T. Senthil and S. N. Majumdar, Phys. Rev. Lett. **76**, 3001 (1996).
- [231] E. Carlon, P. Lajk, and F. Igloi, Phys. Rev. Lett. **88**, 277201 (2001).
- [232] F. C. Alcaraz, J. Phys. A: Math. Gen. **20**, L623 (2009).
- [233] A. V. Fateev and A. B. Zamolodchikov, Sov. Phys. JETP **62**, 215 (1985).
- [234] D. Stauffer and A. Aharony, *Introduction to Percolation Theory* (Taylor and Francis, New York, 1992).
- [235] A. Aharony, in *Directions in Condensed Matter Physics*, edited by G. Grinstein and G. Mazenko (World Scientific, Singapore, 1986).
- [236] P. W. Kasteleyn and G. M. Fortuin, J. Phys. Soc. Japn. **26**, 11 (1969).
- [237] R. B. Stinchcombe, J. Phys. C **14**, 2193 (1981).
- [238] R. B. Stinchcombe, in *Phase Transitions and Critical Phenomena, Vol. 7*, edited by C. Domb and J. L. Lebowitz (Academic, New York, 1983).
- [239] A. P. Young and R. B. Stinchcombe, J. Phys. C **9**, 4419 (1976).
- [240] T. Senthil and S. Sachdev, Phys. Rev. Lett. **77**, 5292 (1996).
- [241] T. Ikegami, S. Miyashita, and H. Rieger, J. Phys. Soc. Jap. **67**, 2671 (1998).
- [242] A. Dutta and R. Loganayagam, Phys. Rev. B **75**, 052405 (2007).
- [243] L. S. Schulman, J. Phys. A **16**, L639 (1983).
- [244] C. M. Newman and L. S. Schulman, Commun. Math. Phys. **104**, 547 (1986).
- [245] H. Hinrichsen, Adv. Phys. **49**, 815 (2000).
- [246] T. Vojta and M. Y. Lee, Phys. Rev. Lett. **96**, 035701 (2006).
- [247] T. Vojta and J. Schamilián, Phys. Rev. Lett. **95**, 237206 (2005).
- [248] C. Monthus, O. Golinelli, and T. Jolicour, Phys. Rev. Lett. **79**, 3254 (1997).
- [249] A. W. Sandvik, Phys. Rev. Lett. **86**, 3209 (2001).
- [250] R. Sknepnek, T. Vojta, and M. Vojta, Phys. Rev. Lett. **93**, 097201 (2004).
- [251] O. P. Vajk and M. Greven, Phys. Rev. Lett. **89**, 177202 (2002).
- [252] O. P. Vajk, R. K. Mang, M. Greven, P. M. Gehring, and J. W. Lynn, Science **295**, 1691 (2002).
- [253] T. Nattermann, in *Spin Glasses and Random Fields* (World Scientific, Singapore, 1998).
- [254] D. P. Belanger and A. P. Young, J. Magn. Magn. Mater. **100**, 272 (1991).
- [255] H. Rieger, in *Annual Review of Computational Physics II* (World Scientific, Singapore, 1995).
- [256] D. P. Belanger, in *Spin Glasses and Random Fields* (World Scientific, Singapore, 1998).
- [257] Y. Imry and S. K. Ma, Phys. Rev. Lett. **35**, 1399 (1975).
- [258] J. Bricmont and A. Kupiainen, Phys. Rev. Lett. **59**, 1829 (1987).
- [259] G. Greinstein, Phys. Rev. Lett. **37**, 944 (1976).
- [260] A. Aharony, Y. Imry, and S. K. Ma, Phys. Rev. Lett. **37**, 1364 (1976).
- [261] J. L. Cardy, Phys. Rev. B **29**, 505 (1984).
- [262] S. Fishman and A. Aharony, J. Phys. C **12**, L729 (1979).
- [263] A. Aharony, Y. Gefen, and Y. Shapir, J. Phys. C **15**, 673 (1982).
- [264] T. Senthil, Phys. Rev. B **57**, 8375 (1998).
- [265] A. Dutta and R. B. Stinchcombe, Phys. Rev. B **61**, 354 (2000).
- [266] R. L. Greenblatt, M. Aizenmann, and J. L. Lebowitz, Phys. Rev. Lett. **103**, 197201 (2009).
- [267] A. J. Bray and M. Moore, J. Phys. C **18**, L297 (1985).
- [268] R. B. Stinchcombe, E. D. Moore, and S. L. A. de Queiroz, Eur. Phys. Lett. **35**, 295 (1996).
- [269] D. S. Fisher, Phys. Rev. Lett. **56**, 416 (1986).
- [270] P. B. Chakraborty, P. Henelius, H. Kjonsberg, A. W. Sandvik, and S. M. Girvin, Phys. Rev. B **70**, 144411 (2004).

- [271] S. M. A. Tabei, M. J. P. Gingras, Y.-J. Kao, and T. Yavors'kii, Phys. Rev. B **78**, 184408 (2008).
- [272] G. I. Mias and S. M. Girvin, Phys. Rev. B **72**, 064411 (2005).
- [273] S. M. A. Tabei, F. Vernay, and M. J. P. Gingras, Phys. Rev. B **77**, 014432 (2008).
- [274] M. Schechter and P. C. E. Stamp, Phys. Rev. B **78**, 054438 (2008).
- [275] M. Schechter, P. C. E. Stamp, and N. Laflorencie, Phys. Rev. B **78**, 054438 (2008).
- [276] M. Schechter and P. C. E. Stamp, Phys. Rev. Lett. **95**, 267208 (2005).
- [277] S. M. A. Tabei, M. J. P. Gingras, Y.-J. Kao, P. Stasiak, and J.-Y. Fortin, Phys. Rev. Lett. **97**, 237203 (2006).
- [278] T. Vojta, D. Belitz, R. Narayanan, and T. Kirkpatrick, Z. Phys. B **103**, 451 (1997).
- [279] D. Belitz, T. R. Kirkpatrick, R. Narayanan, and T. Vojta, Phys. Rev. Lett. **85**, 4602 (2000).
- [280] R. Narayanan, T. Vojta, D. Belitz, and T. R. Kirkpatrick, Phys. Rev. Lett. **82**, 5132 (1999).
- [281] D. Belitz, T. R. Kirkpatrick, and T. Vojta, Phys. Rev. Lett. **82**, 4707 (1999).
- [282] M. E. Fisher and W. Selke, Phys. Rev. Lett. **44**, 1502 (1980).
- [283] W. Selke, Phys. Rep. **170**, 213 (1988).
- [284] W. Selke, in *Phase Transitions and Critical Phenomena, Vol. 15*, edited by C. Domb and J. L. Lebowitz (Academic, New York, 1992).
- [285] E. Muller-Hartmann and J. Zittartz, Z. Phys. B **27**, 261 (1977).
- [286] J. Villain and P. Bak, J. Physique (Paris) **42**, 657 (1981).
- [287] J. Yeomans, in *Solid State Physics, Vol. 41*, edited by H. Ehrenreich and J. L. Turnbull (Academic, New York, 1987).
- [288] P. Sen and B. K. Chakrabarti, Phys. Rev. B **13559**, 43 (1989).
- [289] G. I. Dzhasharidze and A. A. Nersesyan, JETP Lett. **27**, 334 (1978).
- [290] V. L. Pokrovsky and A. L. Talapov, Phys. Rev. Lett. **42**, 65 (1979).
- [291] M. den Nijs, in *Phase Transitions and Critical Phenomena, Vol. 12*, edited by C. Domb and J. L. Lebowitz (Academic, New York, 1988).
- [292] V. Berezinskii, Zh. Eksp. Teor. Fiz. **59**, 907 (1970).
- [293] D. Allen, P. Azaria, and P. Lecheminant, J. Phys. A **34**, L305 (2001).
- [294] A. Dutta and D. Sen, Phys. Rev. B **67**, 094435 (2003).
- [295] P. Sen and B. K. Chakrabarti, Phys. Rev. B **760**, 40 (1988).
- [296] G. Umin and H. Rieger, Z. Phys. B **101**, 597 (1996).
- [297] M. N. Barber and P. M. Duxbury, J. Phys. A **14**, L251 (1981).
- [298] M. N. Barber and P. M. Duxbury, J. Stat. Phys. **29**, 427 (1982).
- [299] M. N. Barber and P. M. Duxbury, J. Phys. A **15**, 3219 (1982).
- [300] P. Rujan, Phys. Rev. B **24**, 6620 (1981).
- [301] I. Peschel and V. J. Emery, Z. Phys. B **43**, 241 (1981).
- [302] J. Kurmann, H. Thomas, and G. Müller, Physica **112A**, 235 (1982).
- [303] G. Müller and R. E. Shrock, Phys. Rev. B **32**, 5845 (1985).
- [304] A. Sato and F. Matsubara, Phys. Rev. B **60**, 10316 (1999).
- [305] T. Shirahata and T. Nakamura, Phys. Rev. B **65**, 024402 (2001).
- [306] M. Beccaria, M. Campostrini, and A. Feo, Phys. Rev. B **76**, 094410 (2007).
- [307] A. K. Chandra and S. Dasgupta, J. Phys. A **40**, 6251 (2007).
- [308] A. K. Chandra and S. Dasgupta, Phys. Rev. E **75**, 021105 (2007).
- [309] T. Giamarchi and H. J. Schulz, J. Physique (Paris) **49**, 819 (1988).
- [310] A. A. Nersesyan, A. Luther, and F. V. Kusmartsev, Phys. Lett. A **176**, 363 (1993).
- [311] V. M. Yakovenko, JETP Lett. **56**, 510 (1992).
- [312] D. V. Dmitriev, V. Y. Krivnov, A. A. Ovchinnikov, and A. Langari, JETP **95**, 538 (2002).
- [313] D. V. Dmitriev, V. Y. Krivnov, and A. A. Ovchinnikov, Phys. Rev. B **65**, 172409 (2002).
- [314] D. C. Cabra, A. Honecker, and P. Pujol, Phys. Rev. B **58**, 6241 (1998).
- [315] D. Sen and B. K. Chakrabarti, Phys. Rev. B **2713**, 41 (1990).
- [316] D. Sen, Phys. Rev. B **43**, 5939 (1991).
- [317] J. Karadamoglou and N. Papanicolau, Phys. Rev. B **60**, 9477 (1999).
- [318] X. Wang, X. Zotos, J. Karadamoglou, and N. Papanicolau, Phys. Rev. B **61**, 14303 (2000).
- [319] T. Sakai and M. Takahashi, Phys. Rev. B **60**, 7295 (1999).
- [320] S. R. White, Phys. Rev. B **48**, 10345 (1993).
- [321] M. Beccaria, M. Campostrini, and A. Feo, Phys. Rev. B **73**, 052402 (2006).
- [322] A. Nagy, New J. Phys. **13**, 023015 (2011).
- [323] J.-S. Caux, F. H. L. Essler, and U. Löw, Phys. Rev. B **68**, 134431 (2003).
- [324] R. Hagemans, J.-S. Caux, and U. Löw, Phys. Rev. B **71**, 014437 (2005).
- [325] M. Kenzelmann, R. Coldea, D. A. Tennant, D. Visser, M. Hofmann, P. Smeibidl, and Z. Tylczynski, Phys. Rev. B **65**, 144432 (2002).
- [326] A. Dutta, B. K. Chakrabarti, and J. K. Bhattacharjee, Phys. Rev. B **55**, 5619 (1997).
- [327] A. Dutta, J. K. Bhattacharjee, and B. K. Chakrabarti, Eur. Phys. J. B **3**, 97 (1998).
- [328] R. Ramazashvili, Phys. Rev. B **60**, 7314 (1999).
- [329] Y. Nishiyama, Phys. Rev. E **75**, 051116 (2007).
- [330] R. M. Hornreich, M. Luban, and B. Strikman, Phys. Rev. Lett. **35**, 1638 (1975).
- [331] R. M. Hornreich, M. Luban, and B. Strikman, Phys. Lett. A **55**, 269 (1975).

- [332] R. M. Hornreich, M. Luban, and B. Strikman, *Physica A* **86**, 465 (1977).
- [333] A. Schroeder, G. Aeppli, E. Bucher, R. Ramazasvilli, and P. Coleman, *Phys. Rev. Lett.* **80**, 5623 (1998).
- [334] B. K. Chakrabarti and J.-I. Inoue, *Ind. J. Phys.* **80**, 609 (2006).
- [335] B. K. Chakrabarti, A. Das, and J.-I. Inoue, *Euro. Phys. J. B* **51**, 321 (2006).
- [336] A. K. Chandra, J.-I. Inoue, and B. K. Chakrabarti, *J. Phys: Conf. ser.* **143**, 012013 (2009).
- [337] A. Chandra, J. I. Inoue, and B. K. Chakrabarti, *Phys. Rev. E* **81**, 021101 (2010).
- [338] A. Ganguli and S. Dasgupta, *Phys. Rev. E* **80**, 031115 (2009).
- [339] R. F. Werner, *Phys. Rev. A* **40**, 4277 (1989).
- [340] C. H. Bennett, D. P. DiVincenzo, J. A. Smolin, and W. K. Wootters, *Phys. Rev. A* **54**, 3824 (1996).
- [341] M. Horodecki, *Quantum Inf. Comput.* **1**, 3 (2001).
- [342] M. A. Nielsen and I. C. Chuang, *Quantum Computation and Quantum Information* (Cambridge University Press, Cambridge, 2009).
- [343] W. K. Wootters, *Quantum Inf. Comput.* **1**, 27 (2001).
- [344] L. Amico, R. Fazio, A. Osterloh, and V. Vedral, *Rev. Mod. Phys.* **80**, 517 (2008).
- [345] S. Ghosh, T. F. Rosenbaum, G. Aeppli, and S. N. Coopersmith, *Nature* **425**, 48 (2003).
- [346] I. Bose and A. Trivedi, in *Quantum Quenching, Annealing and Computation: Lecture Notes in Physics, Vol. 802*, edited by A. Das, A. K. Chandra, and B. K. Chakrabarti (Springer, Heidelberg, 2010).
- [347] L.-A. Wu, M. S. Sarandy, and D. A. Lidar, *Phys. Rev. Lett.* **93**, 250404 (2004).
- [348] S. Hill and W. K. Wootters, *Phys. Rev. Lett.* **78**, 5022 (1997).
- [349] W. K. Wootters, *Phys. Rev. Lett.* **80**, 2245 (1998).
- [350] O. F. Syljuasen, *Phys. Rev. A* **68**, 060301(R) (2003).
- [351] J. Osborne and M. A. Nielsen, *Phys. Rev. A* **66**, 032110 (2002).
- [352] A. Osterloh, L. Amico, G. Falci, and R. Fazio, *Nature* **416**, 608 (2002).
- [353] O. Osenda, Z. Huang, and S. Kais, *Phys. Rev. A* **67**, 062321 (2003).
- [354] Z. Huang, O. Osenda, and S. Kais, *Phys. Lett. A* **322**, 137 (2004).
- [355] F. Verstraete, M. Popp, and J. I. Cirac, *Phys. Rev. Lett.* **92**, 027901 (2004).
- [356] V. Subrahmanyam, *Quant. Inf. Comput.* **11**, 1 (2011).
- [357] L. Amico, A. Osterloh, F. Plastina, G. Palma, and R. Fazio, *Phys. Rev. A* **69**, 022304 (2004).
- [358] V. Subrahmanyam, *Phys. Rev. A* **69**, 034304 (2004).
- [359] A. S. De, U. Sen, and M. Lewenstein, *Phys. Rev. A* **72**, 052319 (2005).
- [360] J. Vidal, R. Mosseri, and J. Dukelsky, *Phys. Rev. A* **69**, 69 (2004).
- [361] I. Bose and E. Chattopadhyay, *Phys. Rev. A* **66**, 062320 (2002).
- [362] F. Alcaraz, A. Saguia, and M. Sarandy, *Phys. Rev. A* **70**, 032333 (2004).
- [363] X. X. Yi, H. Wang, and W. Wang, *Eur. Phys. J. D* **45**(2), 355 (2007).
- [364] A. Peres, *Phys. Rev. Lett.* **77**, 1413 (1996).
- [365] G. Vidal and R. F. Werner, *Phys. Rev. A* **65**, 032314 (2002).
- [366] T. M. Fiola, J. Preskill, A. Strominger, and S. P. Trivedi, *Phys. Rev. D* **50**, 3897 (1994).
- [367] K. Audenaert, K. J. Eisert, M. B. Plenio, and R. F. Werner, *Phys. Rev. A* **66**, 042327 (2002).
- [368] J. I. Latorre and A. Riera, *J. Phys. A* **42**, 504002 (2009), special Issue “Entanglement Entropy in Extended Quantum Systems” edited by P. Calabrese, J. Cardy and B. Doyon.
- [369] M. Srednicki, *Phys. Rev. Lett.* **71**, 666 (1993).
- [370] P. Calabrese and J. Cardy, *J. Phys. A: Math. Theor.* **42**, 504005 (2009), special Issue “Entanglement Entropy in Extended Quantum Systems” edited by P. Calabrese, J. Cardy and B. Doyon.
- [371] P. Calabrese and J. Cardy, *J. Stat. Mech.* P06002 (2004).
- [372] V. E. Korepin, *Phys. Rev. Lett.* **92**, 096402 (2004).
- [373] V. Alba, L. Tagliacozzo, and P. Calabrese, *Phys. Rev. B* **81**, 060411 (2010).
- [374] M. Fagotti and P. Calabrese, *J. Stat. Mech.* P04016 (2010).
- [375] J. I. Latorre, E. Rico, and G. Vidal, *Quant. Inf. Comput.* **4**, 48 (2004).
- [376] B. Jin and V. E. Korepin, *J. Stat. Phys.* **116**, 79 (2004).
- [377] A. R. Its, B. Q. Jin, and V. E. Korepin, *J. Phys. A* **38**, 2975 (2005).
- [378] F. Franchini, A. R. Its, B. Q. Jin, and V. E. Korepin, *arXiv:quant-ph/0606240* (2006) (unpublished).
- [379] P. Calabrese, M. Campostrini, F. Essler, and B. Nienhuis, *Phys. Rev. Lett.* **104**, 095701 (2010).
- [380] P. Calabrese and A. Lefevre, *Phys. Rev. A* **78**, 032329 (2008).
- [381] E. Fradkin, *J. Phys. A: Math. Theor.* **42**, 504011 (2009), special Issue “Entanglement Entropy in Extended Quantum Systems” edited by P. Calabrese, J. Cardy and B. Doyon.
- [382] A. B. Zamolodchikov, *JETP Lett.* **43**, 730 (1986).
- [383] G. Refael and J. E. Moore, *Phys. Rev. Lett.* **93**, 260602 (2004).
- [384] N. Laflorencie, *Phys. Rev. B* **72**, 140408 (2005).
- [385] C. D. Chiara, S. Montangero, P. Calabrese, and R. Fazio, *J. Stat. Mech.* P03001 (2006).
- [386] Y. C. Lin, F. Igloi, and H. Rieger, *Phys. Rev. Lett.* **99**, 147202 (2007).
- [387] I. A. Kovacs and F. Igloi, *Phys. Rev. B* **83**, 174207 (2011).
- [388] H. Olliver and W. H. Zurek, *Phys. Rev. Lett.* **88**, 017901 (2001).
- [389] W. H. Zurek, *Rev. Mod. Phys.* **75**, 715 (2003).
- [390] L. Henderson and V. Vedral, *J. Phys. A* **34**, 6899 (2001).

- [391] V. Vedral, Phys. Rev. Lett. **90**, 050401 (2003).
- [392] S. Luo, Phys. Rev. A **77**, 042303 (2008).
- [393] R. Dillenschneider, Phys. Rev. B **78**, 224413 (2008).
- [394] M. S. Sarandy, Phys. Rev. A **80**, 022108 (2009).
- [395] A. K. Pal and I. Bose, J. Phys. B: At. Mol. Opt. Phys. **44**, 045101 (2011).
- [396] J. Maziero, L. C. Céleri, R. M. Serra, and M. S. Sarandy, Phys. Lett. A **376**, 1540 (2012).
- [397] Y. C. Li and H. Q. Lin, Phys. Rev. A **83**, 052323 (2011).
- [398] B. Tomasello, D. Rossini, A. Hamma, and L. Amico, EPL **96**, 27002 (2011).
- [399] R. Auccaise, J. Maziero, L. C. Céleri, D. O. Soares-Pinto, E. R. deAzevedo, T. J. Bonagamba, R. S. Sarthour, I. S. Oliveira, and R. M. Serra, Phys. Rev. Lett. **107**, 070501 (2011).
- [400] P. W. Anderson, Phys. Rev. Lett. **18**, 1049 (1967).
- [401] E. Bettelheim, A. G. Abanov, and P. Weigmann, Phys. Rev. Lett. **97**, 246402 (2006).
- [402] S. Sachdev, M. Troyer, and M. Vojta, Phys. Rev. Lett. **86**, 2677 (2001).
- [403] P. Zanardi and N. Paunkovic, Phys. Rev. E **74**, 031123 (2006).
- [404] S. J. Gu, Int. J. Mod. Phys. **24**, 4371 (2010).
- [405] S. Pancharatnam, Proc. Indian Acad. Sci. A **44**, 247 (1956).
- [406] M. Berry, Proc. R. Soc. Lond. A **392**, 45 (1984).
- [407] W. L. You, Y.-W. Li, and S.-J. Gu, Phys. Rev. E **76**, 022101 (2007).
- [408] S.-J. Gu, H.-M. Kwok, W.-Q. Ning, and H.-Q. Lin, Phys. Rev. B **77**, 245109 (2008).
- [409] S. J. Gu, Int. J. Mod. Phys. B **24**, 4371 (2010).
- [410] L. C. Venuti and P. Zanardi, Phys. Rev. Lett. **99**, 095701 (2007).
- [411] D. Abasto, A. Hamma, and P. Zanardi, Phys. Rev. A **78**, 010301 (2008).
- [412] L. Venuti, H. Saleur, and P. Zanardi, Phys. Rev. B **79**, 092405 (2009).
- [413] M. Cozzini, P. Giorda, and P. Zanardi, Phys. Rev. B **75**, 014439 (2007).
- [414] P. Zanardi, P. Giorda, and M. Cozzini, Phys. Rev. Lett. **99**, 100603 (2007).
- [415] L. C. Venuti, M. Cozzini, P. Buonsante, F. Massel, N. Bray-Ali, and P. Zanardi, Phys. Rev. B **78**, 115410 (2008).
- [416] S.-J. Gu and H.-Q. Lin, Eur. Phys. Lett. **87**, 10003 (2009).
- [417] B. Li, S.-H. Li, and H.-Q. Zhou, Phys. Rev. E **79**, 060101(R) (2009).
- [418] D. Schwandt, F. Alet, and S. Capponi, Phys. Rev. Lett. **103**, 170501 (2009).
- [419] V. Gritsev and A. Polkovnikov, in *Understanding Quantum Phase Transitions* (Taylor and Francis, Boca Raton, Florida, 2010).
- [420] A. F. Albuquerque, F. Alet, C. Sire, and S. Capponi, Phys. Rev. B **81**, 064418 (2010).
- [421] V. Mukherjee and A. Dutta, Phys. Rev. B **83**, 214302 (2011).
- [422] S. Banerjee, R. R. P. Singh, V. Pardo, and W. E. Pickett, Phys. Rev. Lett. **103**, 016402 (2009).
- [423] P. Bounsante and A. Vezzani, Phys. Rev. Lett. **98**, 101601 (2007).
- [424] V. Mukherjee, A. Polkovnikov, and A. Dutta, Phys. Rev. B **60**, 344 (2011).
- [425] W. K. Wootters, Phys. Rev. D **23**, 357 (2011).
- [426] S. L. Zhu, Phys. Rev. Lett. **96**, 077206 (2006).
- [427] A. C. M. Carollo and J. K. Pachos, Phys. Rev. Lett. **95**, 157203 (2005).
- [428] J. K. Pachos and A. Carollo, Phil. Trans. R. Soc. Lond. A **364**, 3663 (2006).
- [429] S. L. Zhu, Int. J. Mod. Phys. B **22**, 561 (2008).
- [430] A. Hamma, arXiv:quant-ph/0602091 (2006).
- [431] H. T. Cui, K. Li, and X. X. Li, Phys. Lett. A **360**, 243 (2006).
- [432] H. T. Quan, J. Phys. A: Math. Theor **42**, 395002 (2009).
- [433] M. F. Yang, Phys. Rev. B **76**, 180403(R) (2008).
- [434] S. J. Gu, Phys. Rev. E **79**, 061125 (2009).
- [435] J.-H. Zhao and H.-Q. Zhou, Phys. Rev. B **80**, 014403 (2009).
- [436] M. M. Rams and B. Damski, Phys. Rev. A **84**, 032324 (2011).
- [437] S. Garnerone, N. T. Jacobson, S. Haas, and P. Zanardi, Phys. Rev. Lett. **102**, 057205 (2009).
- [438] H.-Q. Zhou, R. Orús, and G. Vidal, Phys. Rev. Lett. **100**, 080601 (2008).
- [439] H. Q. Zhou, J. H. Zhao, and B. Li, J. Phys. A: Math. Theor. **41**, 492002 (2008).
- [440] A. Uhlmann, Rep. Math. Phys. **9**, 273 (1976).
- [441] R. Jozsa, J. Mod. Opt. **41**, 2315 (1994).
- [442] H.-Q. Zhou, arXiv:0704.2945 (2007) (unpublished).
- [443] M. Zindaric and T. Prosen, J. Phys. A: Math. Gen. **36**, 2463 (2003).
- [444] J. Ma, L. Xu, H. N. Xiang, and X. Wang, Phys. Rev. E **78**, 051126 (2008).
- [445] Y. Li, Phys. Lett. A **372**, 6207 (2008).
- [446] J. Ma, L. Xu, and X. Wang, Comm. Theor. Phys. **53**, 175 (2010).
- [447] N. Paunkovic, P. D. Sacramento, P. Nogueira, V. R. Viera, and V. K. Dugaev, Phys. Rev. A **77**, 052302 (2008).
- [448] H. M. Kwok, C. S. Ho, and S. J. Gu, Phys. Rev. A **78**, 062302 (2008).
- [449] E. Eriksson and H. Johannesson, Phys. Rev. A **79**, 060301(R) (2009).
- [450] P. Zanardi, H. T. Quan, X. Wang, and C. P. Sun, Phys. Rev. A **75**, 032109 (2007).
- [451] Y. C. Tzeng, H. H. Hung, Y.-C. Chen, and M.-F. Yang, Phys. Rev. A **77**, 062321 (2008).
- [452] N. Paunkovic and V. R. Viera, Phys. Rev. B **77**, 011129 (2008).

- [453] H. T. Quan and F. M. Cucchiatti, Phys. Rev. E **79**, 031101 (2009).
- [454] P. Zanardi, L. C. Venuti, and P. Giorda, Phys. Rev. A **76**, 062318 (2007).
- [455] W. H. Zurek, Phys. Today **44**, 36 (1991).
- [456] S. Haroche, Phys. Today **51**, 36 (1998).
- [457] E. Joos, H. D. Zeh, C. Keifer, D. Giulini, J. Kupsch, and I.-O. Statatescu, *Decoherence and the Appearance of a Classical World in a Quantum Theory* (Springer Presse, Berlin, 2003).
- [458] A. Peres, *Quantum Theory: Concepts and Methods* (Kluwer Academic Publishers, Dordrecht, 1995).
- [459] Z. P. Karkuszewski, C. Jarzynski, and W. H. Zurek, Phys. Rev. Lett. **89**, 170405 (2002).
- [460] F. M. Cucchiatti, D. A. R. Dalvit, J. P. Paz, and W. H. Zurek, Phys. Rev. Lett. **95**, 105701 (2003).
- [461] R. A. Jalabert and H. M. Pastawski, Phys. Rev. Lett. **86**, 246 (2001).
- [462] W. H. Zurek and J. P. Paz, Phys. Rev. Lett. **72**, 2508 (1994).
- [463] H. T. Quan, Z. Song, X. F. Liu, P. Zanardi, and C. P. Sun, Phys. Rev. Lett. **96**, 140604 (2006).
- [464] Z.-G. Yuan, P. Zhang, and S.-S. Li, Phys. Rev. A **75**, 012102 (2007).
- [465] Y.-C. Ou and H. Fan, J. Phys. A-Math.Gen. **40**, 2455 (2007).
- [466] S. Sharma, V. Mukherjee, and A. Dutta, Eur. Phys. J. B **85**, 143 (2012).
- [467] D. Rossini, T. Calarco, V. Giovannetti, S. Montangero, and R. Fazio, J. Phys. A: Math. Theor. **40**, 8033 (2007).
- [468] J. Zhang, F. M. Cucchiatti, C. M. Chandrashekar, M. Laforest, C. A. Ryan, M. Ditty, A. Hubbard, J. Gamble, and R. Laflamme, Phys. Rev. A **79**, 012305 (2009).
- [469] F. M. Cucchiatti, S. Fernandez-Vidal, and J. P. Paz, Phys. Rev. A **75**, 032337 (2007).
- [470] C. Cormick and J. P. Paz, Phys. Rev. A **77**, 022317 (2008).
- [471] B. Damski, H. T. Quan, and W. H. Zurek, Phys. Rev. A **83**, 062104 (2011).
- [472] P. Mazur, Physica A **43**, 533 (1969).
- [473] L. E. Sadler, J. M. Higbie, S. R. Leslie, M. Vengalattore, and D. M. Stamper-Kurn, Nature **443**, 312 (2006).
- [474] M. Lewenstein, A. Sanpera, V. Ahufinger, B. Damski, A. S. De, and U. Sen, Advances in Physics **56**, 243 (2007).
- [475] I. Bloch, J. Dalibard, and W. Zwerger, Rev. Mod. Phys. **80**, 885 (2008).
- [476] M. Acharyya, B. K. Chakrabarti, and R. B. Stinchcombe, J. Phys. A **27**, 1533 (1994).
- [477] V. Banerjee, S. Dattagupta, and P. Sen, Phys. Rev. E **52**, 1436 (1995).
- [478] A. Das, Phys. Rev. B **82**, 172402 (2010).
- [479] V. Subrahmanyam, Phys. Rev. B **68**, 212407 (2003).
- [480] S. Miyashita, H. D. Raedt, and B. Barbara, Phys. Rev. B **79**, 104422 (2009).
- [481] K. Sengupta, S. Powell, and S. Sachdev, Phys. Rev. A **69**, 053616 (2004).
- [482] E. Fradkin, *Field Theories of Condensed Matter Systems* (Addison-Wesley, Reading, 1991).
- [483] D. Rossini, A. Silva, G. Mussardo, and G. Santoro, Phys. Rev. Lett. **102**, 127204 (2009).
- [484] D. Rossini, S. Suzuki, G. Mussardo, G. E. Santoro, and A. Silva, Phys. Rev. B **82**, 144302 (2010).
- [485] F. Igloi and H. Rieger, Phys. Rev. Lett. **85**, 3233 (2000).
- [486] L. Foini, L. F. Cugiliandolo, and A. Gambassi, Phys. Rev. B **84**, 212404 (2011).
- [487] H. Wichterich and S. Bose, Phys. Rev. A **79**, 060302 (2009).
- [488] L. C. Venuti, S. M. Giampaolo, F. Illuminati, and P. Zanardi, Phys. Rev. A **76**, 052328 (2007).
- [489] D. Gordon and C. M. Savage, Phys. Rev. A **59**, 4623 (1999).
- [490] A. Micheli, D. Jaksch, J. I. Cirac, and P. Zoller, Phys. Rev. A **67**, 013607 (2003).
- [491] A. P. Hines, R. H. McKenzie, and G. J. Milburn, Phys. Rev. A **67**, 013609 (2003).
- [492] A. Simoni, F. Ferlino, G. Roati, G. Modugno, and M. Inguscio, Phys. Rev. Lett. **90**, 163202 (2003).
- [493] J. Cirac, M. Lewenstein, K. Molmer, and P. Zoller, Phys. Rev. A **57**, 1208 (1998).
- [494] G. E. Volovik, *The Universe in a Helium Droplet* (Oxford University Press, Oxford, 2003).
- [495] T. W. B. Kibble, J. Phys. A **9**, 1387 (1976).
- [496] T. W. B. Kibble, Phys. Rep. **67**, 183 (1980).
- [497] W. H. Zurek, Nature **317**, 505 (1985).
- [498] W. H. Zurek, Acta. Physica Polonica. B **24**, 1301 (1993).
- [499] W. H. Zurek, Phys. Rep. **276**, 177 (1996).
- [500] P. Laguna and W. H. Zurek, Phys. Rev. Lett. **78**, 2519 (1997).
- [501] I. L. Chuang, R. Durrer, N. Turok, and B. Yurke, Science **251**, 1336 (1991).
- [502] M. J. Bowick, L. Chandar, E. A. Schiff, and A. M. Srivastava, Science **263**, 943 (1994).
- [503] S. Ducci, P. L. Ramazza, W. González-Vinas, and F. T. Arecchi, Phys. Rev. Lett. **83**, 5210 (1999).
- [504] R. Monaco, M. Aaroe, J. Mygind, R. J. Rivers, and V. P. Koshelets, Phys. Rev. B **74**, 144513 (2006).
- [505] V. M. H. Ruutu, V. B. Eltsov, A. J. Gill, T. W. B. Kibble, M. Krusius, Y. G. Makhlin, B. Placais, G. E. Volovik, and W. Xu, Nature **382**, 334 (1996).
- [506] P. C. Hendry, Nature (London) **368**, 315 (1994).
- [507] M. E. Dodd, Phys. Rev. Lett. **81**, 3703 (1998).
- [508] W. H. Zurek, U. Dorner, and P. Zoller, Phys. Rev. Lett. **95**, 105701 (2005).
- [509] A. Polkovnikov, Phys. Rev. B **72**, R161201 (2005).
- [510] A. Messiah, *Quantum Mechanics* (Dover Publications, Minoela, New York, 1999).
- [511] S. Suzuki and M. Okada, in *Quantum Annealing and Related Optimization Methods*, edited by A. Das and B. K. Chakrabarti (Springer, Heidelberg, 2005).
- [512] B. Damski, Phys. Rev. Lett. **95**, 035701 (2005).

- [513] B. Damski and W. H. Zurek, Phys. Rev. A **73**, 063405 (2006).
- [514] J. Dziarmaga, Phys. Rev. Lett. **95**, 245701 (2005).
- [515] C. D. Grandi, V. Gritsev, and A. Polkovnikov, Phys. Rev. B **81**, 012303 (2010).
- [516] D. Sen, K. Sengupta, and S. Mondal, Phys. Rev. Lett. **101**, 016806 (2008).
- [517] R. Barankov and A. Polkovnikov, Phys. Rev. Lett. **101**, 076801 (2008).
- [518] S. Mondal, K. Sengupta, and D. Sen, Phys. Rev. B **79**, 045128 (2009).
- [519] K. Sengupta, D. Sen, and S. Mondal, Phys. Rev. Lett. **100**, 077204 (2008).
- [520] A. Dutta, R. R. P. Singh, and U. Divakaran, Europhys. Lett. **89**, 67001 (2010).
- [521] A. H. C. Neto, F. Guinea, N. M. R. Peres, K. S. Novoselov, and A. K. Geim, Rev. Mod. Phys. **81**, 109 (2009).
- [522] K. Sun, H. Yao, E. Fradkin, and S. A. Kivelson, Phys. Rev. Lett. **103**, 046811 (2009).
- [523] B. Dora and R. Moessner, Phys. Rev. B **81**, 165431 (2010).
- [524] B. Dora, E. V. Castro, and R. Moessner, Phys. Rev. B **82**, 125441 (2010).
- [525] K. L. Lee, B. Gremaud, R. Han, B.-G. Englert, and C. Miniatura, Phys. Rev. A **80**, 043411 (2009).
- [526] H. Saito, R. G. Hulet, and M. Ueda, Phys. Rev. A **76**, 043613 (2007).
- [527] M. Uhlmann, R. Schützhold, and U. R. Fischer, Phys. Rev. Lett. **99**, 120407 (2007).
- [528] M. Uhlmann, R. Schützhold, and U. R. Fischer, Phys. Rev. D **81**, 025017 (2010).
- [529] M. Uhlmann, R. Schützhold, and U. R. Fischer, New J. Phys. **12**, 094020 (2010).
- [530] A. Bermudez, D. Patane, L. Amico, and M. A. Martin-Delgado, Phys. Rev. Lett. **102**, 135702 (2009).
- [531] A. Bermudez, L. Amico, and M. A. Martin-Delgado, New J. Phys. **12**, 055014 (2010).
- [532] A. Polkovnikov and V. Gritsev, Nature Phys. **4**, 477 (2008).
- [533] A. Fubini, G. Falci, and A. Osterloh, New J. Phys. **9**, 134 (2007).
- [534] L. Mathey and A. Polkovnikov, Phys. Rev. A **81**, 033605 (2010).
- [535] I. Klich, C. Lannert, and G. Refael, Phys. Rev. Lett. **99**, 205303 (2007).
- [536] N. Rosen and C. Zener, Phys. Rev. **40**, 502 (1932).
- [537] J. Dziarmaga, Advances in Physics **59**, 1063 (2010).
- [538] R. Schützhold, J. Low. Temp. Phys. **153**, 228 (2008).
- [539] U. Divakaran, V. Mukherjee, A. Dutta, and D. Sen, in *Quantum Quenching, Annealing and Computation: Lecture Notes in Physics, Vol. 802*, edited by A. Das, A. K. Chandra, and B. K. Chakrabarti (Springer, Heidelberg, 2010).
- [540] C. D. Grandi and A. Polkovnikov, in *Quantum Quenching, Annealing and Computation: Lecture Notes in Physics, Vol. 802*, edited by A. Das, A. K. Chandra, and B. K. Chakrabarti (Springer, Heidelberg, 2010).
- [541] S. Mondal, D. Sen, and K. Sengupta, in *Quantum Quenching, Annealing and Computation: Lecture Notes in Physics, Vol. 802*, edited by A. Das, A. K. Chandra, and B. K. Chakrabarti (Springer, Heidelberg, 2010).
- [542] A. Polkovnikov, K. Sengupta, A. Silva, and M. Vengalattore, Rev. Mod. Phys. **83**, 863 (2011).
- [543] C. D. Grandi, V. Gritsev, and A. Polkovnikov, Phys. Rev. B **81**, 224301 (2010).
- [544] M. Tomka, A. Polkovnikov, and V. Gritsev, Phys. Rev. Lett. **108**, 080404 (2012).
- [545] R. W. Cherng and L. S. Levitov, Phys. Rev. A **73**, 043614 (2006).
- [546] N. V. Vitanov and B. M. Garraway, Phys. Rev. A **53**, 4288 (1996).
- [547] N. V. Vitanov, Phys. Rev. A **59**, 988 (1999).
- [548] S. N. Shevchenko, S. Ashhab, and F. Nori, Phys. Rep. **492**, 1 (2010).
- [549] V. Mukherjee, U. Divakaran, A. Dutta, and D. Sen, Phys. Rev. B **76**, 174303 (2007).
- [550] F. Pollmann, S. Mukerjee, A. M. Turner, and J. E. Moore, Phys. Rev. E **81**, 020101 (2010).
- [551] U. Divakaran, V. Mukherjee, A. Dutta, and D. Sen, J. Stat. Mech. P02007 (2009).
- [552] S. Deng, G. Ortiz, and L. Viola, Phys. Rev. B **80**, 241109(R) (2009).
- [553] V. Mukherjee and A. Dutta, Eur. Phys. Lett. **92**, 37104 (2010).
- [554] S. Deng, G. Ortiz, and L. Viola, Phys. Rev. B **83**, 094304 (2011).
- [555] U. Divakaran, A. Dutta, and D. Sen, Phys. Rev. B **81**, 054306 (2010).
- [556] V. Mukherjee, A. Dutta, and D. Sen, Phys. Rev. B **77**, 214427 (2008).
- [557] Y. Kayanuma, Phys. Rev. B **47**, 9940 (1993).
- [558] Y. Kayanuma, Phys. Rev. A **50**, 843 (1994).
- [559] S. Ashhab, J. R. Johansson, A. M. Zagorin, and F. Nori, Phys. Rev. A **75**, 063414 (2007).
- [560] M. Wubs, K. Saito, S. Kohler, Y. Kayanuma, and P. Hänggi, New J. Phys. **7**, 218 (2005).
- [561] Y. Kayanuma and Y. Mizumoto, Phys. Rev. A **62**, 061401(R) (2000).
- [562] V. Mukherjee and A. Dutta, J. Stat. Mech. P05005 (2009).
- [563] A. Russomanno, A. Silva, and G. E. Santoro, arXiv:1204.5084 (2012) (unpublished).
- [564] F. Pellegrini, S. Montangero, G. E. Santoro, and R. Fazio, Phys. Rev. B **77**, 140404 (2008).
- [565] I. Titvinidze and G. I. Japaridze, Eur. Phys. J. B **383**, 012101 (2003).
- [566] A. A. Zvyagin and G. A. Skorobogat'ko, Phys. Rev. B **73**, 024427 (2006).
- [567] M. Fabrizio, Phys. Rev. B **54**, 10054 (1996).
- [568] R. Arita, K. Kuroki, H. Aoki, and M. Fabrizio, Phys. Rev. B **57**, 10324 (1998).
- [569] D. Chowdhury, U. Divakaran, and A. Dutta, Phys. Rev. E **81**, 012101 (2010).
- [570] J. Dziarmaga, Phys. Rev. B **74**, 064416 (2006).
- [571] T. Caneva, R. Fazio, and G. E. Santoro, Phys. Rev. B **76**, 144427 (2007).
- [572] D. Patane, A. Silva, M. Amico, R. Fazio, and G. E. Santoro, Phys. Rev. Lett. **101**, 175701 (2008).
- [573] D. Patane, L. Amico, A. Silva, R. Fazio, and G. E. Santoro, Phys. Rev. B **80**, 024302 (2009).

- [574] S. Mostame, G. Schaller, and R. Schützhold, Phys. Rev. A **76**, 030304(R) (2007).
- [575] B. Damski and W. H. Zurek, New. J. Physics **11**, 063014 (2009).
- [576] L. Cincio, J. Dziarmaga, J. Meisner, and M. M. Rams, Phys. Rev. B **79**, 094421 (2009).
- [577] K. Sengupta and D. Sen, Phys. Rev. A **80**, 032304 (2009).
- [578] L. Cincio, J. Dziarmaga, M. M. Rams, and W. Zurek, Phys. Rev. A **75**, 052321 (2007).
- [579] A. J. Bray, Advances in Physics **51**, 1460 (2002).
- [580] B. Basu, Phys. Lett. A **374**, 1205 (2010).
- [581] T. Nag, A. Patra, and A. Dutta, J. Stat. Mech: Theor. Expt 08026 (2011).
- [582] S. Deng, G. Ortiz, and L. Viola, arXiv:0802.3941 (2008) (unpublished).
- [583] T. Nag, U. Divakaran, and A. Dutta, Phys. Rev. B **86**, 020401(R) (2012).
- [584] V. Mukherjee, S. Sharma, and A. Dutta, Phys. Rev. B **86**, 020301 (R) (2012).
- [585] P. Calabrese and J. Cardy, J. Stat. Mech. P04010 (2005).
- [586] P. Calabrese and J. Cardy, Phys. Rev. Lett. **96**, 136801 (2006).
- [587] L. C. Venuti and P. Zanardi, Phys. Rev. A **81**, 032113 (2010).
- [588] D. B. Abraham, E. Barouch, G. Gallavotti, and A. Martin-Löf, Studies in Applied Math. **50**, 121 (1971).
- [589] V. Eisler and I. Peschel, J. Stat. Mech. P06005 (2007).
- [590] P. Calabrese and J. Cardy, J. Stat. Mech. P10004 (2007).
- [591] V. Eisler, D. Karevski, T. Platini, and I. Peschel, J. Stat. Mech. P01023 (2008).
- [592] U. Divakaran, F. Igloi, and H. Rieger, arXiv:1105.5317 (2011) (unpublished).
- [593] J.-M. Stephan and J. Dubail, J. Stat. Mech. P08019 (2011).
- [594] S. Sachdev and A. P. Young, Phys. Rev. Lett. **78**, 2220 (1997).
- [595] P. Calabrese and J. Cardy, J. Stat. Mech. P06008 (2007).
- [596] F. Igloi and H. Rieger, Phys. Rev. Lett. **106**, 035701 (2011).
- [597] M. Rigol, V. Dunjko, and M. Olshani, Nature **452**, 854 (2008).
- [598] A. Iucci and M. A. Cazalilla, Phys. Rev. A **80**, 063619 (2009).
- [599] A. Iucci and M. A. Cazalilla, New J. Phys. **12** (2010).
- [600] E. Canovi, D. Rossini, R. Fazio, G. E. Santoro, and A. Silva, Phys. Rev. B **83**, 094431 (2011).
- [601] E. Farhi, J. Goldstone, S. Gutmann, J. Lapan, A. Lundgren, and D. Preda, Science **292**, 472 (2001).
- [602] M. Collura and D. Karevski, Phys. Rev. Lett. **104**, 200601 (2010).
- [603] H. T. Quan and W. H. Zurek, New J. Phys. **12**, 093025 (2010).
- [604] J. Nehrkorn, S. Montangero, A. Ekert, A. Smerzi, R. Fazio, and T. Calarco, arXiv:1105.1707 (2011) (unpublished).
- [605] G. Schaller, Phys. Rev. A **78**, 032328 (2008).
- [606] M. Eckstein and M. Kollar, New. J. Phys. **12**, 055012 (2010).
- [607] A. Das and B. K. Chakrabarti, Rev. Mod. Phys. **80**, 1061 (2008).
- [608] G. E. Santoro and E. Tosatti, J. Phys. A **39**, R393 (2006).
- [609] P. A. Lee and T. V. Ramakrishnan, Rev. Mod. Physics **57**, 287 (1985).
- [610] A. Das, B. K. Chakrabarti, and R. B. Stinchcombe, Phys. Rev. E **72**, 026701 (2005).
- [611] V. N. Smelyanskiy, E. G. Rieffel, S. I. Knysh, C. P. Williams, M. W. Johnson, M. C. Thom, and K. L. P. W. G. Macready, arXiv:1204.2821 (2012) (unpublished).
- [612] P. Amara, D. Huse, and J. E. Straub, J. Phys. Chem. **97**, 6715 (1993).
- [613] A. B. Finnila, M. A. Gomez, C. Sebenik, C. Stenson, and D. J. Doll, Chem. Phys. Lett. **219**, 343 (1994).
- [614] T. Kadowaki and H. Nishimori, Phys. Rev. E **58**, 5355 (1998).
- [615] G. E. Santoro, R. Mortonak, E. Tosatti, and R. Car, Science **295**, 2427 (2002).
- [616] S. Morita and H. Nishimori, J. Math. Phys. **49**, 125210 (2008).
- [617] B. Altshuler, H. Krovi, and J. Roland, Proc. Nat. Acad. Sc., **107**, 12446 (2010).
- [618] A. P. Young, S. Knysh, and V. N. Smelyanskiy, Phys. Rev. Lett. **104**, 020502 (2010).
- [619] E. Farhi, J. Goldstone, D. Gosset, S. Gutmann, H. B. Meyer, and P. Shor, arXiv:0909.4766 (2009) (unpublished).
- [620] M. Amin and V. Choi, Phys. Rev. A **80**, 062326 (2009).
- [621] T. Jorg, F. Krezkala, J. Kurchan, and A. C. Maggs, Phys. Rev. Lett. **101**, 147204 (2008).
- [622] Y. Seki and H. Nishimori, Phys. Rev. E **85**, 051112 (2012).
- [623] J. Jensen and A. R. Mackintosh, *Rare Earth Magnetism* (Clarendon, Oxford, 1991).
- [624] J. M. Luttinger and L. Tisza, Phys. Rev. **70**, 954 (1946).
- [625] P. Beauvillain, J. P. Renard, and L. . P. E. Hansen, J. Phys. C **10**, J. Phys. C **10**, L709 (1977).
- [626] G. Mennenga, L. J. de Jong, and W. J. Huiskamp, J. Magn. Magn. Mat **44**, 48 (1984).
- [627] R. Youngblood, G. Aeppli, J. Axe, and J. Griffin, Phys. Rev. Lett. **49**, 1724 (1982).
- [628] R. Blinc and B. Zeks, Adv. Phys. **91**, 693 (1972).
- [629] Y. Feng, C. Ancona-Torres, T. F. Rosenbaum, D. L. Price, and E. Courtens, Phys. Rev. Lett. **97**, 145501 (1996).
- [630] G. Xu, C. Broholm, Y.-A. Soh, G. Aeppli, J. F. DiTusa, Y. Chen, M. Kenzelmann, C. D. Frost, T. Ito, K. Oka, et al., Science **317**, 1049 (2007).
- [631] T. Bitko, T. F. Rosenbaum, and G. Aeppli, Phys. Rev. Lett. **77**, 940 (1996).
- [632] H. M. Ronnow, J. Jensen, R. Parthasarathy, G. Aeppli, T. F. Rosenbaum, D. F. McMorrow, and C. Kraemer, Phys. Rev. B **75**, 054426 (2007).
- [633] D. H. Reich, T. F. Rosenbaum, G. Aeppli, and H. J. Guggenheim, Phys. Rev. B. **34**, 4956 (1986).
- [634] D. Reich, B. Ellman, I. Yang, T. Rosenbaum, G. Aeppli, and D. P. Belanger, Phys. Rev. B. **42**, 4631 (1990).

- [635] C. Ancona-Torres, D. M. Silevitch, T. F. Rosenbaum, and G. Aeppli, Phys. Rev. Lett. **101**, 057201 (2008).
- [636] P. E. Joensson, R. Mathieu, W. Wernsdorfer, A. M. Tkachuk, and B. Barbara, Phys. Rev. Lett. **98**, 256403 (2007).
- [637] J. A. Quilliam, S. Meng, C. G. A. Mugford, and J. B. Kycia, Phys. Rev. Lett. **101**, 187204 (2008).
- [638] J. A. Quilliam, C. G. A. Mugford, A. Gomez, S. W. Kycia, and J. B. Kycia, Phys. Rev. Lett. **98**, 037203 (2007).
- [639] D. H. Reich, T. F. Rosenbaum, and G. Aeppli, Phys. Rev. Lett. **59**, 1969 (1987).
- [640] R. N. Bhatt and P. A. Lee, Phys. Rev. Lett. **4**, 344 (1982).
- [641] S. Ghosh, R. Parthasarathy, T. Rosenbaum, and G. Aeppli, Science **296**, 2195 (2002).
- [642] S. Ghosh, T. Rosenbaum, and G. Aeppli, Phys. Rev. Lett. **101**, 157205 (2008).
- [643] R. Giraud, W. Wernsdorfer, A. M. Tkachuk, D. Mailly, and B. Barbara, Phys. Rev. Lett. **87**, 057203 (2001).
- [644] M. Schechter, Phys. Rev. B **77**, 020401 (2008).
- [645] D. Silevitch, G. Aeppli, and T. Rosenbaum, PNAS **107**, 2797 (2010).
- [646] D. M. Silevitch, D. Bitko, J. Brooke, S. Ghosh, G. Aeppli, and T. F. Rosenbaum, Nature **448**, 567 (2007).
- [647] J. Brooke, T. F. Rosenbaum, and G. Aeppli, Nature **413**, 610 (2001).
- [648] J. Brooke, D. Bitko, T. F. Rosenbaum, and G. Aeppli, Science **284**, 779 (1999).
- [649] M. W. Johnson, M. H. S. Amin, S. Gildert, T. Lanting, F. Hamze, N. Dickson, R. Harris, A. J. Berkley, J. Johansson, P. Bunyk, et al., Nature **473**, 194 (2011).
- [650] D. Sen, Phys. Rev. B **59**, 43 (1991).
- [651] G. Baskaran, D. Sen, and R. Shankar, Phys. Rev. B **78**, 115116 (2008).
- [652] F. D. M. Haldane, Phys. Rev. Lett. **45**, 1358 (1980).
- [653] F. D. M. Haldane, Phys. Rev. Lett. **47**, 1840 (1981).
- [654] F. D. M. Haldane, J. Phys. C **14**, 2585 (1981).
- [655] H. J. Schulz, in *Proceedings of Les Houches Summer School LXI*, edited by E. Akkermans, G. Montambaux, J. Pichard, and J. Zinn-Justin (Elsevier, Amsterdam, 1995).
- [656] H. J. Schulz, G. Cuniberti, and P. Pieri, in *Field Theories for Low Dimensional Condensed Matter Systems*, edited by G. Morandi, A. Tagliacozzo, and P. Sodano (Springer, Berlin, 2000).
- [657] A. O. Gogolin, A. A. Nersisyan, and A. M. Tsvelik, *Bosonization and Strongly Correlated Systems* (Cambridge University Press, Cambridge, 1998).
- [658] J. von Delft and H. Schoeller, Ann. Phys. (Leipzig) **7**, 225 (1998).
- [659] S. Rao and D. Sen, *Field theories in Condensed Matter Physics* (Hindustan Book Agency, New Delhi, editor: S. Rao, 2001).
- [660] T. Giamarchi, *Quantum Physics in One Dimension* (Oxford University Press, Oxford, 2004).
- [661] G. F. Giuliani and G. Vignale, *Quantum Theory of Electron Liquid* (Cambridge University Press, Cambridge, 2005).
- [662] K. D. Schotte and U. Schotte, Phys. Rev. **182**, 479 (1969).
- [663] D. C. Mattis, J. Math. Phys. **15**, 609 (1974).
- [664] A. Luther and I. Peschel, Phys. Rev. B **12**, 3908 (1975).
- [665] S. Coleman, Phys. Rev. D **11**, 2088 (1975).
- [666] S. Mandelstam, Phys. Rev. D **11**, 3026 (1975).
- [667] I. Affleck, in *Fields, Strings and Critical Phenomena*, edited by E. Brezin and J. Zinn-Justin (North-Holland, Amsterdam, 1989).
- [668] R. J. Baxter, *Exactly Solved Models in Statistical Mechanics* (Academic Press, New York, 1982).
- [669] J. P. Boucher and L. P. Regnault, J. de Phys. I **6**, 1939 (1996).
- [670] S. Pati, R. Chitra, D. Sen, S. Ramasesha, and H. R. Krishnamurthy, J. Phys. Condens. Matter **9**, 219 (1997).
- [671] F. D. M. Haldane, Phys. Rev. B **25**, 4925 (1982).
- [672] K. Okamoto and K. Nomura, Phys. Lett. A **169**, 433 (1992).
- [673] R. J. Bursill, T. Xiang, and G. A. Gehring, J. Phys. A **28**, 2109 (1994).
- [674] R. J. Bursill, G. A. Gehring, D. J. Farnell, J. B. Parkinson, T. Xiang, and C. Zeng, J. Phys. C **7**, 8605 (1995).
- [675] R. Chitra, S. Pati, H. R. Krishnamurthy, D. Sen, and S. Ramasesha, Phys. Rev. B **52**, 6581 (1995).
- [676] S. R. White and I. Affleck, Phys. Rev. B **54**, 9862 (1996).
- [677] U. Schollwöck, T. Jolicoeur, and T. Garel, Phys. Rev. B **53**, 3304 (1996).
- [678] M. Kumar, Z. G. Soos, D. Sen, and S. Ramasesha, Phys. Rev. B **81**, 104406 (2010).
- [679] C. K. Majumdar and D. K. Ghosh, J. Math. Phys. **10**, 1388 and 1399 (1969).
- [680] A. Patra, V. Mukherjee, and A. Dutta, J. Stat. Mech. P03026 (2011).
- [681] X. Peng, S. Wu, D. Suter, and J. Du, Phys. Rev. Lett. **105**, 240405 (2010).
- [682] L. Landau, Phys. Sov. Union **2**, 46 (1932).
- [683] C. Zener, Proc. Roy. Soc. London Ser A **137**, 696 (1932).
- [684] E. C. G. Stueckelberg, Helv. Phys. Acta **5**, 369 (1932).
- [685] E. Majorana, Nuovo Cimento **9**, 43 (1932).
- [686] B. K. Chakrabarti and D. Samanta, Phys. Rev. B **81**, 052301 (2010).
- [687] A. Altland and V. Gurarie, Phys. Rev. Lett. **100**, 063302 (2008).
- [688] A. Altland, V. Gurarie, T. Kriecherbauer, and A. Polkovnikov, Phys. Rev. A **79**, 042703 (2009).
- [689] W. H. Zurek and U. Dorner, Phil. Trans. R. Soc. A **366**, 2953 (2008).
- [690] T. Platini, D. Karevski, and L. Turban, J. Phys: A. Math. Theor. **40**, 1467 (2007).
- [691] M. Collura, D. Karevski, and L. Turban, J. Stat. Mech: Theor Expt. 08007 (2009).
- [692] B. Damski and W. H. Zurek, Phys. Rev. Lett. **99**, 130402 (2007).

- [693] F. Igloi, I. Peschel, and L. Turban, *Adv. Phys.* **42**, 683 (1993).
- [694] M. Campostrini and E. Vicari, *Phys. Rev. Lett.* **102**, 240601 (2009).
- [695] J. Dziarmaga and M. M. Rams, *New J. Phys.* **12**, 103002 (2010).
- [696] J. Dziarmaga and M. M. Rams, *New J. Phys.* **12**, 055007 (2010).
- [697] D. Sen and S. Vishveshwara, *EPL* **91**, 66009 (2010).
- [698] M. Thakurathi, W. DeGottardi, D. Sen, and S. Vishveshwara, *Phys. Rev. B* **85**, 165425 (2012).
- [699] C. D. Grandi, R. Barankov, and A. Polkovnikov, *Phys. Rev. Lett.* **101**, 230402 (2008).
- [700] B. Dora, M. Haque, and G. Zarand, *Phys. Rev. Lett.* **106**, 156406 (2011).
- [701] J. O. Fjaerstad, *J. Stat. Mech.* 07011 (2008).